SULFUR BIOGEOCHEMISTRY OF CIRCUMNEUTRAL MINING WASTEWATERS

IDENTIFICATION OF BIOGEOCHEMICAL INDICATORS TOWARDS ACID GENERATION IN MICROBIAL SULFUR CYCLING OF CIRCUMNEUTRAL MINING WASTEWATERS

By
David Camacho, B.Sc.

A thesis submitted to the School of Graduate Studies in Partial Fulfilment of the Requirements for the Degree Doctor of Philosophy

McMaster University DOCTOR OF PHILOSOPHY (2021)
Hamilton, Ontario (Earth and Environmental Science)

TITLE: Identification of Biogeochemical Indicators Towards Acid Generation in Microbial Sulfur Cycling of Circumneutral Mining Wastewaters
AUTHOR: David Camacho, B.Sc. (University of Guelph).
SUPERVISOR: Professor Lesley Warren
NUMBER OF PAGES: xiii, 231

Abstract

Acid mine drainage (AMD) is a major issue for the mining industry and a global environmental concern. It is facilitated heavily by microbially catalyzed sulfur oxidation/ disproportionation reactions involving reduced sulfide components in mine wastes that result in the release of harmful acidity and metals. The microbial processes catalyzing sulfide mineral leaching of mine waste rock resulting in AMD have been previously studied. However, the initiation of AMD processes in mining wastewaters has not been well studied. Post extraction, highly contaminated, mining wastewater is stored in retention (tailings) impoundments on site and treated to prevent impacts such as toxicity, contamination, and acidity prior to discharge to the receiving environment. Tailings, the waste stream generated through extraction of sulfide ores contains a variety of aqueous sulfur oxidation intermediate compounds (SOIs), such as polysulfides, elemental sulfur, and sulfur oxyanions, of the form $S_xO_y^{2-}$ termed "thiosalts" by the industry, which can also generate AMD. These wastewaters typically initially start off with circumneutral pH, but if thiosalts are present in high enough concentrations, microbial processes can cause net-acid generation leading to AMD. The microbial ecology and functionality of endemic tailings impoundment microbial assemblages in the "pre-net acid generating phase" (PNAG) of circumneutral mine wastewaters, as well as the associated sulfur species and reactions are not well understood. Thus, early-stage indicators that would offer mines proactive monitoring tools for improved tailings impoundment management are currently lacking.

In collaboration with our mining industry partners, who provided tailings impoundment water samples, this dissertation tackles these limitations. This dissertation aimed to identify important microbes and the SOI important to the initiation of AMD in PNAG tailings impoundment wastewaters and to determine potential markers (microbial and/or geochemical) associated with these initiating AMD processes that would inform the development of monitoring tools in mine water management. The objectives of this doctoral research were to constrain the S biogeochemistry of the PNAG phase by characterizing both expression levels of sulfur oxidation genes and sulfur speciation under experimental conditions designed to assess the roles of microbial community, SOI geochemistry and pH. Specifically three well constrained laboratory experiments determined: (1) gene expression by a pure culture of *Acidithiobacillus thiooxidans* and sulfur speciation with either thiosulfate or elemental sulfur added as the starting SOI substrate (Chapter 3); (2) parent mining wastewater communities and associated sulfur oxidizing bacteria (SoxB) enrichments collected seasonally at two mines and grown at either pH 7-5 or pH 5-3 genetically (16S amplicon) (Chapter 4); and (3) geochemical sulfur pathways of three unique mine wastewater SoxB enrichment communities for six distinct simulated mine wastewater thiosulfate and/or tetrathionate treatments (Chapter 5).

Results presented in Chapter 3 expand the understanding of the reactions and enzymes involved in S^0 and $S_2O_3^{2-}$ metabolism by a pure strain sulfur oxidizing bacteria *A. thiooxidans* ATCC 19377 by developing the first models integrating gene expression, solution sulfur

speciation, electron microscopy and spectroscopy. These novel results reveal that *A. thiooxidans* $S_2O_3^{2-}$ metabolism involves the conversion of $S_2O_3^{2-}$ to SO_4^{2-}, S^0 and $S_4O_6^{2-}$, mediated by the sulfur oxidase complex (Sox), tetrathionate hydrolase (TetH), sulfide quinone reductase (Sqr) and heterodisulfate reductase (Hdr) proteins. These same proteins, with the addition of rhodanese (Rhd), were identified to convert S^0 to SO_3^{2-}, $S_2O_3^{2-}$ and polythionates in the *A. thiooxidans* S^0 metabolism model. The results of this chapter advance understanding by revealing (1) the important role specifically of TetH in $S_2O_3^{2-}$ metabolism; (2) Hdr proteins, rather than Sdo proteins, are likely associated with S^0 oxidation; (3) that formation of intracellular $S_2O_3^{2-}$ is a critical step in S^0 metabolism, and (4) that recycling of internally generated SO_3^{2-} occurs, through comproportionating reactions that result in $S_2O_3^{2-}$.

Results summarized in Chapter 4, identify that pH is the most important factor influencing which sulfur oxidizing bacteria (SoxB) occur irrespective of total S concentration of SOI substrate provided in enrichment experiments for two mines of different parent wastewater geochemistry. Mine 1 exhibited a lower total S and reactive soluble sulfur compounds (oxidation state < +VI) concentrations, and greater parent wastewater microbial community diversity with more unique sequences relative to Mine 2. All experimental SoxB enrichment experiment microbial communities evidenced a shift in dominance from primarily *Alphaproteobacteria* (28% - 77%) at circumneutral pH to *Gammaproteobacteria* (>80%) under moderately acidic pH values. A further pH dependent shift was observed at the genus level, from *Halothiobacillus* spp. dominating the circumneutral pH SoxB enrichments to *Thiomonas* spp. dominating the mildly acidic SoxB enrichments. These results provide some of the first putative biological indicators to improve prediction and management of sulfur processes and AMD onset within mining wastewaters.

Chapter 5 results importantly assess the influences of SOI chemistry and SoxB consortia identity on SOI cycling. Results identify that SOI substrate, whether $S_2O_3^{2-}$, $S_4O_6^{2-}$, or $S_2O_3^{2-}$ + $S_4O_6^{2-}$, was a more important determinant of microbial sulfur outcomes than the relative abundances of *Halothiobacillus spp.* and *Thiomonas spp.*. Further, three pH dependent phases of microbial sulfur processing were identified: Phase 1, pH > 5, dis/comproportionation reactions and acid consuming reactions were prevalent alongside oxidation, with $S_2O_3^{2-}$ identified as an important indicator; Phase 2, pH 5 – 3, further dis/comproportionation occurred, with S^0 emerging as an important indicator signalling the progression of the system towards net acid generation with $S_4O_6^{2-}$ or $S_2O_3^{2-}$ as the major S species present and; Phase 3, pH < 3, i.e. full AMD conditions, with dominant oxidation reactions resulting in SO_4^{2-} and acid generation. Collectively, these results identify specific SOI species important at different pH stages in AMD initiation and development across different microbial SoxB, providing new indicators that may serve as signals associated with predictive tool development.

The integration of the novel results of this thesis revealed some of the first biologically informed possible indicators (bacterial and geochemical) that will enable improved management through proactive monitoring tools for AMD initiation in mining wastewaters.

Acknowledgements

I would like to thank my supervisor, Dr. Lesley Warren, for the opportunity to work with her and the rest of the group for the last few years. Being able to study and teach others such a diverse interdisciplinary facet of science, it has been a privilege and phenomenal experience. I would also like to thank the rest of my committee and advisors, Dr. Greg Slater, Dr. Jim Smith and Dr. Luc Bernier, for all their assistance, guidance and comradery during my time as a PhD. student at McMaster.

To the ladies of the lab, Tara, Maya, Michelle, Katy, Darla, Steph, Kelly and Lauren. I could not have gotten through my studies without your assistance in lab troubleshooting and in welcoming me to joke around and putting up with my most likely distracting high-jinx. To the fellas of the lab, Florent, Patrick, Gerdhard, Jiro and of course my lab husband and partner in shenanigans Daniel, thanks for the fun and learning both in the office and out. To the WOBs and the Phoenix crew, thanks for being there to support philosophical discussions both science/work-related and not, making it a good lime every time.

I would definitely like to thank my family and friends throughout my journey from all the places I've been to here, making it a wonderful time full of fun and learning. Especially the ladies in my life who kept pushing me forward no matter what my laid-back self felt. My mum Colleen, always there for me no matter what, ready with a steups if I slack, but loves me regardless. My sisters Lisa and Ariane for pushing me to further myself to University and beyond. My friend Emma who quite literally made sure I had all my forms and applications done in time, without whom I would be far back. My friend Mai, who I could count on to check my writing for me. My professor Lesley who always tried to get the best work out of me, unquestioningly. And lastly, Taren, my love, who made these many years a phenomenal time, through all the degrees and work, being there with love, support, and firmness. Keeping me at my best and encouraging me to go further than I had thought I would, it has been amazing and I look forward to the future each day.

Finally, I would like to thank you… the reader, if you even read this section, or any bit of my thesis I hope you find what you are looking for and it helps you out, big or small, I hope you enjoy it!

Cheers, benches and tables!

David

TABLE OF CONTENTS

List of Figures

List of Tables

Declaration of Academic Achievement

Chapters 1, 2, 5 and 6, in their entirety were completed by me with contributions, revisions and editing provided by Dr. Lesley Warren.

Chapter 3, Experimental Design and Sampling were completed equally by me and Rodolfo Frazao. Analyses were completed mostly by me and Rodolfo Frazao, with minor work completed by Dr. Aurélien Foullien and Dr. Simon Apte. Data interpretation was carried out by me with minor work done by Rodolfo Frazao. Writing was carried out by me, with contributions, revisions and editing provided by Dr. Christian Baron and Dr. Lesley Warren. Equipment, lab space and funding were provided by Dr. Antonio Nanci, Dr. B. Franz Lang, Dr. Simon Apte, Dr. Christian Baron and Dr. Lesley Warren.

Chapter 4, Experimental Design and Sampling were completed by me. Analyses were mostly completed by me, with minor work completed by Dr. Gerdhard Jessen, Dr. Jiro Mori and Chad Jarolimek. Data interpretation and writing was carried out by me, with contributions, revisions and editing provided by Dr. Gerdhard Jessen and Dr. Lesley Warren. Equipment, lab space and funding were provided by Dr. Simon Apte and Dr. Lesley Warren.

Chapter 1

1.1. Review

Sulfur can exist in a range of oxidation states, from -2 to +6, at earth surface pressure and temperature. Between its most reduced form, sulfide (S^{2-}), and its most oxidized form, sulfate (SO_4^{2-}), there exist multiple sulfur oxidation intermediate (SOI) species, including elemental sulfur (S^0), thiosulfate ($S_2O_3^{2-}$), polythionates ($S_xO_y^{2-}$), sulfite (SO_3^{2-}) (Figure 1.1) (Zopfi et al., 2004). This range of oxidative states contributes to a complex important biogeochemical cycle driven by both abiotic and biotic redox reactions (Figure 1.1) (Johnston and McAmish, 1973; Kelly et al., 1990; Pronk et al., 1990; Druschel, 2002; Zopfi et al., 2004; Ghosh and Dam, 2009; Boyd and Druschel, 2013; Wang et al., 2019). The occurrence and concentrations of sulfur species in any environmental system are dependent on many variables, such as pH, temperature, pressure and redox potential (Druschel, 2002), which enable sulfur to occur in a variety of aqueous (solution) species as well as gaseous (H_2S_g), and solid (mineralized) forms (Sato, 1992; Lindsay et al., 2015). This complexity of possible sulfur compounds that can occur, makes accurate prediction of possible sulfur compounds occurring in any given system challenging (Canfield et al., 2010; Jamieson et al., 2015, Camacho et al., 2020a).

Sulfur plays a central role in the generation of acid mine drainage (AMD) or acid rock drainage (ARD) systems (Amos et al., 2015; Lindsay et al., 2015). Sulfur's primary role in AMD reflects the oxidation of sulfur within sulfide minerals associated with waste rock and tailings that results in the generation of acid (H^+ ions) and SO_4^{2-}, which eventually leads to the leaching of metals from the sulfide minerals as pH decreases (Pronk et al., 1990; Druschel, 2002; Sheoran and Sheoran, 2006; Moncur et al., 2015; Nordstrom et al., 2015). The generation of these compounds is driven by microbially initiated oxidation of sulfide minerals present in exposed ores, waste rock

and tailings (Table 1.1) (Schippers and Sand, 1999; Jamieson et al., 2015; Lindsay et al., 2015). Most of the world's metals come from sulfide minerals, underscoring the widespread and significant volumes of sulfur associated with mining activities that pose AMD/ARD risks (Jamieson et al. 2015; Lindsay et al., 2015). The quantity of tailings produced and the quality (i.e., percentage of sulfur in tailings) is dependent on the site, the ore mined and the extraction practices used (Smuda et al., 2008). Hence a better understanding of sulfur biogeochemical cycling within mining waste contexts is critical to mitigate and ultimately prevent AMD (Schippers et al., 1996; Bernier and Warren, 2005; Castendyk et al., 2015; Moncur et al., 2015).

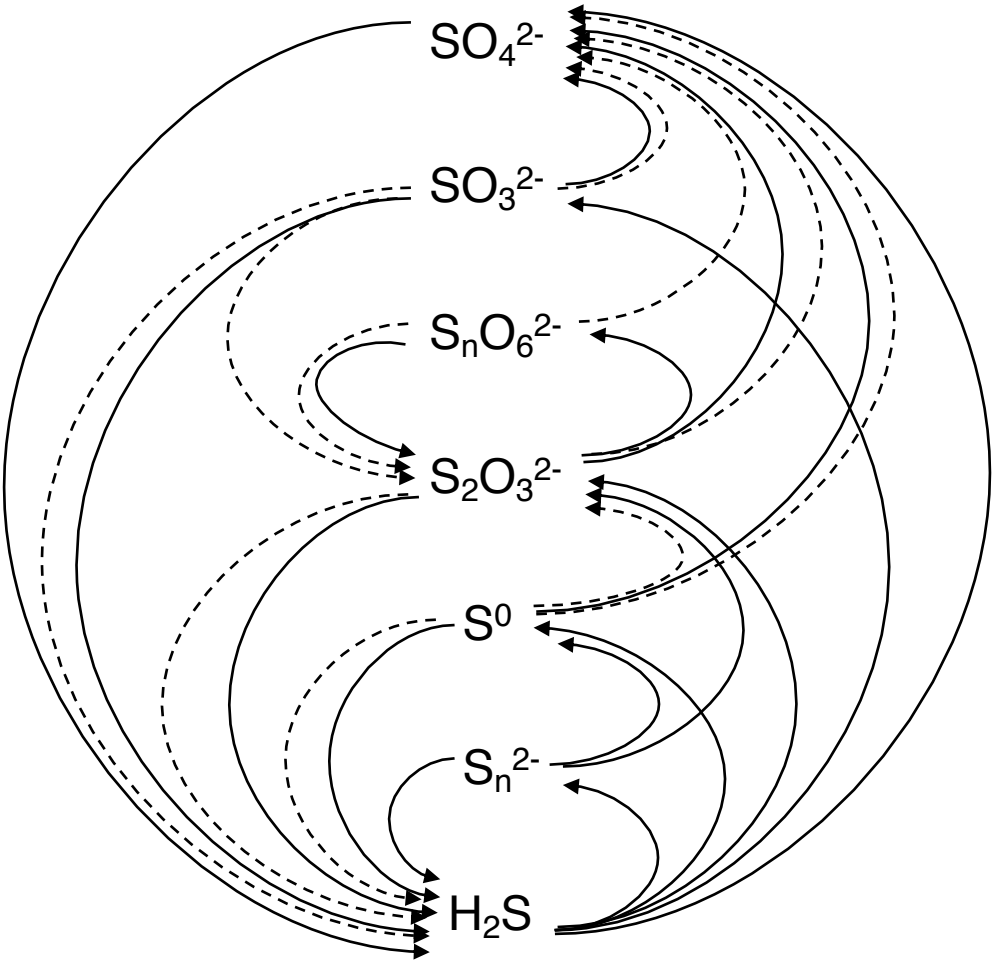

Figure 1.1: A non-exhaustive suite of aqueous sulfur compounds from most reduced (i.e. H_2S) to most oxidized (i.e SO_4^{2-}), illustrating the complexity of possible reduction (on left) and oxidation (on right) pathways (solid lines), and bacterial disproportionation (dashed lines) of select S species.

Table 1.1: Sulfide containing minerals found in mined ores.

Mineral	Chemical Structure
Chalcopyrite	$CuFeS_2$
Cinnabar	HgS
Cobaltite	$CoAsS$
Enargite	Cu_3AsS_4
Galena	PbS
Hauerite	MnS_2
Marcasite	FeS_2
Molybdenite	MoS_2
Orpiment	As_2S_3
Pentlandite	$(Fe,Ni)_9S_8$
Pyrite	FeS_2
Pyrrhotite	$Fe_{(1-x)}S$
Realgar	As_4S_4
Sphalerite	$(Zn,Fe)S$
Stibnite	Sb_2S_3
Tetrahedrite–Tennantite	$(Cu,Fe)_{12}Sb_4S_{13}$–$(Cu,Fe)_{12}As_4S_{13}$

Mining systems generate large volumes of waste primarily in the forms of waste rock (overburden removed to facilitate access of ores; mostly large solids), tailings (an aqueous slurry of post extraction processed fine particulates and chemicals) and wastewater associated with the tailings waste stream generated by mineral processing (Amos et al., 2015; Jamieson et al., 2015; Moncur et al., 2015; Nordstrom et al., 2015). Canada annually produces an estimated 475,000,000 tonnes of waste rock and tailings and more than 600,000,000 tonnes (m^3) of wastewater (Statistics Canada, 2012). The majority of water withdrawals (71%) by mines is used as process water and discharged (post treatment) to surface water (71%), and groundwater (8%) or held in tailings ponds (13%) (Statistics Canada, 2016). In 2013, mineral extraction industries spent $179 million on water, for acquisition, discharge, and treatment, of which the metal ore mining industry represented

70% of the total costs paid (Statistics Canada, 2016). In Canada and the US, remediation for mine waste was estimated to be 1-2 billion US$ per annum (Dold, 2008). This highlights the economic importance of constraining the biogeochemical processes occurring in all forms of mine waste to improve monitoring techniques, reduce deleterious water quality and thus reduce remediation costs.

Not all mining waste develops AMD conditions, and those that eventually form AMD sites start at circumneutral pH (Dold and Fontbonté, 2001; Smuda et al., 2008; Dockrey et al., 2014; Nordstrom, 2015; Nordstrom et al., 2015, Whaley et al., 2019). However, the majority of research on sulfur dynamics in mining to date has focused on the waste rock piles and tailings that have already reached AMD conditions, i.e., acidic with high metal concentrations (Schippers et al., 2010). Very little published research has assessed the wastewater retained in tailings ponds, prior to treatment and discharge to the receiving environment. These mine tailings wastewaters differ from well-studied AMD, having higher pH and the inclusion of SOI sulfur oxyanions in the form $S_xO_y^{2-}$ termed "thiosalts" generated by extraction processes (Miranda-Trevino et al., 2013). These thiosalts species occur primarily in the forms of thiosulfate ($S_2O_3^{2-}$), trithionate ($S_3O_6^{2-}$) and tetrathionate ($S_4O_6^{2-}$), with the speciation and concentration dependent on variables such as the ore or chemical extractions methods used in the mining and milling processes (Negeri et al., 1999; Miranda-Trevino et al., 2013). Mine modeling and management have focused on these SOI species due to their presumed dominance in wastewaters (Whaley-Martin et al., 2020) and possible recalcitrance to treatment, resulting in their discharge into receiving environments where they may cause impacts (Kuyucak and Yaschyshyn, 2007; Whaley-Martin et al., 2019). These models are based on the dominating, ubiquitous presence of these specific SOI species in tailings generated by extraction of sulfide ores and the assumption that they will continue to dominate within the

retention or tailings ponds, where they are held on site; i.e. any possible biogeochemical reactivity is not currently considered. However, increasing evidence indicates that thiosalts SOI species enter a larger sulfur biogeochemical cycle with diverse potential outcomes dependent on variables such as impoundment geochemistry, physico-chemistry, seasonality, and tailings characteristics (Druschel, 2002; Vongporm, 2008; Wang et al., 2019; Whaley Martin et al., 2019).

For many mines, tailings pond management models are based on abiotic and thus oxygen driven thiosalts oxidation, i.e., the key markers of sulfur oxidation routinely monitored are H^+ ions and/or SO_4^{2-} concentrations (Kuyucak and Yaschyshyn, 2007). However, the relationship between H^+ and SO_4^{2-} is less evident under microbial S cycling due to a greater suite of SOI species that can be potentially generated and more diverse pathways, that do not necessarily result immediately in sulfuate and acidity, than are currently modelled (Figure 1.1) (Johnston and McAmish, 1973; Druschel, 2002; Druschel et al., 2003; Bernier and Warren 2007; Warren et al., 2008; Camacho et al., 2020a). Once net acid generation occurs, i.e., AMD conditions initiate (Figure 1.2), management of further acid generation becomes highly challenging due to the positive feedback in acid mine waste reactions (Schippers et al., 1996; Warren et al., 2008). Therefore, the conventional use of an increase in H^+ (i.e., pH depression) and/or SO_4^{2-} production as the signal of the start of AMD generation can let these processes go undetected until too late to mitigate or reverse the reactions.

In order to gain a better understanding of an effective monitoring approach for aqueous SOI species in mining impacted wastewaters, this review provides a summary of sulfur reactions and the roles that oxidation and disproportionation reactions can play under abiotic or biotic catalysis in more well researched mine waste rock and tailings sites already exhibiting AMD conditions; as well as current understanding of pre net acid generating (PNAG) conditions and

those that may be associated with AMD initiation in circumneutral mining wastewaters, the specific mine waste context of interest for the research in this thesis. In addition, this chapter will provide a summary of current and emerging genetic approaches that will be important to the development new more accurate (microbially informed) monitoring of these processes *in situ*.

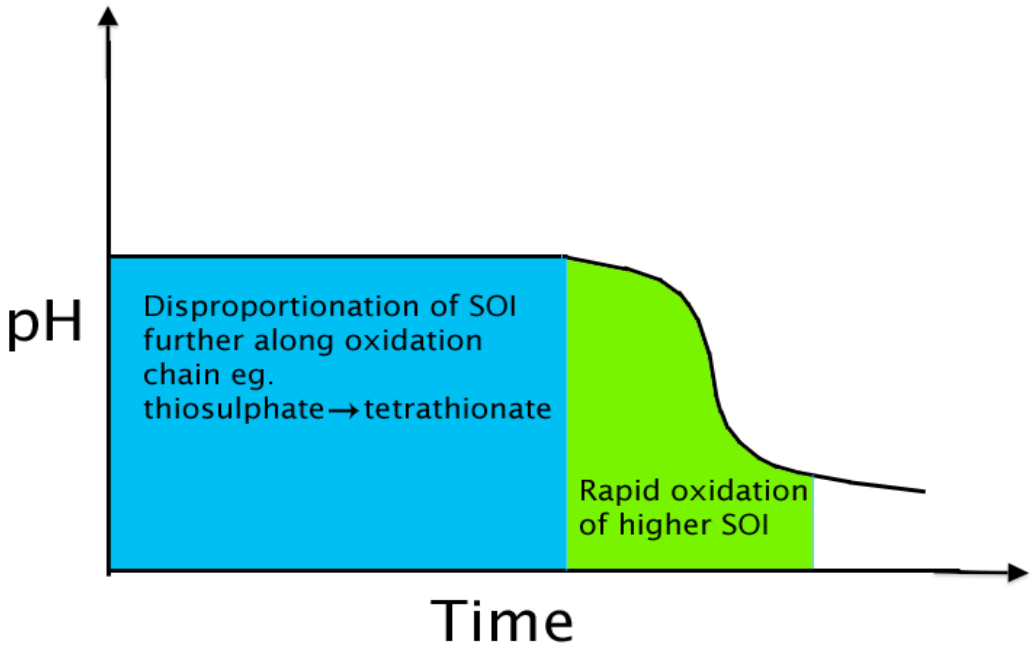

Figure 1.2: Simplified hypothetical dynamics of the process resulting in eventual AMD conditions over time in mine wastewaters.

1.1.1. Sulfur dynamics in mining contexts

The factors affecting sulfur oxidation leading to AMD conditions in mining systems are dynamic and interactive. Kinetics of abiotic reactions are influenced by identities and concentrations of sulfur species, as well as pH, temperature, organic carbon, [O_2] and parent material (ore) (Sato 1992; Druschel 2002; Boyd and Druschel 2013; Lindsay et al., 2015). Biological sulfur oxidation occurs via an array of metabolic pathways dependent on the microbes present, the types and concentrations of S species and solid S phases present, environmental concentrations of possible

e- acceptors such as O_2, Fe^{3+}, NO_3^- as well as temperature and pH (Suzuki et al., 1999; Ghosh and Dam, 2009; Houghton et al., 2016; Wang et al., 2019; Camacho et al., 2020a). As these important variables differ amongst waste rock, dewatered tailings undergoing reclamation and active tailings ponds, it is more than likely that the nature of reactions and the microorganisms involved in possible S biogeochemical cycling will also differ.

Oxygen as the electron acceptor for oxidation of reduced sulfur species, is important to both abiotic and biotic S oxidation processes. Sulfite, a common thiosalt species, is rapidly oxidized to sulfate, both abiotically (Eq 1) or biotically (Eq 2).

$$SO_3^{2-} + ½O_2 \rightarrow SO_4^{2-} \quad (1)$$

$$SO_3^{2-} + H_2O \rightarrow SO_4^{2-} + 2H^+ + 2e^- \quad (2)$$

Sulfur oxidizing microbes catalyzing Eq (2) can use sulfite oxidases (SO) enzymes that use O_2 as an e-acceptor and result in the production of hydrogen peroxide (H_2O_2) (Kappler, 2011). However, oxygen is not the only electron acceptor capable of oxidizing reduced forms of sulfur and has even been shown to be less effective (i.e., slower rate of oxidization) than Fe^{3+} for the oxidation of reduced sulfur species under certain conditions (Druschel, 2002). The rate is dependent on the specific reduced sulfur species, such that at very low pH values, i.e., 1.5, tetrathionate oxidizes at a rate of an order of magnitude (factor of 10) faster with Fe^{3+} than with oxygen, while elemental sulfur oxidizes at a factor of two faster rate with Fe^{3+} than with oxygen (Druschel, 2002). Iron has been well noted as being a major contributor to abiotic sulfur oxidation and thereby acid generation, both by increasing rates of oxidation and by the reaction pathways it takes (Schippers and Sand, 1999; Druschel et al., 2003). However, soluble Fe^{3+} will only be present at low pH values (i.e., <~ pH 3; Sato, 1992; Druschel et al., 2003). Therefore, abiotic Fe^{3+} driven sulfide oxidation only becomes significant at acidic pH values.

As mentioned previously, most studies on sulfur dynamics to date have focused on waste rock and tailings. In these mine contexts the reduced sulfur source is primarily the sulfide minerals present which influences the potential oxidation mechanisms through sulfide mineral structure (Schippers and Sand, 1999) (Figure 1.3). A "thiosulfate mechanism" exists for acid-insoluble minerals (e.g. pyrite (FeS_2) and molybdenite (MoS_2)), which are first oxidatively dissolved to aqueous thiosulfate then subsequently oxidized to sulfate (Figure 1.3A). A "polysulfide mechanism" can occur in oxidation of acid-soluble minerals (e.g. sphalerite, chalcopyrite, or galena) (Table 1.1), in which they are progressively oxidized to polysulfides, elemental S and finally to sulfate (Figure 1.3B).

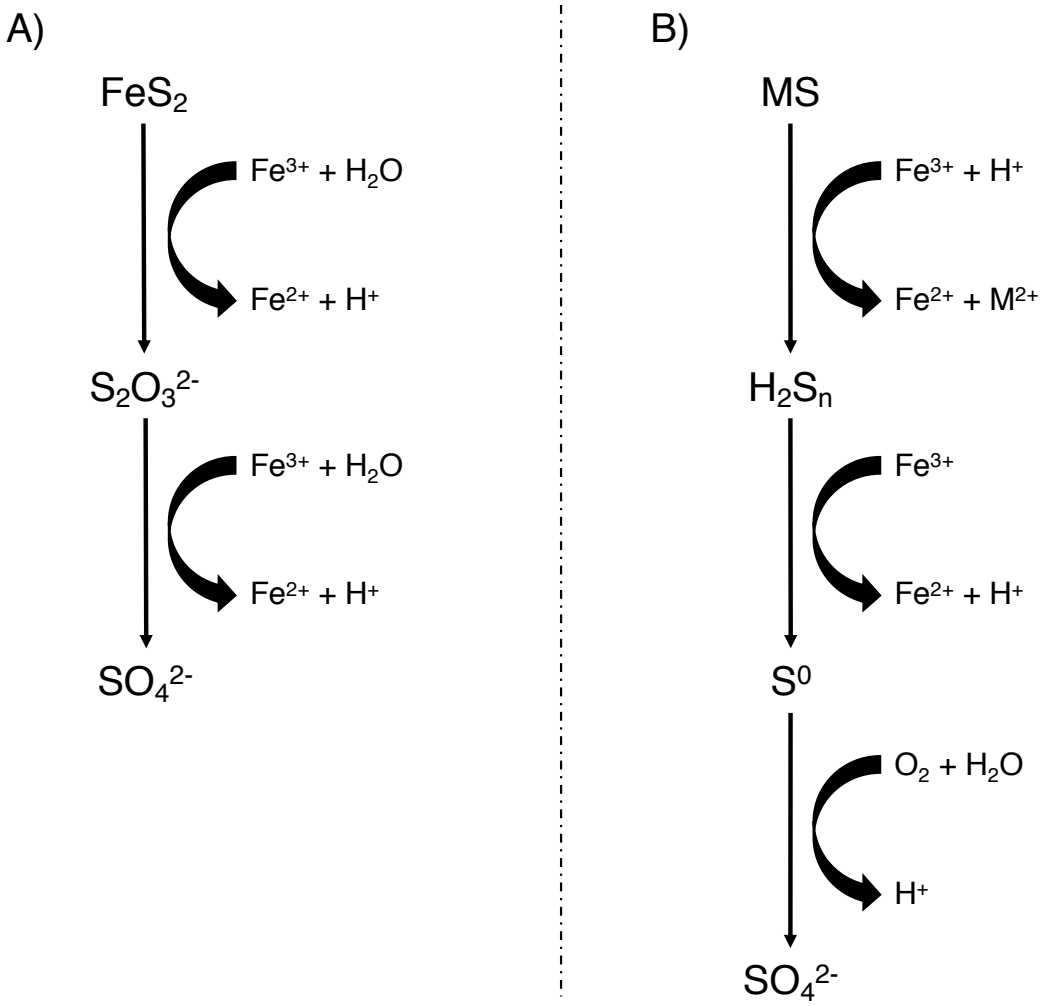

Figure 1.3: Simplified schematic of sulfur oxidation mechanisms based on sulfide mineral structure. **A)** "thiosulfate mechanism" for acid-insoluble minerals. **B)** "polysulfide mechanism" for acid-soluble minerals. Adapted from Schippers and Sand (1999).

In the "polysulfide mechanism", Boyd and Druschel (2013) showed that the rate of elemental sulfur formed from polysulfide was dependent on pH and organic carbon, due to polysulfide instability at acidic pH values. The oxidation of elemental S also requires microbial catalysis (Ghosh and Dam, 2009). Thus, as a result, sulfide minerals undergoing the "polysulfide mechanism" pathway would produce elemental sulfur as the final S species under strict abiotic control. This is due to the abiotically slow reaction rate with O_2 (first order rate constants 10^{-8}-10^{-}

^{10}) or with Fe^{3+} (2 x O_2 rates) at the e- acceptor (Druschel, 2002) resulting in no net increase of H^+. These results underline the importance of microbial catalysis in tandem with abiotic processes to fully drive systems towards AMD conditions and provide evidence that similar processes occur in wastewater contexts, i.e., a lag in acidity generation associated with initial S oxidation processes that then results in acidity generation and potentially swift pH depression (Figure 1.2).

The specific rates and percentages of sulfur compounds produced by the proposed "thiosulfate mechanism" pathway requires a soluble supply of Fe^{3+}, i.e., acidic pH values (Figure 1.3A; Schippers and Sand, 1999). This requirement is due to the disproportionation and rearrangement of $S_2O_3^{2-}$ that occurs at acidic pH values with no Fe^{3+} present (Johnston and McAmish, 1973) versus its oxidation when Fe^{3+} is present Druschel 2002; Druschel et al., 2003) respectively. Under acidic conditions (pH < 4) with no Fe^{3+} present, thiosulfate undergoes disproportionation (Eq 3) (Johnston and McAmish, 1973).

$$S_2O_3^{2-} + H^+ \rightarrow S^0 + HSO_3^- \qquad (3)$$

Therefore, in AMD systems at pH < 4, thiosulfate produced in the "thiosulfate mechanism" (Figure 1.3A) should undergo this disproportionation reaction which would result in a buildup of acid-stable elemental sulfur, while non-acid stable sulfite would quickly oxidize to sulfate (Eq 1 and 2). This disproportionation of thiosulfate favoured at low pH values with no Fe^{3+}, contrasts Fe^{3+} driven oxidation of thiosulfate at low pH values to form tetrathionate (Eq 4) (Figure 1.3A). (Williamson and Rimstidt, 1993).

$$2Fe^{3+} + 2S_2O_3^{2-} \leftrightarrow 2FeS_2O_3^+ \rightarrow 2Fe^{2+} + S_4O_6^{2-} \qquad (4)$$

This pathway was demonstrated by Schippers et al. (1996), identifying that the kinetic rate of oxidation via Fe^{3+} is affected by O_2 concentration (Williamson and Rimstidt, 1994). Building on this understanding, Druschel et al. (2003) compared the kinetics in the presence of both oxygen

and excess Fe^{3+}, showing that almost 100% of thiosulfate oxidizes to tetrathionate when Fe^{3+} is present, since the kinetic rate is much faster for Eq (4) than Eq (3). Thus, for the proposed oxidation of thiosulfate in the "thiosulfate mechanism" to fully occur (Figure 1.3A), Fe^{3+} must be initially present allowing Eq (4) to happen, after which the oxidation of tetrathionate to sulfate can occur. However, tetrathionate has a very slow rate of abiotic oxidation (Druschel, 2002). Although in extremely acidic (pH < 1) solution, acid-stable tetrathionate undergoes a rearrangement reaction into trithionate and pentathionate, of which trithionate has a much faster rate of oxidation than tetrathionate (Druschel et al., 2003). At circumneutral pH values typical of mine tailings ponds, the occurrence and rates of possible reactions for each of these S species will differ. In particular, these studies highlight the importance of biological catalysis to drive oxidation of thiosulfate (often the dominant thiosalts species in sulfide mineral associated tailings) towards its end point of sulfate, as well as providing evidence for the accumulation of higher oxidation state SOI in mine tailings ponds (Figure 1.2).

In mining wastewaters (i.e., tailings ponds), sulfur species are thought to be dominated by thiosalts, the industry term for $S_nO_x^{2-}$ species generated by extraction of sulfide ores (Miranda-Trevino et al., 2013; Camacho et al., 2020b; Whaley-Martin et al., 2020). The possible reactions and rates of reactions that can occur for various "thiosalts" species (e.g., thiosulfate, tetrathionate, sulfite) will be vary as a function of pH and temperature (Vongporm, 2008). In the reverse of what is observed in acidic contexts, thiosulfate would be expected to be stable in tailings ponds, reflecting the more basic pH values typically occurring in these systems, whilst tetrathionate dissociation would be predicted to occur associated with the higher pH values Eq (5) (Vongporm, 2008) resulting in thiosulfate and trithionate.

$$3S_4O_6^{2-} + 6OH^- \rightarrow 3S_2O_3^{2-} + 2S_3O_6^{2-} + 3H_2O \qquad (5)$$

Further, the occurrence of a matrix of S species rather than a single S species can create a different stability field for the kinetics associated with various thiosalts oxidation and disproportionation reactions (Vongporm, 2008). Eq (6) identifies the reduced stability of tetrathionate and increased stability of trithionate that occurs at neutral pH values in the presence of other thiosalts species.

$$2S_4O_6^{2-} + 3H_2O \rightarrow S_2O_3^{2-} + 2S_3O_6^{2-} + 6H^+ \quad (6)$$

These equations illustrate some of the variability and complexity of possible SOI reactions that can occur under varying pH, [O_2] and [Fe^{3+}] conditions. However, they suggest that in neutral to acidic pH mining wastewater impoundments, tetrathionate would be an important sulfur species to monitor, due to its acid-stability and ability for rearrangement. While in neutral to alkaline wastewaters, thiosulfate would be an important sulfur species to monitor for its stability in neutral pH and its prevalence in many important reaction steps. These reactions also highlight that [Fe^{3+}] can play an increasingly important role at lower pH values. However, the abiotic oxidation rates are relatively slow even under oxidizing (high Eh) and acidic (low pH, < 3) conditions (Sato, 1992; Druschel, 2002) indicating biological oxidation of Fe^{2+} to Fe^{3+} Eq (7) is a critical pathway to generate a source of Fe^{3+}.

$$Fe^{2+} + ¼O_2 + H^+ \rightarrow Fe^{3+} + ½H_2O \quad (7)$$

Experimental work has shown that pH is the strongest variable in determining whether abiotic or biotic is more prevalent to Fe^{2+} oxidation (Kirby et al., 1999). Biological catalysis influences Fe^{2+} oxidation more when pH < 5, while at pH 5 – 6.4 abiotic reactions dominate being positively correlated to pH, and at pH > 6.4, Fe^{2+} oxidation becomes independent of pH, having no change in rates (Kirby et al., 1999). Thus, the need for case specific assessment in AMD wasterock and tailings and pre-acidification in the mine wastewater ponds is essential for developing effective monitoring approaches for these differing S rich contexts. However, the collective understanding

to date identifies that generation of AMD conditions via abiotic processes alone is extremely slow underscoring the critical role of microbial S oxidation pathways in this process. As microbial S cycling pathways, controls and outcomes differ from those that can occur abiotically, monitoring methods and models based only on abiotic process understanding will not be capture the potential AMD producing capabilities of mine wastewater tailings impoundments.

1.1.2. Microbial sulfur metabolic groups in mining contexts

Noted and emphasized above were key reactions that are driven by or greatly increased by biological catalysis; namely the oxidation of elemental S, tetrathionate and of ferrous iron at acidic pH. Underscoring how important microbial sulfur cycling is likely to be in mining wastewaters, the capacity for biological sulfur oxidation is widespread, occurring in multiple domains, such as bacteria, archaea and fungi (Kletzin, 1989; Kelly et al., 1990; Baker and Banfield, 2003; Cowie et al., 2009; Ghosh and Dam, 2009; Huang et al., 2011; Whaley-Martin et al., 2019; Camacho et al., 2020b). Not only is the capability for sulfur oxidation widespread in the microbial world, numerous metabolic strategies to gain energy from sulfur oxidation exist, dependent on differing types and concentrations of SOI species, e- acceptors and physico-chemical conditions. This versatility in sulfur oxidation metabolism is due to the plethora of reduced sulfur compounds thermodynamic favourability for energy release and their ability to donate electrons, allowing energy and electron gain for the organism (Warren et al., 2008).

Microbial sulfur oxidation occurs via photo/chemo- litho/organo- auto/hetero trophy, in both aerobic and anaerobic conditions (Kletzin, 1989,1992; Kelly et al., 1990; Meulenberg et al., 1992; Bacelar-Nicolau and Johnson, 1999; Druschel et al., 2004; Beller et al., 2006; Houghton et al., 2016; Wang et al., 2019). The metabolism of sulfur oxidation is dependent on the specific

organism being considered. However, some exist that are capable of all or many of these metabolisms, such as *Allochromatium vinosum* (Ghosh and Dam, 2009). There is a great diversity of microorganisms involved in S oxidation reactions in mining contexts. To date, both phototrophic and chemotrophic metabolic microbes have been found, whose diversities have been shown to be influenced by environmental conditions (Hiraishi et al., 2001; Hallberg and Johnson, 2003; Kimura et al., 2011; Jones et al., 2014). This evidence identifies that delineating the possible metabolic reaction pathways, genetic makeup and ecology of biological sulfur oxidation will be highly complex.

Photolithotrophic bacteria are a major group of known sulfur oxidizing bacteria (SoxB), utilizing light as an energy source and reduced sulfur for electrons. Interestingly, no archaea or any other organisms besides bacteria have yet been found to exploit a phototrophic metabolism for sulfur oxidation (Ghosh and Dam, 2009; Niu et al., 2016). Based on current genomic studies and ecological studies, very few phototrophic organisms can exist in the harsh acidic environments found in AMD systems (Korehi et al., 2014; Niu et al., 2016). Moreover, little is known of their relevance or abundance in pre-AMD systems due to the limited research on such contexts (Korehi et al., 2014; Whaley-Martin et al., 2019). In AMD sites exposed to sunlight, it would be possible for phototrophs to acquire and represent an important source of fixed carbon and energy (Hiriashi et al., 2000) while their possible contributions to biogeochemical cycling would be negligible to nonexistent in subsurface, i.e., dark AMD systems (Baker and Banfield, 2003). The primary metabolic processes associated with AMD sites and what little is known of pre-AMD contexts identified to date are: chemolithoautotrophs that oxidize ferrous iron and sulfide released by pyrite and other sulfide/ferrous iron containing minerals to gain energy; chemoorganoheterotrophs, which consume the carbon produced by the autotrophs; and chemolithoheterotrophs oxidizing iron

and sulfur while utilizing organic carbon (Johnson and Hallberg, 2003; Diaby et al., 2007; Kuang et al., 2013; Niu et al., 2016; Rameez et al., 2020). The chemotrophs, unlike the phototrophs, encompass organisms from all domains in mine waste microbial ecology (Ghosh and Dam, 2009; Niu et al., 2016). These organisms are responsible for most biological geochemical cycling occurring in AMD systems (Tyson et al., 2004).

1.1.3. AMD vs pre-AMD microbes

Only highly adapted microbes can withstand the high levels of acidity and metal contamination occurring in severe AMD systems (Druschel et al., 2004). This makes the potential community variability and species richness smaller relative to more neutral pH ecological niches (Baker and Banfield, 2003). However, biological interactions of consortia formed between bacteria (Norlund et al., 2009), as well as consortia formed between protists and bacteria (Baker and Banfield, 2003) occur in AMD conditions to mutually benefit their partners. For instance, Norlund et al. (2009) identified that a S oxidizer and a S reducer formed micro-scale aggregates that enabled redox recycling of S compounds supplying each partner's required substrates that enabled them both to survive the bulk geochemical conditions under which these aggregates formed (Figure 1.1). This microbial cycling of redox reactive species at the microscale, makes it challenging to accurately identify key geochemical processes occurring in systems via reaction rates determined at bulk scale (Norlund et al., 2009). It also increases the potential for a higher variation of microbe function and diversity than expected, due to variable ecological niches present, such as bacteria living in neutral pH within a protist, which protects it from acidic conditions (Baker and Banfield, 2003).

While microscale consortial biogeochemical cycling is likely occurring in these contexts, the microbes present in AMD communities of waste rock and tailings sites have been shown to largely

be comprised of sulfur and iron oxidizers, especially in iron-rich ores (Leduc et al., 2002; Baker and Banfield, 2003; Huang et al., 2011; Kimura et al., 2011; Korehi et al., 2014). As identified previously, at low pH values, the kinetics of abiotic Fe^{2+} oxidation slow down considerably, thus acidophilic Fe oxidizers can catalyze the reaction and gain the energy (Druschel et al., 2004). Iron oxidizing bacteria, *Leptosprillium* and archaea, *Ferraplasma* and *Thermoplasmatales* are prevalent in AMD systems containing high levels of ferrous iron (Druschel et al., 2004; Tyson et al., 2004; Huang et al., 2011; Kuang et al., 2013). As for sulfur oxidizers, the common and well-studied organisms represented are *Proteobacteria*: mainly *Gammaproteobacteria* belonging to *Acidithiobacilli*, *Alphaproteobacteria* belonging to *Acidiphilum* and a few *Beta/Deltaproteobacteria* (Kelly and Wood, 2000; Baker and Banfield, 2003; Rameez et al., 2020). Sulfur oxidizing bacteria, *Sulfobacillus* and archaea, *Sulfolobales* have also been found in acidic sites (Baker and Banfield, 2003; Kimura et al., 2011; Korehi et al., 2014). The archaea are mainly found in natural geothermal acidic environments rather than AMD sites (Baker and Banfield, 2003). These results identify that while there is some variability in metabolism dependent on the conditions occurring, typically they are associated with a select few genetic groups: *Nitrospira, Proteobacteria, Firmicutes, Sulfolobales* and *Actinobacteria* (Johnson and Hallberg, 2003; Liu et al., 2014).

As indicated previously most research on microbial sulfur oxidizing bacteria in acidic environments has identified that *Proteobacteria* are common and often dominate communities (Liu et al., 2014). In AMD systems, *Gammaproteobacteria* studied include *Acidithiobacilli* spp. such as *A.thiooxidans, A.caldus* and *A.ferrooxidans,* which can oxidize both reduced sulfur and iron species (Pronk et al., 1990; Hallberg et al., 1996; Schippers et al., 1996; Kelly and Wood, 2000; Rohwerder and Sand, 2003). Another well-researched *Gammaproteobacteria* is the highly

versatile, facultative phototroph *A.vinosum,* which can exist in variable conditions including AMD sites and pre-acidification mine tailings ponds, thought to reflect its versatility in metabolic capabilities (Dahl et al., 2005; Henson et al., 2006). The *Alphaproteobacteria* mainly studied belong to the *Acidiphilum* spp. such as *A.cryptum* and *A.acidophilum* (Meulenberg et al. 1992, 1993a,b; Norlund et al., 2009). These microbes are commonly used as model reference organisms in the investigation of S metabolism for mining contexts, however, they are not likely to represent all the possible and potentially important microbial S cycling that can occur, as their respective presence and abundance will be influenced interactively by physico-chemical, geochemical and seasonal factors, such as DO, pH and temperature (Baker and Banfield, 2003; Johnson and Hallberg, 2003).

pH is thought to be the main driver of the microbial ecology in mining systems (Elbering et al., 2000; Kuang et al., 2013; Liu et al., 2014). As less well studied pre-acidification mine wastewater impoundments typically range in pH values between moderately acidic to circumneutral pH, 3 – 8 (Schippers et al., 2010), the microbial and ecological links from possible PNAG initiating conditions to evident AMD are not well known. However, there have been some studies assessing the microbial ecology in mine tailings that are between pH 3 – 7. Hallberg and Johnson (2003) evaluated microbial and geochemical conditions in wastewaters at two sites, an abandoned tin mine with a pH 3.4 and an abandoned coalmine with a pH 6.3. Their microbial results showed high counts of Fe oxidizers at the pH 3.4 site and very low counts at the pH 6.3 site. Illustrating the point brought up earlier that biological iron oxidation is important at pH < 5 (Eq 7). Furthermore, the dominance of "moderate acidophiles" in these pre-AMD tailings should be noted, characterized by different species than those found in AMD systems. Specifically, organisms such as a moderately acidophilic iron oxidizer highly related to *Halothiobacillus*

neapolitanus was found to occur in the pH 3.4 site, and a neutrophilic thiosulfate oxidizing *Thiomonas* spp. occurred in the pH 6.3 site (Hallberg and Johnson, 2003) and in other pre-AMD tailings and wastewater ponds (Leduc et al., 2002; Whaley-Martin et al., 2019; Camacho et al., 2020b). Both genera belong to *Proteobacteria*, the former a *Gammaproteobacteria* and the latter previously classified as a *Betaproteobacteria* (Johnson and Hallberg, 2003).

Korehi et al. (2014), examined microbial communities with 16S rRNA gene sequencing, within the tailings of three separate mines at various depths and ranging in pH 3.2 - 6.5. Their results identified the dominant bacterial phyla and families to include: *Firmicutes,* families *Alicyclobacillaceae* and *Peptococcaceae*; *Proteobacteria*, family *Hydrogenophilaceae*; and *Actinobacteria,* family *Micrococcaceae*. However, *Proteobacteria* were only detected in surfacial depth samples (Korehi et al., 2014).

Whaley-Martin et al. (2019) determined that in circumneutral mining wastewater samples (pH 6 – 7.3) microbial communities are primarily *Proteobacteria*; dominated by the *Alphaproteobacteria* families *Sphingomonadaceae*, *Rhodobacteraceae* and *Caulobacteraceae*; and partially by *Gammaproteobacteria* families *Burkholderiaceae* and *Hydrogenophilaceae*. Interestingly Whaley-Martin et al. (2019) found that at two moderately acidic sites *Gammaproteobacteria* dominated, at a site of pH=4.7 by the family *Halothiobacillaceae* and at a site of pH = 4.3 by *Halothiobacillaceae* and *Burkholderiaceae*. Although studies for AMD sites have focused heavily on *Proteobacteria*, seemingly, it is also a relevant genetic group identified for pre-acidification tailings and wastewaters. Thus, *Proteobacteria* and taxa examined at a more refined classification level within it, may be highly significant in the creation of AMD and an important biological characteristic to explore in development for a monitoring tool.

In assessing effective monitoring tools, it is critical to understand all the variables and

parameters of the system. For instance, the difference between pre-AMD and AMD characteristics in mine wastewater contexts may be temporal, found with variation over seasons (Leduc et al., 2002), or spatial, varying with depth or location (Dold and Fontboté, 2001; Johnson and Hallberg, 2003; Diaby et al., 2007). These temporal or spatial variations enable exploration of a wide range of conditions to identify those relevant to pre-acidification mine wastewater impoundments to AMD systems. For example, in studies by Dold and Fontboté (2001) and Diaby et al. (2007), the neutralization zone (Figure 1.4) was observed to be subsequently oxidized once the water level dropped due to drainage resulting in acid pH values. This process shares multiple characteristics with pre-AMD settings (i.e., moderately acidic to circumneutral pH and presence of sulfide minerals). In concurrence with microbial results presented in Diaby et al. (2007), they also determined that sulfur oxidizers and S reducers were present, while iron oxidizers were negligible. Their results are also consistent with microbial sulfur disproportionation/oxidation of thiosalts as the likely initiating pathways in PNAG wastewaters.

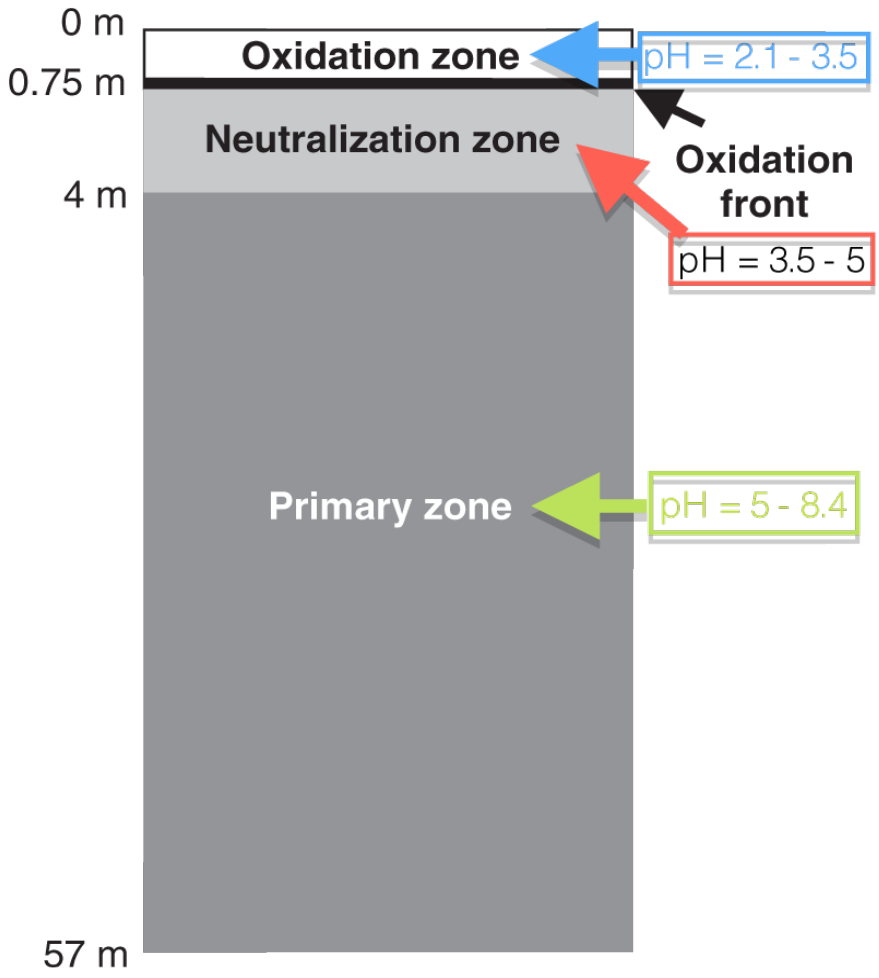

Figure 1.4: Profile and pH of Piuquenes tailings impoundment at the La Andina mine, Chile. Modified from Diaby et al. (2007), based on Dold and Fontboté (2001) geochemical data.

1.1.4. Key sulfur microbial metabolisms in mining contexts

It is important to identify the current microbial sulfur metabolisms that may play a role in oxidation and acidification associated with mining wastewaters derived from sulfide hosted ore extraction. Sulfur oxidizing microbes have been found to possess highly variable metabolic pathways even within a genus as well as dependent on which SOI species is used as the S substrate (Hallberg et al., 1996; Wang et al., 2019). Bernier and Warren (2007) illustrate this determination of different thiosulfate reaction arrays catalyzed by *Acidithiobacilli* spp. and mining wastewater microbial

enrichments under identical experimental conditions. The two major biological sulfur oxidation pathways currently identified are the Sox pathway and the S_4I pathway, although a third reverse DSR (rDSR) pathway is emerging (Watanabe et al., 2019).

The Sox pathway, also known as the "Kelly-Friedrich pathway" was first identified in research by Kelly et al. (1997) and Friedrich et al. (2001). This pathway takes a reduced form of sulfur and oxidizes it directly to sulfate, provided that the entire Sox gene complex is present. It was originally observed for the oxidation of thiosulfate; but has since been shown to work for other reduced forms of sulfur (Table 1.2) (Friedrich et al., 2001; Sauvé et al., 2007). The Sox complex contains proteins encoded from multiple genes (*soxTRS-VW-XYZABCDEFGH*) of which the entire complex or parts (eg *sox XYZAB* only) are present, dependent of the species of bacteria. No archaea are known to have any *sox* genes and they therefore utilize other pathways to undergo sulfur oxidation/disproportionation reactions (Ghosh and Dam, 2009). Summarized, the major pathways of the Sox complex are from the encoded proteins SoxXA, SoxYZ, SoxB and $Sox(CD)_2$. Initially, SoxXA attaches the thiosulfate (S^--SO_3^-) to SoxYZ, which holds it for the rest of the reaction. SoxB hydrolyzes the sulfone (SO_3^-) to sulfate, $Sox(CD)_2$ oxidizes the sulfane (S^-) to a sulfone, then SoxB hydrolyzes the new sulfone off the SoxYZ (Figure 1.5). Sox proteins are found catalyzing reactions mainly in bacteria living at neutral pH, with only *Alphaproteobacteria* containing all the regulatory and structural *sox* genes, important for the ability to oxidize pre-AMD wastewater into AMD identified to date (Ghosh and Dam, 2009). However, consortia such as with *Alphaproteobacteria* living at near neutral pH within protists in AMD pH < 1, may allow the Sox pathway to be utilized within AMD systems (Baker and Banfield, 2003). As well as recent results of this thesis (Chapter 3, Camacho et al., 2020a) which demonstrated RNA expression of *sox* genes at low pH values of 1.5. However, the Sox pathway promotes oxidation only (Eq 8) and has no

mechanism for disproportionation, except in bacteria lacking the *soxCD* gene which results in the formation of elemental S globules (Hensen et al., 2006; Ghosh and Dam, 2009; Wang et al., 2019).

$$-SSO_3 + 5H_2O \rightarrow 2SO_4^{2-} + 8e^- + 10H^+ \quad (8)$$

Other possible pathways can also store elemental S globules depending on the microbe and homolog of the gene. For instance, mediation by the *sqr* sulfide:quinone oxidoreductase gene results in storage of S globules inside or outside of the cells (Table 1.2) (Jones et al., 2014). In mining contexts, it is common to see products of disproportionation. In fact, these are important intermediates associated with the S transformation chain that ultimately lead to full AMD (Figure 1.2). However, as the Sox pathway is based in oxidation reactions only, these important disproportionation pathway species would not be captured (Bernier and Warren, 2005, 2007; Warren et al., 2008).

Table 1.2: Genes and proposed reactant/products in microbial sulfur oxidation/disproportionation reaction pathways.

Position	Gene	Reactants	Products	Reference(s)
Periplasm	sdo (sulfur dioxygenase)	S^- from GSSH	SO_3^{2-}	Rohwerder and Sand (2003)
Periplasm	sox complex	$S_2O_3^{2-}$, S^{2-}, S^0, $S_4O_6^{2-}$, SO_3^{2-}	S^0, SO_4^{2-}	Kelly *et al*. (1997), Freidrich *et al*. (2001), Hensen *et al*. (2006), Sauvé *et al*. (2007)
Periplasm/ Inner membrane	sqr (sulfide:quinone oxidoreductase)	S^{2-}	S^0, S_n^{2-}	Griesbeck (2002), Quatrini *et al*. (2009), Valdes *et al*. (2011), Jones *et al*. (2014)
Periplasm/ Inner membrane	doxD (thiosulfate:quinone oxidoreductase)	$S_2O_3^{2-}$	$S_4O_6^{2-}$	Meulenberg *et al*. (1993a), Müller et al. (2004), Valdes *et al*. (2011)
Periplasm	tetH (tetrathionate hydrolase)	$S_4O_6^{2-}$	$S_2O_3^{2-}$, S^0, SO_4^{2-}, $S_xO_y^{2-}$	Steudal *et al*. (1987), Pronk *et al*. (1990), Meulenberg *et al*. (1992), Hallberg *et al*. (1996), Rzhepishevska *et al*. (2007)
Cytoplasm	sor (sulfur oxygenase reductase)	S^0	S^{2-}, $S_2O_3^{2-}$, SO_3^{2-}	Kletzin (1989;1992), Jones *et al*. (2014)
Cytoplasm	rhd (rhodanese) or thiosulfate sulfur transferase	$S_2O_3^{2-}$	S^0, SO_3^{2-}	Beller *et al*. (2006), Yin *et al.* (2014)
Cytoplasm	hdr (heterodisulfide reductase)	RSSH	RSH, SO_3^{2-}	Quatrini *et al*. (2009) , Yin *et al.* (2014)
Cytoplasm	paps (phosphoadenosine phosphosulfate reductase)	SO_3^{2-}	PAPS	Beller *et al*. (2006) , Yin *et al.* (2014)
Cytoplasm	aps (ATP sulfurylase)	PAPS	SO_4^{2-}	Beller *et al*. (2006) , Yin *et al.* (2014)

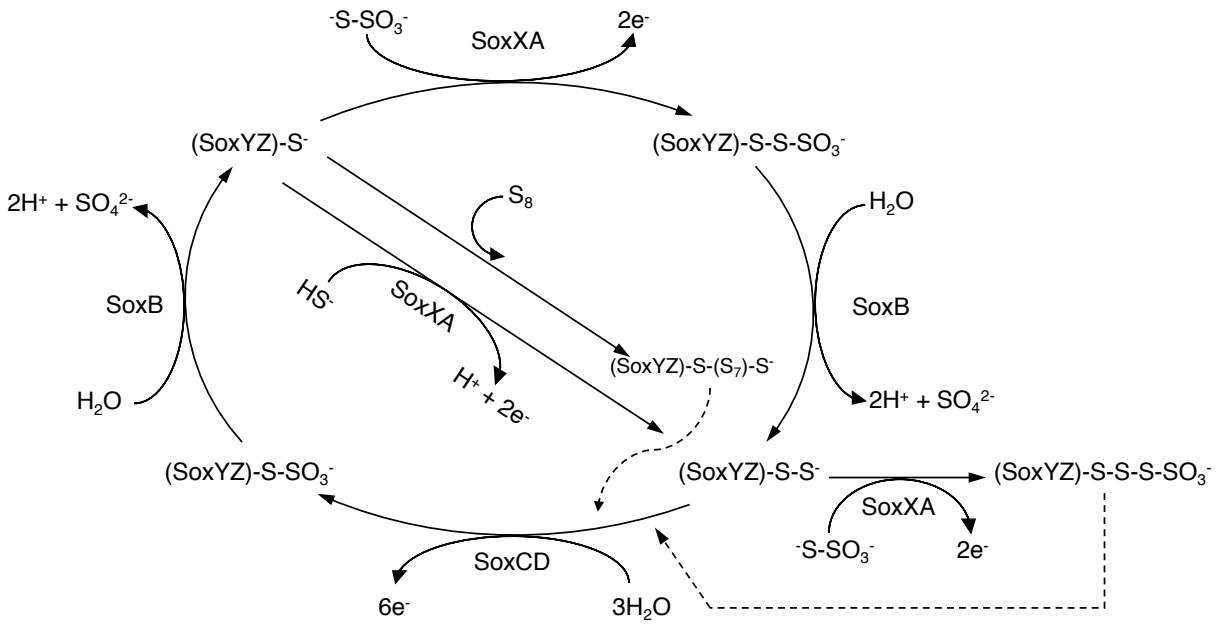

Figure 1.5: Summarized diagram for the Sox pathway, also known as "Kelly-Friedrich pathway". (Adapted from Ghosh and Dam (2009)).

The S_4I, "tetrathionate intermediate pathway", is less well-characterized than the Sox pathway, but has been identified to use *doxD* (thiosulfate:quinone oxidoreductase*)* and *tetH* (tetrathionate hydrolase) genes (Wang *et al.*, 2019). It has mainly been found in *Beta/Gammaproteobacteria* to date and the proposed mechanisms have been identified from a combination of enzymatic, theoretical and geochemical data from a variety of groups looking at diverse microbes, including bacteria and archaea (Steudel et al., 1987; Kletzin, 1989,1992; Pronk et al., 1990; Meulenburg 1992, 1993a, b; Hallberg et al., 1996; Schippers et al., 1996; Rzhepishevska et al., 2007; Wang et al., 2019). Schippers et al. (1996) proposed a cyclic mechanism using tetrathionate hydrolysis to produce polysulfane-monosulfonic acid (PMSA) and sulfate (Eq 9) as was first identified by Steudel et al. (1987) in *A.ferrooxidans*.

$$S_4O_6^{2-} + H_2O \rightarrow HSSSO_3^- + SO_4^{2-} + H^+ \qquad (9)$$

This highly reactive PMSA then allows for the formation of other polythionates (Eq 10 – 13).

$$S_3O_3^{2-} + S_2O_3^{2-} + 0.5O_2 + 2H^+ \rightarrow 3S_5O_6^{2-} + H_2O \quad (10)$$

$$S_3O_3^{2-} + S_4O_6^{2-} \rightarrow S_2O_3^{2-} + S_5O_6^{2-} \quad (11)$$

$$S_3O_3^{2-} + 1.5O_2 \rightarrow S_3O_6^{2-} \quad (12)$$

$$4S_3O_3^{2-} \rightarrow S_8 + 4SO_3^{2-} \quad (13)$$

Schippers et al. (1996) showed the formation of these PMSAs occurred over a range of pH from acidic to neutral, identifying that Fe^{3+} influence did not change over the experimental conditions investigated. In this study, the only difference observed over the range of pH values tested was the specific polythionate outcomes from PMSA. In acidic experiments, formation of pentathionate and elemental sulfur was observed to be prevalent (Eq 10, 11 and 13), while in neutral pH conditions, trithionate (Eq 12) and some thiosulfate were formed (Schippers et al., 1996). Unlike the Sox pathway, S_4I accurately predicts biological reactions capable of disproportionation and formation of variable reduced sulfur species found in AMD and pre-acid AMD environments. Abiotic processes oxidizing reduced sulfur up the oxidation chain to tetrathionate but unable to fully oxidize to sulfate because of slow reaction rates, further confirm this biological pathway. Since little tetrathionate is present in environmental samples containing microbes, i.e., biological oxidation/disproportionation reactions catalyzing the tetrathionate (Druschel, 2002).

1.1.5. Genetic capabilities and monitoring approach

The importance of integrating genomic data in tandem with geochemical data has been emphasized and proven to be highly effective in generating a more accurate understanding of an environment (Newman and Banfield, 2002; Reysenbach and Shock, 2002; Whaley-Martin et al., 2019). Methods such as metagenomics are already demonstrating their worth, when applied with geochemical characterization in the development of critical understanding of microbial community

function and dynamics (e.g., Inskeep et al., 2010; Lewin et al., 2013). More specifically, full-length genome readings of microbes will assist in identification of genes common across species as well as searching across species for specific genes, allowing identification based on potential metabolic pathways and capabilities (Beller et al., 2006; Crane III, 2019; Rameez et al., 2020). Genes that have been identified associated with the S_4I system are: a thiosulfate:quinone oxidoreductase (TQO) discovered in archaea *A. ambivalens,* coded *doxDA* that is found in *A. ferrooxidans* (Müller et al., 2004) and *A. caldus* (Rzhepishevska et al., 2007); and a thiosulfate dehydrogenase found in *A. vinosum* (Table 1.2) (Hensen et al., 2006). Integrating microorganism identity, metagenomics and carbon isotope fractionation can provide us with a better understanding of the microbial S cycle interactions (Cowie et al., 2009) and reveal potential bio-indicators that may serve as more effective, proactive monitoring assays. An example of this possible approach is shown in the tandem analysis of Table 1.2 and Figure 1.6, which incorporates geochemical data to more comprehensively identify the possible/actual sulfur oxidation/disproportionation biological reactions occurring and pathways involved, while determining the important genes.

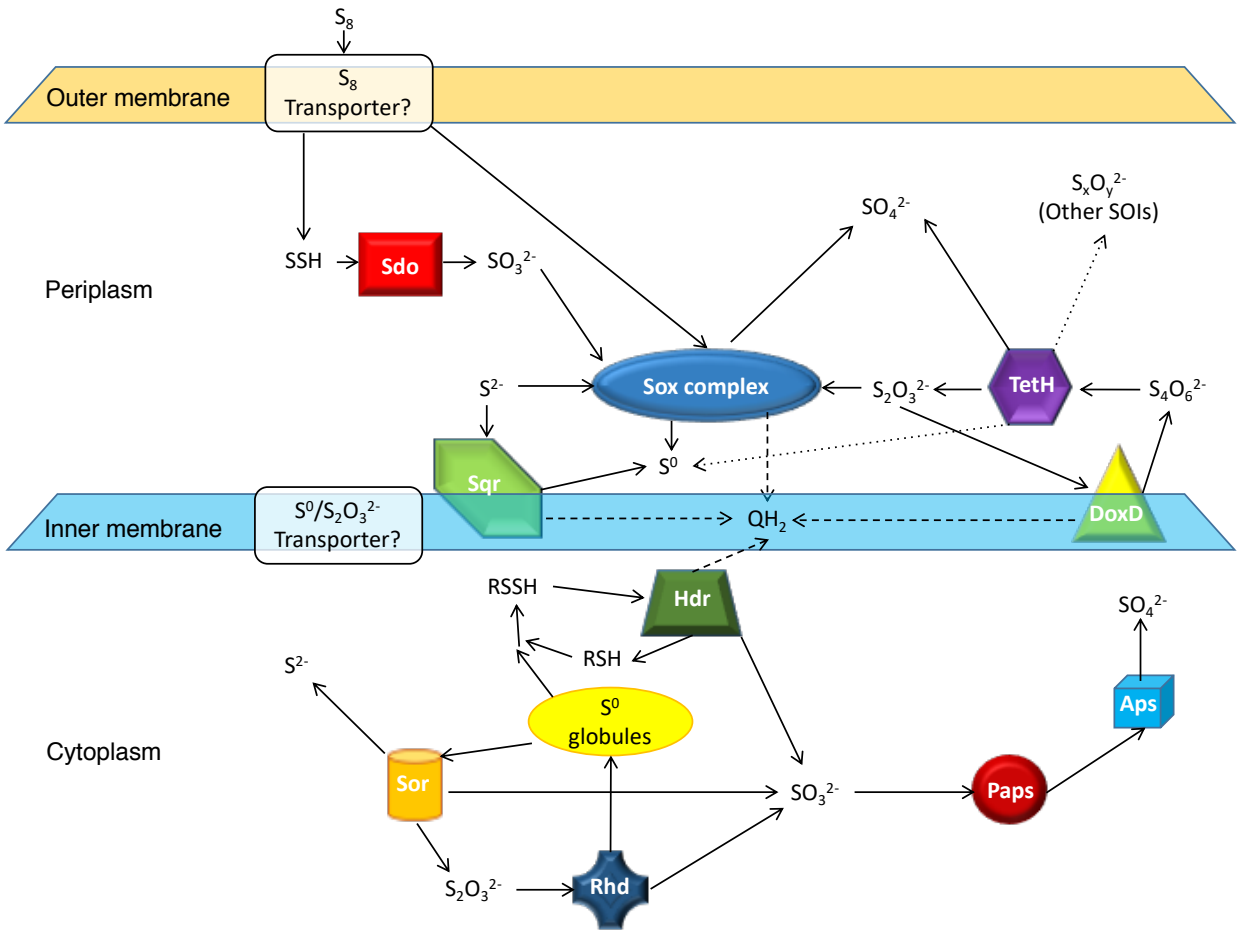

Figure 1.6: Gene map with S species reactions in *A.thiooxidans* ATCC 19733 (Solid line = known S reactions; Dotted line = theorized reactions; and Dashed line = Q/cytochrome c reactions). Based on accumulative literature in Table 1.2.

Evidence identifies that once waters held within mine tailings impoundments gets below a threshold pH of ~ 3, oxidation processes occur more rapidly (Bernier and Warren, 2007). This can be attributed to Fe^{3+} remaining in solution and accelerating acidity generation associated with sulfur oxidation processes and reducing disproportionation, Eq (3) and (4). Thus, it would be beneficial to have robust monitoring approaches tailored to target these "pre-net acid generation (PNAG)" conditions. However, many knowledge gaps of the microbial ecology and functionality of endemic mine wastewater impoundment microbial assemblages, as well as the sulfur species and reaction pathways involved in this pre-net acid generating phase (Figure 1.2) exist.

Consequently, early indicators that would offer mines a proactive monitoring tool for tailings management, are currently lacking.

As summarized previously, thiosulfate will be an important sulfur species to monitor considering its widespread and abundant presence in sulfide associated tailings ponds and the possibility of its oxidation by both abiotic and biotic processes. Furthermore, thiosulfate is an important precursor to the generation of other SOIs ultimately leading to sulfate through oxidation/disproportionation reactions (Figure 1.1) (Warren et al., 2008). Thus, systematic investigation of the important sulfur oxidizing bacteria, pathways (genes) alongside sulfur geochemistry of mining wastewaters will generate a new integrated understanding of relevant factors linked to pre-net acid generation stages of the mine wastewater.

1.2. Objectives

The overarching objective of this PhD research is to constrain the S biogeochemistry of the PNAG phase by integrating molecular microbiology and analytical sulfur chemistry in a series of experiments that cumulatively identify the roles of sulfur oxidizing bacteria (SoxB), SOI speciation and pH in SOI reaction arrays and S outcomes.

Experimentally, this objective was addressed through three research goals:

(1) determine gene expression and sulfur speciation with either thiosulfate or elemental sulfur added as the starting SOI substrate with a pure culture of *Acidithiobacillus thiooxidans* in well constrained laboratory experiments (Chapter 3);

(2) genetically characterize (16S amplicon) seasonal mining wastewater parent communities and associated SoxB enrichments grown at either pH 7-5 or pH 5-3 from two mines in well constrained laboratory experiments (Chapter 4); and

(3) determine the sulfur pathways mediated by three unique mine wastewater SoxB enrichment communities in well constrained laboratory experiments assessing six distinct simulated mine wastewater thiosulfate and tetrathionate treatments (Chapter 5).

Hypotheses:

The hypotheses tested by the research are:

1) Metabolism (Gene expression) (Research goal 1; Chapter 3):
    - Sulfur reactions catalyzed by the same pure strain SoxB species, *A. thiooxidans* will differ dependent on which SOI species is provided as their starting sulfur

substrate.

2) Microbial Ecology (Research goal 2; Chapter 4):

- A pH dependent shift in dominant SoxB genera will occur as pH decreases in experiments, irrespective of which sulfur substrate is provided.

3) Geochemistry (Research goal 3; Chapter 5):

- Sulfur substrate speciation, rather than SoxB enrichment identity, will determine microbial sulfur cycling reaction pathways.

The second main objective is to identify potential indicators (bacterial and/or geochemical) for the development of monitoring tools in mine wastewater management by integrating the results of the three research goals.

Hypothesis:

- S^0, $S_2O_3^{2-}$ and/or $S_4O_6^{2-}$ will indicate changes in system pH associated with shifts from PNAG – NAG conditions.

References

Amos RT, Blowes DW, Bailey BL, Sego DC, Smith L, Ritchie AIM. 2015. Waste-rock hydrogeology and geochemistry. *Appl. Geochem.* 57:140-156.

Bacelar-Nicolau P, Johnson DB. 1999. Leaching of pyrite by acidophilic heterotrophic iron-oxidizing bacteria in pure and mixed cultures. *Appl. Environ. Microbiol*. 65:585-590.

Baker BJ, Banfield JF. 2003. Microbial communities in acid mine drainage. *FEMS Microbiol*. Ecol. 44:139-152.

Beller HR, Chain PS, Letain TE, Chakicherla A, Larimer FW, Richardson PM, *et al.* 2006. The genome sequence of the obligately chemolithoautotrophic, facultatively anaerobic bacterium *Thiobacillus denitrificans*. *J. Bacteriol*. 188:1473-1488. doi: 10.1128/JB.188.4.1473-1488.2006.

Bernier L, Warren L. 2005. Microbially driven acidity generation in a tailings lake. *Geobiology*. 3:115-133.

Bernier L, Warren LA. 2007. Geochemical diversity in S processes mediated by culture-adapted and environmental-enrichments of *Acidithiobacillus* spp. *Geochim. Cosmochim. Acta.* 71:5684-5697.

Boyd ES, Druschel GK. 2013. Involvement of intermediate sulfur species in biological reduction of elemental sulfur under acidic, hydrothermal conditions. *Appl. Environ. Microbiol*. 79:2061-2068. doi: 10.1128/AEM.03160-12; 10.1128/AEM.03160-12.

Camacho D, Frazao R, Fouillen A, Nanci A, Lang BF, Apte SC, *et al.* 2020. New insights into *Acidithiobacillus thiooxidans* sulfur metabolism through coupled gene expression, solution chemistry, microscopy and spectroscopy analyses. *Front. Microbiol.* 11:411. doi: 10.3389/fmicb.2020.00411

Camacho D, Jessen GL, Mori JF, Apte SC, Jarolimek CV, Warren LA. 2020. Microbial succession signals the initiation of acidification in mining wastewaters. *Mine Water Environ.* 39:669-683. doi.org/10.1007/s10230-020-00711-9.

Canfield DE, Stewart FJ, Thamdrup B, De Brabandere L, Dalsgaard T, Delong EF, *et al.* 2010. A cryptic sulfur cycle in oxygen-minimum–zone waters off the Chilean coast. *Science*. 330:1375-1378.

Castendyk DN, Eary LE, Balistrieri LS. 2015. Modeling and management of pit lake water chemistry 1: Theory. *Appl. Geochem.* 57:267-288.

Cowie BR, Slater GF, Bernier L, Warren LA. 2009. Carbon isotope fractionation in phospholipid fatty acid biomarkers of bacteria and fungi native to an acid mine drainage lake. *Org. Geochem*. 40:956-962.

Crane III, EJ. 2019. Sulfur-dependent microbial lifestyles: deceptively flexible roles for biochemically versatile enzymes. *Curr. Opin. Chem. Biol*. 49:139-145.

Dahl C, Engels S, Pott-Sperling AS, Schulte A, Sander J, Lubbe Y, *et al.* 2005. Novel genes of the *dsr* gene cluster and evidence for close interaction of Dsr proteins during sulfur oxidation in the phototrophic sulfur bacterium *Allochromatium vinosum*. *J. Bacteriol*. 187:1392-1404. doi: 10.1128/JB.187.4.1392-1404.2005.

Diaby N, Dold B, Pfeifer H, Holliger C, Johnson DB, Hallberg KB. 2007. Microbial communities in a porphyry copper tailings impoundment and their impact on the geochemical dynamics of the mine waste. *Environ. Microbiol*. 9:298-307.

Dockrey J, Lindsay M, Mayer K, Beckie R, Norlund K, Warren L, *et al*. 2014. Acidic microenvironments in waste rock characterized by neutral drainage: Bacteria–mineral interactions at sulfide surfaces. *Minerals*. 4:170-190.

Dold B. 2008. Sustainability in metal mining: from exploration, over processing to mine waste management. *Rev. Environ. Sci. Bio*. 7: 275.

Dold B, Fontboté L. 2001. Element cycling and secondary mineralogy in porphyry copper tailings as a function of climate, primary mineralogy, and mineral processing. *J. Geochem. Explor*. 74:3-55.

Druschel GK. 2002. Sulfur Biochemistry: Kinetics of Intermediate Sulfur Species Reactions in the Environment. PhD Dissertation University of Wisconsin - Madison.

Druschel GK, Baker BJ, Gihring TM, Banfield JF. 2004. Acid mine drainage biogeochemistry at Iron Mountain, California. *Geochem T*. 5:13-32.

Druschel GK, Hamers RJ, Banfield JF. 2003. Kinetics and mechanism of polythionate oxidation to sulfate at low pH by O_2 and Fe^{3+}. *Geochim. Cosmochim. Acta*. 67:4457-4469.

Elberling B, Schippers A, Sand W. 2000. Bacterial and chemical oxidation of pyritic mine tailings at low temperatures. *J. Contam. Hydrol*. 41:225-238.

Friedrich CG, Rother D, Bardischewsky F, Quentmeier A, Fischer J. 2001. Oxidation of reduced inorganic sulfur compounds by bacteria: emergence of a common mechanism? *Appl. Environ. Microbiol*. 67:2873-2882. doi: 10.1128/AEM.67.7.2873-2882.2001.

Ghosh W, Dam B. 2009. Biochemistry and molecular biology of lithotrophic sulfur oxidation by taxonomically and ecologically diverse bacteria and archaea. *FEMS Microbiol. Rev*. 33:999-1043.

Hallberg KB, Dopson M, Lindstrom EB. 1996. Reduced sulfur compound oxidation by *Thiobacillus caldus*. *J. Bacteriol*. 178:6-11.

Hallberg KB, Johnson DB. 2003. Novel acidophiles isolated from moderately acidic mine drainage waters. *Hydrometallurgy*. 71:139-148.

Hensen D, Sperling D, Trüper HG, Brune DC, Dahl C. 2006. Thiosulphate oxidation in the phototrophic sulphur bacterium *Allochromatium vinosum*. *Mol. Microbiol*. 62:794-810.

Hiraishi A, Matsuzawa Y, Kanbe T, Wakao N. 2000. *Acidisphaera rubrifaciens* gen. nov., sp. nov., an aerobic bacteriochlorophyll-containing bacterium isolated from acidic environments. *Int. J. Syst. Evol. Microbiol*. 50 Pt 4:1539-1546.

Houghton JL, Foustoukos DI, Flynn TM, Vetriani C, Bradley AS, Fike DA. 2016. Thiosulfate oxidation by *Thiomicrospira thermophila*: metabolic flexibility in response to ambient geochemistry. *Environ. Microbiol*. 18:3057-3072.

Huang LN, Zhou WH, Hallberg KB, Wan CY, Li J, Shu WS. 2011. Spatial and temporal analysis of the microbial community in the tailings of a Pb-Zn mine generating acidic drainage. *Appl. Environ. Microbiol.*, 77(15), 5540-5544.

Inskeep WP, Rusch DB, Jay ZJ, Herrgard MJ, Kozubal MA, *et al.* 2010. Metagenomes from high-temperature chemotrophic systems reveal geochemical controls on microbial community structure and function. *PloS One*. 5:e9773.

Jamieson HE, Walker SR, Parsons MB. 2015. Mineralogical characterization of mine waste. *Appl. Geochem*. 57:85-105.

Johnson DB, Hallberg KB. 2003. The microbiology of acidic mine waters. *Res. Microbiol*. 154:466-473.

Johnston F, McAmish L. 1973. A study of the rates of sulfur production in acid thiosulfate solutions using S-35. *J. Colloid Interface Sci*. 42:112-119.

Jones DS, Schaperdoth I, Macalady JL. 2014. Metagenomic Evidence for Sulfide Oxidation in Extremely Acidic Cave Biofilms. *Geomicrobiol. J.* 31, 194–204. DOI: 10.1080/01490451.2013.834008

Kappler U. 2011. Bacterial sulfite-oxidizing enzymes. *BBA-Bioenergetics*. 1807:1-10.

Kelly DP, Baker SC. 1990. The organosulphur cycle: aerobic and anaerobic processes leading to turnover of C_1 -sulphur compounds. *FEMS Microbiol. Lett*. 87:241-246.

Kelly DP, Shergill JK, Lu W, Wood AP. 1997. Oxidative metabolism of inorganic sulfur compounds by bacteria. *Antonie Van Leeuwenhoek*. 71:95-107.

Kelly DP, Wood AP. 2000. Reclassification of some species of Thiobacillus to the newly designated genera Acidithiobacillus gen. nov., Halothiobacillus gen. nov. and Thermithiobacillus gen. nov. *Int. J. Syst. Evol. Microbiol.* 50: 511–516.

Kimura S, Bryan CG, Hallberg KB, Johnson DB. 2011. Biodiversity and geochemistry of an extremely acidic, low-temperature subterranean environment sustained by chemolithotrophy. *Environ. Microbiol.* 13: 2092–2104. doi:10.1111/j.1462-2920.2011.02434.x.

Kirby C, Thomas H, Southam G, Donald R. 1999. Relative contributions of abiotic and biological factors in Fe (II) oxidation in mine drainage. *Appl. Geochem*. 14:511-530.

Kletzin A. 1992. Molecular characterization of the *sor* gene, which encodes the sulfur oxygenase/reductase of the thermoacidophilic Archaeum *Desulfurolobus ambivalens*. *J. Bacteriol*. 174:5854-5859.

Kletzin A. 1989. Coupled enzymatic production of sulfite, thiosulfate, and hydrogen sulfide from sulfur: purification and properties of a sulfur oxygenase reductase from the facultatively anaerobic archaebacterium *Desulfurolobus ambivalens*. *J. Bacteriol*. 171:1638-1643.

Korehi H, Blöthe M, Schippers A. 2014. Microbial diversity at the moderate acidic stage in three different sulfidic mine tailings dumps generating acid mine drainage. *Res. Microbiol.* 165: 713-718.

Kuang JL, Huang LN, Chen LX, Hua ZS, Li SJ, Hu M, *et al*. 2013. Contemporary environmental variation determines microbial diversity patterns in acid mine drainage. *ISME J*. 7: 1038.

Kuyucak N, Yaschyshyn D. 2007. Managing thiosalts in mill effluents, Studies conducted at the Kidd metallurgical site. *Mining and environment IV conference, Sandbury, Canada*.

Leduc D, Leduc L, Ferroni G. 2002. Quantification of bacterial populations indigenous to acidic drainage streams. *Water Air Soil Pollut.* 135:1-21.

Lewin A, Wentzel A, Valla S. 2013. Metagenomics of microbial life in extreme temperature environments. *Curr. Opin. Biotechnol.* 24:516-525.

Lindsay MB, Moncur MC, Bain JG, Jambor JL, Ptacek CJ, Blowes DW. 2015. Geochemical and mineralogical aspects of sulfide mine tailings. *Appl. Geochem*. 57:157-177.

Liu J, Hua Z, Chen L, Kuang J, Li S, Shu W, *et al*. 2014. Correlating Microbial Diversity Patterns with Geochemistry in an Extreme and Heterogeneous Environment of Mine Tailings. *Appl. Environ. Microbiol*. 80: 3677–3686. doi:10.1128/AEM.00294-14.

Malkin SY, Rao AM, Seitaj D, Vasquez-Cardenas D, Zetsche E, Hidalgo-Martinez S, *et al.* 2014. Natural occurrence of microbial sulphur oxidation by long-range electron transport in the seafloor. *ISME J*. 8:1843-1854.

Meulenberg R, Pronk JT, Hazeu W, Bos P, Kuenen JG. 1992. Oxidation of reduced sulphur compounds by intact cells of *Thiobacillus acidophilus*. *Arch. Microbiol*. 157:161-168.

Meulenberg R, Pronk JT, Hazeu W, van Dijken JP, Frank J, Bos P, *et al.* 1993. Purification and partial characterization of thiosulphate dehydrogenase from *Thiobacillus acidophilus*. *J. Gen. Microbiol.* 139:2033-2039.

Meulenberg R, Scheer EJ, Pronk JT, Hazeu W, Bos P, Gijs Kuenen J. 1993. Metabolism of tetrathionate in *Thiobacillus acidophilus*. *FEMS Microbiol. Lett*. 112:167-172.

Miranda-Trevino JC, Pappoe M, Hawboldt K, Bottaro C. 2013. The Importance of Thiosalts Speciation: Review of Analytical Methods, Kinetics, and Treatment. *Crit. Rev. Env. Sci. Tec.* 43:19:2013-2070. DOI: 10.1080/10643389.2012.672047

Moncur MC, Ptacek CJ, Lindsay MB, Blowes DW, Jambor JL. 2015. Long-term mineralogical and geochemical evolution of sulfide mine tailings under a shallow water cover. *Appl. Geochem.* 57:178-193.

Müller FH, Bandeiras TM, Urich T, Teixeira M, Gomes CM, Kletzin A. 2004. Coupling of the pathway of sulphur oxidation to dioxygen reduction: characterization of a novel membrane-bound thiosulphate: quinone oxidoreductase. *Mol. Microbiol*. 53:1147-1160.

Negeri T, Paktunc AD, Boisclair M, Kingston DM. 1999. Characterization of thiosalts generation during millings of sulfide ores. *CANMET Report*: CANMET- MMSL.

Newman DK, Banfield JF. 2002. Geomicrobiology: how molecular-scale interactions underpin biogeochemical systems. *Science*. 296:1071-1077. doi: 10.1126/science.1010716.

Niu J, Deng J, Xiao Y, He Z, Zhang X, Van Nostrand JD, *et al.* 2016. The shift of microbial communities and their roles in sulfur and iron cycling in a copper ore bioleaching system. *Sci Rep*. 6:34744. doi: 10.1038/srep34744.

Nordstrom DK. 2015. Baseline and premining geochemical characterization of mined sites. *Appl Geochem.* 57:17-34.

Nordstrom DK, Blowes DW, Ptacek CJ. 2015. Hydrogeochemistry and microbiology of mine drainage: an update. *Appl. Geochem.* 57:3-16.

Norlund KL, Southam G, Tyliszczak T, Hu Y, Karunakaran C, Obst M, *et al.* 2009. Microbial architecture of environmental sulfur processes: a novel syntrophic sulfur-metabolizing consortia. *Environ. Sci. Technol*. 43:8781-8786.

Pronk J, Meulenberg R, Hazeu W, Bos P, Kuenen J. 1990. Oxidation of reduced inorganic sulphur compounds by acidophilic thiobacilli. *FEMS Microbiol. Lett.* 75:293-306.

Quatrini R, Appia-Ayme C, Denis Y, Jedlicki E, Holmes DS, Bonnefoy V. 2009. Extending the models for iron and sulfur oxidation in the extreme acidophile *Acidithiobacillus ferrooxidans*. *BMC Genomics*. 10:394

Rameez MJ, Pyne P, Mandal S, Chatterjee S, Alam M, Bhattacharya S, *et al.* 2020. Two pathways for thiosulfate oxidation in the alphaproteobacterial chemolithotroph *Paracoccus thiocyanatus* SST. *Microbiol. Res*. 230:126345.

Rohwerder T, Sand W. 2003. The sulfane sulfur of persulfides is the actual substrate of the sulfur-oxidizing enzymes from *Acidithiobacillus* and *Acidiphilium* spp. *Microbiology*. 149:1699-1710.

Rzhepishevska OI, Valdes J, Marcinkeviciene L, Gallardo CA, Meskys R, Bonnefoy V, *et al.* 2007. Regulation of a novel *Acidithiobacillus caldus* gene cluster involved in metabolism of reduced inorganic sulfur compounds. *Appl. Environ. Microbiol*. 73:7367-7372. doi: 10.1128/AEM.01497-07.

Sato M. 1992. Persistency-field Eh-pH diagrams for sulfides and their application to supergene oxidation and enrichment of sulfide ore bodies. *Geochim. Cosmochim. Acta*. 56:3133-3156.

Schippers A, Breuker A, Blazejak A, Bosecker K, Kock D, Wright TL. 2010. The biogeochemistry and microbiology of sulfidic mine waste and bioleaching dumps and heaps, and novel Fe(II)-oxidizing bacteria. *Hydrometallurgy* 104: 342–350. doi:10.1016/j.hydromet.2010.01.012.

Schippers A, Sand W. 1999. Bacterial leaching of metal sulfides proceeds by two indirect mechanisms via thiosulfate or via polysulfides and sulfur. *Appl. Environ. Microbiol.* 65:319-321.

Schippers A, Jozsa P, Sand W. 1996. Sulfur chemistry in bacterial leaching of pyrite. *Appl. Environ. Microbiol.* 62:3424-3431.

Sheoran AS, Sheoran V. 2006. Heavy metal removal mechanism of acid mine drainage in wetlands: a critical review. *Miner. Eng*. 19:105-116.

Smuda J, Dold B, Spangenberg JE, Pfeifer H. 2008. Geochemistry and stable isotope composition of fresh alkaline porphyry copper tailings: Implications on sources and mobility of elements during transport and early stages of deposition. *Chem. Geol.* 256:62-76.

Statistics Canada. 2012. Human Activity and the Environment 2012 Waste Management in Canada. Statistics Canada Catalogue No 16-201-x2012000. Ottawa, Ontario https://www150.statcan.gc.ca/n1/en/pub/16-201-x/16-201-x2012000-eng.pdf?st=l8YkhLHx (Accessed October 7, 2019). Annually.

Statistics Canada. 2016. Human Activity and the Environment 2016 Freshwater in Canada. Statistics Canada Catalogue No 16-201-x2017000. Ottawa, Ontario. https://www150.statcan.gc.ca/n1/en/pub/16-201-x/16-201-x2017000-eng.pdf?st=f6B980R8 (Accessed October 7, 2019). Annually.

Steudel R, Holdt G, Göbel T, Hazeu W. 1987. Chromatographic Separation of Higher Polythionates SnO 62θ(n= 3… 22) and Their Detection in Cultures of *Thiobacillus ferroxidans*; Molecular Composition of Bacterial Sulfur Secretions. *Angew. Chem. Int. Edit*. 26:151-153.

Suzuki I, Lee D, Mackay B, Harahuc L, Oh JK. 1999. Effect of various ions, pH, and osmotic pressure on oxidation of elemental sulfur by *Thiobacillus thiooxidans*. *Appl. Environ. Microbiol.* 65:5163-5168.

Tyson GW, Chapman J, Hugenholtz P, Allen EE, Ram RJ, Richardson PM, *et al.* 2004. Community structure and metabolism through reconstruction of microbial genomes from the environment. *Nature*. 428:37-43.

Vongporm Y. 2008. Thiosalt behaviour in aqueous media. MEng Thesis: Memorial University of Newfoundland.

Wang R, Lin JQ, Liu XM, Pang X, Zhang CJ, Gao XY, *et al.* 2019. Sulfur oxidation in the acidophilic autotrophic *Acidithiobacillus* spp. *Front. Microbiol.* 9:3290.

Warren L, Norlund KI, Bernier L. 2008. Microbial thiosulphate reaction arrays: The interactive roles of Fe (III), O2 and microbial strain on disproportionation and oxidation pathways. *Geobiology*. 6:461-470.

Watanabe T, Kojima H, Umezawa K, Hori C, Takasuka TE, Kato Y, *et al.* 2019. Genomes of neutrophilic sulfur-oxidizing chemolithoautotrophs representing 9 proteobacterial species from 8 genera. *Front. Microbiol*. 10:316.

Whaley-Martin KJ, Jessen G, Nelson TC, Mori J, Apte S, Jarolimek C, *et al*. 2019. The potential role of Halothiobacillus spp. in sulphur oxidation and acid generation in circum-neutral mine tailings reservoirs. *Front. Microbiol*. 10:297.

Whaley-Martin K, Marshall S, Nelson TE, Twible L, Jarolimek CV, King JJ, *et al.* 2020. A mass-balance tool for monitoring potential dissolved sulfur oxidation risks in mining impacted waters. *Mine Water Environ.* 39:291–307. https://doi.org/10.1007/s10230-020-00671-0

Williamson MA, Rimstidt JD. 1993. The rate of decomposition of the ferric-thiosulfate complex in acidic aqueous solutions. *Geochim. Cosmochim. Acta.* 57:3555-3561.

Williamson MA, Rimstidt JD. 1994. The kinetics and electrochemical rate-determining step of aqueous pyrite oxidation. *Geochim. Cosmochim. Acta.* 58:5443-5454.

Zopfi J, Ferdelman TG, Fossing H. 2004. Distribution and fate of sulfur intermediates−−sulfite, tetrathionate, thiosulfate, and elemental sulfur −−in marine sediments. *Geol. Soc. Am. Spec. Papers.* 379: 97-116 doi: 10.1130/0-8137-2379-5.97.

Chapter 2

2.1. Experimental Design

To assess and meet the objectives and research goals in this thesis, three experimental procedures were used. First, genetic expression + geochemistry integrated analyses to monitor both activity of S metabolic genes as well as changes in S speciation in media for a pure strain *A. thiooxidans* with two different starting S substrates, elemental Sulfur (S^0) or thiosulfate ($S_2O_3^{2-}$). Second, small-scale enrichments termed "Microcosms", were used to enrich sulfur oxidizing bacteria (SoxB) from endemic mine waters in sulfur oxidizing media with either neutrophilic (NSOM) or acidophilic (ASOM) media under different pH ranges (7-5 and 5-3). Third, medium-scale biogeochemical experiments termed "Mesocosms", were used to identify seasonal endemic microbial communities and compare SOI cycling for two different mine wastewaters.

Microcosm and mesocosm experiments included simple (synthetic) simulated mine waters and complex endemic mine wastewaters, of various S species occurrence and concentrations. Both were subjected to either the model AMD organism *A.thiooxidans*, or with enriched sulfur oxidizing microbes from the mine wastewaters. The endemic wastewaters treatment contained tailings impoundment wastewater samples from our industry partners with sampling both temporally/seasonally (Summer, Winter and Spring, over two years from August 2014 to September 2015) and spatially/geochemically (two different mine sites, different source rock and milling procedures, as described further below) (Table 2.1), i.e. acquiring/constraining varying endemic microbial communities, with a variety of S species and concentrations and other physicochemical components (eg. Temperature, O_2, Fe, DOC, salts).

Table 2.1: Mine wastewater samples collected for microcosm and mesocosm experiments.

	Summer 2014	Winter 2015	Spring 2015	Summer 2015
Mine 1	✔	✔	✔	✔
Mine 2	✔	✖	✔	✔

2.1.1. Genetic expression + geochemistry collaborative tests

For the collaborative tests, the strict sulfur oxidizing/disproportionating microbe, pure strain *A. thiooxidans* ATCC 19377, was inoculated in ASOM with either S^0 or $S_2O_3^{2-}$ as the reduced S source. These were used to characterize both the levels of gene expression at high resolution (RNA-Seq) for *A. thiooxidans,* and the changes in sulfur speciation and concentration associated with its experimental growth on either S^0 or $S_2O_3^{2-}$. This tandem approach would allow a more robust generation of sulfur metabolism models for *A. thiooxidans* than currently available (Wang *et al*., 2019). Also providing potential novel insights into sulfur metabolic pathways for these S sources, and key genes or S species of interest in this important metabolism judged to drive acidification in mines.

For the geochemistry tests, the experimental procedure utilized nine sterile 1 L flasks, six containing ASOM with S^0 and three with $S_2O_3^{2-}$. Concentrations were prepared identical to the Genetic Expression experiments done by Colleagues at UdM, for RNA via RT-qPCR and RNA-Seq. 1% or 10g/L S^0 and 0.2% or 2g/L NaS_2O_3. Similarly, the inoculation of *A.thiooxidans* was replicated as in the Genetic Expression experiments. Whereby cultures were inoculated at 5% v/v with cultures pre-grown in the corresponding medias. The bacteria were washed with sterile NaCl 1% before inoculation to prevent acid contamination into the fresh media. Cultures were grown under aerobic conditions at 120 rpm and 30 ^oC. Sampling times for the two treatments varied: ASOM-S^0 was sampled on days 0, 1, 2, 3, 4, and 5; ASOM-$S_2O_3^{2-}$ was sampled on days 0, 2 and

4. Each sampling point used one flask. The geochemistry sampled was in triplicate for pH, $\sum S_{aq}$, SO_4^{2-}, S^{2-}, $S_2O_3^{2-}$, S^0 and SO_3^{2-}.

2.1.2. Microcosms: enrichment experiments

Microcosms contained small volumes (150 mL) of the mine wastewaters enriched in media at variable conditions such as pH, S concentration, S species available, Carbon availability etc. for assessing microbial ecology and communities (DNA) (Figure 2.1). These were used to identify potential microbes of metabolic and functional importance and isolate those that are critical in these mining systems dependent on the variations within the mine wastewaters. The enrichments were also used for microbial communities in mesocosm experiments.

Figure 2.1: Illustrating the size difference between microcosm (on left with orange outline) and mesocosm (on right with green outline) experiments.

The microcosm experimental procedure mixed endemic mine wastewaters with NSOM or ASOM with S_2O_3 as the S source at ≈ 28 ˚C. $S_2O_3^{2-}$ was selected due to its importance as a major SOI in sulfur oxidation metabolism and its relevance to mining wastewaters as a widespread,

abundant and recalcitrant byproduct found in wastewaters after processing of sulfide hosted ores (Druschel *et al.*, 2004; Bernier and Warren, 2005; Bernier and Warren, 2007; Warren *et al.*, 2008; Bobadilla Fazzini *et al.*, 2013; Miranda-Trevino *et al.*, 2013; Whaley-Martin *et al.,* 2019). The enrichments were cycled with fresh media dependent on their pH corrals of 5-7 for both media and 3-5 additionally for ASOM (Figure 2.2), to examine potential microbial communities both as a function of media and pH value for each mine site and sampling time point (Table 2.1). DNA was sampled at cycles 1, 3, 5, 10 and 15 and stored at -20 ˚C until analysed via metagenomics Illumina Hi-Seq or 16S DNA Illumina Mi-seq. This was to examine the effects of succession in microbial enrichment communities, functionality and ecology associated with pH. Lastly, cryogenic samples were taken at cycles 1-5, 10 and 15 and stored in 20% glycerol at -80 ˚C, to create a microbial library for future culture growths and experimentation.

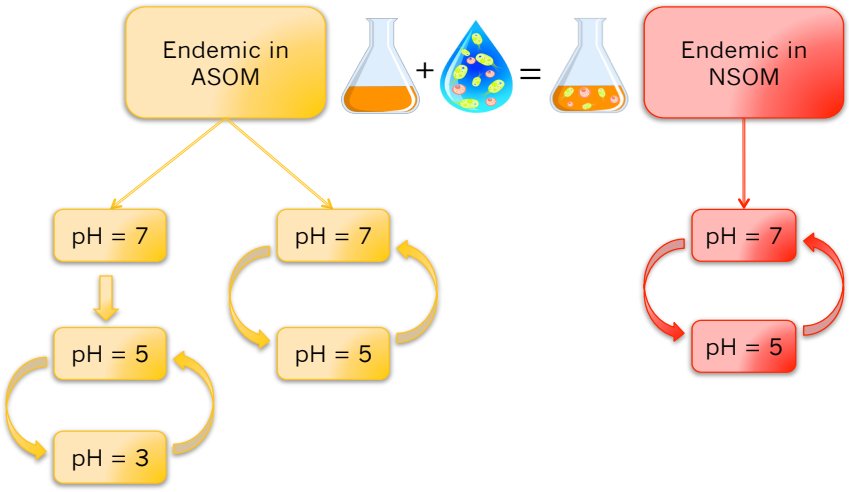

Figure 2.2: Illustration for cycling method of microcosm experiments.

2.1.3. Mesocosms: biogeochemical experiments

Mesocosms contained large volumes (5 L) of the synthetic or endemic mine wastewaters, with either abiotic or biotic (pure strain, endemic or select microcosm enrichments) additions, to assess

the changes in geochemistry and microbial communities (Figure 2.1). These were used in tandem to evaluate and connect potential important traits throughout the mining systems. The experiments tested were to identify the thiosalt concentrations, the interactions of geochemical (abiotic) and/or microbial (biotic) reactions on the thiosalts. Additionally, the potential biogeochemical pathways or reactions occurring in mine tailing wastewaters to assist in identifying monitoring tools.

2.1.3.1. Endemic mine wastewater based mesocosms

The experimental procedure for endemic mine wastewater samples were to initially sample for DNA and geochemical analyses for all seven samples collected before undergoing further experimentation or treatment (Table 2.1). This was both to examine the endemic variables comparing seasonal and geochemical trends and ensuring a reference point for each individual Microcosm and Mesocosm experiment. A "treatment" was then undergone, which each seasonal time point had varying treatment types, i.e., abiotic (filter sterilized mine water at <0.22 μm), endemic (plain mine water sample, no treatment) and enriched with microbial communities/pure strain (filter sterilized mine water at <0.22 μm, inoculated with *A. thiooxidans* or SoxB enrichment microcosms). The treatment types varied only seasonally for both mine site samples (Table 2.2). All enrichments used in the treatments were from the last cycle/generation of Summer'14 microcosms to maintain consistency in microbial community structure and function. Geochemistry was sampled periodically throughout the experiments and DNA for the endemic samples were sampled once more when the experiments were finished. The geochemical analyzes sampled were in triplicate for S^{2-}, S^0, $S_2O_3^{2-}$, SO_3^{2-}, SO_4^{2-}, $\sum S_{aq}$, TOC/DOC, NO_3^-, Fe^{2+}, Fe_T and pH.

Summer'14 had three biological treatments: abiotic, endemic and pure strain *A. thiooxidans*. Also tested alongside was the simulated mine wastewater (ASOM) with the pure

strain *A. thiooxidans.* These tests were used to assess the difference in geochemical pathways of a complex endemic community vs a pure strain. As well as to identify if endemic parent waters were given a specific SoxB, if they will become acid generating, i.e., comparing if the mining wastewater systems were geochemically or microbially driven.

Winter'15 had four biological treatments: abiotic, endemic and two enrichments, NSOM 7-5 and ASOM 7-5. Since only one mine was sampled, this was a preliminary test to examine possible microcosm enrichments (SoxB grown from the endemic parent waters) effects on parent wastewaters; i.e., to compare endemic microbial effects vs select enriched SoxB from the endemic community on parent water geochemistry.

Spring'15 had five biological treatments: abiotic, endemic and three enrichments, NSOM 7-5, ASOM 7-5 and ASOM 5-3. These tests were used to compare endemic microbial effects vs select enriched SoxB from the endemic community on parent water geochemistry. In order to determine if the microbes that are present but may be usually limited or not abundant can drive the system acidic, i.e., if the mining wastewater system is geochemically or microbially limited.

Summer'15 had five biological treatments: abiotic, endemic and three enrichments, NSOM 7-5, ASOM 7-5 and ASOM 5-3. Enrichments and wastewaters were then mixed such that Mine 1 enriched micro-organisms were added to Mine 2 wastewaters and Mine 2 enrichment micro-organisms were added to Mine 1 wastewaters. These tests examined both the dependence of the microbes and geochemistry compared to the Spring'15 tests in determining the acid generation potential or capabilities of the mine wastewaters.

Table 2.2: Treatment types of mesocosm experiments for each sampling time point of mine wastewaters.

Season	Treatments				
	1	2	3	4	5
Summer'14	Abiotic (sterile) ASOM	Endemic mine water	*A.thio* + sterile mine water	*A.thio* + ASOM	
Winter'15	Abiotic (sterile) mine water	Endemic mine water	NSOM 7-5 enrich + sterile mine water	ASOM 7-5 enrich + sterile mine water	
Spring'15	Abiotic (sterile) mine water	Endemic mine water	NSOM 7-5 enrich + sterile mine water	ASOM 7-5 enrich + sterile mine water	ASOM 5-3 enrich + sterile mine water
Summer'15	Abiotic (sterile) mine water	Endemic mine water	Other mine's NSOM 7-5 enrich + sterile mine water	Other mine's ASOM 7-5 enrich + sterile mine water	Other mine's ASOM 5-3 enrich + sterile mine water

2.1.3.2. Synthetic mine wastewater based mesocosms

A combination of synthetic mine wastewater mesocosms with SoxB microbe enrichment microcosms were tested. This was to assess how communities of the SoxB microbes found in mine wastewater enrichments metabolise different starting reduced S substrates in simulated waters. These experiments were to better constrain key sulfur oxidation intermediate geochemical pathways by these selective prominent sulfur micro-organisms, endemic to the mine wastewaters.

The experimental procedure simulated mine wastewaters based on the sulfur data collected for the two endemic parent mine wastewaters. Two concentrations: a low S concentration, similar to Mine 1 (4mM) and a high S concentration similar to Mine 2 (20mM) (based on mM of S) were assessed in experiments. Further, to assess possible microbial alteration of these common important mining wastewater associated SOI species, three sulfur cocktails were chosen as microbial sulfur substrates: S_2O_3, S_2O_3 + S_4O_6 and S_4O_6. Each at both low S and high S concentrations for a total of six chemical treatments (Figure 2.3). Four biological treatments were tested with each of the six different S cocktail simulated wastewaters, an abiotic control and three enrichments: Mine 1 Summer'14 ASOM 5-3, Mine 2 Summer'14 ASOM 5-3 and Mine 2 Summer'15 ASOM 5-3 (Figure 2.3). These enrichments were chosen due to the highly different S geochemistry of the parent waters from these samples. As well as the results from the mesocosms in the tests in section 1.3.1. with the ASOM 5-3 enrichments being of interest and more robust than the other pH corrals. Thus, in total 24 treatments were undergone and ran for total of 15 days, with the enrichment treatments inoculated each with $1x10^5$ cells/mL after cell counts of the respective enrichment and being rinsed with 0.01M potassium phosphate buffer to prevent acid contamination or sulfur cross-over from the enrichment to the mesocosm. Cell counts were also taken on day 5 and 15 to assess potential microbial growth on the various sulfur cocktails. All

samples started at pH=7, and 20 sampling times points were taken for geochemical analyses over 15 days: every 12 hours for the first 4 days, then once a day from day 5- day 15. The geochemistry was sampled in triplicate for pH, $\sum S_{UF}$, $\sum S_{0.2\mu m}$, SO_4^{2-}, S^{2-}, $S_2O_3^{2-}$, S^0 and SO_3^{2-} analyses.

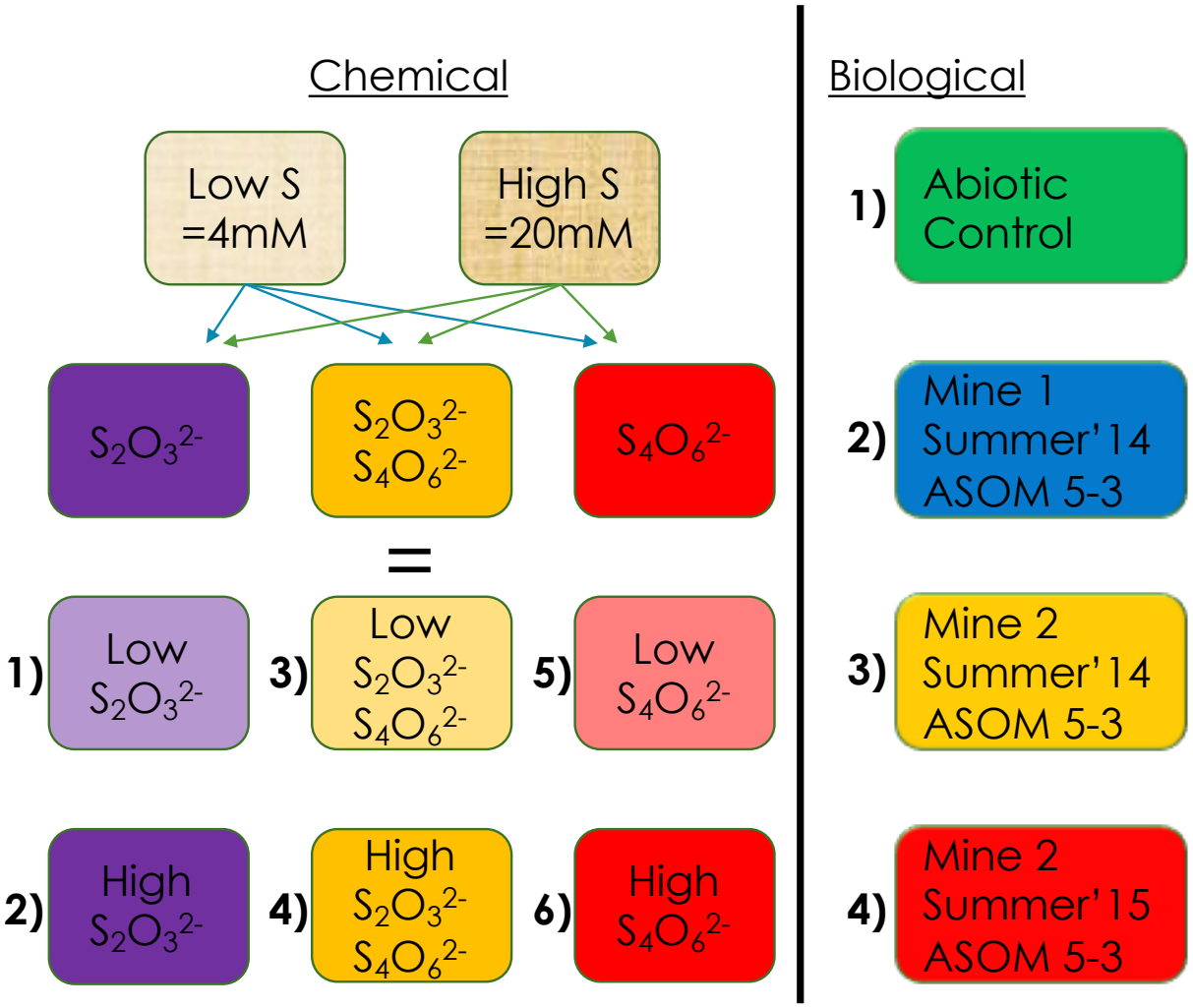

Figure 2.3: Illustration for experimental design of the synthetic mine wastewater mesocosms. showing the six chemical treatments and the four biological treatments, for a total of 24 mesocosms.

2.2. Methods

2.2.1. Mine wastewater sampling

2.2.1.1. Spatial and Temporal Sampling of Sites

Seven samples were collected from two mines sites Mine 1 (Cu, Ni; Sudbury, Ontario), and Mine 2 (Co, Cu, Ni; Newfoundland and Labrador) between August 2014 and September 2015 (Table 2.1). Mine 1 has been an important site for past and current research investigating the biogeochemical cycling of sulfur associated with acid generation in mine wastewaters and tailings (Bernier and Warren, 2005; Warren *et al*., 2008, Whaley-Martin *et al.*, 2019). Mine 2 was selected due to its differing wastewater sulfur chemistry in comparison to Mine 1. Wastewaters from the tailings ponds were collected at both mines for Summer 2014, Spring 2015 and Summer 2015, and Mine 1 was also sampled in Winter 2015. Each of the seven parent wastewater samples were: 1) geochemically characterized for pH, total dissolved S ($\sum S_{aq}$; < 0.45 μm) and SOI species (S^{2-}, S^0, $S_2O_3^{2-}$, SO_3^{2-}, SO_4^{2-}); 2) characterized for microbial community structure (16S rRNA, via Illumina Mi-Seq and metagenomic Illumina Hi-Seq); 3) experimentally enriched for sulfur oxidizing consortia (SoxB) in the three types of media-pH treatments, which were subsequently genetically characterized as above for wastewater parent communities; and 4) used for each samples endemic parent mine wastewater geochemistry in mesocosm experiments undergoing biological treatments as stated in section 1.3.1.

2.2.1.2. Mine wastewater sample collection

For both sites, water samples were collected into ethanol sterilized, lined and 20 L containers that were immediately sealed (Whaley-Martin *et al.*, 2019). At Mine 1, samples were collected directly

from the tailings reservoir surface, using a sampling beaker that was rinsed first with 70% ethanol and then rinsed with the mine water three times prior to collection. These samples were brought back to the laboratory (McMaster University, Hamilton, Ontario) within 1-3 days via ground transport for analyses. Mine 2 samples were taken directly from the mine wastewater effluent discharge point to the receiving environment into the sterilized lined containers. Due to the remote location of Mine 2, once collected, water samples were air shipped arriving within 3-10 days at the laboratory (McMaster University). Assessments have shown that the sulfur speciation of the major identified species of concern (e.g., S^0, $S_2O_3^{2-}$, $S_4O_6^{2-}$, SO_4^{2-}) remain stable within this time frame (1-10 days), for these circumneutral mine wastewaters (Whaley-Martin *et al*., 2019, 2020). The lack of any significant change in SOI speciation is also consistent with the notion that associated sulfur oxidizing microbes in these waters show low activity rates during shipment and thus no significant changes to their composition occur within this transportation time frame is a reasonable assumption (Whaley-Martin *et al*., 2019, 2020).

2.2.2. Media and synthetic wastewater recipes for experiments

2.2.2.1. Media for pure strain A. thiooxidans

A. thiooxidans ATCC 19377 cells were grown in liquid elemental sulfur or thiosulfate media (Staley *et al*., 1989). The media contained two components, a salt medium and a sulfur source. Elemental sulfur salt medium: $(NH_4)_2SO_4$, 0.2 g; $MgSO_4$ x 7 H_2O, 0.5 g; $CaCl_2$ x 2 H_2O, 0.331 g; KH_2PO_4, 3.0 g; $FeSO_4$ x 7 H_2O, 9.15 mg; distilled water, 1 000 mL. The salt medium was sterilized by passing through a 0.22 µm filter. Elemental sulfur powder was heated in an oven at 100^{o}C for 30 minutes and the cycle was repeated three times. The salt medium was then added to the culture

flasks and the final sulfur concentration was 1% (m/v). Thiosulfate medium: salt medium as above and $Na_2S_2O_3$ was added at 0.2% (m/v), followed by filter sterilization (0.22 μm filter).

2.2.2.2. Microcosm enrichment media creation

Two types of media, a neutrophilic sulfur oxidizing media (NSOM), and an acidophilic sulfur oxidizing media (ASOM), that both used $S_2O_3^{2-}$ as the sulfur substrate were used in the experiments.

NSOM was created in 1 L batches as follows. Part 1: 90 mL of 1.1% (w/v) K_2HPO_4 was added to 400 mL of tap water. Part 2: 5 g of $Na_2S_2O_3$, 90 mL of 0.44% (w/v) NH_4Cl, 90 mL of 0.11% (w/v) $MgSO_4$, 2.2 mL of Solution T and 320 mL of tap water. Part 1 and 2 were sterilized separately by either filtration (<0.2 μm) into autoclaved glassware and then combined. Solution T was made by: 50 g of EDTA disodium salt dissolved into 400 mL of water, followed by 9 g of NaOH added to EDTA solution, then the following salts were added individually to 30 mL of water before being added to the EDTA solution: 5 g of $ZnSO_4.7H_2O$, 5 g of $CaCl_2$ (or 7.34 g of $CaCl_2.2H_2O$), 2.5 g of $MnCl_2.6H_2O$, 0.5 g of $CoCl_2.6H_2O$, 0.5 g of $(NH_4)_6Mo_7O_{24}.4H_2O$, 5 g of $FeSO_4.7H_2O$ and 0.2 g of $CuSO_4.5H_2O$.

ASOM was made in 1 L batches as follows. In 1 000 mL of distilled water the following salts were added individually until dissolved, 5 g of $Na_2S_2O_3$, 0.2 g $(NH_4)_2SO_4$, 0.5 g $MgSO_4.7$ H_2O, 0.36 g $CaCl_2.2$ H_2O, 3 g KH_2PO_4 and 10 mg $FeSO_4$. The solution was then filter sterilized (<0.2 μm) into autoclaved glassware.

2.2.2.3. Synthetic mine wastewater sulfur cocktails

Six types of sulfur cocktails were created: two concentrations of reduced S source, a low at 4 mM (in mM of S) and a high 20 mM (in mM of S), for three different combinations of reduced S species, $S_2O_3^{2-}$, $S_2O_3^{2-}$ + $S_4O_6^{2-}$ and $S_4O_6^{2-}$ (Figure 2.3). The choice of these concentrations and S species cocktails was due to as mentioned, the concentration of reduced S species found at each of the two mine sites. As well as $S_2O_3^{2-}$ being an important S species and $S_4O_6^{2-}$ also being known as a major SOI in sulfur oxidation metabolism further up the oxidation chain and a key step in $S_2O_3^{2-}$ metabolism (Suzuki, 1999; Li *et al.*, 2017; Wang *et al*., 2019).

The synthetic waters were created in 5 L batches as follows: First, a base solution was created with 5 000 mL of distilled water and the following salts added individually until dissolved, 1 g $(NH_4)_2SO_4$, 1.25 g $MgSO_4.7\ H_2O$, 1.8 g $CaCl_2.2\ H_2O$, 2.5 g KH_2PO_4 and 90 mg $FeSO_4.7\ H_2O$. The reduced S source was then added dependent on the cocktail needed. For i) $S_2O_3^{2-}$ 4 mM, 2.48 g $Na_2S_2O_3.5\ H_2O$; ii) $S_2O_3^{2-}$ 20 mM, 12.4 g $Na_2S_2O_3.5\ H_2O$; iii) $S_2O_3^{2-}$ + $S_4O_6^{2-}$ 4 mM, 1.24 g $Na_2S_2O_3.5\ H_2O$ + 0.756 g $K_2S_4O_6$; iv) $S_2O_3^{2-}$ + $S_4O_6^{2-}$ 20 mM, 6.2 g $Na_2S_2O_3.5\ H_2O$ + 3.93 g $K_2S_4O_6$; v) $S_4O_6^{2-}$ 4 mM, 1.512 g $K_2S_4O_6$; vi) $S_4O_6^{2-}$ 20 mM, 7.56 g $K_2S_4O_6$. Thus, for the $S_2O_3^{2-}$ + $S_4O_6^{2-}$ combination having equal concentrations of S for each reduced sulfur source, i.e. for the 4 mM cocktail, 2 mM of S as $S_2O_3^{2-}$ and 2 mM of S as $S_4O_6^{2-}$, and for the 20 mM cocktail, 10 mM of S as $S_2O_3^{2-}$ and 10 mM of S as $S_4O_6^{2-}$. The solution was then filter sterilized (<0.2 μm) and placed in an autoclaved 8 L carboy.

2.2.3. Microbial inoculation, growth and preservation for experiments

2.2.3.1. Pure strain A. thiooxidans

For both experiments (elemental sulfur or thiosulfate sulfur substrate), the total volume of medium corresponded to a fifth of the total volume of the autoclaved Erlenmeyer flask. All cultures were initially inoculated at 5% v/v with cultures pre-grown in the corresponding media; the inoculant bacteria were washed with sterile 1% NaCl solution prior to inoculation to prevent acid contamination into the fresh media. All cultures were grown under aerobic conditions at 30 ^{o}C and flasks were shaken at 120 rpm.

2.2.3.2. Microcosm enrichments growth

All seven of the water samples collected from the mines wastewaters underwent the three enrichment strategies: 1) NSOM within a pH corral between 7-5 (NSOM 7-5); 2) ASOM within a pH corral between 7-5 (ASOM 7-5); and 3) ASOM within a pH corral between 5-3 (ASOM 5-3). These pH corrals were chosen to identify key sulfur oxidizing microbes of mine wastewaters as potential bioindicators as acid generation occurs, as well as to identify possible microbial SoxB consortia progression from neutral to mildly acidic pH (7-5) and subsequently to moderately acidic pH (5-3) conditions. The endemic microbial communities were enriched initially with a 1:1 ratio of endemic mine wastewater to media, to make 150 mL of enrichment within sterile autoclaved 250 mL Erlenmeyer flasks, i.e., 75 mL of endemic mine wastewater and 75 mL of media. These were then buffered to start at pH 7 with dilute sterile (0.2µm filtered) NaOH and HCl. The enrichments were kept static in incubators @ 28 ˚C with 12-hour diurnal light. pH was tested at intervals as described in Whaley-Martin *et al.* (2019) until each enrichment achieved the final pH of its specific pH corral, i.e., pH = 5 for the 7-5 enrichments, or pH = 3 for the 5-3 enrichments.

Once the final pH was achieved, a new run/cycle/generation(gen) was then created using a 1:2 ratio of the current enrichment to fresh media, i.e., 50 mL of current enrichment cycle and 100 mL of fresh media. It was then buffered to the starting pH of the enrichment type corral, i.e. NSOM 7-5 and ASOM 7-5, starting pH = 7, and for ASOM 5-3 starting pH = 5 (Figure 2.2).

2.2.3.3. Microbial microcosms enrichment preservation and re-growth

To utilize the SoxB microbial communities cultivated in the microcosm experiments for future tests, cells were harvested to allow for further experimentation. Cells were harvested by placing 40-50 mL of the microcosm enrichment into 50 mL tubes and centrifuging @ 5000 rpm, for 30 min, at 4 ˚C. The supernatant was discarded, then cells washed with sterile 0.01 M potassium phosphate buffer solution (PBS) (pH 7.0) and centrifuged again. The supernatant was discarded again, and cells resuspended in 20% v/v glycerol and fresh initial media (NSOM/ASOM), then placed in cryotubes and frozen @ -80 ˚C.

To regrow the preserved microbial enrichment communities, the sample was taken out of the -80 ˚C freezer to thaw at room temperature. Once thawed, the tube was shaken/vortexed to ensure cells were suspended in the sample, then poured into fresh media of the same type and grown under identical conditions of the initial sample enrichment, as described previously.

2.2.3.4. Mine wastewater mesocosms

The different treatment types for the mesocosms described in section 2.1.3.1. overall used seven different biological treatments, the pure strain *A. thiooxidans* and six enrichments: one of each of the three enrichment types (NSOM 7-5, ASOM 7-5 and ASOM 5-3) for both Mine 1 and Mine 2 Summer 2014 latest generation microcosms (Table 2.2).

The *A. thiooxidans* was grown on elemental sulfur media for this experiment, ensuring growth by OD_{600}, testing for change in pH to ensure cells were actively oxidizing S and examining under microscope for active cells. Autoclaved 8 L carboy containers were filled with 5 L of either the filter sterilized (<0.2 μm) mine wastewaters or ASOM, and 100 mL of media with active *A. thiooxidans* was poured directly into each. The treatment mesocosms were buffered by dilute sterile (0.2 μm filtered) NaOH and HCl to the initial pH of the endemic mine wastewater. These were kept static in incubators @ 28 ˚C with 12-hour diurnal light and the geochemistry was sampled periodically throughout the experiments.

The enrichments were re-grown from the preserved microcosm enrichments as described above. Autoclaved 8 L carboy containers were filled with 5 L of the filter sterilized (<0.2 μm) mine wastewaters, and once the enrichments reached the low end of their respective pH corrals, the 150 mL enrichments were filtered through 0.2 μm membranes, then the membranes were aseptically removed and placed in the 5 L sterile mine wastewater containers. This strategy was used to add the SoxB enrichment microbial community, while preventing any change to the mine wastewater geochemistry due to addition of S sources or acid contamination from the enrichment media.

2.2.3.5. Synthetic wastewater "S cocktail" enrichment mesocosms

Four biological treatments were assessed for these experiments including an abiotic control and three SoxB enrichments (Mine 1 Summer'14 ASOM 5-3, Mine 2 Summer'14 ASOM 5-3 and Mine 2 Summer'15 ASOM 5-3) (Figure 2.3). The enrichments were re-grown from the preserved microcosm enrichments of the latest generations for the samples. Once the enrichment reached the minimum value of its pH corral (pH = 3), cells were counted via fluorescence and microscopy

described below. Enrichments were centrifuged @10 000 rpm at 4 ˚C for 20 min, the supernatant discarded, and cells then washed with 0.01 M PBS (pH 7.0). Then cells were centrifuged again, the supernatant discarded, and the cell pellet resuspended in sterile MQ water. The now washed SoxB enrichment was then added to the 5 L synthetic wastewater mesocosm to ensure $1x10^5$ cells/mL for each mesocosm. Mesocosms were buffered to pH = 7 by dilute sterile (0.2 μm filtered) NaOH and HCl and were kept static in incubators @ 28 ˚C under a 12-hour diurnal light regime.

Cells counts were done by first drawing a 1 cm circle on microscope slide, then washing slide with 10% v/v HCl and after a couple hours rinsing with MQ water. A 1% w/v Agarose solution (1 g per 100 mL) was cooked until the agarose dissolved, then the solution was poured on the slides and left for a couple hours until it hardened. 10 μL of the enrichment sample was spread onto the 1 cm^2 area and left to dry. Once dried, 3 μL of SYTO™ 9 (Invitrogen™) (diluted to a 30μM solution) and 7 μL MQ water was added and spread onto the 1 cm^2 area then placed in the dark to stain for a few minutes. 12-15 field views per slide were then counted via fluorescence microscopy (Leica DM R, Wetzlar, Germany) at 100x magnification under UV light and through the GFP filter. Then cell count extrapolation based on the area of the field of view for magnification and number of fields for the 1 cm^2 of sample.

2.2.4. Microbial genetic analyses and characterization (16S rRNA)

2.2.4.1. Biases in genetic analyses

Bias in community structure identification can be introduced through a variety of steps associated with environmental sampling (Brooks et al., 2015), DNA extraction (Glassing et al. 2016; Salter et al. 2014) and sequencing artifacts (van der Loos and Nijland, 2020). Here, methods relied on both environmental sampling as well as lab mesocosms with non-replicate samples and thus some

bias in interpretation is likely. In particular, the possible non detection of rare community members. Wherever possible, bias in DNA extraction, primer selection, PCR protocols and chimera formation and trimming steps was mitigated as described in subsequent sections.

2.2.4.2. DNA extraction and quantification

The endemic mine wastewater samples (3-7 L depending on sample) and SoxB enrichment samples (75 mL) were filtered on 0.2µm filter towers (Thermo Scientific™ Nalgene™ Rapid-Flow™ Sterile Disposable Filter Units with CN Membrane). The filters were then aseptically transferred into sterile tubes and frozen @-20 ˚C until DNA extraction. The Qiagen's DNeasy® PowerWater® Kit was used to extract DNA from the filters as per manufacturer's guidelines and to reduce DNA biases from environmental variables (van der Loos and Nijland, 2020). Samples of extracted DNA, alongside DNA extraction blanks to ensure non-contamination from the kits (Glassing et al. 2016; Salter et al. 2014) for 16S rRNA were sent to the McMaster Farncombe DNA Sequencing Facility (Hamilton, Ontario) for analysis. Eight samples (All from Summer'14; the two endemic parent mine wastewater samples, and the latest generation of the three enrichment types from both mines) underwent metagenomic sequencing for a more comprehensive understanding of the mine tailing wastewater microbial community ecology and metabolic potential, of which 16S rRNA data were also extracted from metagenome results as described below. The samples library construction and sequencing were performed at the Farncombe Metagenomics Facility at McMaster University (Hamilton, Ontario). Quantitative PCR (qPCR) was used to quantify the extracted DNA from all samples and its concentrations adjusted for each step of the subsequent molecular protocol.

2.2.4.3. Genomic sequencing for 16S rRNA gene only samples

For the 16S rRNA only sequencing, standard protocols of the Earth Microbiome Project (Caporaso *et al.*, 2011; 2012) and Illumina adapted primers as Bartram *et al.* (2011) were used on aliquots of purified DNA to amplify region V4 of the 16S rRNA gene by PCR. The 806r (GGACTACNVGGGTWTCTAAT) and 515f (GTGYCAGCMGCCGCGGTAA) variable regions of archaeal and bacterial 16S rRNA gene were amplified via modified primers. PCR was accomplished using 50 ng of template and the PCR mix comprised 1U of recombinant Taq DNA Polymerase (Invitrogen™), 1x buffer, 0.2 mmol L-1dNTPs, 0.4 mg mL-1 BSA, 1.5 mmol L-1MgCl2, and 5 pM of each primer. The reaction was carried out at 98 °C for 5 min, 35 cycles (98 °C) for 30 min, then 30 min (50 °C) and 30 min (72 °C), with a final extension of 72 °C for 10 min. The PCR products were examined by electrophoresis and sent for sequencing. Illumina Mi-Seq sequencing was undergone for all amplicons normalized to 1.25 ng μL-1 using the SequalPrep normalization kit (ThermoFisher#A1051001). Bimera checking was performed on the data through DADA2 (version 1.6.0). The 3-5% of reads that were detected as bimeras were subsequently excluded from further analyses as outlined in Whaley-Martin *et al.* (2019).

In the eight samples where metagenome data were used, all available DNA (up to 1 μg) from each sample was fragmented using the Covaris S220 Ultrasonicator. Parameters for 500 bp shearing with 50 μL input were: 175W PIP, 5% duty factor, 200 cpb, 35 sec. Dual-indexed shotgun libraries were prepared with the NEBNext Ultra DNA Library Prep Kit for Illumina (New England Biolabs Inc.). The libraries were quantitated by qPCR, pooled in equimolar volumes and sequenced using the Illumina HiSeq 1500 platform (Rapid v2 chemistry with onboard cluster generation; 151 bp pair-end reads). Raw data was processed with HCS v2.2.58 (RTA v1.18.64).

File conversion and demultiplexing were performed with CASAVA v1.8.2 allowing 1 mismatch in the indexes.

2.2.4.4. 16S rRNA extraction from metagenomic sequences

FastQC [http://www.bioinformatics.babraham.ac.uk/projects/fastqc/] was run to inspect read quality on all samples. Cutadapt (Martin, 2011) was used to trim Illumina adapters, filtering quality at 28 and trimming any Ns from the ends. Trimmed reads shorter than 50bp were discarded. After trimming, the number of read pairs per sample ranged from 6.8M to 18.3M with a mean of 9.7M. To identify which reads came from the 16S rRNA gene, the reads were mapped to the SILVA 16S database (version 1.3.2, (Quast *et al.*, 2013)) with Bowtie2 (Langmead and Salzberg, 2012) using default parameters (allowing discordant mapping and keeping only the best mapping of each read). The number of individual reads (not pairs) that mapped to the SILVA database from each sample ranged from 6 540 to 19 318 with a mean of 10 492. A fasta file was generated from the SAM file of mapped reads using SAMtools (Li *et al.*, 2009). Then taxonomy was assigned to the reads using the DADA2 (version 1.6.0) (Callahan *et al*., 2016) implementation of the RDP classifier (Wang *et al*., 2007).

2.2.5. Geochemical methods and analyses

2.2.5.1. Total sulfur - determination by ICP-AES

Dependent on the experiment total S was sampled for unfiltered total sulfur ($\sum S_{UF}$), filtered (< 0.2 µm) total sulfur ($\sum S_{0.2\mu m}$) and dissolved (< 0.45 µm) total sulfur ($\sum S_{aq}$). 40 mL of sample was either unfiltered ($\sum S_{UF}$) or filtered ($\sum S_{0.2\mu m}$) by Pall Acrodisc® 25mm 0.2 µm Supor® membrane or filtered ($\sum S_{aq}$) by Pall Acrodisc® 25mm 0.45 µm Supor® membrane via polypropylene syringes

into 50 mL Falcon™ tubes, immediately after 80 µL of HNO_3 (Optima grade, Fisher Chemical) was added to each tube, and stored at 4°C until further processed at CSIRO Land and Water laboratory (New South Wales, Australia). Analyses for total S were carried out using inductively coupled argon plasma emission spectrometry (ICP-AES) (Varian730 ES, Mulgrave, VIC), with sulfur calibration standards prepared from a certified reference stock solution (AccuStandard New Haven, CT, USA) in 2 % v/v HNO_3. By measuring intensity at the 181.972 nm sulfur emission line concentrations were determined with a limit of detection (LOD) for sulfur of 1 mg L^{-1} (0.03mM). The quality control/quality assurance included duplicate analysis and drift analysis on at least 10 % of samples.

2.2.5.2. SO_4^{2-} and S^{2-} - determination by spectrophotometry

At each sampling time point, samples were immediately fixed and analyzed using the HACH SulfaVer 4 Method and Methylene Blue Method for SO_4^{2-} and S^{2-}, respectively (Hach company, Colorado, USA) by spectrophotometry (Pharmacia Biotech Ultrospec 3000 UV/Visible Spectrophotometer).

2.2.5.3. $S_2O_3^{2-}$, S^0 and SO_3^{2-} - determination by HPLC

SOI species $S_2O_3^{2-}$, SO_3^{2-} and S^0 sampling and analyses were collected simultaneously with those for total S, and redox end member species, SO_4^{2-} and S^{2-}, and immediately preserved using a monobromobimane derivatization procedure for SOI analyses by HPLC (Rethmeier *et al.*, 1997). The Shimadzu LC-20AD prominence HPLC instrument with Alltima HP C18 (5 µm x 150 mm x 4.6 mm Grace™) reverse phase column was used for all SOI species analyses. Solvents used in protocols were A=Water, B=Methanol, C=Acetonitrile, D=Acetic acid 0.25% v/v pH 3.5 adjusted

with NaOH (1N). $S_2O_3^{2-}$ and SO_3^{2-} were analyzed via fluorescence excitation at 380 nm and emission at 480 nm. Standards and calibrations for $S_2O_3^{2-}$ (0-10 mM) and SO_3^{2-} (0-1.7 mM) were made with $Na_2S_2O_3$ (Sigma Aldrich, 99% purity) and Na_2SO_3 (Sigma Aldrich, ≥98% purity), respectively. The initial thiosulfate and sulfite elution protocol was as follows: 0-1min, 1 mL/min flow; 1-6 min, 1 mL/min to 0.85 mL/min flow linear gradient; 0-8 min B 35%, D 65% to B 40%, D 60% linear gradient, oven heated to 35 ˚C. Sample size was 5 µL and elution times were 3 min for SO_3^{2-} and 6.5 min for $S_2O_3^{2-}$. This protocol was replaced as analytical tests were undergone to develop more efficient methodologies. Two protocols were used, either better for the health of the column as follows: i) Isocratic mobile phase B 35%, D 65%, flow rate of 0.5 mL/min and oven heated to 35 ˚C for a run time of 20 min. Sample size was 5 µL and elution times were 5 min for SO_3^{2-} and 6 min for $S_2O_3^{2-}$. Or by a more accurate protocol, particularly for lower concentration samples: ii) Isocratic mobile phase B 35%, D 65%, flow rate of 1 mL/min and oven heated to 35 ˚C for a run time of 15 min. Sample size was 10 µL and elution times were 3 min for SO_3^{2-} and 4 min for $S_2O_3^{2-}$.

S^0 was extracted with chloroform from both filtered (<0.45 µm, i.e colloidal) and unfiltered samples (i.e., particulate and/or colloidal) and analyzed with reverse-phase HPLC and UV-absorption at 263 nm. Standards and calibrations (0-32 mM) were made from S^0 (Fisher, 99.5% purity) dissolved in chloroform. S^0 elution protocol: Isocratic mobile phase B 65%, C 35%, flow rate of 1 mL/min, run time of 10 min. The sample size was 10 µL and the elution time was at 5 min. This protocol was replaced as analytical tests were undergone to develop a more efficient methodology for acquiring more accurate measurements particularly in samples with lower S^0 concentration as follows: Isocratic mobile phase A 5%, B 95%, flow rate of 1 mL/min, run time of 12 min. The sample size was 20 µL and the elution time was at 8 min.

2.2.5.4. Unresolved and reactive sulfur pools

To quantify any unresolved or "Other SOI" within both parent and enrichment waters, the sum of all measured solution sulfur species concentrations, (i.e., $\sum (SO_4^{2-}, S^{2-}, S_2O_3^{2-}, SO_3^{2-}$ and $S^0)$) was subtracted from the total S concentration. Lastly, by subtracting SO_4^{2-}, the end state of S oxidation, from the Total S, we were able to determine the reactive S pool available for oxidation.

2.2.5.5. pH, carbon, nitrogen and iron analyses

pH was measured immediately (Denver Instrument Model 225, NY, USA) prior to sampling for any geochemical analyses.

For carbon analysis 100 mL of sample was taken and stored in carbon-clean amber glass bottles and stored at -20 ˚C until analysed. DOC was separated by filtering samples with 0.45 μm filters. Samples were run on the Shimadzu TOC-$L_{CPH/CPN}$ analyser.

NO_3^-, Fe^{2+} and Fe_T, samples were taken immediately and analysed using HACH *NitraVer 5 Method*, *Ferrous Iron Reagent Method* and *FerroVer Iron Reagent Method* for NO_3^-, Fe^{2+} and Fe_T, respectively by spectrophotometry.

References

Bartram A.K., Lynch M.D.J., Stearns J.C., Moreno-Hagelsieb G., Neufeld J.D. (2011) Generation of multimillion-sequence 16S rRNA gene libraries from complex microbial communities by assembling paired-end Illumina reads. *Appl. Environ. Microbiol.* 77: 3846–3852. doi:10.1128/AEM.02772-10.

Bernier L., Warren L. (2005) Microbially driven acidity generation in a tailings lake. *Geobiology*. 3: 115-133.

Bernier L., Warren L.A. (2007) Geochemical diversity in S processes mediated by culture-adapted and environmental-enrichments of *Acidithiobacillus* spp. *Geochim. Cosmochim. Acta.* 71: 5684-5697.

Bobadilla Fazzini R.A., Cortés M.P., Padilla L., Maturana D., Budinich M., Maass A., *et al*. (2013) Stoichiometric modeling of oxidation of reduced inorganic sulfur compounds (Riscs) in *Acidithiobacillus thiooxidans*. *Biotechnol. Bioeng.* 110: 2242-2251.

Brooks J.P., Edwards D.J., Harwich M.D., Rivera M.C., Fettweis J.M., Serrano, M.G., *et al* (2015) The truth about metagenomics: quantifying and counteracting bias in 16S rRNA studies. *BMC Microbiol*, 15: 1-14.

Callahan B.J., McMurdie P.J., Rosen M.J., Han A.W., Johnson A.J.A., Holmes S.P. (2016) DADA2: High-resolution sample inference from Illumina amplicon data. *Nat. Methods*. 13: 581

Caporaso J.G., Lauber C.L., Walters W.A. Berg-Lyons D., Huntley J., Fierer N., *et al*. (2012) Ultra-high-throughput microbial community analysis on the Illumina HiSeq and MiSeq platforms. *ISME J.* 6: 1621–1624. doi:10.1038/ismej.2012.8.

Caporaso J.G., Lauber C.L., Walters W.A., Berg-Lyons D., Lozupone C.A., Turnbaugh P.J., *et al*. (2011) Global patterns of 16S rRNA diversity at a depth of millions of sequences per sample. *Proc. Natl. Acad. Sci.* 108: 4516–4522. doi:10.1073/pnas.1000080107.

Druschel G.K., Baker B.J., Gihring T.M., Banfield J.F. (2004) Acid mine drainage biogeochemistry at Iron Mountain, California. *Geochem T* 5: 13-32.

Glassing A., Dowd S.E., Galandiuk S., Davis B., Chiodini R.J. (2016) Inherent bacterial DNA contamination of extraction and sequencing reagents may affect interpretation of microbiota in low bacterial biomass samples. *Gut. Pathog.* 8:24. doi: 10.1186/s13099-016-0103-7.

Langmead B., Salzberg S.L. (2012) Fast gapped-read alignment with Bowtie 2. *Nat Methods*. 9: 357–9.

Li H., Handsaker B., Wysoker A., Fennell T., Ruan J., Homer N., *et al*. (2009) The Sequence Alignment/Map format and SAMtools. *Bioinforma. Oxf. Engl*. 25: 2078–9.

Li L.F., Fu L.J., Lin J.Q., Pang X., Liu X.M., Wang R., *et al.* (2017) The sigma(54)-dependent two-component system regulating sulfur oxidization (Sox) system in *Acidithiobacillus caldus* and some chemolithotrophic bacteria. *Appl. Microbiol. Biotechnol.* 101, 2079–2092.

Martin M. (2011) Cutadapt removes adapter sequences from high-throughput sequencing reads. *EMBnet.journal*. 17:10–2.

Miranda-Trevino J.C., Pappoe M., Hawboldt K., Bottaro C. (2013) The Importance of Thiosalts Speciation: Review of Analytical Methods, Kinetics, and Treatment. *Crit. Rev. Env. Sci. Tec.* 43: 2013-2070. doi: 10.1080/10643389.2012.672047.

Quast C., Pruesse E., Yilmaz P., Gerken J., Schweer T., Yarza P., *et al*. (2013) The SILVA ribosomal RNA gene database project: improved data processing and web-based tools. *Nucleic Acids Res*. 41: D590–6.

Rethmeier J., Rabenstein A., Langer M., Fischer U. (1997) Detection of traces of oxidized and reduced sulfur compounds in small samples by combination of different high-performance liquid chromatography methods. *J Chromatogr A*. 760: 295-302.

Salter S.J., Cox M.J., Turek E.M., Calus S.T., Cookson W.O., Moffatt M.F., Turner P., Parkhill J., Loman N.J., Walker A.W. (2014). Reagent and laboratory contamination can critically impact sequence-based microbiome analyses. *BMC Biol.* 12:87. doi: 10.1186/s12915-014-0087-z

Staley J.T., Bryant M.P., Pfennig N., Holt J.G. (1989) *Acidithiobacillus*. In: *Bergey's Manual of Systematic Bacteriology vol 3*. Edited by Wilkins Wa, vol. 3, 1st edn. Baltimore 1842-1858.

Suzuki I. (1999) Oxidation of inorganic sulfur compounds: chemical and enzymatic reactions. *Can J Microbiol* 45: 97-105.

van der Loos, L. M., & Nijland, R. (2020). Biases in bulk: DNA metabarcoding of marine communities and the methodology involved. *Mol. Ecol.*

Wang Q., Garrity G.M., Tiedje J.M., Cole J.R. (2007) Naïve Bayesian Classifier for Rapid Assignment of rRNA Sequences into the New Bacterial Taxonomy. *Appl Environ Microbiol*. 73: 5261–7.

Wang R., Lin J.Q., Liu X.M., Pang X., Zhang C.J., Gao X.Y., *et al.* (2019) Sulfur oxidation in the acidophilic autotrophic *Acidithiobacillus* spp. *Front Microbiol 9*: 3290.

Warren L., Norlund K.I., Bernier L. (2008) Microbial thiosulphate reaction arrays: The interactive roles of Fe (III), O2 and microbial strain on disproportionation and oxidation pathways. *Geobiology* 6: 461-470.

Whaley-Martin K.J., Jessen G., Nelson T.C., Mori J., Apte S., Jarolimek C., *et al*. (2019) The potential role of *Halothiobacillus* spp. in sulphur oxidation and acid generation in circum-neutral mine tailings reservoirs. *Front. Microbiol*. 10: 297.

Whaley-Martin K., Marshall S., Nelson T.E., Twible L., Jarolimek C.V., King J.J., *et al.*(2020) A mass-balance tool for monitoring potential dissolved sulfur oxidation risks in mining impacted waters. *Mine Water Environ* 1-17.

Chapter 3

New insights into *Acidithiobacillus thiooxidans* Sulfur Metabolism through Coupled Gene Expression, Solution Chemistry, Microscopy and Spectroscopy Analyses

David Camacho[1], Rodolfo Frazao[2], Aurélien Fouillen[2,3], Antonio Nanci[2,3], B. Franz Lang[2], Simon C. Apte[4], Christian Baron[2] and Lesley A. Warren[1,5]

[1]School of Geography and Earth Science, Faculty of Science, McMaster University, Hamilton, ON, CA;
[2]Department of Biochemistry and Molecular Medicine, Faculty of Medicine, Université de Montréal, Montréal, QC, CA;
[3]Laboratory for the Study of Calcified Tissues and Biomaterials, Faculty of Dentistry, Université de Montréal, Montréal, QC, CAN;
[4]CSIRO, Land and Water, Lucas Heights NSW, AU;
[5]Department of Civil and Mineral Engineering, Faculty of Applied Science and Engineering, University of Toronto, Toronto, ON, CA;

Citation: Camacho D., Frazao R., Fouillen A., Nanci A., Lang B.F., Apte S.C., Baron C., Warren L.A. (2020) New Insights Into *Acidithiobacillus thiooxidans* Sulfur Metabolism Through Coupled Gene Expression, Solution Chemistry, Microscopy, and Spectroscopy Analyses. *Front. Microbiol*. 11:411. doi: 10.3389/fmicb.2020.00411

Abstract

Here, we experimentally expand understanding of the reactions and enzymes involved in *A. thiooxidans* ATCC 19377 S^0 and $S_2O_3^{2-}$ metabolism by developing models that integrate gene expression analyzed by RNA-Seq, solution sulfur speciation, electron microscopy and spectroscopy. The *A. thiooxidans* $S_2O_3^{2-}$ metabolism model involves the conversion of $S_2O_3^{2-}$ to SO_4^{2-}, S^0 and $S_4O_6^{2-}$, mediated by the sulfur oxidase complex (Sox), tetrathionate hydrolase (TetH), sulfide quinone reductase (Sqr) and heterodisulfate reductase (Hdr) proteins. These same proteins, with the addition of rhodanese (Rhd), were identified to convert S^0 to SO_3^{2-}, $S_2O_3^{2-}$ and polythionates in the *A. thiooxidans* S^0 metabolism model. Our combined results shed light onto the important role specifically of TetH in $S_2O_3^{2-}$ metabolism. Also, we show that activity of Hdr proteins rather than Sdo are likely associated with S^0 oxidation. Finally, our data suggest that formation of intracellular $S_2O_3^{2-}$ is a critical step in S^0 metabolism, and that recycling of internally generated SO_3^{2-} occurs, through comproportionating reactions that result in $S_2O_3^{2-}$. Electron microscopy and spectroscopy confirmed intracellular production and storage of S^0 during growth on both S^0 and $S_2O_3^{2-}$ substrates.

3.1. Introduction

The stepwise oxidation of reduced sulfur species from sulfide to sulfate can occur via several pathways involving a variety of sulfur oxidation intermediate (SOI) compounds that are dynamically influenced by environmental and geochemical characteristics as well as the microbes involved (Schippers *et al*., 1996; Schippers and Sand, 1999; Nordstrom, 2015). This range of sulfur oxidation states contributes to a complex, and only partially constrained biogeochemical cycle in which sulfur compounds can be variably reduced, oxidized and disproportionated via abiotic and/or biotic processes depending on environmental conditions (Johnston and McAmish, 1973; Kelly and Baker, 1990; Pronk *et al*., 1990; Druschel, 2002; Zopfi *et al*., 2004; Bernier and Warren, 2007; Boyd and Druschel, 2013). The geochemical challenges to closing the sulfur biogeochemical cycle reflect the existence of multiple semi-stable SOI compounds, which are either not comprehensively constrained to date and/or lack readily available analytical methods for their characterization (Miranda-Trevino *et al.*, 2013). For instance, the challenges in measuring polythionates and other higher oxidation state sulfur compounds have impeded the delineation of their roles in the chain of reactions culminating in sulfate (Johnson and Hallberg, 2003; Nordstrom *et al.*, 2015). The complexities of sulfur chemistry underscore the need for mass balance of all sulfur within systems, in order to quantify how much sulfur may be tied up in a currently unidentified or, as referred to here, "other SOI" pool. However, sulfur mass balance is rarely employed in studies of sulfur cycling.

Further, microbial catalysis, dependent on the specific bacteria, growth stage and sulfur substrates involved, is important for initiating or accelerating rates for some of these sulfur oxidation reactions (Bacelar-Nicolau and Johnson, 1999; Druschel *et al.*, 2004; Bernier and

Warren, 2005; Beller *et al.*, 2006; Bernier and Warren, 2007; Warren *et al.*, 2008; Bobadilla Fazzini *et al.*, 2013). Several studies have demonstrated flexibility of the sulfur oxidation metabolism by assessing the solution chemical changes in some intermediate sulfur species, or inferred pathways from what is known about identified sulfur metabolism genes within an organism or community (Bobadilla Fazzini *et al.*, 2013; Jones *et al.*, 2014; Yin *et al.*, 2014; Houghton *et al.*, 2016). Intermediate species of sulfur, especially S^0, $S_2O_3^{2-}$ and polythionates ($S_nO_6^{2-}$ (n>2)), are important in microbial processing of sulfur, even though their concentrations in solution may be low. Indeed, these intermediate sulfur compounds are thought to be involved in the so-called "cryptic" sulfur cycle, an enigmatic process in which sulfur is recycled amongst lower state sulfur species that is not well characterized to date (Thamdrup *et al.*, 1994; Jørgensen and Nelson, 2004; Canfield *et al.*, 2010; Houghton *et al.*, 2016).

Further, gaps in understanding of which proteins catalyze specific sulfur pathways also exist (Friedrich *et al.*, 2001; Sauvé *et al.*, 2007; Valdes *et al.*, 2011; Jones *et al.*, 2014). The literature to date indicates that some sulfur metabolic enzymes catalyze a broad suite of sulfur oxidative reactions, e.g. the Sox (sulfur oxidizing) complex, while others seem to catalyze more specific sulfur reactions, e.g. Sdo (sulfur dioxygenase) (Kelly *et al.*, 1997; Friedrich *et al.*, 2001; Rowerder and Sand, 2003; Hensen *et al*., 2006; Sauvé *et al.*, 2007; Wang *et al.*, 2019). Some microorganisms capable of sulfur oxidation can possess a suite of these genes, enabling them to carry out many different reactions, while others have a more limited set of sulfur genes, restricting them to select reactions only (Hallberg and Johnson, 2003; Ghosh and Dam, 2009; Zhu *et al*., 2012; Nuñez *et al.*, 2017). Recent works reviewing *Acidithiobacillus spp.* sulfur metabolism have identified diverse pathways for this genus dependent on the species, as well as the sulfur substrate(s) (S^0, $S_2O_3^{2-}$, $S_4O_6^{2-}$) and the different sulfur metabolism genes available to them (Wang

et al., 2019; Zhan *et al*., 2019). These studies have provided updated models for *A. caldus* and *A. ferrooxidans* based on the existing literature of studies using either genomics, proteomics or sulfur chemistry analyses. For both species, S^0 metabolism is proposed as oxidation to SO_3^{2-} via Sdo, followed by oxidation to SO_4^{2-} via the sulfate adenylyltransferase dissimilatory-type (SAT) gene (Wang *et al.*, 2019). While the $S_2O_3^{2-}$ metabolism is proposed to differ between the two species, where in *A. caldus* it is through the S_4I pathway and Sox complex, and in *A. ferrooxidans* via the S_4I pathway and thiosulfate dehydrogenase (TSD) (Wang *et al.*, 2019; Zhan *et al*., 2019). The S_4I pathway utilizing the *doxD* (thiosulfate:quinone oxidoreductase*)* and *tetH* (tetrathionate hydrolase) genes (Wang *et al.*, 2019). While further notable genes present in the sulfur metabolism for *Acidithiobacillus spp.* include the *sqr* (sulfide quinone reductase*)*, *sor* (sulfur oxygenase reductase), *rhd* (rhodanese) and the heterodisulfide reductase or Hdr-like complex (*hdrA*, *hdrB* and *hdrC*) (Ghosh and Dam, 2009; Valdes *et al.*, 2011; Jones *et al.*, 2014; Yin *et al*., 2014; Wang *et al*., 2019).

Here, the objectives were to characterize both the levels of gene expression at high resolution (RNA-Seq) for *Acidithiobacillus thiooxidans,* and the changes in sulfur speciation associated with its experimental growth on either S^0 or $S_2O_3^{2-}$ to generate models for *A. thiooxidans* sulfur metabolism. *A. thiooxidans* is a strict autotroph only able to carry out sulfur oxidation/disproportionation reactions (Figure 3.1a) and a well-studied sulfur oxidizing microorganism (Kelly *et al.*, 1997; Suzuki *et al.*, 1999; Masau *et al*., 2001; Rowerder and Sand, 2003). The model organism *A. thiooxidans* ATCC 19377 used here, encodes at least 10 known proteins or protein complexes thought to be involved in sulfur metabolism, which includes the aforementioned S_4I pathway and Sox complex in the periplasm, and the Hdr-like complex in the cytoplasm (Valdes *et al.*, 2011; Bobadilla Fazzini *et al.*, 2013; Yin *et al*., 2014) (Figure 3.1b). Our

integrated approach provides important novel insights since previous studies have designed models for this species based solely on solution chemistry (Bobadilla Fazzini *et al.*, 2013) or gene expression (Yin *et al.*, 2014).

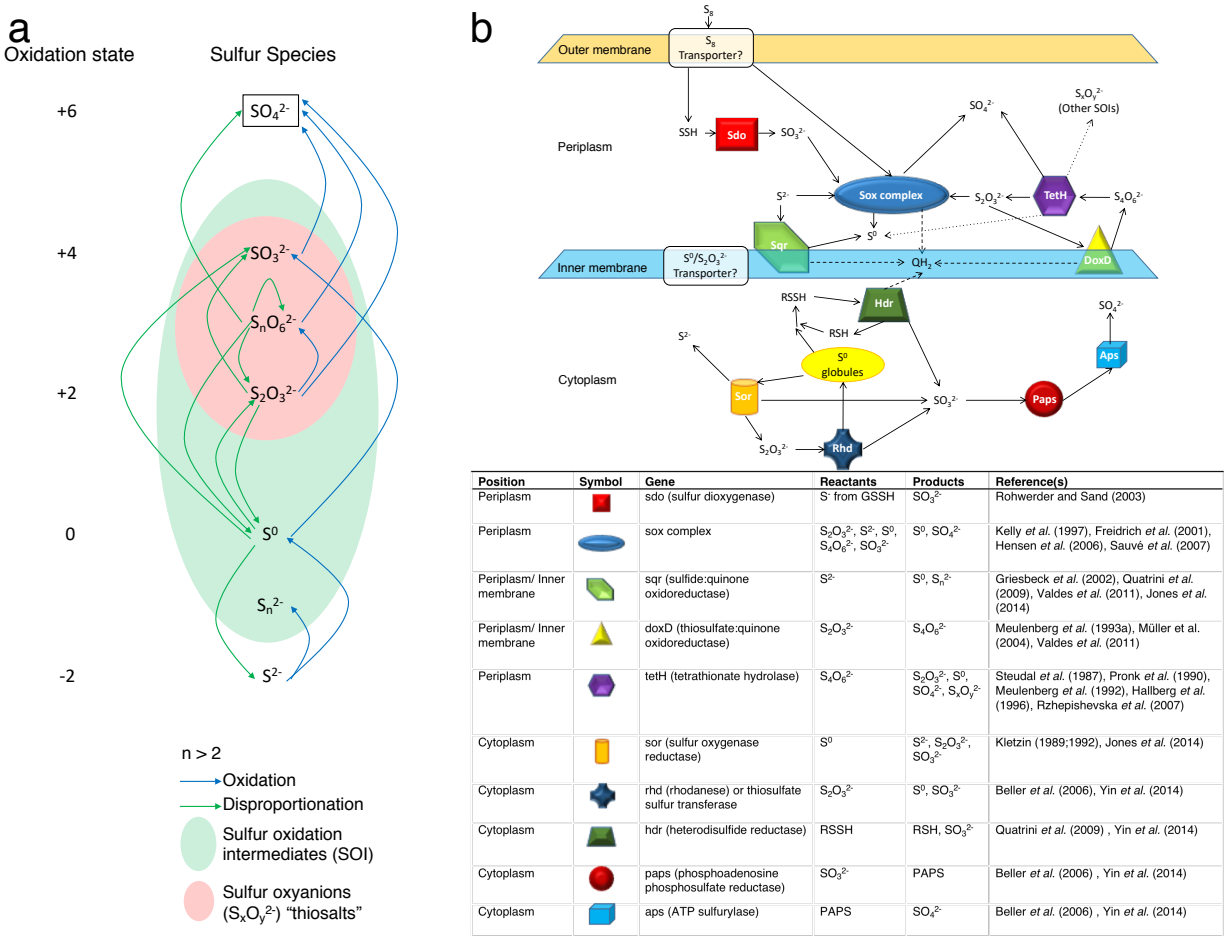

Position	Symbol	Gene	Reactants	Products	Reference(s)
Periplasm		sdo (sulfur dioxygenase)	S· from GSSH	SO_3^{2-}	Rohwerder and Sand (2003)
Periplasm		sox complex	$S_2O_3^{2-}$, S^{2-}, S^0, $S_4O_6^{2-}$, SO_3^{2-}	S^0, SO_4^{2-}	Kelly *et al.* (1997), Freidrich *et al.* (2001), Hensen *et al.* (2006), Sauvé *et al.* (2007)
Periplasm/ Inner membrane		sqr (sulfide:quinone oxidoreductase)	S^{2-}	S^0, S_n^{2-}	Griesbeck *et al.* (2002), Quatrini *et al.* (2009), Valdes *et al.* (2011), Jones *et al.* (2014)
Periplasm/ Inner membrane		doxD (thiosulfate:quinone oxidoreductase)	$S_2O_3^{2-}$	$S_4O_6^{2-}$	Meulenberg *et al.* (1993a), Müller et al. (2004), Valdes *et al.* (2011)
Periplasm		tetH (tetrathionate hydrolase)	$S_4O_6^{2-}$	$S_2O_3^{2-}$, S^0, SO_4^{2-}, $S_xO_y^{2-}$	Steudal *et al.* (1987), Pronk *et al.* (1990), Meulenberg *et al.* (1992), Hallberg *et al.* (1996), Rzhepishevska *et al.* (2007)
Cytoplasm		sor (sulfur oxygenase reductase)	S^0	S^{2-}, $S_2O_3^{2-}$, SO_3^{2-}	Kletzin (1989;1992), Jones *et al.* (2014)
Cytoplasm		rhd (rhodanese) or thiosulfate sulfur transferase	$S_2O_3^{2-}$	S^0, SO_3^{2-}	Beller *et al.* (2006), Yin *et al.* (2014)
Cytoplasm		hdr (heterodisulfide reductase)	RSSH	RSH, SO_3^{2-}	Quatrini *et al.* (2009) , Yin *et al.* (2014)
Cytoplasm		paps (phosphoadenosine phosphosulfate reductase)	SO_3^{2-}	PAPS	Beller *et al.* (2006) , Yin *et al.* (2014)
Cytoplasm		aps (ATP sulfurylase)	PAPS	SO_4^{2-}	Beller *et al.* (2006) , Yin *et al.* (2014)

Figure 3.1: **Biological sulfur capabilities and gene layout for *A. thiooxidans.*** (**a**) Biological sulfur reaction capabilities across all known sulfur species and oxidation states and **(b)** a theoretical map for the locations of sulfur genes analysed and information on potential reactants and products of these genes. Showing proven sulfur reactions in solid arrows, theorized reactions in dotted arrows and cytochrome C proton reactions in dashed arrows. Based on the referenced literature.

3.2. Materials and Methods

3.2.1 Experimental design, cell growth and counting

3.2.1.1. Experimental design

In order to jointly assess both gene expression and changes in sulfur speciation, the experimental design included collection of samples for cell counts, gene expression, microscopy, S speciation and pH for *A. thiooxidans* grown in both S^0 and $S_2O_3^{2-}$ treatments over 12 days to ensure both exponential and stationary phases were encompassed in the characterization. Greater details on collection and analyses of samples for each of these variables are provided subsequently.

3.2.1.2. Culture conditions

A. thiooxidans ATCC 19377 cells were grown in liquid elemental sulfur or thiosulfate media (Staley *et al*., 1989). The media contained two components, the salt medium and the sulfur source. Elemental sulfur salt medium: $(NH_4)_2SO_4$, 0.2g; $MgSO_4$ x 7 H_2O, 0.5g; $CaCl_2$ x 2 H_2O, 0.331g; KH_2PO_4, 3.0g; $FeSO_4$ x 7 H_2O, 9.15 mg; distilled water, 1 000ml. The salt medium was sterilized by passing through a 0.22 µm filter. Elemental sulfur powder was heated in an oven at 100ºC for 30 minutes and the cycle was repeated three times. The salt medium was then added to the culture flasks and the final sulfur concentration was 1% (m/v). Thiosulfate medium: salt medium as above and $Na_2S_2O_3$ was added at 0.2% (m/v), followed by filter sterilization (0.22 µm filter). For both cultures, the total volume of medium corresponded to a fifth of the total volume of the Erlenmeyer flask. All cultures were initially inoculated at 5% v/v with cultures pre-grown in the corresponding media; the inoculant bacteria were washed with sterile 1% NaCl solution prior to inoculation. All cultures were grown under aerobic conditions at 30ºC and flasks were shaken at 120 rpm.

3.2.1.3. Fluorescence-activated cell sorting (FACS)

Cells were harvested at the desired time points (days 1, 2, 3, 4, 5, 8, 10 and 12) and washed with 1% NaCl. Optical density (O.D.) values were determined to generate cell counts; however errors introduced by S^0 clumping precluded their use for these experiments. Thus, for the growth curves, 2 µl of the Live/Dead marker mixture of component A and component B at a ratio of 1:1 (L7012 LIVE/DEAD® BacLight, Bacterial Viability Kit, ThermoFisher Scientific) were added to 1.5 ml of bacterial suspension. The rationale behind the Live/Dead stain is that all cells will be stained green, because SYTO 9 penetrates into live and dead cells and stains their DNA, whereas propidium iodide (red stain) penetrates only into dead or damaged cells with leaky membranes staining their DNA. For the negative control (dead cells), the cells were first washed with 1% NaCl and then incubated in 70% ethanol for one hour, followed by washing with 1% NaCl. Propidium iodide (Component B) was added (0.66 µl for 1 ml of bacterial suspension). For the positive control, 0.66 µl of SYTO 9 (Component A) was added to 1 ml of bacterial suspension. All samples were incubated in the dark at room temperature for 15 minutes, followed by counting in a FACS BD Canto II instrument. Experiments were conducted in triplicates.

3.2.2. Genetic methods and analyses

3.2.2.1. DNA purification

Genomic DNA was purified from cells from 50 ml bacterial culture grown on elemental sulfur by manual cell disruption with a pestle in the presence of small glass beads (< 106 µm diameter; sufficient to form a thick paste). Genomic DNA was purified from combined washes with TE buffer (10 mM Tris, 1 mM EDTA, pH 8) following essentially the instructions of the Qiagen Genomic G20 kit, resulting in 10 µg of purified total DNA.

3.2.2.2. Illumina DNA sequencing

For paired-end Illumina sequencing (MISEQ-PE300, i.e. 300 nucleotides read length), a TruSeq library was constructed with sized DNA fragments (570 to 650 bp). The reads received from the sequencing service (McGill and Génome Québec Innovation Centre; Montréal) were cleaned from adapters and quality-clipped with the Trimmomatic software (Bolger *et al*., 2014), resulting in a total of 2 254 174 read pairs. In addition, a Nextera mate-pair library (insert size 7-8 kbp) was sequenced on two flow cells of Illumina HISEQ (rapid mode; 150 nucleotides read length), and cleaned with Trimmomatic (8 224 769 read pairs).

3.2.2.3. Genome assembly and annotation

The genome was assembled with Spades v. 3.6.1 (Bankevich et al., 2012) using a coverage cutoff value of 3.0. The resulting set of contigs was annotated with Prokka v.1.13.3 (Seemann, 2014).

3.2.2.4. Total RNA extraction

Cells were harvested on day 3 (exponential phase; pH 2.5) and 5 (stationary phase; pH 1.5) for S^0 media and day 5 (stationary phase; pH 2.5) for $S_2O_3^{2-}$ media, and washed with ice-cold NaCl 1%. They were then lysed and total RNA was extracted using the High Pure RNA Isolation Kit (Roche). Instead of 4 µl of lysozyme as indicated in the kit, 20 µl were added to efficiently break the cells. The lysozyme solution was prepared from egg white lysozyme (Bio Basic Inc; activity: 20 000 U/mg) at a final concentration of 50 mg/ml. The genomic DNA was removed using the TURBO DNA-*free*™ Kit (Ambion). The concentration of total RNA was determined using a Nanodrop instrument and the quality of the preparation was assessed by agarose gel electrophoresis to

monitor 16S and 23S ribosomal RNA. Samples were conserved at -80ºC; experiments were conducted in biological triplicates.

3.2.2.5. High-throughput RNA sequencing and bioinformatics

Sequencing was done using Illumina Hi-seq technology (100 bases paired-end). Quality controls, DNA library construction from isolated RNA and sequencing were performed at the Génome Québec Innovation Centre (Montréal, Canada). Bioinformatics analysis was done using software available on the Galaxy server (https://usegalaxy.org/) (Giardine *et al*., 2005; Blankenberg *et al*., 2010; Goecks *et al*., 2010). Full-length reads (100 bases) were trimmed so that only portion 11 to 80 of each read was conserved. Quality control of the reads was done using FastQC (Galaxy Tool Version 0.63) before and after trimming to ensure quality of the reads. The quality format was changed to "Sanger & Illumina 1.8+" using FASTQ Groomer (Galaxy Tool Version 1.0.4). Reads were mapped as paired-end using Tophat (Galaxy Tool Version 0.9). The mean inner distance between mate pairs was set to 150 bases and the standard deviation to 20. The reference genome of *A. thiooxidans* (Valdes *et al.*, 2011) was used as guide to help align the reads and the defaults parameters of Tophat were selected. Finally, differential expression was analysed using Cufflinks (Galaxy Tool Version 2.2.1.0). The "max intron length" was set to 300 000, the "min isoform fraction" was set to 0.1 and the "pre mRNA fraction" to 0.15. Cufflinks only counted fragments compatible with the reference annotation of the genome and it performed a biased correction using the genome assembly. Default Cufflinks parameters were selected.

3.2.3. Sulfur chemistry methods and analyses

3.2.3.1. Biogeochemical experiments

Nine sterile 1L flasks were prepared for batch experimentation: six containing salt medium with 1% S^0 and three with 0.2% $S_2O_3^{2-}$ culture medium, followed by *A. thiobacillus* inoculation as described above. For each treatment, one flask was sacrificed for sulfur chemical analyses from the S^0 cultures on days 0, 1, 2, 3, 4 and 5 and from the $S_2O_3^{2-}$ cultures on days 0, 2 and 4. For each sampling time, the bulk solution pH was measured (Denver Instrument Model 225, NY, USA) prior to sampling for sulfur analyses. Triplicate samples were then collected for dissolved (< 0.45 µm), total sulfur ($\sum S_{aq}$) and sulfur speciation (SO_4^{2-}, S^{2-}, $S_2O_3^{2-}$, S^0 and SO_3^{2-}) analyses as described subsequently.

3.2.3.2. $\sum S_{aq}$ – determination by ICP-AES

For total S ($\sum S_{aq}$), 40ml of water samples were filtered by Pall Acrodisc® 25mm 0.45 µm Supor® membrane via polypropylene syringes into 50ml Falcon™ tubes, followed immediately by addition of 80 µL of HNO_3 (Optima grade, Fisher Chemical) to each tube before storing at 4°C until analyses. To enable sulfur mass balance calculations, $\sum S_{aq}$ analyses were performed by inductively coupled argon plasma emission spectrometry (ICPAES) (Varian730 ES, Mulgrave, VIC) using the operating conditions recommended by the manufacturer. Sulfur calibration standards were prepared from certified reference stock solutions (AccuStandard New Haven, CT, USA) in 2 % v/v HNO_3. The limit of detection (LOD) for sulfur was 1 mg L^{-1} (calculated as three times the standard deviation of the mean blank). Subtracting the sum of all measured solution sulfur species concentrations, described subsequently (SO_4^{2-}, S^{2-}, $S_2O_3^{2-}$, S^0, and SO_3^{2-}) from the

total sulfur ($\sum S_{aq}$) concentration, allowed us to quantify the concentration of S occurring within an unresolved or "Other" SOI pool.

3.2.3.3. SO_4^{2-} and S^{2-} - determination by spectrophotometry

At each sampling time point, samples were immediately fixed and analyzed using the HACH SulfaVer 4 Method and Methylene Blue Method for SO_4^{2-} and S^{2-}, respectively (Hach company, Colorado, USA) by spectrophotometry (Pharmacia Biotech Ultrospec 3000 UV/Visible Spectrophotometer).

3.2.3.4. $S_2O_3^{2-}$, S^0 and SO_3^{2-} - determination by HPLC

Sampling and analyses for individual SOI species $S_2O_3^{2-}$, S^0 and SO_3^{2-} were concomitant with those for total S, $\sum S_{aq}$, and redox end members, SO_4^{2-} and S^{2-}. At each sampling time point, samples were taken and immediately preserved using a monobromobimane derivatization procedure for SOI analyses by HPLC (Rethmeier *et al.*, 1997). The Alltima HP C18 (5µm x 150mm x 4.6mm) reverse phase column and Shimadzu LC-20AD prominence HPLC instrument were used for all SOI analyses. Solvents used in protocols were: A=Water, B=Methanol, C=Acetonitrile, D=Acetic acid 0.25% v/v pH 3.5 adjusted with NaOH (1N). $S_2O_3^{2-}$ and SO_3^{2-} were assessed via fluorescence excitation at 380 nm and emission at 480 nm. Standards and calibrations for $S_2O_3^{2-}$ (0-10 mM) and SO_3^{2-} (0-1.7 mM) were made with $Na_2S_2O_3^{2-}$ and $Na_2SO_3^{2-}$, respectively. The thiosulfate and sulfite elution protocol was as follows: 0-1min, 1ml/min flow; 1-6 min, 1 ml/min to 0.85 ml/min flow linear gradient; 0-8 min B 35%, D 65% to B 40%, D 60% linear gradient, oven heated to 35˚C. Sample size was 5 µl and elution times were 3 min for SO_3^{2-} and 6.5 min for $S_2O_3^{2-}$. S^0 was extracted with chloroform from both filtered (<0.45 µm, i.e colloidal)

and unfiltered samples (i.e. particulate and/or colloidal) and analyzed with reverse-phase HPLC and UV-absorption at 263 nm. Standards and calibrations (0-32 mM) were made from S^0 dissolved in chloroform. S^0 elution protocol: 1 ml/min flow, B 65%, C 35% isocratic; the sample size was 10 µl and the elution time was at 5 min.

3.2.4. Microscopy and Spectroscopy analyses

3.2.4.1. Transmission electron microscopic (TEM) analysis

25 ml cultures of bacteria were grown in 1% S^0 or 0.2% $S_2O_3^{2-}$ media, respectively. Cells were sedimented and rinsed three times with 0.1 M phosphate buffer at pH 7.2 to eliminate the remaining medium. Cells were fixed with 4% paraformaldehyde (Acros organics, Morris Plains, N.J., USA) and 0.1% glutaraldehyde (Electron Microscopy Sciences, Fort Washington, Pa., USA) for 30 min at 4°C, followed by three wash with 0.1 M phosphate buffer before osmification using 1% osmium tetroxide for 1 h at room temperature. The pellets were dehydrated using a graded ethyl-alcohol series and then processed for embedding in epon (Marivac, Halifax, NS, Canada). Ultrathin sections of 80–100 nm thickness were cut with a diamond knife, collected on Formvar-carbon (polyvinyl formate) coated 200-mesh nickel grids. Sections were then stained with 2% uranyl acetate and lead citrate and examined with a FEI Tecnai 12 (Eindhoven, The Netherlands) transmission electron microscope operating at 80kV.

3.2.4.2. Energy-Dispersive X-ray Spectroscopy and Wavelength-Dispersive Spectroscopy analysis

Bacterial sections were imaged using a transmission electron microscope (Jeol JEM-2100F, JEOL Ltd, Tokyo, Japan) equipped for elemental analysis by energy-dispersive X-ray spectroscopy (EDS). In addition, a scanning electron microscope (Jeol JSM-7600F, JEOL Ltd, Tokyo, Japan)

was used for wavelength dispersive X-ray Spectroscopy (WDS) analysis to obtain a better isolation of the peaks of interest for quantitative analysis.

3.2.5. Statistical Analyses

Growth curve and pH results for the two treatments were compared by T-test analyses: paired two samples for means via Microsoft Excel 2016, with each treatment having three replicates per data point. RNA-seq analysis is a whole genome approach allowing the detection of low and highly expressed genes using the parameter fragments per kilobase of transcript per million mapped reads (FPKM), and the standard deviations between each treatment's triplicates. Further analyses on FPKM values was carried out to make pairwise comparisons using independent t-test on the FPKM between RNA-seq experiments and for the relative levels of gene expression based on Log2 values between samples for the suite of known sulfur genes: (1) across growth curve stage within the S^0 media, (2) between S^0 and $S_2O_3^{2-}$ media at the same solution pH and (3) at the same growth curve stage via Microsoft Excel 2016. The chemical relationships between the different S species and $[H^+]$ (pH) were tested using ANOVA regression statistics via Microsoft Excel 2016 and significance of p value <0.05 are stated. Intracellular S^0 globules were analyzed after TEM to determine the quantity and size of globules found inside the cells using Image J software (https://imagej.nih.gov/ij/). Manual modelling and stoichiometric balancing methodology is presented in Supplementary text .

3.3. Results

3.3.1. Growth, pH and sulfur species related to gene expression

We cultivated *A. thiooxidans* on minimal media with S^0 or $S_2O_3^{2-}$ as the source of energy. The results indicate that the organism can extract energy with equal efficiency from both compounds, as evidenced by statistically identical growth patterns for the two media ($p<0.05$) (Figure 3.2a). However, the amount of acid generated was higher in the S^0 media (final pH of 1.5 compared to 2.5 in the $S_2O_3^{2-}$ media) with a corresponding higher slope of pH decrease (0.68 vs 0.45) as compared to the results on $S_2O_3^{2-}$ media over the experimental time period (day 0-5) (Figure 3.2b). These results indicate *A. thiooxidans* catalyzes sulfur substrate-dependent metabolic reactions, which may correspondingly be reflected in differential gene induction profiles.

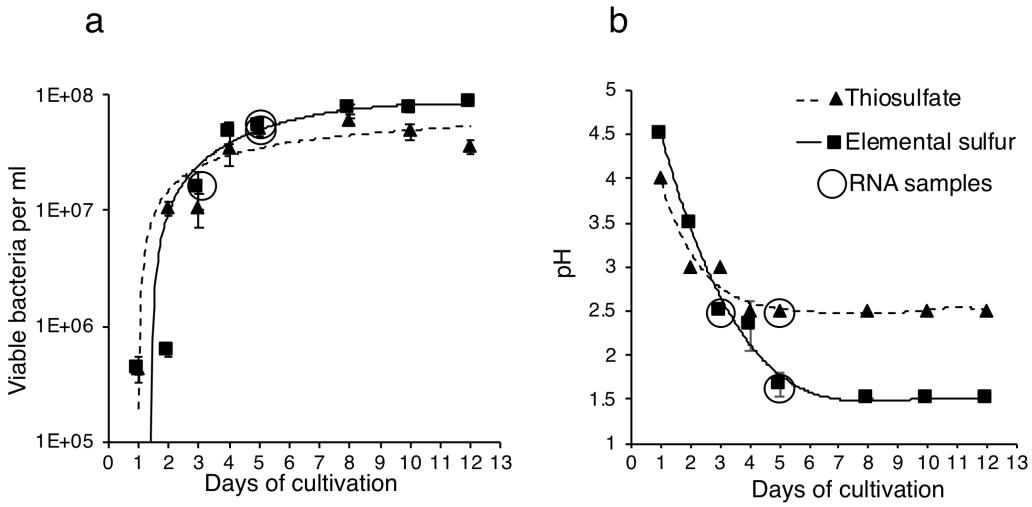

Figure 3.2: Identification of growth and changes of pH for *A. thiooxidans* grown with alternative energy sources. (**a**) Growth curves for *A. thiooxidans* grown with S^0 (squares, solid line) and $S_2O_3^{2-}$ (triangles, dotted line) as energy source. (**b**) Changes of pH in the media for *A. thiooxidans* grown with S^0 (squares, solid line) and $S_2O_3^{2-}$ (triangles, dotted line) as energy source. Time points of samples analyzed by RNA-Seq analyses are indicated by circles. The data are the result of analyses conducted in triplicates and where not visible, error bars for pH measurements were smaller than the symbols plotted for mean pH values.

3.3.2. Genomic analyses

3.3.2.1. Sequencing, assembly and annotation of the A. thiooxidans genome

To correlate the results of the analysis of sulfur species in the medium with expression of the sulfur metabolism genes using RNA-seq we first needed to generate a more robust genome sequence than the available draft version (Valdes *et al*., 2011). The published draft genome sequence (Genbank: AFOH01000000) has 164 contigs at low coverage and a total genome size of 3 019 868 bp, which may lead to incomplete transcriptome analyses. For this reason, we re-sequenced the genome of *A. thiooxidans* ATCC 19377 and Table 3.1 shows the characteristics of the assembly comprising 22 unique contigs and a total of 3 404 101 bp (almost 13% larger than previously published), with the largest contig (2 390 830 bp) spanning 70% of the total sequence. Two contigs have a highly elevated genome coverage, most likely representing circular plasmids. 27 small contigs (size range between 129 – 7 095 bp) carry polymorphic sites and are therefore not counted in the total genome size but included in the GenBank submission. This Whole Genome Shotgun project has been deposited at DDBJ/ENA/GenBank under the accession SZUV00000000. The version described in this paper is version SZUV01000000. A significantly larger fraction of RNA-seq reads (92% for all growth conditions) aligned to our new genome assembly as compared to the previous draft (29-60%) showing that the quality of assembly was greatly improved over the published GenBank record (Table 3.2). Gene annotation identified all known genes encoding enzymes of sulfur metabolism such as *sdo* (sulfur dioxygenase), the Sox (sulfur oxidation) complex (*soxA*, *soxB*, *soxX*, *soxY* and *soxZ)*, *sqr* (sulfide quinone reductase*)*, *doxD* (thiosulfate:quinone oxidoreductase*)*, *tetH* (tetrathionate hydrolase), *sor* (sulfur oxygenase reductase), *rhd* (rhodanese), the heterodisulfide reductase (*hdrA*, *hdrB* and *hdrC)*, *paps* (phosphoadenosine phosphosulfate reductase*)* and *aps* (ATP sulfurylase) (Figure 3.3,

Supplemental Tables S1-4) (Kletzin, 1989; Kletzin, 1992; Griesbeck et al., 2002; Rzhepishevska *et* al., 2007; Valdes *et al*., 2008; Quatrini *et al*., 2009; Valdes *et al*., 2009; Mangold *et al*., 2011; You *et al*., 2011). The genome contains three copies of *sdo,* two operons encoding the Sox complex, two copies of *rhd* and three copies of *hdrA*. The plasmids apparently do not code for genes that are of interest in this context, with the potential exception of a gene for a "divalent metal cation transporter" (MntH), which may have been recruited via a plasmid to manage the high metal ion concentrations in its natural environment.

Table 3.1: Assembly and annotation of the *Acidithiobacillus thiooxidans* genome ATCC 19377.

Characteristic	**Value**
Total genome size	3 404 101 bp
Total number of unique contigs (including two potential circular plasmids)	22
Largest contig	2 390 830 bp
Contigs carrying polymorphisms	27
Average % GC	52.6
Number of tRNA genes	64
Number of rRNA genes	4
Total number of coding sequences	3 505
Number of proteins with known function	2 242
Number of hypothetical proteins	1 263

Table 3.2: Comparison of the percentage of concordant pair alignments between RNA-seq data and the new assembly of the *A. thiooxidans* ATCC 19377 genome and the published draft genome with 164 contigs.

Genome	Elemental sulfur pH 2.5	Elemental sulfur pH 1.5	Thiosulfate pH 2.5
44 contigs genome	92.1	92.3	92.4
164 contigs genome	59.5	29.5	56.8

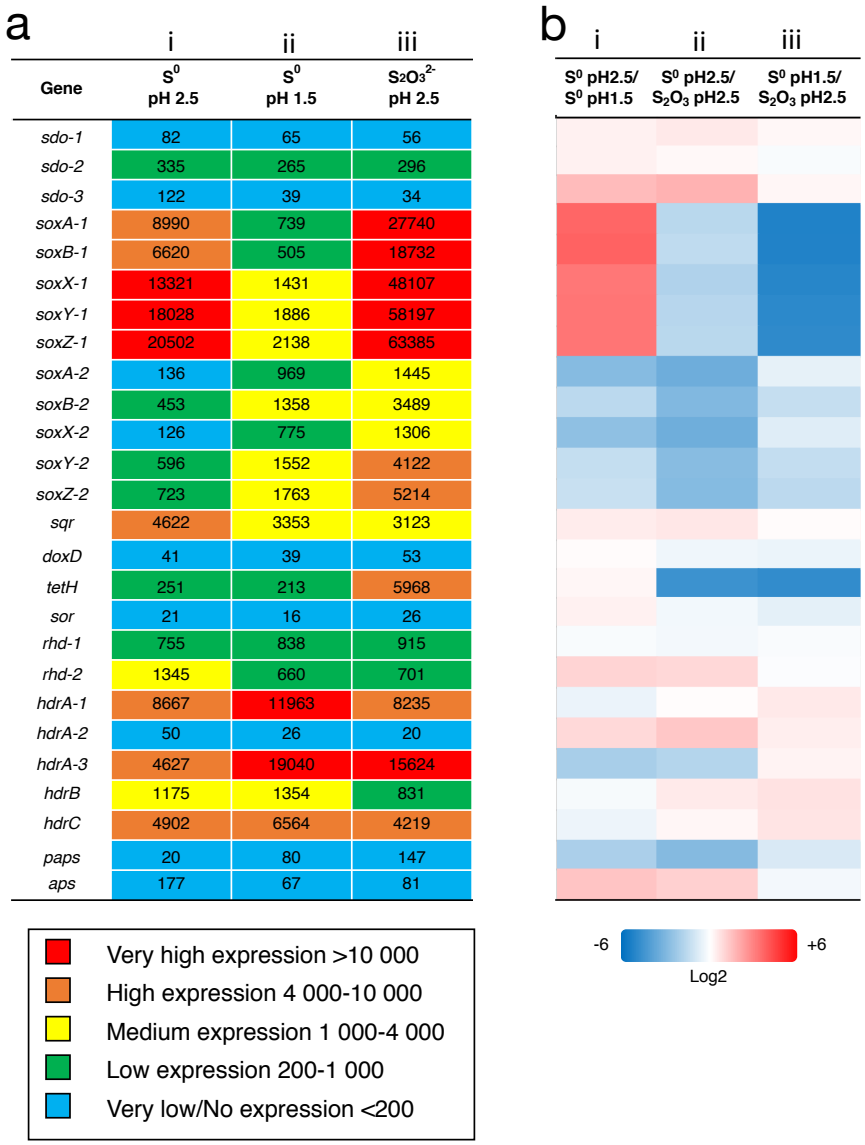

Figure 3.3: Analysis of gene expression after growth with S^0 or $S_2O_3^{2-}$ as energy source. (**a**) Gene expression based on FPKM values was analyzed after growth on S^0 to (i) pH-value 2.5 and at (ii) 1.5 and on (iii) $S_2O_3^{2-}$ to pH-value 2.5. Color scale against indicates relative expression values with blue very low, green low, yellow intermediate, orange high and red very highly expressed genes. **(b)** Comparative gene expression for FPKM values based on Log2 ratio. (i) Growth on same substrate (S^0) at different points on pH and growth curve (pH 2.5 = day 3 / pH 1.5 = day 5), (ii) growth to same pH (2.5) on different substrates and points on growth curve (S^0 = day 3 / $S_2O_3^{2-}$ = day 5), (iii) growth until day 5 on different substrates and to different pH values (S^0 = pH 1.5 / $S_2O_3^{2-}$ = pH 2.5). Color scale against each comparison test based on Log2 values; blue = -6 (i.e., numerator expressed less than denominator), white = 0 (i.e., expression equal), red = +6 (i.e., numerator expressed more than denominator).

3.3.2.2. Expression analysis of the sulfur metabolism genes using RNA-Seq

For transcriptome analysis, we collected total RNA from cultures of *A. thiooxidans* grown on elemental S^0 and on $S_2O_3^{2-}$ media (three biological replicates) to compare gene expression on two differing oxidation state sulfur substrates. RNA-Seq analysis is a whole genome approach allowing the detection of low and highly expressed genes using the parameter fragments per kilobase of transcript per million mapped reads (FPKM) (Sequence Read Archive (SRA) accession: PRJNA541131). To assess the quality of mapping of the RNA-Seq sequences on the genome assembly, we compared the percentage of concordant pair alignments using the same raw RNA-Seq data and the two available genomes (our new assembly and the previously published draft genome (Valdes *et al*., 2011)). We observed an increase of more than 30% of the total concordant pair alignments of the RNA-Seq data for the newly assembled genome for each individual sample as compared to the draft (Table 3.2). These data underline the quality of the new genome assembly that was used for all the following analyses. A direct representation of the FPKM values, i.e. relative expression levels for the three growth conditions (exponential and stationary growth phases on S^0 and stationary growth phase on $S_2O_3^{2-}$) is shown in Figure 3.3a. FPKM values under 200 are interpreted as low to no expression, as compared to low expression (200 - 1 000 FPKM), medium expression (1 000 - 4 000 FPKM), high (4 000 - 10 000 FPKM), and very highly expressed (more than 10 000 FPKM).

The genes encoding the Sox complex (*soxA*, *B*, *X*, *Y*, *Z*) are generally highly expressed, but interestingly the relative expression of the two *sox* operons changes during growth on elemental sulfur at pH 2.5 (day 3) and pH 1.5 (day 5); *sox-1* strongly decreases and *sox-2* increases to medium levels). In contrast, the *sox-1* operon is very highly expressed during growth on $S_2O_3^{2-}$ and we also

observe medium to high expression of the *sox-2* operon showing the importance of the gene products under this condition.

The *sqr* gene is medium to highly expressed in all three conditions at comparable levels suggesting that the gene product sulfide quinone reductase also plays an important role in *A. thiooxidans* S metabolism. Other genes are relatively weakly expressed, and whereas there is some variation of gene expression, it is difficult to assess whether they provide major contributions to sulfur metabolism under these conditions (*aps*, *doxD*, *sor* and *paps*). We observe low expression of the *rhd* gene and medium to very high expression of *hdrA*, *hdrB*, *hdrC* genes under all conditions. In the case of *sdo*, encoding sulfur dioxygenase required for the entry of elemental sulfur into the cell, the expression of one copy is low under all conditions, whereas two gene copies are below 200 FKPM values (Figure 3.3a).

3.3.2.3. Further pairwise expression analysis of the sulfur metabolism genes using RNA-seq

Expression of most of the *A. thiooxidans* sulfur genes (with exceptions of the *sox-2* operon, *hdr,* all but *hdrA-2,* and *paps* genes) was higher on day 3 during exponential growth on S^0 media, as compared to day 5 when cells were in the stationary phase (Figure 3.3b-i). It thus appears that *A. thiooxidans* exhibits greater metabolic variability in the genes involved, producing higher oxidation state sulfur species (e.g. polythionates) (Figure 3.1a), during exponential phase, which shifts during stationary phase to a greater processing of polythionates and decreasing pH values (Figure 3.2). In addition, *hdrA-1* and *hdrA-3* expression strongly increases at pH 1.5 as compared to pH 2.5 during growth on sulfur, suggesting an increased importance of heterodisulfide reductase in the late growth phase. In contrast, the tetrathionate hydrolase encoding gene (*tetH*) is highly

expressed only during stationary growth on thiosulfate (day 5), suggesting that this protein plays a specific role in growth on this SOI compound.

A. thiooxidans gene expression also differed between the two growth media, when an identical pH of 2.5 had been reached. Higher expression levels of the *sox* complex, *tetH*, *hdrA-3* and *paps* genes were observed for growth on $S_2O_3^{2-}$ (day 5, stationary phase), whilst higher expression levels of the all the *sdo* copies, *sqr*, *rhd-2*, *aps* and all the *hdr* genes except *hdrA-3* were observed during growth on S^0 (day 3, exponential phase) (Figure 3.3b-ii). Gene expression levels also differed for day 5 (stationary phase) for *A. thiooxidans* growth in the two sulfur media (Figure 3.3b-iii): all sulfur genes with the exceptions of *sdo-1, sdo-3, sqr* and all *hdr* genes were more highly expressed when grown on $S_2O_3^{2-}$ compared to growth on S^0.

3.3.2.4. Genome wide analysis of gene expression

While the analysis of sulfur genes is vital to the comprehension of autotrophic metabolism, the analysis of the complete transcriptome may lead to the identification of genes that are correlated with this metabolic adaptation. To this effect, we conducted pairwise comparisons of relative gene expression levels (FPKM values) to identify additional up- and down-regulated genes. Analysis of gene expression after growth on elemental sulfur at pH 2.5 compared to pH 1.5 (Supplementary Figure S1a), showed that 20% of the genes (660) are upregulated and 12% (404) are downregulated. The top 50 upregulated genes with the highest degree of differential expression are presented in Supplementary Table S5; several of these genes encode chemotaxis and flagellar components. We also analyzed the top 50 downregulated genes and most encode hypothetical proteins (Supplementary Table S6). Analysis of gene expression after growth on elemental sulfur at pH 2.5 compared to thiosulfate pH 2.5 (Supplementary Figure S1b), shows that 18% (594) are

upregulated and 8% (269) are downregulated. The top 50 upregulated genes comprise genes encoding chemotaxis components as well as ATP synthase subunits (Supplementary Table S7). We analyzed the top 50 downregulated genes finding hypothetical proteins as well as transcription factors involved in osmoregulation as well as proteins cytochrome C biogenesis among them (Supplementary Table S8). Finally, analysis of gene expression after growth on thiosulfate at pH 2.5 compared to elemental sulfur at pH 1.5 (Supplementary Figure S1c) shows that 8% of the genes are upregulated (271) and 11% are downregulated (347). The top 50 upregulated genes comprise genes encoding components of cytochrome C biogenesis and of proteins involved in protein folding and outer membrane stability (Supplementary Table S9). Analysis of the top 50 downregulated showed that most encode hypothetical proteins (Supplementary Table S10). Further discussion on these broader metabolic characteristics can be found in Supplemental text.

3.3.3. Insights into sulfur pathways catalyzed by A. thiooxidans grown on S^0 and $S_2O_3^{2-}$

Consistent with the notion that *A. thiooxidans* catalyzes sulfur substrate-dependent metabolic reactions suggested by differential acid production (Figure 3.2), solution sulfur speciation also differed in the two growth media (Figure 3.4). *A. thiooxidans* growth on S^0 resulted in relatively higher concentrations of produced *Other SOI*, (i.e. unresolved S species; 25.3 mM versus 6.9 mM on $S_2O_3^{2-}$) and SO_4^{2-} (13.7 mM versus 7.8 mM on $S_2O_3^{2-}$; Figure 3.4a, b), while growth on $S_2O_3^{2-}$ resulted in near equal generation of *Other SOI*, sulfate and S^0 (Figure 3.4a, b). Further, S^{2-} and SO_3^{2-} were largely non-detectable in solution, with the exception of a very low amount of SO_3^{2-} on day 5 in the S^0 growth experiment, (Supplementary Table S11), while both sulfur species were detected at low concentrations (<0.5 mM) throughout growth on $S_2O_3^{2-}$ (Supplementary Table S11).

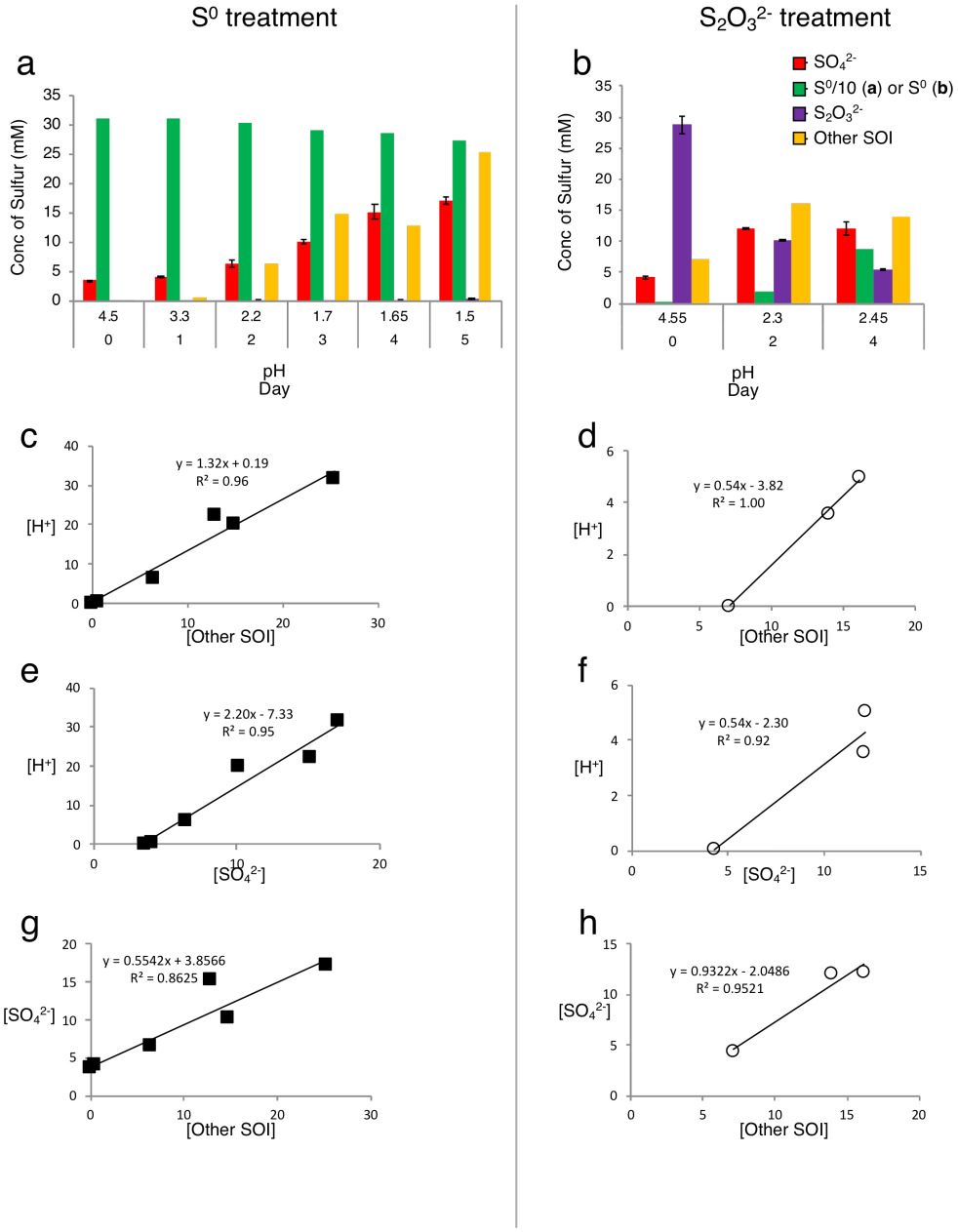

Figure 3.4: **Analysis of sulfur chemistry after growth with S^0 or $S_2O_3^{2-}$ as energy source.** *A. thiooxidans* was cultivated with different substrates for up to 5 days, followed by determination of the production of different sulfur species in the media and comparison of $[H^+]$ production to S species on S^0 media (filled squares) and $S_2O_3^{2-}$ media (empty circles). (**a**) Production of sulfur species during growth on S^0. (**b**) Production of sulfur species during growth on $S_2O_3^{2-}$. (**c-d**) $[H^+]$ production vs [Other SOI], (**e-f**) $[H^+]$ production vs $[SO_4^{2-}]$, (**g-h**) $[SO_4^{2-}]$ production vs [Other SOI]. **Note** the difference in S^0 concentration scale between figures, where in (**a**) the value shown is in 1/10 actual value. Concentrations of all S species are given in mM in mol of S (e.g. 1 mM of SO_4^{2-} = 1 mm S, while 1 mM $S_2O_3^{2-}$ = 2 mM S).

Sulfur mass balance identified that concentrations of unresolved sulfur species, *Other SOI*, occurred at appreciable levels under both growth conditions (Figure 3.4a, b). This *Other SOI* pool may variably comprise a number of possible sulfur intermediate oxidation compounds, such as species associated with oxidation pathways, i.e. polythionates, as well as products of disproportionation reactions, i.e., polysulfides. While our results do not identify the specific species sulfur species occurring within this pool, insights provided through analysis of the relationships between changes in (1) [*Other SOI*] and (2) [SO_4^{2-}] to [H^+] (Figure 3.4c-h), suggest that the unresolved sulfur species differ in their composition between the two growth treatments. The high correlations and statistical significance (p-value <0.05) for Figures 3.4c-h assist in providing a strong rationale for the basis of stoichiometric reactions occurring in the respective sulfur substrates individual metabolism. The higher slopes observed during growth on S^0 (Figure 3.4c and e) alongside the greater overall H^+ generation (10-fold higher total H^+ increase) imply greater overall oxidation compared to growth on $S_2O_3^{2-}$ (Figure 3.4d and f; Supplementary Figure S2a). During growth on S^0, a decrease in ΔS^0, and increases in both Δ*Other SOI* and ΔSO_4^{2-} imply that S^0 is first converted to higher oxidation state SOI, e.g. polythionate species, and ultimately to SO_4^{2-} (Supplementary Figure S2a); consistent with predominantly oxidative (i.e. acid generating) pathways (i.e. Eq 2-6; Table 3.3). During growth on $S_2O_3^{2-}$, Δ*Other SOI* and ΔSO_4^{2-} increase from day 0-2, while, Δ*Other SOI* subsequently decreases and ΔSO_4^{2-} does not change from day 2-4 (Supplementary Figure S2b), These results are consistent with oxidative pathways occurring initially (i.e. Eq 5, 6, 9 and 10; Table 3.3), followed by disproportionating pathways (eg. Eq 11; Table 3.3; as shown further and in Supplementary text), reflected in an increase in ΔS^0. Consistent with a potential shift from oxidative (i.e. greater acid generating) to disproportionating reactions

dominating, $\Delta[H^+]$ increased between day 0-2, and subsequently decreased from day 2-4 (Supplementary Figure S2b).

Table 3.3: Mass balance S reactions for the two treatments and potential S abiotic and biotic reactions important for stoichiometric balancing.

Formula	Eq #	Reference
$6S^0 \rightarrow 2SO_4^{2-} + 4S^{Other\ SOI} + 5H^+$	1	This paper, S^0 treatment day 0-5
$S^0 + O_2 + H_2O \rightarrow SO_3^{2-} + 2H^+$	2	Based on Suzuki (1999)
$SO_3^{2-} + 0.5O_2 \rightarrow SO_4^{2-}$	3	Based on Suzuki (1999)
$S^0 + SO_3^{2-} \leftrightarrow S_2O_3^{2-}$	4	Based on Johnston and McAmish (1973); Suzuki (1999)
$2S_2O_3^{2-} + 0.5O_2 + 2H^+ \rightarrow S_4O_6^{2-} + H_2O$	5	Based on Suzuki (1999)
$S_4O_6^{2-} + 3.5O_2 + 3H_2O \rightarrow 4SO_4^{2-} + 6H^+$	6	Based on Suzuki (1999)
$37S_2O_3^{2-} + 0.5SO_3^{2-} \rightarrow 7S^0 + 31.5SO_4^{2-} + 36S^{Other\ SOI} + 20H^+$	7	This paper, $S_2O_3^{2-}$ treatment day 0-2
$3S_2O_3^{2-} \rightarrow 2S^0 + 2SO_4^{2-} + 2S^{Other\ SOI} + H^+$	8	This paper, $S_2O_3^{2-}$ treatment day 0-4
$SO_3^{2-} + H_2O \rightarrow SO_4^{2-} + 2H^+$	9	Based on Suzuki (1999)
$S_4O_6^{2-} + H_2O \rightarrow S_3O_3^{2-} + SO_4^{2-} + 2H^+$	10	Based on Pronk *et al.* (1990); Suzuki (1999)
$4S_3O_3^{2-} \rightarrow 8S^0 + 4SO_3^{2-}$	11	Based on Steudel *et al.* (1987); Pronk *et al.* (1990)

3.3.4. Electron microscopic and spectroscopic analyses of intracellular S^0 storage

Transmission electron microscopy in tandem with energy-dispersive X-ray spectroscopy (EDS) and wavelength dispersive spectroscopy (WDS) revealed sulfur globule formation in the cells (Figure 3.5a-h). The globules did not differ in size (Supplementary Figure S3), but quantification

indicated that a higher number (45.6 per 100 bacteria) were observed for *A. thiooxidans* grown on S^0, while a lower number of internal S^0 globules (13.5 per 100 bacteria) occurred for *A. thiooxidans* grown on $S_2O_3^{2-}$ (Figure 3.5a and b vs 3.5c and d), consistent with sulfur speciation and mass balance results (Supplementary Table S12).

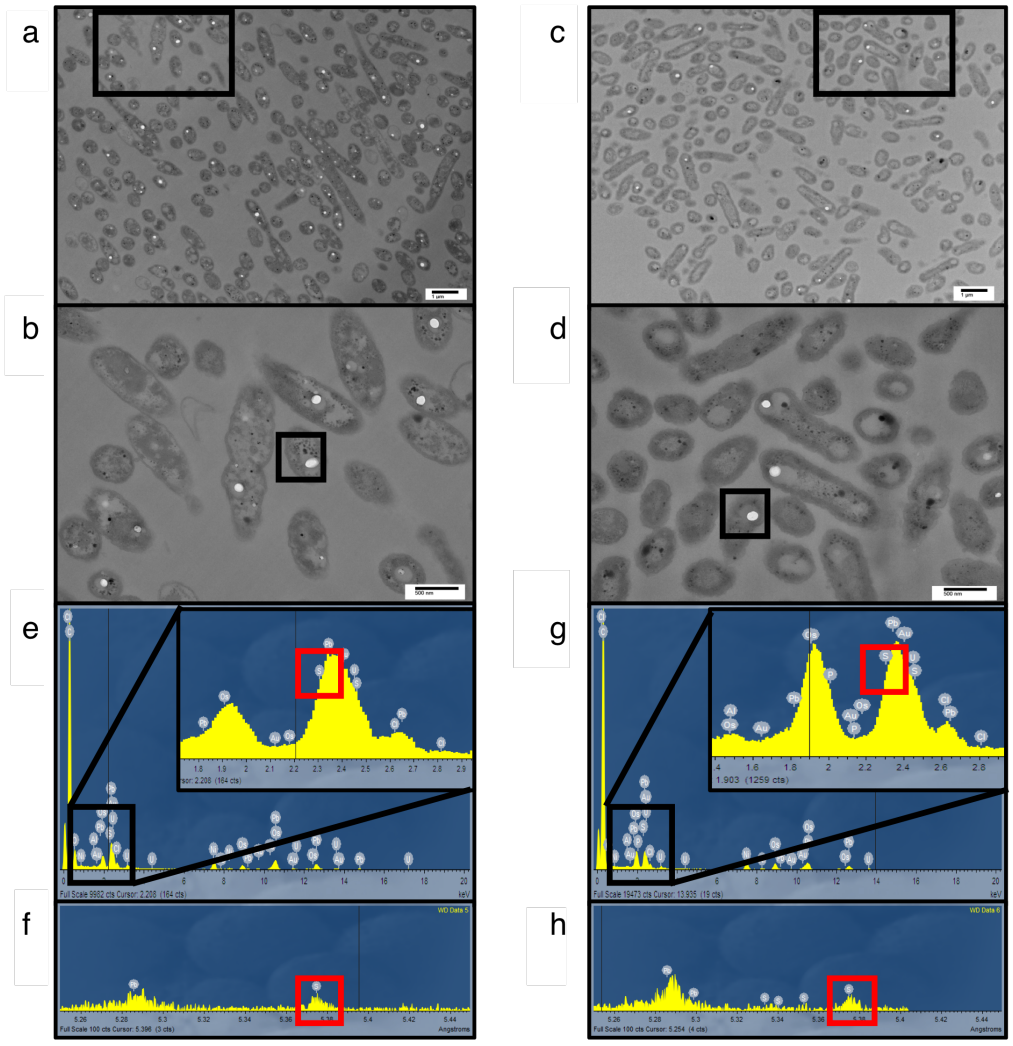

Figure 3.5: **Electron microscopic analysis of sulfur globule formation.** (**a-d**) Transmission Electron microscopy of *A. thiooxidans* cells grown in S^0 media at pH 1.5 or 2.5 (**a, b**) and $S_2O_3^{2-}$ media at pH 2.5 (**c, d**), respectively. Scale bars in **a**) and **c**) indicate 1 µm and 500 nm in **b**) and **d**). **(e, g)** Energy-dispersive X-ray spectroscopy (EDS) analysis was conducted on the sulfur globules indicated in **b**) and **d**), revealing the presence of different elements shown by their characteristic emission energies. **(f, h)**: To better separate the signals, wavelength-dispersive X-ray spectroscopy (WDS) analysis was conducted on the sulfur globules indicated in **b**) and **d**), confirming the presence of sulfur.

3.3.5. Sulfur metabolism models

3.3.5.1. Stoichiometric sulfur metabolism arrays

We developed *A. thiooxidans* metabolism models by combining observed solution S speciation and [H^+] changes with FPKM gene expression levels to elucidate the most likely pathways being catalyzed. The generated *A. thiooxidans* S^0 metabolism model identifies conversion of S^0 into 1/3 SO_4^{2-} and 2/3 $S^{Other\ SOI}$ (Eq 1; assumption of initial *Other SOI* generated to be $S_4O_6^{2-}$; the initial metabolism reaction from $S_2O_3^{2-}$ (Eq 5, Table 3.3)). While there are uncertainties as to whether the *Other SOI* pool is solely polythionate species and/or comprises the same polythionates at any given sampling point in either treatment, the highly significant correlations between acid generation and this specific sulfur pool (Figure 3.4g and h) are consistent with this assumption (Eq 1, 7 and 8 Table 3.3; Figure 3.6a, b and c, respectively).

$$6S^0 \rightarrow 2SO_4^{2-} + 4S^{Other\ SOI} + 5H^+ \qquad \text{(Table 3.3, Eq 1)}$$

Thus our *A. thiooxidans* S^0 metabolism model identifies the following suite of reactions occur throughout the time course of the experiment (Figure 3.6a).

$$S^0 + O_2 + H_2O \rightarrow SO_3^{2-} + 2H^+ \qquad \text{(Table 3.3, Eq 2)}$$

$$SO_3^{2-} + 0.5O_2 \rightarrow SO_4^{2-} \qquad \text{(Table 3.3, Eq 3)}$$

$$S^0 + SO_3^{2-} \leftrightarrow S_2O_3^{2-} \qquad \text{(Table 3.3, Eq 4)}$$

$$2S_2O_3^{2-} + 0.5O_2 + 2H^+ \rightarrow S_4O_6^{2-} + H_2O \qquad \text{(Table 3.3, Eq 5)}$$

The model stoichiometrically balances the observed changes in elemental sulfur concentration. However, the model predicts a greater acid generation than observed. Specifically, the model predicts production of $6H^+$ for every $6S^0$ converted to $2SO_4^{2-}$ and 4S (as *Other SOI*); whereas we observe $5H^+$. The same observed lower H^+ generation relative to expected, also occurs for a model

incorporating successive oxidative processing of sulfur by an alternative set of pathways that would exclude SO_3^{2-} oxidation to SO_4^{2-} (Eq 3), and proceed via oxidation of $S_2O_3^{2-}$ and $S_4O_6^{2-}$ and other polythionates to SO_4^{2-} (Table 3.3, Eq 5 and 6).

$$S_4O_6^{2-} + 3.5O_2 + 3H_2O \rightarrow 4SO_4^{2-} + 6H^+ \qquad \text{(Table 3.3, Eq 6)}$$

A stoichiometrically balanced sulfur and H^+ model of *A. thiooxidans* $S_2O_3^{2-}$ metabolism developed for day 0-2 or for the entire time course of day 0-4 (Table 3.3; Eq 7 and 8, respectively) identifies the most likely occurring reactions would include conversion of $S_2O_3^{2-}$ to SO_3^{2-}, S^0 and polythionates (*Other SOI*) and ultimately to SO_4^{2-}, with the reverse of Eq 4 followed by Eq 3, 5, 6 and 9 as the dominant reactions (Table 3.3) (Figure 3.6b).

$$37S_2O_3^{2-} + 0.5SO_3^{2-} \rightarrow 7S^0 + 31.5SO_4^{2-} + 36S^{\text{Other SOI}} + 20H^+ \qquad \text{(Table 3.3, Eq 7)}$$

$$3S_2O_3^{2-} \rightarrow 2S^0 + 2SO_4^{2-} + 2S^{\text{Other SOI}} + H^+ \qquad \text{(Table 3.3, Eq 8)}$$

$$SO_3^{2-} + H_2O \rightarrow SO_4^{2-} + 2H^+ \qquad \text{(Table 3.3, Eq 9)}$$

However, the $S_2O_3^{2-}$ metabolism model of *A. thiooxidans* for day 2-4 indicates disproportionation of $S_4O_6^{2-}$ and $S_3O_3^{2-}$ to S^0 and SO_3^{2-} are occurring (Table 3, Eq 10 and 11).

$$S_4O_6^{2-} + H_2O \rightarrow S_3O_3^{2-} + SO_4^{2-} + 2H^+ \qquad \text{(Table 3.3, Eq 10)}$$

$$4S_3O_3^{2-} \rightarrow 8S^0 + 4SO_3^{2-} \qquad \text{(Table 3.3, Eq 11)}$$

These disproportionation reactions would recycle sulfur back to $S_2O_3^{2-}$, continuing to consume H^+ via regenerated reduced SOI species such as $S_2O_3^{2-}$ and S^0 over the time period of day 2-4. $S_2O_3^{2-}$ model reaction arrays (Figure 3.6b and c) can also be stoichiometrically balanced via other pathways involving oxidation of polythionates and thiosulfate to sulfate. However, informed by gene expression, results, S metabolism for day 0-2 and day 2-4 is more consistent with the reactions identified above. The most robust model for day 0-4 based on currently theorized/known sulfur

reactions follows the series of reactions shown in Figure 3.6c, identifying the important formation and accumulation of S^0. Stepwise reactions for Figure 3.6 are identified in Supplementary text.

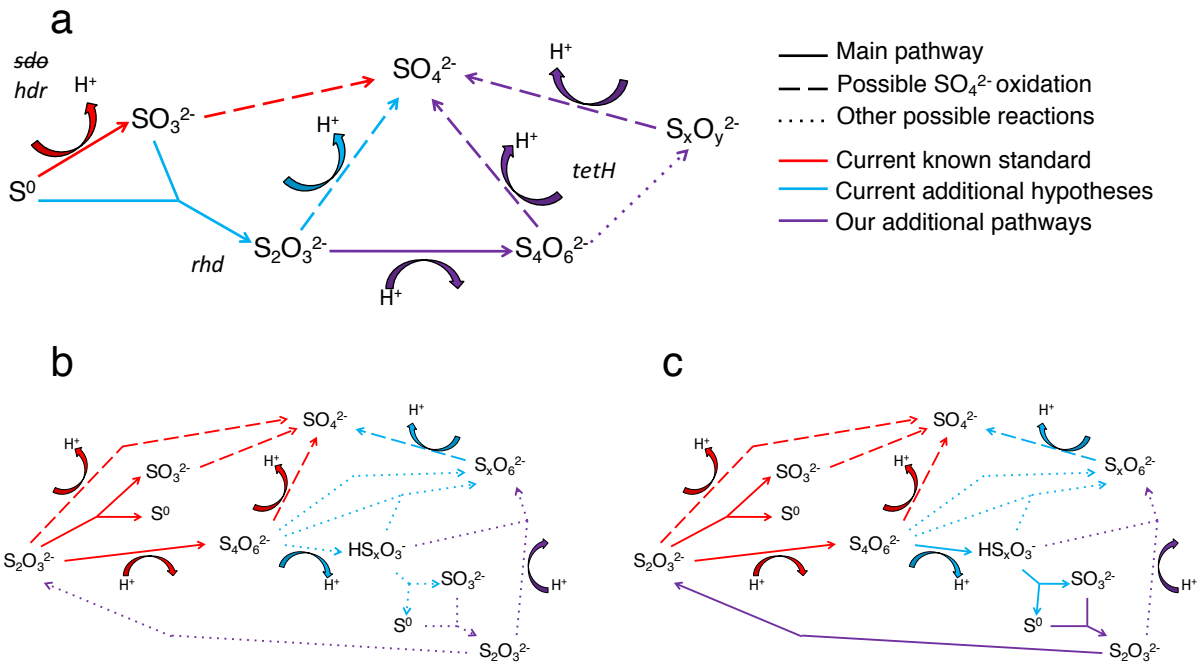

Figure 3.6: **Models of theorized *A.thiooxidans* metabolism for different S reaction pathways, the genes catalysing them and H^+ consumption or production reactions based on observed experiments' mass balance and known potential reactions in literature.** (**a**) S^0 initial reduced S source over total time of experiment (Day 0-5). (**b**) $S_2O_3^{2-}$ initial reduced S source early reactions (day 0-2). (**c**) $S_2O_3^{2-}$ initial reduced S source for total time of experiment (day 0-4). **Note** SO_3^{2-} can be oxidized both biotically via H_2O releasing H^+ and abiotically via O_2 which is neutral.

3.3.5.2. Models of A. thiooxidans S^0 and $S_2O_3^{2-}$ metabolism

By combining the analysis of gene expression, solution sulfur speciation and electron microscopy, our results provide new insights into *A. thiooxidans* sulfur metabolism revealing the importance of intracellular pathways. Based on these data we propose models for the metabolism of *A. thiooxidans* grown on S^0, (Figure 3.7a and b) suggesting that the Sox complex plays a major role initiating metabolism after entry of S^0 into the cell via unknown transporters. There is little

published information on the transport of S^0 into cells to date, however, it has been postulated by other studies to occur via outer membrane proteins (Sugio *et al*., 1991; Buonfiglio *et al*., 1999; Rohwerder and Sand, 2003). Sdo is not highly expressed, but it may also contribute to S^0 metabolism. The intracellular S^0 is metabolized subsequently through both oxidative and comproportionating pathways. Cytoplasmic Hdr catalyzes S^0 oxidation generating intracellular SO_3^{2-}. While it is not certain which gene(s) are involved in intracellular S^0 comproportionation and buildup of sulfur granules, the high expression of genes responsible for SO_3^{2-} production (*hdr*) yet low concentrations in bulk solution, suggest that this pathway generates $S_2O_3^{2-}$. We believe that this pathway is active, because we observe medium-level expression of Rhd known to catalyze $S_2O_3^{2-}$ disproportionation (Figure 3.7a), possibly acting in a reverse reaction utilizing the high intracellular S^0 and SO_3^{2-} to produce $S_2O_3^{2-}$, which is then oxidized to higher order S species (e.g. tetra- and other polythionates). This possibility is consistent with the observed increased concentration of the *Other SOI* pool and ultimately SO_4^{2-} (Figure 3.4a). These higher oxidation state S species (i.e. $S_4O_6^{2-}$ and/or other higher chain polythionates represented, we believe, in the *Other SOI* fraction based on S speciation, $[H^+]$ changes and gene expression results presented above) generated through S^0 comproportionation are oxidized through TetH catalysis resulting in SO_4^{2-}. The observed increase in Hdr expression from exponential growth (Figure 3.7a) to stationary growth (Figure 3.7b) supports the notion that this pathway would catalyze growth through intracellular recycling of sulfur, and implies the synthesis of sulfur storage granules.

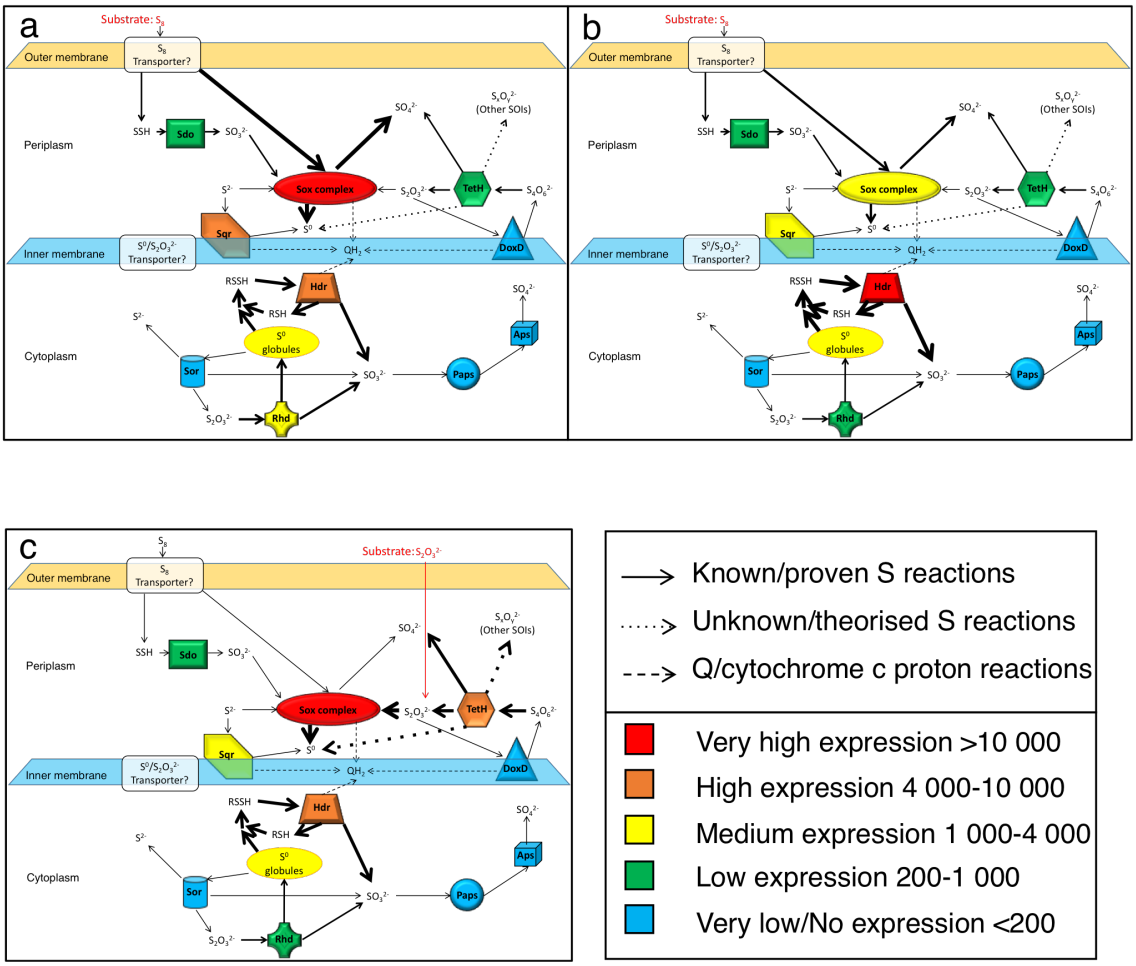

Figure 3.7: **Model of *A. thiooxidans* S metabolism based on the analyses of the expression of key genes encoding S-metabolizing enzymes and of S solution chemistry.** Gene expression values are based on the results shown in Figure 3.3a (FPKM). (**a**) Model for exponential growth phase in S^0 media (day 3, pH 2.5); (**b**) model for stationary growth phase in S^0 media (day 5, pH 1.5); (**c**) model for stationary growth phase in $S_2O_3^{2-}$ media (day 5, pH 2.5); models taking results of gene expression analysis and sulfur chemistry into account. Thickness of the arrows reflects importance of the pathways.

The model for growth of *A. thiooxidans* on $S_2O_3^{2-}$ implies that the Sox complex catalyzes $S_2O_3^{2-}$ disproportionation to S^0 and SO_4^{2-} (Figure 3.7c), while TetH catalyzes oxidation and conversion of $S_4O_6^{2-}$ to other higher chain polythionates (consistent with detection of *Other SOI,* which would include these unresolved S compounds (Figure 3.4b)). These higher oxidation S compounds are

then disproportionated via the Sox complex and/or TetH catalysis, resulting in intracellular S^0, and the subsequent intracellular generation of SO_3^{2-} indicated to occur by the high level of Hdr expression (Figure 3.7c). Comproportionation reforming $S_2O_3^{2-}$ from the high intracellular S^0 and SO_3^{2-}catalyzed by Rhd may also be possible, thereby recycling S within the cell. Alternatively, the low levels of expression of DoxD (Figure 3.3a), suggest that either TetH may be catalysing a reverse reaction from $S_2O_3^{2-}$ to $S_4O_6^{2-}$ (or to *Other SOI*), or there may be other proteins responsible for $S_2O_3^{2-}$ oxidation to higher chain polythionates.

3.4. Discussion

3.4.1. Novel insights into S-metabolism: Importance of S^0, $S_2O_3^{2-}$, SO_3^{2-} and intracellular reactions

3.4.1.1. Comparisons to previous literature

The models of *A. thiooxidans* sulfur metabolism that were developed through integrated analysis of gene expression, sulfur chemistry, sulfur mass balance and electron microscopy reveal new insights into the importance of intracellular reactions involving TetH- and Hdr-catalyzed transformation of S^0 into SO_3^{2-} species, compared to previous models. Bobadilla Fazzini *et al.* (2013) analyzed the solution concentrations of two sulfur species, S^0 and $S_2O_3^{2-}$, for *A. thiooxidans* DSM 17318 at stationary phase when grown in S^0 and $S_4O_6^{2-}$ media at low pH (1.8 and 2.5, respectively). Their chemically based model identified the same comproportionation reaction involving S^0 and SO_3^{2-} to form $S_2O_3^{2-}$ (Eq 4; Table 3.3) as identified here for *A. thiooxidans* S^0 growth. However, they speculated that Sdo was the most important protein for SO_3^{2-} production, while our results are more consistent with the Hdr protein catalyzing this reaction. Further, their S^0 metabolism model does not account for activity of the TetH enzyme, resulting in less S^0 storage and *Other SOI* (e.g. polythionates) production. Bobadilla Fazzini *et al*. (2013) also modelled *A. thiooxidans* growth on $S_4O_6^{2-}$ and suggest, based only on their chemical analyses of S^0 and $S_2O_3^{2-}$ that S^0 production from polythionates occurs with no involvement of TetH. In contrast, our combined chemical and gene expression results assessing *A. thiooxidans* growth on $S_2O_3^{2-}$, show that TetH is highly expressed (Figure 3.7c) and associated with the evident production of intracellular S^0 determined by microscopy and elemental analyses (Figure 3.5c). This intracellular S^0 plays a central role in $S_2O_3^{2-}$ metabolism (Figure 3.6c). The Bobadilla Fazzini *et al*. (2013)

model did not predict any S^0 storage for *A. thiooxidans* grown on S^0, or storage in tandem with TetH activity for *A. thiooxidans* grown on $S_4O_6^{2-}$ and did not include the *hdr*, *rhd*, *paps* and *aps* genes.

Yin *et al.* (2014) examined *A. thiooxidans* A01 via gene expression proposing a similar sulfur gene model to our *A. thiooxidans* ATCC 19377 model. Due to our improved draft genome of *A. thiooxidans* ATCC 19377, we were able to find and confirm the previously elusive *sor* gene (Valdes *et al*., 2011) identifying that the same sulfur genes are present in the two strains (Figure 3.1b). However, differences in the number of gene copies identified for *hdrA*, *rhd*, *paps* and *aps* exist between the strains, where for *A. thiooxidans* ATCC 19377, we found three copies of *hdrA,* two copies of *rhd* and one copy each for *paps* and *aps* (Figure 3.3). In contrast, for *A. thiooxidans* A01 one copy of *hdrA*, five copies of *rhd*, three copies of *paps* and two copies of *aps* were identified (Yin *et al.*, 2014). That study found that most sulfur metabolic genes were more strongly expressed in *A. thiooxidans* A01 when grown on S^0 compared to $S_2O_3^{2-}$ during exponential growth phase (Yin *et al.*, 2014), showing opposing results to our relative expression levels for *A. thiooxidans* ATCC 19377 stationary phase growth on S^0 compared to $S_2O_3^{2-}$ (Figure 3.3b-iii), These results suggest that relative gene expression switches from lower to higher in $S_2O_3^{2-}$, and higher to lower in S^0, as *A. thiooxidans* goes from exponential to stationary growth phase. However, the Yin *et al.* 2014 study only examined gene expression during exponential growth phase, and their hypothetic models included pathways identified from previous studies depicting models for other *Acidithiobacillus* species (Yin *et al.,* 2014). Thus, their model was not able to identify the importance of intracellular S^0, and SO_3^{2-} and the *hdr* gene as observed here.

In comparison to other *Acidithiobacillus* species models of S metabolism, our gene model for *A. thiooxidans* shows closest similarity to *A. caldus*. Differing only that in *A. caldus,* Sdo has

been determined to be located in the cytoplasm instead of the periplasm (Wu *et al*., 2017) and it has the addition of SAT responsible for oxidation of sulfite to sulfate (Wang *et al*., 2019). While the *A. ferrooxidans* gene model shows greater differences to our *A.thiooxidans* model, most notably in its absence of the Sox complex and *sor* gene, and its inclusion of SAT and TSD (Wang *et al*., 2019; Zhan *et al*., 2019). For *A. caldus* and *A. ferrooxidans*, the current S^0 metabolism is proposed to be oxidation to SO_3^{2-} via Sdo, followed by oxidation to SO_4^{2-} via SAT, with the bacteria acquiring S^0 from extracellular sources (Mangold *et al*., 2011; Zhan *et al*., 2019). This differs to our proposed S^0 metabolic pathway (Figure 3.6a), which is elaborated upon further below. The current proposed model of $S_2O_3^{2-}$ oxidation metabolism, shows that both *A. caldus* and *A. ferrooxidans* utilize the S_4I pathway, however, *A. caldus* also uses the Sox system while *A. ferrooxidans* also uses TSD (Ghosh and Dam, 2009; Wang *et al*., 2019). Our *A. thiooxidans* S metabolism model follows the same $S_2O_3^{2-}$ oxidation metabolism as *A. caldus* employing both the S_4I pathway and the Sox system.

3.4.1.2 Integrated gene expression and sulfur chemistry A. thiooxidans metabolism models

The models generated here provide new insights into the likely pathways involved in *A. thiooxidans* sulfur metabolism, closing some of the gaps in the current understanding. Specifically, our results identify internal cell S^0 generation, storage and use, as well as the importance and rapid conversion of SO_3^{2-} in these models, both confirming the speculated importance of these two S compounds (Suzuki *et al*., 1992) and explaining why they have not previously been definitively confirmed by solution chemical characterization alone.

Based on the published studies to date, the first step in microbial S^0 metabolism is thought to be a relatively linear pathway beginning with oxidation to SO_3^{2-}, followed by further oxidation

to SO_4^{2-} (Suzuki *et al*., 1992; Rohwerder and Sand, 2003). However, here the model developed through combined sulfur chemical and gene expression analyses indicates that $S_2O_3^{2-}$ oxidation/disproportionation reactions are occurring as formation of significant amounts of *Other SOI* (i.e. indicating the presence of polythionates) and small amounts of $S_2O_3^{2-}$ are observed (Figure 3.4a). Consistent with these pathways, expression specifically of *tetH* and *rhd*, genes known to encode enzymes for $S_2O_3^{2-}$ and polythionate oxidation/disproportionation reactions were being expressed (Figure 3.7a and b) (Meulenberg *et al.*, 1992; Hallberg *et al.*, 1996; Beller *et al.*, 2006; Rzhepishevska *et al.*, 2007).

Further lending support to these alternative pathways, higher relative expression of the *hdr* genes was observed (Figure 3.3a), which should result in high levels of SO_3^{2-}, and thus subsequent high SO_4^{2-} values. However, our results here indicate lower values of SO_4^{2-} than expected, consistent with recycling of this SO_3^{2-} through comproportionating reactions that would generate $S_2O_3^{2-}$ instead. The specific presence of $S_2O_3^{2-}$, despite likely abiotic disproportionation at this low pH <2, SO_3^{2-} (Supplementary Table S11) and activity of *hdr* genes associated with sulfur back reactions, underscore the formation of $S_2O_3^{2-}$ as a critical step in S^0 metabolism (Figure 3.6a) generating the precursor to most reactions involving the increased pool of *Other SOI*, e.g. polythionates (Meulenberg *et al.*, 1993; Müller *et al.*, 2004).

The formation of $S_2O_3^{2-}$ from SO_3^{2-} comproportionation during *A. thiooxidans* S^0 metabolism is supported by three lines of evidence. First, the intracellular neutral pH of *A. thiooxidans* (Suzuki *et al*., 1999) makes the neutrophilic reaction combining S^0 with SO_3^{2-} to form $S_2O_3^{2-}$ favourable (Eq 4, Table 3.1). Second, *A. thiooxidans* possesses rhodanese/sulfur transferase (Yin *et al*., 2014), which may include a rhodanese capable of binding a sulfane group sulfur (eg. S^0) to SO_3^{2-} to form $S_2O_3^{2-}$ (Hildebrandt and Grieshaber, 2008; Zhang *et al*., 2013). Third, the

metabolic bonding of S^0 with SO_3^{2-} is mediated via the Sox complex, which is highly expressed by *A. thiooxidans* grown on S^0 (Figure 3.7a and b). The versatility of the Sox complex would support this pathway (Sauvé *et al.*, 2007; Wang *et al.,* 2019). The gene expression results are consistent with comproportionation, as results here identify that within the Sox complex, SoxYZ (carriers) and SoxAX (binders) are more highly expressed than the oxidizing enzyme (SoxB) in all analyses (Figure 3.3a).

Metabolic modeling results from growth on $S_2O_3^{2-}$ indicate *A. thiooxidans* $S_2O_3^{2-}$ oxidation closely follows the S_4I pathway proposed in the literature, further suggesting higher oxidation chain polythionate formation (Figure 3.6b and c; Supplementary text) (Hallberg *et al.*, 1996; Masau *et al.*, 2001; Müller *et al.*, 2004; Ghosh and Dam, 2009). However, the ability to effectively measure all the possible sulfur species remains an analytical challenge (Houghton *et al.*, 2016), which precludes 100% certainty in our model fitting.

The occurrence of S^0 within the cells when grown on S^0, can be attributed to the intake of the sulfur globules from the media via transport enzymes and outer membrane proteins (Rohwerder and Sand, 2003), and/or from SOI cycling through mechanisms such as $S_2O_3^{2-}$ oxidation via the Sox complex when missing SoxCD*,* a characteristic for sulfur globule formation in bacteria species (Figure 3.5a) (Steudal *et al.*, 1987; Pronk *et al.*, 1990). However, formation of S^0 within the cells was also observed when *A. thiooxidans* was grown on $S_2O_3^{2-}$ associated with SOI cycling (Figure 3.5c), though at lower levels than that observed for *A. thiooxidans* grown on S^0 (Figure 3.5a vs c).

3.4.2. Relevance of gene expression analysis

3.4.2.1. Relative expression levels between variable conditions in S metabolism

Results assessing relative changes in gene expression identify that the Sox complex, Sqr, Hdr, TetH and Rhd are important in both S^0 and $S_2O_3^{2-}$ metabolism by *A. thiooxidans*. While measurements of gene expression does not allow firm conclusions on absolute protein levels or enzyme activities, they do identify specific genes and encoded enzymes likely to be important in a metabolic pathway. Relative levels of expression of these genes however differ between the two sulfur media and between growth stages for S^0 (Figure 3.3a). The results illustrate the importance of the Sox complex and of TetH for $S_2O_3^{2-}$ metabolism (Figure 3.7c). The Sox complex is a very important metabolic enzyme complex during growth on both substrates since it is highly expressed under all conditions (Figure 3.3a). Gene expression results indicate the *sox*-1 operon is active in cells at less acidic pH values and underscore the geochemical flexibility and viability of the Sox complex as expression of the *sox*-2 operon is used under more acidic conditions and with higher thiosulfate concentrations (Figure 3.3a). These observations are similar to those reported by others (Zhu *et al.,* 2012; Jones *et al*., 2014; Yin *et al.*, 2014; Li *et al.*, 2017; Wang *et al.,* 2019), whereby different gene copies of the same enzyme express at differing levels due to environmental parameters. The differential expression of these gene copies (Figure 3.3a) indicates that gene expression can provide insights into the geochemical conditions associated with sulfur metabolism.

3.4.2.2. Insight into the importance of Hdr towards S metabolism

Our results identify a key role of Hdr in *A. thiooxidans* ATCC 19377 S^0 metabolism expanding the understanding of important genes and their roles in *A. thiooxidans* sulfur metabolism.

Relatively high *hdr* expression levels were observed under all conditions in comparison to the low levels of *sdo* (Figure 3.3a). The inclusion of solution chemical data and electron microscopy suggest that Hdr is likely the primary S^0 oxidizing enzyme rather than Sdo, which was previously identified as important for internal generation of SO_3^{2-} and $S_2O_3^{2-}$ during growth on S^0 (Rohwerder and Sand, 2003; Bobadilla Fazzini *et al*., 2013; Yin *et al*., 2014; Koch and Dahl, 2018). Catalysis by Hdr rather than Sdo is energetically more favourable since conversion of S^0 to SO_3^{2-} is a non-quinone/cytochrome metabolic step for Sdo. Thus it would result in a loss of approximately 50% of the available potential energy considering the ΔG of -500 to 550kJ per mol S in oxidation of S^0 to SO_4^{2-} (Kelly, 1999). In contrast, catalysis of the *hdr* gene also found in *A. caldus* (Mangold *et al*, 2011), *A. ferrooxidans* (Quatrini *et al*., 2009) and *A. thiooxidans* A01 (Yin *et al*., 2014) enables *A. thiooxidans* to metabolize and access this energy. The identification of its role in sulfur metabolism here, may assist taxonomic classification and facilitate better understanding of the potential for sulfur metabolism across all *Acidithiobacilli* (Nuñez *et al*., 2017; Cao *et al*., 2018; Koch and Dahl, 2018; Wang *et al*., 2019) and other sulfur oxidizing microbes.

3.5. Conclusions

Here we are able to provide greater insight into the specific reactions being catalyzed by known sulfur genes and newly highlight the role of Hdr in *A. thiooxidans* sulfur metabolism by integrating gene expression levels with bulk solution S speciation. Our results further confirm the importance specifically of $S_2O_3^{2-}$ and SO_3^{2-} in *A. thiooxidans* sulfur metabolism, which have been widely accepted in the literature to be important, though not definitively shown to date prior to this study (Suzuki *et al.*, 1992; Suzuki, 1999; Bobadilla Fazzini *et al*., 2013). Further, our results generate new insights into the central role of intracellular S^0 generation, transformation and pathways in both $S_2O_3^{2-}$ and S^0 metabolism and that SO_3^{2-} comproportionation to $S_2O_3^{2-}$ is a critical step in S^0 metabolism. Collectively these results highlight how the integration of molecular biology and chemistry approaches can better inform our understanding of biogeochemical cycling of sulfur by microbes.

References

Bacelar-Nicolau P., Johnson D.B. (1999) Leaching of pyrite by acidophilic heterotrophic iron-oxidizing bacteria in pure and mixed cultures. *Appl Environ Microbiol* 65: 585-590.

Bankevich A., Nurk S., Antipov D., Gurevich A.A., Dvorkin M., Kulikov A.S., *et al*. (2012) SPAdes: a new genome assembly algorithm and its applications to single-cell sequencing. *J Comp Biol* 19: 455-477.

Beller H.R., Chain P.S., Letain T.E., Chakicherla A., Larimer F.W., Richardson P.M., *et al*. (2006) The genome sequence of the obligately chemolithoautotrophic, facultatively anaerobic bacterium *Thiobacillus denitrificans*. *J Bacteriol* 188: 1473-1488, doi: 10.1128/JB.188.4.1473-1488.2006.

Bernier L., Warren L. (2005) Microbially driven acidity generation in a tailings lake. *Geobiology*. 3: 115-133.

Bernier L., Warren L.A. (2007) Geochemical diversity in S processes mediated by culture-adapted and environmental-enrichments of *Acidithiobacillus* spp. *Geochim Cosmochim Acta* 71: 5684-5697.

Blankenberg D., Von Kuster G., Coraor N., Ananda G., Lazarus R., Mangan M., *et al.* (2010) Galaxy: a web-based genome analysis tool for experimentalists. *Current protocols in molecular biology / edited by Frederick M Ausubel [et al]* Chapter 19: Unit 19 10 11-21.

Bobadilla Fazzini R.A., Cortés M.P., Padilla L., Maturana D., Budinich M., Maass A., *et al*. (2013) Stoichiometric modeling of oxidation of reduced inorganic sulfur compounds (Riscs) in *Acidithiobacillus thiooxidans*. *Biotechnol bioeng* 110: 2242-2251.

Bolger A.M., Lohse M., Usadel B. (2014) Trimmomatic: a flexible trimmer for Illumina sequence data. *Bioinformatics* 30: 2114-2120.

Boyd E.S., Druschel G.K. (2013) Involvement of intermediate sulfur species in biological reduction of elemental sulfur under acidic, hydrothermal conditions. *Appl Environ Microbiol* 79: 2061-2068. doi: 10.1128/AEM.03160-12; 10.1128/AEM.03160-12.

Buonfiglio, V., Polidoro, M., Soyer, F., Valenti, P., Shively, J. (1999) A novel gene encoding a sulfur-regulated outer membrane protein in *Thiobacillus ferrooxidans*. *J Biotechnol*, 72:85-93.

Canfield D.E., Stewart F.J., Thamdrup B., De Brabandere L., Dalsgaard T., Delong E.F., *et al*. (2010) A cryptic sulfur cycle in oxygen-minimum–zone waters off the Chilean coast. *Science* 330: 1375-1378.

Cao X., Koch T., Steffens L., Finkensieper J., Zigann R., Cronan J.E., *et al.* (2018) Lipoate-binding proteins and specific lipoate-protein ligases in microbial sulfur oxidation reveal an atpyical role for an old cofactor. *Elife* 7: 37439.

Druschel G.K. (2002) Sulfur Biochemistry: Kinetics of Intermediate Sulfur Species Reactions in the Environment. PhD Dissertation University of Wisconsin - Madison.

Druschel G.K., Baker B.J., Gihring T.M., Banfield J.F. (2004) Acid mine drainage biogeochemistry at Iron Mountain, California. *Geochem T* 5: 13-32.

Friedrich C.G., Rother D., Bardischewsky F., Quentmeier A., Fischer J. (2001) Oxidation of reduced inorganic sulfur compounds by bacteria: emergence of a common mechanism? *Appl Environ Microbiol* 67: 2873-2882, doi: 10.1128/AEM.67.7.2873-2882.2001.

Ghosh W., Dam B. (2009) Biochemistry and molecular biology of lithotrophic sulfur oxidation by taxonomically and ecologically diverse bacteria and archaea. *FEMS Microbiol Rev* 33: 999-1043.

Giardine B., Riemer C., Hardison R.C., Burhans R., Elnitski L., Shah P., *et al*. (2005) Galaxy: a platform for interactive large-scale genome analysis. *Genome Res* 15: 1451-1455.

Goecks J., Nekrutenko A., Taylor J., Galaxy T. (2010) Galaxy: a comprehensive approach for supporting accessible, reproducible, and transparent computational research in the life sciences. *Genome biology* 11: R86.

Griesbeck C., Schütz M., Schödl T., Bathe S., Nausch L., Mederer N., *et al*. (2002) Mechanism of sulfide-quinone reductase investigated using site-directed mutagenesis and sulfur analysis. *Biochemistry* 41: 11552-11565.

Hallberg K.B., Dopson M., Lindstrom E.B. (1996) Reduced sulfur compound oxidation by *Thiobacillus caldus*. *J Bacteriol* 178: 6-11.

Hallberg K.B., Johnson D.B. (2003) Novel acidophiles isolated from moderately acidic mine drainage waters. *Hydrometallurgy*. 71: 139-148.

Hensen D., Sperling D., Trüper H.G., Brune D.C., Dahl C. (2006) Thiosulphate oxidation in the phototrophic sulphur bacterium *Allochromatium vinosum*. *Mol Microbiol* 62: 794-810.

Hildebrandt T.M., Grieshaber M.K. (2008) Three enzymatic activities catalyze the oxidation of sulfide to thiosulfate in mammalian and invertebrate mitochondria. *Febs Journal* 275: 3352-3361.

Houghton J.L., Foustoukos D., Flynn T.M., Vetriani C., Bradley A.S., Fike D.A. (2016) Thiosulfate oxidation by *Thiomicrospira thermophila*: metabolic flexibility in response to ambient geochemistry. *Environ Microbiol*. 18: 3057–3072

Johnson D.B., Hallberg K.B. (2003) The microbiology of acidic mine waters. *Res Microbiol* 154: 466-473.

Johnston F., McAmish L. (1973) A study of the rates of sulfur production in acid thiosulfate solutions using S-35. *J Colloid Interf Sci* 42: 112-119.

Jones D.S., Schaperdoth I., Macalady J.L. (2014) Metagenomic Evidence for Sulfide Oxidation in Extremely Acidic Cave Biofilms. *Geomicrobiol J* 31: 194–204, doi: 10.1080/01490451.2013.834008.

Jørgensen B.B., Nelson D.C. (2004) Sulfide oxidation in marine sediments: geochemistry meets microbiology. *Geol S Am S* 379: 63-81.

Kelly D.P. (1999) Thermodynamic aspects of energy conservation by chemolithotrophic sulfur bacteria in relation to the sulfur oxidation pathways. *Arch Microbiol* 171: 219–229.

Kelly D.P., Baker S.C. (1990) The organosulphur cycle: aerobic and anaerobic processes leading to turnover of C_1 -sulphur compounds. *FEMS Microbiol Lett* 87: 241-246.

Kelly D.P., Shergill J.K., Lu W., Wood A.P. (1997) Oxidative metabolism of inorganic sulfur compounds by bacteria. *Antonie Van Leeuwenhoek*. 71: 95-107.

Kletzin A. (1989) Coupled enzymatic production of sulfite, thiosulfate, and hydrogen sulfide from sulfur: purification and properties of a sulfur oxygenase reductase from the facultatively anaerobic archaebacterium *Desulfurolobus ambivalens*. *J Bacteriol* 171: 1638-1643.

Kletzin A. (1992) Molecular characterization of the *sor* gene, which encodes the sulfur oxygenase/reductase of the thermoacidophilic Archaeum *Desulfurolobus ambivalens*. *J Bacteriol* 174: 5854-5859.

Koch T., Dahl C. (2018) A novel bacterial sulfur oxidation pathway provides a new link between the cycles of organic and inorganic sulfur compounds. *ISME J* 12: 2479.

Li L.F., Fu L.J., Lin J.Q., Pang X., Liu X.M., Wang R., *et al.* (2017) The sigma(54)-dependent two-component system regulating sulfur oxidization (Sox) system in *Acidithiobacillus caldus* and some chemolithotrophic bacteria. *Appl. Microbiol. Biotechnol.* 101: 2079–2092. doi: 10.1007/s00253-016- 8026-2

Mangold S., Valdes J., Holmes D.S., Dopson M. (2011) Sulfur metabolism in the extreme acidophile acidithiobacillus caldus. *Front Microbiol* 2: 17.

Masau R.J.Y., Oh J.K., Suzuki I. (2001) Mechanism of oxidation of inorganic sulfur compounds by thiosulfate-grown *Thiobacillus thiooxidans*. *Can J Microbiol* 47: 348–358.

Meulenberg R., Pronk J.T., Hazeu W., Bos P., Kuenen J.G. (1992) Oxidation of reduced sulphur compounds by intact cells of *Thiobacillus acidophilus. Arch Microbiol* 157: 161-168.

Meulenberg R., Pronk J.T., Hazeu W., van Dijken J.P., Frank J., Bos P., *et al*. (1993) Purification and partial characterization of thiosulphate dehydrogenase from *Thiobacillus acidophilus*. *J Gen Microbiol* 139: 2033-2039.

Miranda-Trevino J.C., Pappoe M., Hawboldt K., Bottaro C. (2013) The Importance of Thiosalts Speciation: Review of Analytical Methods, Kinetics, and Treatment. *Crit Rev Env Sci Tec* 43: 2013-2070, doi: 10.1080/10643389.2012.672047.

Müller F.H., Bandeiras T.M., Urich T., Teixeira M., Gomes C.M., Kletzin A. (2004) Coupling of the pathway of sulphur oxidation to dioxygen reduction: characterization of a novel membrane-bound thiosulphate: quinone oxidoreductase. *Mol Microbiol* 53: 1147-1160.

Nordstrom D.K. (2015) Baseline and premining geochemical characterization of mined sites. *Appl Geochem* 57: 17–34.

Nordstrom D.K., Blowes D.W., Ptacek C.J. (2015) Hydrogeochemistry and microbiology of mine drainage: An update. *Appl Geochem* 57: 3–16.

Nuñez H., Moya-Beltrán A., Covarrubias P.C., Issotta F., Cardenas J.P., Gonzalez M., *et al*. (2017) Molecular systematics of the genus *Acidithiobacillus*: insights into the phylogenetic structure and diversification of the taxon. *Front Microbiol* 8: 30.

Pronk J., Meulenberg R., Hazeu W., Bos P., Kuenen J. (1990) Oxidation of reduced inorganic sulphur compounds by acidophilic thiobacilli. *FEMS Microbiol Lett* 75: 293-306.

Quatrini R., Appia-Ayme C., Denis Y., Jedlicki E., Holmes D.S., Bonnefoy, V. (2009) Extending the models for iron and sulfur oxidation in the extreme acidophile *Acidithiobacillus ferrooxidans*. *BMC genomics* 10: 394

Rethmeier J., Rabenstein A., Langer M., Fischer U. (1997) Detection of traces of oxidized and reduced sulfur compounds in small samples by combination of different high-performance liquid chromatography methods. *J. Chromatogr A* 760: 295-302.

Rohwerder T., Sand W. (2003) The sulfane sulfur of persulfides is the actual substrate of the sulfur-oxidizing enzymes from *Acidithiobacillus* and *Acidiphilium* spp. *Microbiology*. 149: 1699-1710.

Rzhepishevska O.I., Valdes J., Marcinkeviciene L., Gallardo C.A., Meskys R., Bonnefoy V., *et al*. (2007) Regulation of a novel *Acidithiobacillus caldus* gene cluster involved in metabolism of reduced inorganic sulfur compounds. *Appl Environ Microbiol* 73: 7367-7372, doi: 10.1128/AEM.01497-07.

Sauvé V., Bruno S., Berks B.C., Hemmings A.M. (2007) The SoxYZ complex carries sulfur cycle intermediates on a peptide swinging arm. *J Biol Chem* 282: 23194-23204.

Schippers A., Jozsa P., Sand W. (1996) Sulfur chemistry in bacterial leaching of pyrite. *Appl Environ Microbiol* 62: 3424-3431.

Schippers A., Sand W. (1999) Bacterial leaching of metal sulfides proceeds by two indirect mechanisms via thiosulfate or via polysulfides and sulfur. *Appl Environ Microbiol* 65: 319-321.

Seemann T. (2014) Prokka: rapid prokaryotic genome annotation. *Bioinformatics* 30: 2068-2069.

Staley J.T., Bryant M.P., Pfennig N., Holt J.G. (1989) *Acidithiobacillus*. In: *Bergey's Manual of Systematic Bacteriology vol 3.* Edited by Wilkins Wa, vol. 3, 1st edn. Baltimore 1842-1858.

Steudel R., Holdt G., Göbel T., Hazeu W. (1987) Chromatographic Separation of Higher Polythionates SnO 62⊖(n= 3… 22) and Their Detection in Cultures of *Thiobacillus ferroxidans*; Molecular Composition of Bacterial Sulfur Secretions. Angewandte Chemie International Edition in English. 26:151-153.

Sugio, T., Suzuki, H., Oto, A., Inagaki, K., Tanaka, H., Tano, T. (1991) Purification and some properties of a hydrogen sulfide- binding protein that is involved in sulfur oxidation of *Thiobacillus ferrooxidans*. *Agric Biol Chem* 55:2091–2097.

Suzuki I. (1999) Oxidation of inorganic sulfur compounds: chemical and enzymatic reactions. *Can J Microbiol* 45: 97-105.

Suzuki I., Chan C.W., Takeuchi T.L. (1992) Oxidation of elemental sulfur to sulfite by *Thiobacillus thiooxidans* cells. *Appl Environ Microbiol* 58: 3767-3769.

Suzuki I., Lee D., Mackay B., Harahuc L., Oh J.K. (1999) Effect of various ions, pH, and osmotic pressure on oxidation of elemental sulfur by *Thiobacillus thiooxidans*. *Appl Environ Microbiol* 65: 5163-5168.

Thamdrup B., Fossing H., Jørgensen, B.B. (1994) Manganese, iron and sulfur cycling in a coastal marine sediment, Aarhus Bay, Denmark. *Geochim Cosmochim Ac* 58: 5115-5129.

Valdes J., Ossandon F., Quatrini R., Dopson M., Holmes D.S. (2011) Draft genome sequence of the extremely acidophilic biomining bacterium *Acidithiobacillus thiooxidans* ATCC 19377 provides insights into the evolution of the *Acidithiobacillus* genus. *J Bacteriol* 193: 7003-7004.

Valdes J., Pedroso I., Quatrini R., Dodson R.J., Tettelin H., Blake R. (2008) 2nd, Eisen JA, Holmes DS: *Acidithiobacillus ferrooxidans* metabolism: from genome sequence to industrial applications. *BMC genomics* 9: 597.

Valdes J,. Quatrini R., Hallberg K., Dopson M., Valenzuela P.D., Holmes D.S. (2009) Draft genome sequence of the extremely acidophilic bacterium *Acidithiobacillus caldus* ATCC 51756 reveals metabolic versatility in the genus *Acidithiobacillus*. *J Bacteriol* 191: 5877-5878.

Wang R., Lin J.Q., Liu X.M., Pang X., Zhang C.J., Gao X.Y., *et al.* (2019) Sulfur oxidation in the acidophilic autotrophic *Acidithiobacillus* spp. *Front Microbiol 9*: 3290.

Warren L., Norlund K.I., Bernier L. (2008) Microbial thiosulphate reaction arrays: The interactive roles of Fe (III), O2 and microbial strain on disproportionation and oxidation pathways. *Geobiology* 6: 461-470.

Wu W., Pang X., Lin J., Liu X., Wang R., Lin J., *et al.* (2017) Discovery of a new subgroup of sulfur dioxygenases and characterization of sulfur dioxygenases in the sulfur metabolic network of *Acidithiobacillus caldus*. *PLoS One* 12:e0183668. doi: 10.1371/journal.pone.0183668

Yin H., Zhang X., Li X., He Z., Liang Y., Guo X., *et al*. (2014) Whole-genome sequencing reveals novel insights into sulfur oxidation in the extremophile *Acidithiobacillus thiooxidans*. *BMC microbiol* 14: 179.

You X.Y., Guo X., Zheng H.J., Zhang M.J., Liu L.J., Zhu Y.Q., *et al.* (2011) Unraveling the *Acidithiobacillus caldus* complete genome and its central metabolisms for carbon assimilation. *Journal of genetics and genomics = Yi chuan xue bao* 38: 243-252.

Zhan Y., Yang M., Zhang S., Zhao D., Duan J., Wang, W., *et al.* (2019) Iron and sulfur oxidation pathways of *Acidithiobacillus ferrooxidans*. *World J Microb Biot 35*: 60, doi: 10.1007/s11274-019-2632-y

Zhang L., Liu X., Liu J., Zhang Z. (2013) Characteristics and function of sulfur dioxygenase in echiuran worm *Urechis unicinctus*. *PloS one*, 8: e81885.

Zhu J., Jiao W., Li Q., Liu X., Qin W., Qiu G., *et al*. (2012) Investigation of energy gene expressions and community structures of free and attached acidophilic bacteria in chalcopyrite bioleaching. *J Ind Microbiol Biotechnol* 39: 1833–1840, doi: 10.1007/s10295-012-1190-1.

Zopfi J., Ferdelman T.G., Fossing H. (2004) Distribution and fate of sulfur intermediates−−sulfite, tetrathionate, thiosulfate, and elemental sulfur −−in marine sediments. In: Amend, J.P., Edwards, K., Lyons, T.W. (Eds.), Sulfur Biogeochemistry — Past and Present: *Geol Soc Am Spec Papers* 379: 97-116, doi: 10.1130/0-8137-2379-5.97.

Chapter 4

Microbial Succession Signals the Initiation of Acidification in Mining Wastewaters

David Camacho[1], Gerdhard L. Jessen[2†], Jiro F. Mori[2§], Simon C. Apte[3], Chad V. Jarolimek[3], and Lesley A. Warren[1,2]

[1]School of Geography and Earth Science, Faculty of Science, McMaster University, Hamilton, ON, CA;
[2]Department of Civil and Mineral Engineering, Faculty of Applied Science and Engineering, University of Toronto, Toronto, ON, CA;
[3]CSIRO, Land and Water, Lucas Heights, NSW 2234, AU;

[†]Present address: Institute of Marine and Limnological Sciences, Faculty of Sciences, University Austral of Chile

[§]Present address: Graduate School of Nanobiosciences, Yokohama City University, Yokohama, Japan

Citation: Camacho D., Jessen G.L., Mori J.F., Apte S.C., Jarolimek C.V., Warren L.A. (2020) Microbial succession signals the initiation of acidification in mining wastewaters. *Mine Water Environ.* 39:669-683. doi.org/10.1007/s10230-020-00711-9.

Abstract

We characterized the sulfur geochemistry and microbial community structure of seven circumneutral wastewaters from two Canadian nickel mines collected between 2014 and 2015, seasonally in Summer, Winter and Spring. We also established and characterized sulfur oxidizing enrichments for these wastewater samples grown under two pH corrals of 7 to 5 and 5 to 3. Mine 1 exhibited lower contents of total soluble sulfur compounds and reactive soluble sulfur compounds (oxidation state < +VI) relative to Mine 2. This coincided to Mine 1 exhibiting greater wastewater microbial community diversity with more unique sequences relative to Mine 2 and resulting in clear NMDS differentiation and Bray-Curtis dissimilarity between the two mines microbial communities. *Proteobacteria* dominated all wastewater samples and enrichments communities ranging between 58% - 99% of the total of sequences retrieved from the corresponding samples. However, a shift in dominance occurred from primarily *Alphaproteobacteria* (28% - 77%) in the circumneutral wastewater communities to *Gammaproteobacteria* (>80%) in the moderately acidic enrichment communities. A further pH dependent shift occurred from *Halothiobacillus* spp. dominating the pH 7 to 5 enrichments to *Thiomonas* spp. dominating the pH 5 to 3 enrichments. These results provide putative biological indicators for better prediction and management of sulfur processes and AMD onset within mining wastewaters.

4.1. Introduction

Acid mine drainage (AMD) remains an environmental concern for mines worldwide. AMD is strongly enhanced by microbial sulfur oxidation/disproportionation, which can result in high concentrations of H^+ and metal ions, leading to severe environmental impacts (Lindsay et al. 2015; Sheoran and Sheoran 2006). Research primarily on waste rock (i.e. unprocessed overburden) associated AMD geomicrobiology has shown that iron and sulfur oxidizing organisms dominate most of these acidic sites (Baker and Banfield 2003; Cowie et al. 2009; Druschel et al. 2004; Moncur et al. 2015; Schippers and Sand 1999; Schippers et al. 2010; Sheoran and Sheoran 2006; Tyson et al. 2004). The prevalent organisms include chemotrophic bacteria and some archaea, e.g. iron oxidizing bacteria of the genera, *Leptosprillium* and *Acidithiobacillus*, and archaea, *Ferroplasma* and other *Thermoplasmatales* (Druschel et al. 2004; Huang et al. 2011; Tyson et al. 2004). As well as, sulfur oxidizing bacteria belonging to the *Proteobacteria*, comprised mainly of *Gammaproteobacteria* including the genus (*Acidithiobacillus)*, *Alphaproteobacteria* (*Acidiphilum)* and a few *Betaproteobacteria* and *Deltaproteobacteria* (Baker and Banfield 2003; Kelly and Wood 2000; Kimura et al. 2011; Kuang et al. 2013).

However, mine tailings, the post extraction waste consisting of an aqueous, highly processed, slurry (< 40% solids), which requires treatment prior to water discharge into receiving environments is less well studied in regard to geomicrobiological investigation to date. In contrast to waste rock, wastewater associated with tailings is often alkaline and can contain a wide variety of sulfur oxidation intermediate compounds (SOI; Whaley-Martin et al. 2020). As some SOI are recalcitrant dependant on the available wastewater treatments applied (Miranda-Trevino et al. 2013), they can pass through into receiving environments. If they are present in high enough

concentrations, their oxidation can cause pH depression, toxicity as well as O_2 consumption and potential fish kills (Bernier and Warren 2007; Lindsay et al. 2015; Schippers et al. 1996; Sheoran and Sheoran 2006).

Research from AMD sites has shown a clear link between pH values and microbial community structure (Kuang et al. 2013; Liu et al. 2014). Thus, tailings impoundment wastewaters, which are commonly circumneutral, likely host different microbial players important to sulfur cycling than those observed in waste rock AMD contexts.

The limited comparative literature that exists does identify distinct differences in the microbial ecology of wastewaters (Whaley-Martin et al. 2019) compared to waste rock associated AMD sites (Dockery et al. 2014) and tailings dumps (Korehi et al. 2014). Whaley-Martin et al. (2019) characterized the parent microbial communities as well as the consortia associated with sulfur oxidizing bacteria (SoxB) enrichment experiments from wastewaters collected from four circumneutral (pH > 6) metal mine tailings impoundments, as well as their receiving environments. Contrasting the well documented *Thiobacilli* dominance of waste rock, this study identified *Halothiobacilliaceae*, and specifically *Halothiobacillus* spp. to dominate seven of the nine communities that were responsible for driving the pH < 4 in enrichment experiments. Interestingly, that study also observed *Halothiobacillus* spp. to occur in high abundance in the parent communities of the acidic wastewater and receiving environment samples, providing field-based evidence supporting their likely importance in sulfur reactions that can lead to AMD conditions (Whaley-Martin et al. 2019).

The objectives of this study were to identify the sulfur oxidizing microorganisms through enrichments (SoxB) and examine any pH dependent trends in enrichment community structure for circumneutral wastewaters collected seasonally from two Ni mines contrasting in their sulfur

concentrations. An enrichment strategy specifically targeted the composition of circumneutral versus acidophilic SoxB enrichment communities. Enrichment experiments were grown from the seven parent circumneutral wastewater samples, in both neutrophilic and acidophilic S oxidizing media using two pH corrals of 7-5 (both media types) and 5-3 (acidophilic media only). The microbial community was analyzed by examining the 16S rRNA gene sequencing for both the wastewater and enrichment samples.

4.2. Materials and Methods

4.2.1. Spatial and temporal sampling of sites

Seven tailings impoundment water samples were collected from two Canadian mine sites; Mine 1 (referred to as Mine 3 in Whaley-Martin et al. 2019; Cu, Ni mine; Sudbury, Ontario), and Mine 2 (Co, Cu, Ni mine; Newfoundland and Labrador) between August 2014 and September 2015. Wastewaters from Mine 1 have been previously investigated for both sulfur geochemistry and microbial communities (Bernier and Warren 2005; Warren et al. 2008; Whaley-Martin et al. 2019). Mine 2 was selected due to its differing wastewater sulfur chemistry in comparison to Mine 1 and its lack of any published information on either SOI speciation or microbial communities and important microbes for S cycling. Wastewaters were collected from the tailings ponds at both mines for Summer 2014, Spring 2015 and Summer 2015, and Mine 1 was also sampled in Winter 2015. Each of these seven parent wastewater samples were: i) characterized for pH, total dissolved S ($\sum S_{aq}$; < 0.45 μm) and SOI species (S^0, $S_2O_3^{2-}$, SO_3^{2-}) as well as S^{2-} and SO_4^{2-}; ii) characterized for microbial community structure (16S rRNA, via Illumina Mi-Seq and metagenomic Illumina Hi-Seq); and iii) experimentally enriched for sulfur oxidizing consortia (SoxB) in the three types of media-pH treatments (pH 7-5 neutrophilic, pH 7-5 acidophilic, and pH 5-3 acidophilic), which microbial community structure were subsequently characterized as above for wastewater parent communities.

4.2.2. Mine wastewater sample collection

For both sites, water samples were collected into ethanol sterilized, lined and sealed 20 L containers (Whaley-Martin et al. 2019). Mine 1 samples were collected directly from the surface

of the tailings reservoir into the containers, using a sampling beaker that was rinsed first with 70% ethanol and then rinsed with the mine water three times prior to collection of the water sample. These samples were brought back to the laboratory (McMaster University, Hamilton, Ontario) within 1-3 days via ground transport for analyses. Mine 2 samples were taken directly from the mine wastewater effluent discharge point to the receiving environment into the sterilized lined containers. Due to the remote location of Mine 2, once collected, water samples were air shipped arriving within 3-10 days at the laboratory (McMaster University). Assessments have shown that the sulfur speciation of the major identified species of concern (e.g. S^0, $S_2O_3^{2-}$, $S_4O_6^{2-}$, SO_4^{2-}) remain stable within this time-frame (1-10 days) for these circumneutral mine wastewaters (Whaley-Martin et al. 2019, 2020). The lack of any significant change in SOI speciation is also consistent with the notion that associated sulfur oxidizing microbes in these waters show low activity rates during shipment and thus no significant changes to their composition occur within this transportation time frame is a reasonable assumption (Whaley-Martin et al. 2019, 2020).

4.2.3. Geochemical analysis

Once samples arrived in the laboratory, pH was measured immediately (Denver Instrument Model 225, NY, USA) prior to sampling for sulfur analyses. Triplicate samples were then collected for dissolved (< 0.45 µm), total sulfur ($\sum S_{aq}$) and sulfur speciation (SO_4^{2-}, S^{2-}, $S_2O_3^{2-}$, SO_3^{2-} and S^0). For $\sum S_{aq}$, 40 mL of water samples were filtered (25 mm Pall Acrodisc® 0.45 µm Supor® membrane) via polypropylene syringes into 50 mL (Falcon™) tubes, immediately after 80 µL of HNO_3 (Optima grade, Fisher Chemical) was added to each tube, and stored at 4°C until further processed at CSIRO Land and Water laboratory (New South Wales, Australia). Analyses for total S were carried out using inductively coupled argon plasma emission spectrometry (ICP-AES)

(Varian730 ES, Mulgrave, VIC), with sulfur calibration standards prepared from a certified reference stock solution (AccuStandard New Haven, CT, USA) in 2% *v*/*v* HNO_3. By measuring intensity at the 181.972 nm sulfur emission line concentrations were determined with a limit of detection (LOD) for sulfur of 1 mg L^{-1} (0.03 mM). SO_4^{2-} and S^{2-} concentrations were quantified via spectrophotometry (Pharmacia Biotech Ultrospec 3000 UV/Visible Spectrophotometer) as described previously (Camacho et al. 2020).

SOI species $S_2O_3^{2-}$, SO_3^{2-} and S^0 were immediately preserved using a monobromobimane derivatization procedure for SOI analyses by HPLC (Rethmeier et al. 1997) and collected simultaneously with those for total S, ($\sum S_{aq}$), and redox end member species, SO_4^{2-} and S^{2-}. SOI species analyses were carried out with the Shimadzu LC-20AD prominence HPLC instrument with Alltima HP C18 (5 µm x 150 mm x 4.6 mm Grace™) reverse phase column. Solvents used in protocols were: A=Water, B=Methanol, C=Acetonitrile, D=Acetic acid 0.25% *v*/*v* pH 3.5 adjusted with NaOH (1 N). $S_2O_3^{2-}$ and SO_3^{2-} were analyzed via fluorescence excitation at 380 nm and emission at 480 nm. Standards and calibrations for $S_2O_3^{2-}$ (0-10 mM) and SO_3^{2-} (0-1.7 mM) were made with $Na_2S_2O_3$ (Sigma Aldrich, 99% purity) and Na_2SO_3 (Sigma Aldrich, ≥98% purity), respectively. The thiosulfate and sulfite elution protocol used an isocratic mobile phase B 35%, D 65%, with a flow rate of 0.5 mL min^{-1} and oven heated to 35˚C for a run time of 20 min. The sample size was 5 µL and elution times were 5 min for SO_3^{2-} and 6 min for $S_2O_3^{2-}$. S^0 was extracted with chloroform from the water samples and analyzed with reverse-phase HPLC and UV-absorption at 263 nm. Standards and calibrations (0-32 mM) were made from S^0 (Fisher, 99.5% purity) dissolved in chloroform. S^0 elution protocol used an isocratic mobile phase B 65%, C 35%, with a flow rate of 1 mL min^{-1} and run time of 10 min. The sample size was 10 µL and the elution time was at 5 min.

A mass balance enabled quantification of any unresolved or "Other SOI" S species not directly analyzed within this study for wastewater samples was determined by the difference between the sum of all measured solution sulfur species concentrations, (i.e. ∑ (SO_4^{2-}, S^{2-}, $S_2O_3^{2-}$, SO_3^{2-} and S^0) and the Total S ($\sum S_{aq}$) concentration. Lastly, by subtracting SO_4^{2-}, the end state of S oxidation, from $\sum S_{aq}$, we also determined the reactive S pool (S_{react}; Whaley-Martin et al. 2020) available for oxidation.

4.2.4. Microbial enrichments of mining wastewaters

4.2.4.1. Media preparation

Two types of media, a neutrophilic sulfur oxidizing media (NSOM), and an acidophilic sulfur oxidizing media (ASOM), that both used $S_2O_3^{2-}$ as the sulfur substrate were used in the SoxB experiments. $S_2O_3^{2-}$ was selected due to its importance as a major SOI in sulfur oxidation metabolism and its relevance to mining wastewaters as a widespread, abundant and recalcitrant byproduct found in wastewaters after processing of sulfide hosted ores (Bernier and Warren 2005, 2007; Bobadilla Fazzini et al. 2013; Druschel et al. 2004; Miranda-Trevino et al. 2013; Warren et al. 2008). Additionally, to link and expand upon its use in the Whaley-Martin et al. (2019) study.

NSOM was created in 1 L batches as follows: Part 1: 90 mL of 1.1% (*w*/*v*) K_2HPO_4 was added to 400 mL of tap water. Part 2: 5 g of $Na_2S_2O_3$, 90 mL of 0.44% (*w*/*v*) NH_4Cl, 90 mL of 0.11% (*w*/*v*) $MgSO_4$, 2.2 mL of Solution T and 320 mL of tap water. Part 1 and 2 were sterilized separately by either filtration (<0.2 μm) or autoclaving and then combined. Solution T was made by: 50 g of EDTA disodium salt dissolved into 400 mL of water, followed by 9 g of NaOH added to EDTA solution, then the following salts were added individually to 30 mL of water before being added to the EDTA solution: 5 g of $ZnSO_4.7H_2O$, 5 g of $CaCl_2$ (or 7.34 g of $CaCl_2.2H_2O$), 2.5 g

of $MnCl_2.6H_2O$, 0.5 g of $CoCl_2.6H_2O$, 0.5 g of $(NH_4)_6Mo_7O_{24}.4H_2O$, 5 g of $FeSO_4.7H_2O$ and 0.2 g of $CuSO_4.5H_2O$.

ASOM was made in 1 L batches incorporating 1 000 mL of distilled water, 5 g of $Na_2S_2O_3$, 0.2 g $(NH_4)_2SO_4$, 0.5 g $MgSO_4.7\ H_2O$, 0.36 g $CaCl_2.2\ H_2O$, 3 g KH_2PO_4, and 10 mg $FeSO_4$. The subsequent solution was then filter sterilized (<0.2 µm) or autoclaved.

4.2.4.2. Enrichment experimental design and sampling

All seven of the water samples underwent the three enrichment strategies: i) NSOM within a pH corral between 7-5 (NSOM 7-5); ii) ASOM within a pH corral between 7-5 (ASOM 7-5); and iii) ASOM within a pH corral between 5-3 (ASOM 5-3); meaning that the pH of the enrichment experiments was kept between 7-5 or 5-3. These pH corrals were chosen to identify key sulfur oxidizing microbes and identify possible microbial SoxB consortia progression from neutral to mildly acidic pH (7-5) and subsequently to moderately acidic pH (5-3) conditions.

The endemic microbial communities were enriched initially with a 1:1 ratio of unfiltered endemic mine wastewater to media, to make 150 mL of enrichment within sterile autoclaved 250 mL Erlenmeyer flasks, i.e. 75 mL of wastewater originating from the mine and 75 mL of media. These were then buffered to start at pH 7 with dilute sterile (0.2 µm filtered) NaOH and HCl. The enrichments were kept static in incubators at 28˚C with a 12 hour diel light. The pH was measured as described in Whaley-Martin et al. (2019) until each enrichment achieved the final lower pH of its specific pH corral, i.e. pH= 5 for the 7-5 enrichments, or pH= 3 for the 5-3 enrichments. Once the final pH was achieved a new run/cycle/generation(gen) was then created, with bacteria transferred to fresh media at a ratio of 1:2, i.e. 50 mL of current enrichment cycle and 100 mL of fresh media. This next gen flask was then buffered to the starting pH of the enrichment corral, i.e.

NSOM 7-5 and ASOM 7-5, starting pH= 7, and ASOM 5-3 starting pH= 5. Samples were collected at enrichment cycle generations 1, 3, 5, 10 and 15 (or latest generation before new sampling regime). A total of 46 sulfur oxidizing enrichment samples across all three enrichment strategies were analysed for DNA characterization as described below.

4.2.5. Microbial genetic analyses and characterization (16S rRNA gene)

4.2.5.1. DNA extraction and quantification

The endemic mine wastewater samples (3-7 L depending on sample) and SoxB enrichment samples (75 mL) were filtered on 0.2 μm filter towers (Thermo Scientific™ Nalgene™ Rapid-Flow™ Sterile Disposable Filter Units with CN Membrane). The filters were then aseptically transferred into sterile tubes and frozen at -20˚C until DNA extraction. The Qiagen's DNeasy® PowerWater® Kit was used to extract DNA from the filters as per manufacturer's guidelines. Samples of extracted DNA, alongside DNA extraction blanks to ensure non-contamination from the kits (Glassing et al. 2016; Salter et al. 2014), were sent to the McMaster Farncombe DNA Sequencing Facility (McMaster University, Hamilton, Ontario) for analysis. For eight samples, 16S rRNA gene data were extracted from metagenome results as described below. The samples library construction and sequencing were performed at the Farncombe Metagenomics Facility. Quantitative PCR (qPCR) was used to quantify the extracted 16S rRNA gene DNA from all samples and its concentrations adjusted for each step of the subsequent molecular protocol.

4.2.5.2. Genomic sequencing for 16S rRNA gene only samples

For the 16S rRNA gene sequencing, standard protocols of the Earth Microbiome Project (Caporaso et al. 2011, 2012) and Illumina adapted primers as Bartram et al. (2011) were used on aliquots of

purified DNA to amplify region V4 of the 16S rRNA gene by PCR. The 806r (GGACTACNVGGGTWTCTAAT) and 515f (GTGYCAGCMGCCGCGGTAA) variable regions of archaeal and bacterial 16S rRNA gene were amplified via modified primers. PCR was accomplished using 50 ng of template and the PCR mix comprised 1U of recombinant Taq DNA Polymerase (Invitrogen™), 1x buffer, 0.2 mmol L^{-1} dNTPs, 0.4 mg mL^{-1} BSA, 1.5 mmol L^{-1} MgCl2, and 5 pM of each primer. The reaction was carried out at 98°C for 5 min, 35 s (98°C) for 30 min, then 30 min (50°C) and 30 min (72°C), with a final extension of 72°C for 10 min. The PCR products were examined by electrophoresis and sent for sequencing. Illumina Mi-Seq sequencing was performed with all amplicons normalized to 1.25 ng μL^{-1} using the SequalPrep normalization kit (ThermoFisher#A1051001). Bimera checking was performed on the data through DADA2 (version 1.6.0). The 3-5% of reads that were detected as bimeras were subsequently excluded from further analyses as outlined in Whaley-Martin et al. (2019).

4.2.5.3. Genomic sequencing for metagenome samples

In the eight samples where metagenome data were sequenced, all available DNA (up to 1 µg) from each sample was fragmented using the Covaris S220 Ultrasonicator. Parameters for 500 bp shearing with 50 µL input were: 175W PIP, 5% duty factor, 200 cpb, 35 s. Dual-indexed shotgun libraries were prepared with the NEBNext Ultra DNA Library Prep Kit for Illumina (New England Biolabs Inc.). The libraries were quantitated by qPCR, pooled in equimolar amounts and sequenced using the Illumina HiSeq 1500 platform (Rapid v2 chemistry with onboard cluster generation, 151 bp paired-end reads). Raw data was processed with HCS v2.2.58 (RTA v1.18.64). File conversion and demultiplexing were performed with CASAVA v1.8.2 allowing 1 mismatch in the indexes.

4.2.5.4. 16S rRNA gene extraction from metagenomic sequences

FastQC [http://www.bioinformatics.babraham.ac.uk/projects/fastqc/] (Andrews 2018) was run to inspect read quality on all the samples. Cutadapt (Martin 2011) was used to trim Illumina adapters, filtering quality at 28 and trimming any Ns from the ends. Trimmed reads shorter than 50bp were discarded. After trimming, the number of read pairs per sample ranged from 6.8M to 18.3M with a mean of 9.7M. To identify which reads came from the 16S rRNA gene, the reads were mapped to the SILVA 16S database (version 1.3.2, (Quast et al. 2013)) with Bowtie2 (Langmead and Salzberg 2012) using default parameters (allowing discordant mapping and keeping only the best mapping of each read). The number of individual reads (not pairs) that mapped to the SILVA database from each sample ranged from 6,540 to 19,318 with a mean of 10,492. A fasta file was generated from the SAM file of mapped reads using SAMtools (Li et al. 2009). Then taxonomy was assigned to the reads using the DADA2 (version 1.6.0) (Callahan et al. 2016) implementation of the RDP classifier (Wang et al. 2007).

4.2.5.5. Bioinformatics and statistical analyses

In the 16S rRNA gene sequences, Cutadapt was used to trim raw sequences with a minimum quality score of 30 and a minimum read length of 100bp. DADA2 resolved sequence variants and its reads were filtered and trimmed based on the quality for each individual Illumina run. The sequence variant tables were amalgamated to combine all data from individual Illumina runs, while sequences identified as chloroplasts or mitochondria and bimeras were deleted. SILVA database version 132 was used to assign taxonomy, while microbial function was deduced from cultured representatives of the identified sequences. Sequences obtained in this study were deposited at NCBI under the bioproject accession number PRJNA636215.

To examine potential microbial community arrangements non-metric multidimensional scaling (NMDS) and hierarchical clustering, based on Bray–Curtis dissimilarities was used to determine any patterns after all samples underwent Hellinger transformation. To ascertain the difference between groups (i.e. endemic vs enrichment, and ASOM 7-5 vs ASOM 5-3) an analysis of similarity (ANOSIM) was implemented and p-values corrected using Bonferroni's correction. Vegan R scripts (Oksanen et al. 2010) (version 3.4.4; www.R-project.org) were used for these statistical analysis similarly done by Buttigieg and Ramette (2014) and Ramette (2007). To compare the relationship between the two prevalent genera *Halothiobacillus* and *Thiomonas* a linear regression on enrichment samples was analysed.

For the detailed phylogenetic characterization of 16S rRNA gene amplicons assigned as *Halothiobacillaceae* and *Thiomonas* spp., a phylogenetic tree based on maximum-likelihood was created using MEGA (ver. 7.0.26; Kumar et al. 2016). The 16S rRNA gene sequences of the related bacterial strains obtained from the database of SILVA (ver. 132), as well as *Halothiobacillaceae* detected from four mine tailing wastewater sites in a previous study (Whaley-Martin et al. 2019) were used as the reference. The nucleic acid sequences were aligned using ClustalW in MEGA, and the tree was created using Tamura-Nei model with 1000 bootstrap iterations.

4.3. Results

4.3.1. Geochemistry of mine wastewaters

The parent wastewater geochemistry reveals distinct differences between the two Ni mines and seasonally for each mine. Both mines exhibited circumneutral pH values over the sampling period. pH fluctuated between 6.2 (Summer 2014) and 7.2 (Winter and Summer 2015) at Mine 1, while Mine 2 exhibited a slightly higher initial pH in Summer 2014 (8.4), that decreased over time to 7.3 (Summer 2015) (Table 4.1). Total S concentration ($\sum S_{aq}$) was ≈2-3x higher at Mine 2 (16 mM – 23 mM) compared to Mine 1 (6 mM – 9 mM) (Table 4.1). Total S concentration decreased over time at Mine 2 from 27.9 mM to 16.0 mM, while Mine 1 showed no evident time dependent trend (Table 4.1). SOI speciation and concentrations also varied between the two mines. For Mine 1, the majority of S occurred as SO_4^{2-} (between 3.6 mM to 6.7 mM) followed by the Other SOI pool (i.e. unresolved S species, between 2.9 mM to 4.4 mM), with very low to non-existent concentrations of S^{2-}, S^0, $S_2O_3^{2-}$, SO_3^{2-} (Table 4.1). Reactive sulfur values for Mine 1 samples were < 46% of the total S pool (Table 4.1). Mine 2 parent wastewater SOI speciation and distribution also differed from that observed in Mine 1. $S_2O_3^{2-}$ and SO_4^{2-} were important SOI species ranging between 7.6 mM – 9.5 mM and 6.5 mM – 7.7 mM respectively (Table 4.1), S^{2-} and SO_3^{2-} concentrations were negligible, S^0 was consistently present at relatively low concentrations throughout (0.06 mM – 0.1 mM), and the Other SOI pool decreased over time from 13.2 mM to 1.7 mM, which was reflected in the decreasing S_{react} value over time (76.7% to 58.8%; Table 4.1).

Table 4.1: Sulfur geochemistry and pH of all endemic mine site samples. Concentrations of all S species are given in mM in mol of S (e.g. 1 mM of SO_4^{2-} = 1 mm S, while 1 mM $S_2O_3^{2-}$ = 2 mM S).

Mine site (Season)	pH	Total S (mM)	S^{2-} (mM)	S^0 (mM)	$S_2O_3^{2-}$ (mM)	SO_3^{2-} (mM)	SO_4^{2-} (mM)	Other SOI (mM)	S_{react} (Total S-SO_4^{2-}) (mM)	S_{react} Proportion (%)
Mine 1 (Summer 2014)	6.2	9.8	0	0	0.09 ± 0.02	<0.002	5.3 ± 0.2	4.4	4.5	45.9
Mine 1 (Winter 2015)	7.2	9.9	0	0	0.04 ± 0.001	0.005 ± <0.001	6.7 ± 0.1	3.1	3.2	32.3
Mine 1 (Spring 2015)	6.4	6.5	0	0	0.01 ± 0.002	0.003 ± 0.001	3.6 ± 0.3	2.9	2.9	44.6
Mine 1 (Summer 2015)	7.2	8.2	0	0	0.06 ± 0.006	0	4.9 ± 0.3	3.2	3.3	40.2
Mine 2 (Summer 2014)	8.4	27.9	0	0.06 ± <0.001	8.2 ± 0.3	0.008 ± <0.001	6.5 ± 0.4	13.2	21.4	76.7
Mine 2 (Spring 2015)	7.9	26.7	0	0.08 ± <0.001	9.5 ± 0.5	0.01 ± <0.001	7.7 ± 0.08	9.4	19	71.2
Mine 2 (Summer 2015)	7.3	16	0	0.1 ± 0.003	7.6 ± 0.07	0	6.6 ± 0.6	1.7	9.4	58.8

Thus, parent wastewater S geochemistry differs markedly between the two mines. Mine 1 has a relatively lower $\sum S_{aq}$ and the majority of its S occurs as SO_4^{2-} with < 46% of SOI occurring as S_{react}, the majority of which occurs as "Other SOI", i.e. unresolved intermediate oxidation state S species. In contrast, Mine 2 has a higher $\sum S_{aq}$, a higher S_{react} proportion occurring principally as $S_2O_3^{2-}$ and "Other SOI", and also evidently marked changes over time in its relative SOI distribution (Table 4.1). These variations in the SOI formed from many factors from the initial mineral ore, to the milling practices and chemical treatment procedures undergone (Mazuelos et al. 2019; Miranda-Trevino et al. 2013).

4.3.2. Microbial Communities

4.3.2.1 Endemic parent circumneutral mine wastewater microbial communities

A total of 378,301 reads were recovered for the seven endemic mine wastewater samples (Supplementary Table S1). Endemic microbial community diversity (Shannon Diversity) was higher for Mine 1 (3.02 – 3.46) which had a lower $\sum S_{aq}$ concentration and S_{react} proportion, compared to the same time point for Mine 2 (1.94 – 2.35) (Supplementary Table S2). Seasonal community trends also differed between the two mines. The Mine 1 Winter sample had the lowest number of unique sequences (55), and the highest (154) for the Spring sample for this site (Supplementary Table S2). In contrast, the Mine 2 Spring sample had the lowest number of unique sequences (38) of all samples (Supplementary Table S2). Further, a higher number of unique sequences were observed for Mine 1 (99 – 154) relative to Mine 2 (38 – 53) (Supplementary Table S2).

Proteobacteria dominated all seven of the wastewater parent samples collected at both mine sites. Ranging in relative abundance from 58% (Spring) - 77% (Summer) in Mine 1 and

increasing from 93% - 99% in Mine 2 over the sampling period of Summer 2014 to Summer 2015 (Figure 4.1A, Supplementary Table S2). In Mine 1, additional phyla were present in high relative abundance including *Bacteroidetes* decreasing from 27% - 18% over time and *Verrucomicrobia* (19%) in high abundance only during Spring (Figure 4.1A, Supplementary Table S2). The majority of *Proteobacteria* consisted of *Alphaproteobacteria* and *Gammaproteobacteria* across all samples (Figure 4.1B). In Mine 1, *Alphaproteobacteria* ranged from 36% - 60% relative abundance and *Gammaproteobacteria* ranged from 16% - 32%, while in Mine 2 *Alphaproteobacteria* ranged from 58% - 77% and *Gammaproteobacteria* 18% - 35% (Figure 4.1B, Supplementary Table S2).

The *Alphaproteobacteria* consisted mainly of families *Caulobacteraceae*, *Rhodobacteraceae*, *Sphingomonadaceae* and *Xanthobacteraceae* across all samples (Supplementary Table S2). *Sphingomonadaceae* was the most prevalent in Mine 1 ranging from 9% - 35% and a high abundance of the nitrogen fixing *Xanthobacteraceae* (19%) was also observed specifically for Summer 2015 in Mine 1. For Mine 2, *Sphingomonadaceae* was also the most dominant family, ranging from 2% - 49%, while *Caulobacteraceae* was highly abundant initially, decreasing over time from 44% to 19% (Supplementary Table S2). For *Gammaproteobacteria*, five families comprise the majority of abundance across this phylum, *Burkholderiaceae*, *Halothiobacillaceae*, *Hydrogenophilaceae*, *Legionellaceae* and *Methylophilaceae* (Supplementary Table S2). In Mine 1, *Burkholderiaceae* was the most prevalent ranging from 1% - 15% and in Mine 2, *Burkholderiaceae* decreased over time from 14% to <1% (Supplementary Table S2). In Mine 2, *Hydrogenophilaceae* was relatively high during both Summer 2014 and 2015 samples (17% and 20%) and low during Spring (<1%), while *Methylophilaceae* showed a reverse trend, lowest for Summer samples (both at 1%) and highest during Spring (12%) (Supplementary Table S2).

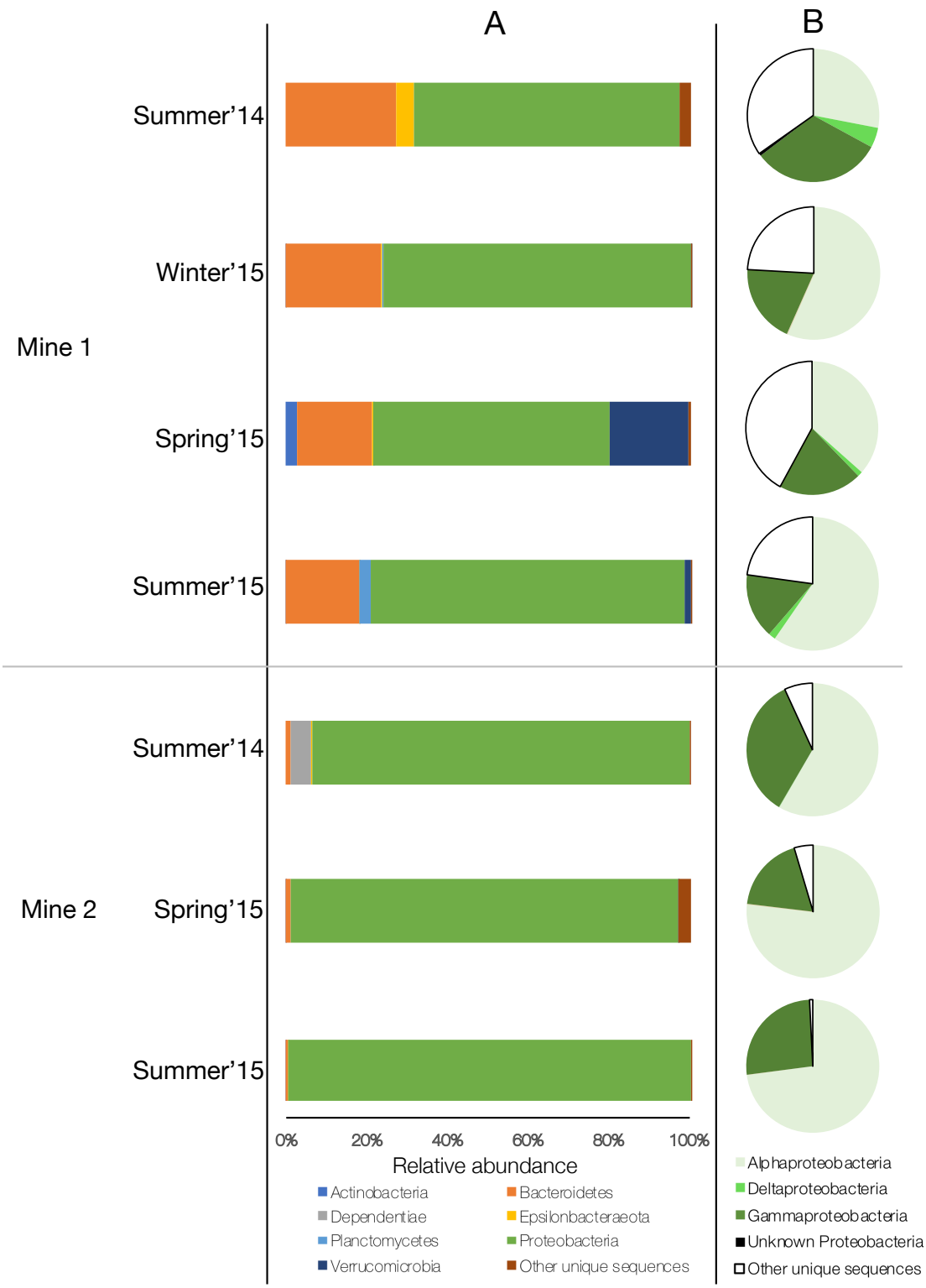

Figure 4.1: Relative sequence abundance of endemic community in both mines over seasons **A**) classified by bacterial phyla, ("Other unique sequences" are phyla with low abundance) and (**B**) classified by bacterial class for P*roteobacteria*, ("Other unique sequences" are remaining organisms not within *Proteobacteria)*.

Hierarchal clustering of endemic samples using Bray-Curtis dissimilarities at the genera taxon level revealed endemic parent communities clustered by mine site (Supplementary Figure S1). Mine 1 parent communities dissimilarity ranged between 62% and 77%, Mine 2 ranged between 56% and 71%, with dissimilarity between Mine 1 and Mine 2 at 86% (Supplementary Figure S1).

4.3.2.2. Sulfur oxidizing enrichment microbial communities

A total of 3,841,246 reads were recovered for the 46 sulfur oxidizing enrichment samples across all three enrichment strategies (Supplementary Table S1). As expected, Shannon Diversity and the number of unique sequences across all SoxB enrichments were lower than the endemic communities (Supplementary Table S1). NMDS statistics showed significant differences in community structure between the 7 endemic and 46 enrichment communities (ANOSIM R^2=0.96, P<0.001, Stress=0.11) (Figure 4.2), with clustering visible in enrichments irrespective of the initial mine site parent community (Figure 4.2, Supplementary Figure S1).

Similar to the results observed for the parent wastewater communities, *Proteobacteria* dominated >98% of every SoxB enrichment community. However, in a reverse abundance pattern observed in parent wastewater communities at the Class level, *Gammaproteobacteria* dominated all SoxB enrichments (>80% relative abundance), with *Alphaproteobacteria* comprising the remainder (Table 4.2). Further analysis identified two families, *Burkholderiaceae* and *Halothiobacillaceae* dominated the *Gammaproteobacteria* for 17 of the enrichments, representing > 69% of community abundance (Table 4.2). Only three Spring enrichments showed lower abundance levels for these two families, Mine 1 Spring 2015 NSOM 7-5 (47%), Mine 2 Spring 2015 NSOM 7-5 (54%) and Mine 2 Spring 2015 ASOM 5-3 (55%) (Table 4.2). Though parent

wastewater communities evidenced *Gammaproteobacteria* families *Hydrogenophilaceae*, *Legionellaceae* and *Methylophilaceae* (Supplementary Table S1), these were not prevalent in SoxB enrichments (Table 4.2). In contrast, *Rhodanobacteraceae* and *Xanthomonadaceae* were abundant only in the enrichments, representing up to 46% and 28% respectively (Table 4.2).

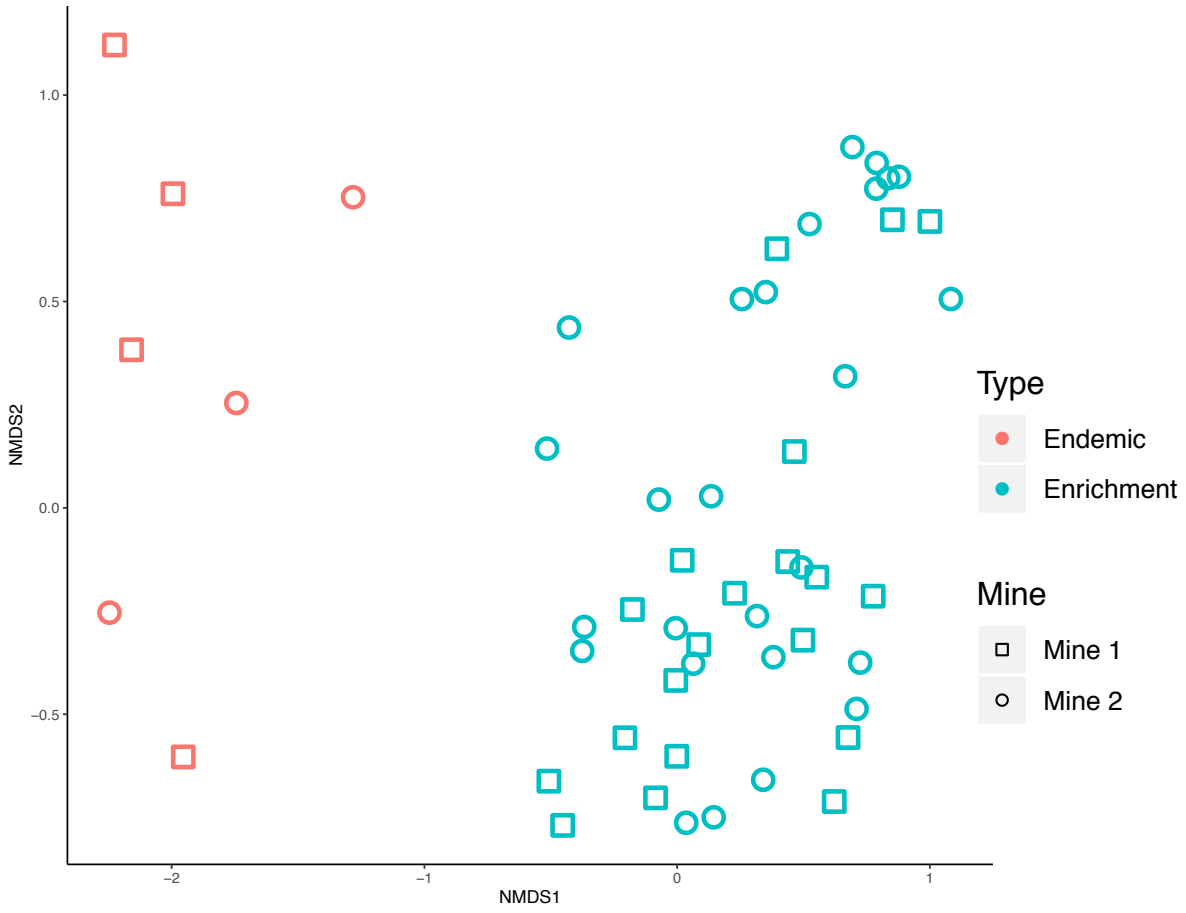

Figure 4.2: Microbial community structure depicting differences between enrichments and endemic parent communities. Non-metric multidimensional scaling (NMDS) plot of all 53 samples at sequence variants level (based on Bray-Curtis dissimilarity from Illumina sequencing of 16S rRNA gene amplicons) (ANOSIM R^2=0.96, P<0.001, Stress=0.11).

Table 4.2: Relative sequence abundance of end-point enrichment community for all enrichments. Classified by the family taxa of *Gammaproteobacteria*. "*Alphaproteobacteria*" relative abundance of the total class taxa. "Other unique sequences" is the remainder of organisms.

Mine Site	Season	Enrichment	Aeromonadaceae	Burkholderiaceae	Cardiobacteriaceae	Endozoicomonadaceae	Enterobacteriaceae	Halothiobacillaceae	Hydrogenophilaceae	Legionellaceae	Methylophilaceae	Pasteurellaceae	Pseudomonadaceae	Rhodanobacteraceae	Solimonadaceae	Unknown Gammaproteobacteria	Wohlfahrtiimonadaceae	Xanthomonadaceae	Alphaproteobacteria	Other unique sequences
Mine 1	Summer'14	NSOM 7-5 (run 15)	0	10	1	1	0	78	0	0	0	0	0	1	0	5	2	1	0	1
		ASOM 7-5 (run 14)	0	21	1	1	0	66	0	0	0	0	0	2	0	4	<1	4	0	1
		ASOM 5-3 (run 15)	0	43	<1	1	0	48	0	0	0	0	0	6	0	3	0	0	0	0
	Winter'15	NSOM 7-5 (run 10)	0	89	0	0	0	<1	0	0	0	0	0	11	0	0	0	<1	<1	<1
		ASOM 7-5 (run 10)	0	2	0	0	0	72	0	0	0	0	3	1	0	0	0	12	9	<1
		ASOM 5-3 (run 10)	0	27	0	0	0	50	0	0	0	0	<1	7	0	0	0	15	<1	2
	Spring'15	NSOM 7-5 (run 10)	0	6	0	0	0	41	0	0	0	0	25	<1	0	0	0	11	17	<1
		ASOM 7-5 (run 10)	0	19	0	0	0	62	0	<1	0	0	1	<1	0	0	0	8	10	<1
		ASOM 5-3 (run 10)	0	68	0	0	0	<1	<1	0	0	0	2	8	0	0	0	4	19	<1
	Summer'15	NSOM 7-5	-	-	-	-	-	-	-	-	-	-	-	-	-	-	-	-	-	-
		ASOM 7-5 (run 10)	0	30	0	0	0	70	<1	0	0	0	0	0	0	0	0	<1	<1	<1
		ASOM 5-3 (run 10)	0	97	0	0	0	<1	0	0	0	0	<1	3	0	0	0	<1	<1	<1
Mine 2	Summer'14	NSOM 7-5 (run 10)	0	32	1	1	0	61	0	0	0	0	0	1	<1	3	1	<1	<1	<1
		ASOM 7-5 (run 5)	1	26	<1	1	0	47	0	0	0	0	2	1	0	3	<1	10	7	0
		ASOM 5-3 (run 8)	0	24	1	1	0	69	0	0	0	0	0	0	0	4	1	0	0	<1
	Spring'15	NSOM 7-5 (run 10)	0	53	0	0	0	1	0	0	0	0	<1	2	0	0	0	28	15	<1
		ASOM 7-5 (run 10)	0	17	0	0	0	68	0	0	0	0	0	1	0	0	0	7	6	<1
		ASOM 5-3 (run 10)	0	54	0	0	0	<1	0	0	0	0	0	46	0	0	0	<1	<1	<1
	Summer'15	NSOM 7-5 (run 10)	0	>99	0	0	0	<1	0	0	0	0	0	<1	0	0	0	<1	<1	<1
		ASOM 7-5 (run 10)	0	98	0	0	<1	<1	0	0	<1	<1	<1	<1	0	0	0	<1	<1	1
		ASOM 5-3 (run 10)	0	>99	0	0	0	<1	0	0	0	0	<1	0	0	0	0	0	<1	<1

4.3.2.3. Comparison of pH corrals on enrichment community and microbial progression

NMDS statistics showed a significant difference occurred (ANOSIM R^2=0.24, P<0.001, Stress=0.12) between the microbial community structure of the ASOM 7-5 and 5-3 enrichments (identical media, pH the only variable of 7-5 vs 5-3; Supplementary Figure S2), identifying the

key control of pH on sulfur oxidizing microbial community composition. Statistics for the number of generations, media type, mine type or season showed no significant correlation across enrichment samples. *Halothiobacillus* spp (*Halothiobacillaceae)* dominated the experiments when pH was kept between 7 and 5, while *Thiomonas* spp. (*Burkholderiaceae*) dominated the enrichments when the pH was kept between 5 and 3 (Figure 4.3). For six of the seven wastewater samples investigated, *Halothiobacillus* spp. dominated community abundance in ASOM 7-5 enrichments (exception of Mine 2 Summer 2015; Figure 4.3). Further, *Halothiobacillus* spp. exhibited higher relative abundance in ASOM 7-5 compared to ASOM 5-3 enrichments (Figure 4.3). ASOM 5-3 enrichment results identified *Halothiobacillus* spp. dominating three samples (Summer 2014 for both mines and Winter 2015 Mine 1), with *Thiomonas* spp. dominating the remainder of samples. Across all ASOM enrichments, ASOM 5-3 had higher *Thiomonas* spp. abundance relative to ASOM 7-5 (Figure 4.3). These results are consistent with a pH dependent dominance of particularly the *Halothiobacillus* spp. between circumneutral pH (7) to mildly acidic (5), that is then replaced by *Thiomonas* spp. between mildly acidic pH (5) to moderately acidic (3) pH values.

Analyses examining the SoxB enrichment community composition across successive media cycles/generations (Gen 1, 3 and 5), revealed how quickly these bacterial consortia developed as a function of the pH corrals (Supplementary Data and Supplementary Figure S3). The dominate genera found in the SoxB enrichments were *Gammaproteobacteria* including the *Burkholderiaceae* and the *Halothiobacillaceae* families, and specifically genera *Halothiobacillus, Thiomonas* and *Thiovirga*. Results identify a progression within the *Halothiobacillaceae* family. Both *Halothiobacillus* and *Thiovirga* occurred in the higher pH corral 7-5 enrichment experiments; however *Halothiobacillus* outcompeted *Thiovirga* as successive generations occurred (Figure 4.3

and Supplementary Figure S3). In the lower pH corral 5-3 enrichment experiments, *Thiomonas* succeeded *Halothiobacillus* as generations proceeded (Supplementary Data and Supplementary Figure S3). Indeed, *Thiomonas* abundance was significantly negatively correlated to *Halothiobacillus* abundance across all 46 enrichment samples (linear regression R^2= 0.68, P<0.001) (Figure 4.4).

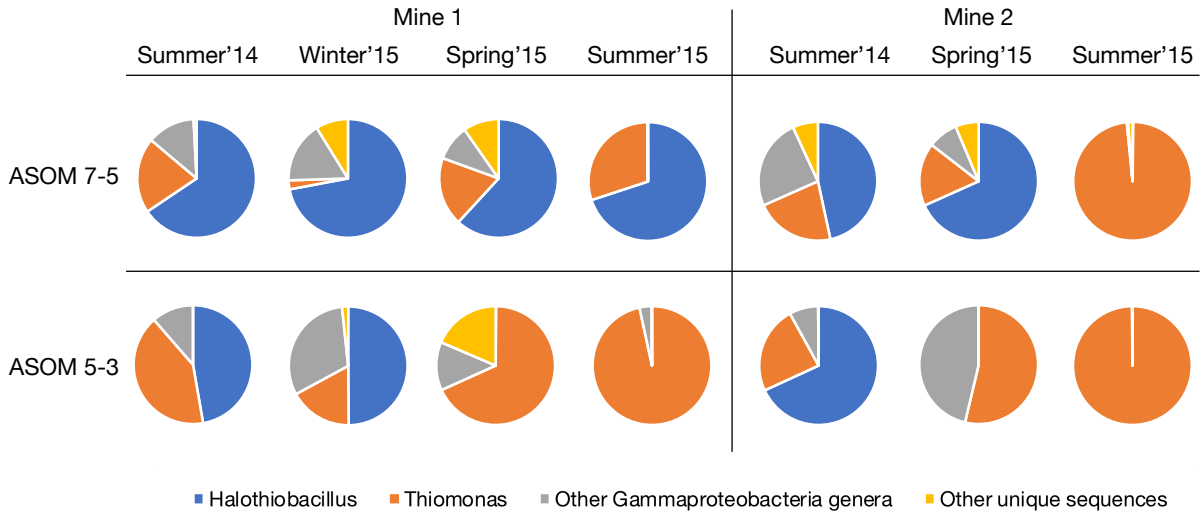

Figure 4.3: Relative sequence abundance of end-point generation samples between the two enrichment pH corrals ASOM 7-5 and ASOM 5-3 communities in both mines over seasons. Showing genera of *Halothiobacillus* spp. and *Thiomonas* spp., "Other *Gammaproteobacteria* genera" are organisms which belong to *Gammaproteobacteria* class but are not part of *Halothiobacillus* or *Thiomonas*, "Other unique sequences" is the remainder of organisms.

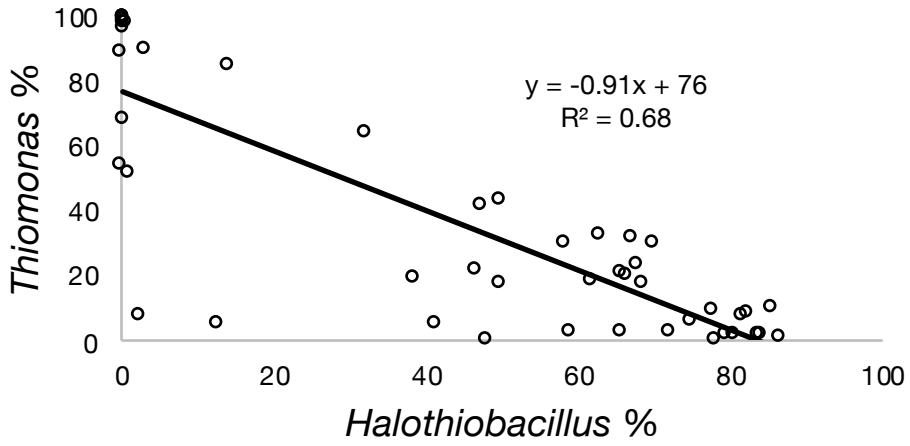

Figure 4.4: Relative abundance for *Thiomonas* vs *Halothiobacillus* in all enrichment samples. Showing linear regression relationship between the two genera (R^2=0.68, P<0.001).

4.3.2.4. Similarity of important identified genera in enrichments to previous study and related strains

Twelve distinct 16S rRNA gene sequences were found for *Halothiobacillus* spp., four for *Thiovirga* spp., one unclassified *Halothiobacillaceae* and six for *Thiomonas* spp. across all sequenced samples (Figure 4.5). Eight of the *Halothiobacillus* spp. showed high similarity with *Halothiobacillus neapolitanus*, alongside sequences found also in mine wastewaters reported on by Whaley-Martin et al. (2019) (Figure 4.5). The *Thiovirga* spp. showed similarity with *Thiovirga sulfuroxydans* and sequences from Whaley-Martin et al. (2019) (Figure 4.5). Our single unclassified *Halothiobacillaceae* also matched to unclassified *Halothiobacillaceae* found in their work and interestingly these unclassified sequences have closer similarity to the *Burkholderiaceae* family *Thiomonas* spp. than the other identified *Halothiobacillaceae* genera (Figure 4.5). For the *Thiomonas,* five of the six sequences relate best to *Thiomonas arsenitoxydans* and the other (*Thiomonas* D3) shows closer similarity to *Thiomonas delicata* (Figure 4.5).

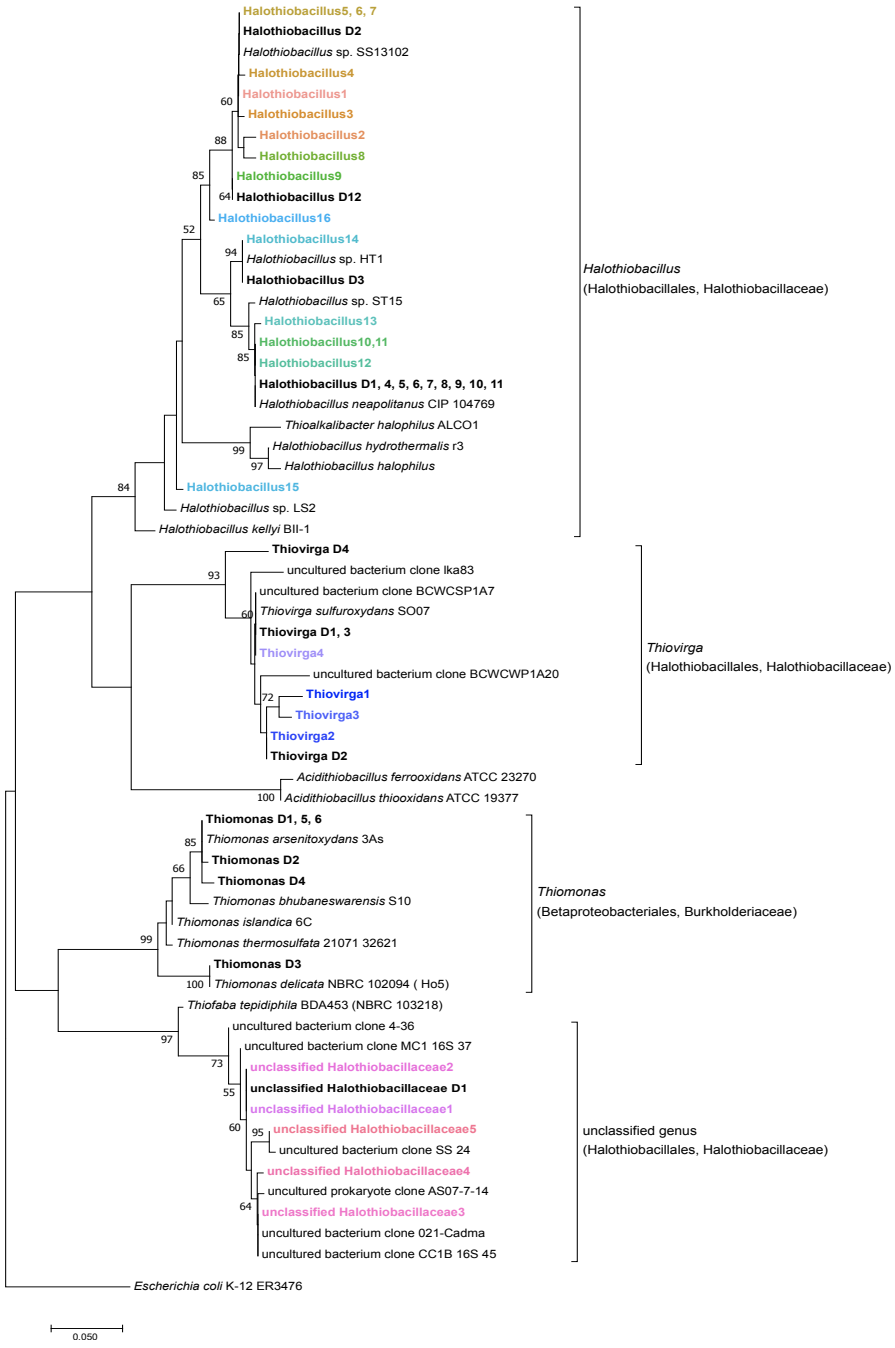

Figure 4.5: A maximum-likelihood phylogenetic tree of 16S rRNA gene amplicons (~264 bp) of the family *Halothiobacillaceae* and *Thiomonas* spp. Detected from this study's different mine tailing wastewater sites and enrichments (in bold, black) and a previous study (Whaley-Martin et al. 2019; bold, colors) showing the affiliation of sequences of the family *Halothiobacillaceae*. Reference genes of known *Halothiobacillaceae* and *Thiomonas* spp (isolates and uncultured clones), and *Acidithiobacillus* spp. in the databases of SILVA and NCBI are also shown and the tree was rooted with *E. coli* K-12. The tree was created with 1000 bootstrap iteration and the values below 50% are not reported. The scale bar represents 5% sequence divergence.

4.4. Discussion

4.4.1. AMD vs Circumneutral Wastewater Sulfur Oxidizing Microbes

The results show that microbial communities for seven samples collected from two circumneutral Ni mine wastewaters sites (pH 6.2 – 8.4; Table 4.1) across three seasons and two years were dominated primarily by *Proteobacteria* (Figure 4.1). Specifically, these communities comprised *Alphaproteobacteria* families *Sphingomonadaceae*, *Rhodobacteraceae* and *Caulobacteraceae*; and partially by *Gammaproteobacteria* families *Burkholderiaceae* and *Hydrogenophilaceae* (Supplementary Table S2). These results mirror those obtained by Whaley-Martin et al. (2019) for four mine wastewater systems ranging in pH from 6 to 7.3, which included Mine 1 in this study (M3 in that study; samples collected in 2017). Interestingly, Whaley-Martin et al. (2019) observed that *Gammaproteobacteria* dominated at two moderately acidic sites, specifically *Halothiobacillaceae* (pH=4.7) and by *Halothiobacillaceae* and *Burkholderiaceae* at a site with a pH of 4.3. Those results are consistent with the results of this study, which identify a shift in dominance from *Alphaproteobacteria* in circumneutral parent wastewater communities to *Gammaproteobacteria* in SoxB enrichments (Figure 4.1, Table 4.2).

pH has been found to be the main driver of the microbial ecology and community structure occurring in mining impacted wastes (Kuang et al. 2013; Liu et al. 2014). The majority of microbes found to occur in AMD (majority associated with waste rock) systems are bacteria, although, archaea are also common and more rarely observed, eukaryotes, such as fungi and protists (Baker and Banfield 2003; Huang et al. 2011; Kimura et al. 2011; Korehi et al. 2014; Leduc et al. 2002). An AMD community typically contains a dominance of iron oxidizers, especially in iron-rich ores, and sulfur oxidizers reflecting the opportunities to gain energy from both sulfur and iron

metabolism as pH decreases below 3. The common and thus well-studied AMD sulfur oxidizing organisms belong to *Proteobacteria*, mainly *Gammaproteobacteria* including *Acidithiobacilli*, *Alphaproteobacteria* including *Acidiphilum*, and to a lesser extent *Betaproteobacteria* and *Deltaproteobacteria* (Baker and Banfield 2003; Kelly and Wood 2000; Kimura et al. 2011). Sulfur oxidizing bacteria, *Sulfobacillus* and archaea, *Sulfolobales* have also been found in acidic sites, though the sulfur oxidizing archaea have been mainly found in natural geothermal acidic environments rather than AMD sites (Niu et al. 2016). These studies identify that the sulfur oxidizing microbes occurring in AMD contexts appear to belong to a select few genetic groups: *Nitrospira, Proteobacteria, Firmicutes, Sulfolobales* and *Actinobacteria* (Johnson and Hallberg 2003; Kimura et al. 2011; Kuang et al. 2013).

As identified previously, far fewer studies exist that have assessed mining wastewaters associated with tailings ponds and non-acidified pH specifically. Leduc et al. (2002) examined the tailings pond microbial communities at four mines with pH ranging between 3-6, i.e. in the moderately acidic range, identifying sulfur oxidizers *Halothiobacillus neopolitanus*, *Starkeya novella* and *Thiomonas intermedia*. Interestingly, Hallberg and Johnson (2003) also found the presence of *Halothiobacillus neopolitanus* and *Thiomonas* spp. to be the prevalent microbes present in tailings ponds at two mines exhibiting pH values of 6.3 and 3.4. Korehi et al. (2014) found bacteria predominated within the tailings dumps at various depths and pH (3.2 - 6.5) of three separate mines. That study observed bacterial communities were dominated by *Firmicutes,* families *Alicyclobacillaceae* and *Peptococcaceae*; and *Proteobacteria,* family *Hydrogenophilaceae*; and *Actinobacteria,* family *Micrococcaceae*. However, the *Proteobacteria* were only detected for surface depth samples where the pH was highest (3.6 – 6.5) in these tailings dumps (Korehi et al. 2014).

Interestingly, the results of Korehi et al. (2014) corroborate our observed pH dependent microbial community SoxB enrichment experimental results, that the microbial communities of wastewater, tailings dumps and waste rock of mining contexts are each composed of unique microbial community structures, differentiated by the pH of these different contexts.

4.4.2. Seasonal vs Geochemical endemic microbial community changes

4.4.2.1. Geochemical dependent microbial trends

All mine wastewater samples recorded circumneutral pH values (pH 6.2 – 8.4; Table 4.1). Mine 2 had higher Total S concentrations and a higher relative proportion of S_{react} (defined as all S with an oxidation state < +VI and therefore capable of oxidation and impact generation; determined as [Total S] - [sulfate]; Whaley-Martin et al. 2020) across comparable Summer 2014, Spring 2015 and Summer 2015 sampling times (Table 4.1). Over the time course examined, parent waters at Mine 2 decreased in pH and Total S while no discernible seasonal or time course trends emerged for Mine 1 (Table 4.1). It has been shown that pH and geochemical concentrations play an important role in the microbial community structure in mining systems (Korehi et al. 2014; Kuang et al. 2013; Liu et al. 2014; Niu et al. 2016). This geochemical driven difference in microbial community structure was observed between the two mine sites. Although both mines had abundant *Proteobacteria* (58% – 99%) primarily as *Alphaproteobacteria* (28% – 77%), Mine 2 was solely dominated by *Proteobacteria* (93% – 99%) compared to a significant proportion of *Bacteroidetes* (18% – 27%) in Mine 1. Mine 1 also demonstrated a higher Shannon Diversity, evenness and number of unique sequences across all samples (Figure 4.1, Supplementary Table S2). This result was likely due to the lower total sulfur concentration and/or reactive sulfur proportion, which may enable a greater diversity of microbes to inhabit these wastewaters at Mine 1 due to the low reactive

S allowing for greater competition in other microbial metabolisms like nitrogen or carbon (Kuang et al. 2013; Niu et al. 2016; Whaley-Martin et al. 2019). The hierarchal clustering of microbial communities by mine site based on Bray-Curtis dissimilarity (Supplementary Figure S1) is also consistent with the observed sulfur geochemical differentiation of the two mines wastewaters.

4.4.2.2. Seasonal dependent microbial trends

For Mine 1, the community diversity as assessed by all measures; diversity index, evenness and number of unique sequences, was reduced for the Winter 2015 sample followed by the greatest diversity and number of unique sequences in the Spring 2015 sample (Table S2). This result may be reflected by the colder temperature and ice cover on the tailings pond which reduced community diversity in winter. The spring thaw and surface run-off including natural water sources, into the tailings pond would enable the influx of other microbes, consistent with the lowest relative abundance of *Proteobacteria* observed for all samples (58%) (Figure 4.1, Supplementary Table S2).

Literature examining the microbial communities of any mining waste systems over multiple seasons is very limited, particularly on circumneutral wastewaters. Leduc et al. (2002) examined multiple moderately acidic tailings impacted streams over a year, using the culture dependent most probable number technique. Huang et al. (2011) studied a tailings dump of an acidified site over a summer, winter and spring using both culture dependent and independent techniques. Neither of these studies on acidic sites noted any seasonal community trends.

4.4.3. Enrichment succession *Halothiobacillus* spp. to *Thiomonas* spp.

Our results for the enrichments further highlighted a pH-dependent succession of *Alphaproteobacteria* to *Gammaproteobacteria* in the endemic microbial communities as observed in Whaley-Martin et al. (2019). The potential microbial indicator *Halothiobacillus* spp suggested by Whaley-Martin et al. (2019) is corroborated by our results here, as an indicator of pH decline from circumneutral to mildly acidic pH (Figure 4.3). This trend in decreasing pH and shift in endemic community structure to *Halothiobacillaceae* was also observed for the parent wastewater sample collected in 2015, (Mine 1 Summer 2015 this study) and in 2017 Whaley-Martin et al. (2019; M3 that study Summer 2017).

Results here assessing SoxB enrichment consortia structure as a function of pH (7-5 and 5-3 corrals), more conclusively reveal the potential for the increasing abundance of *Halothiobacillus* spp to serve as an early warning indicator of AMD initiation, when pH values may not yet have decreased. As well as, the shift from *Halothiobacillus* spp to *Thiomonas* spp to serve as a biological indicator that signals an important acceleration in acid generation associated with decreasing *Halothiobacillus* spp relative to *Thiomonas* spp (Figures 3, 4 and Supplementary Figure S3). This trend is evident also in parent wastewater communities, even though they may only be present at very low abundances at circumneutral pH (Supplementary Table S2). These results support those first suggested by Whaley-Martin et al. (2019). This relationship with progressive changes to microbial community structure associated to decreasing pH has been recorded previously in tailings dumps across circumneutral to acidic conditions, correlating with the *Alphaproteobacteria* (Liu et al. 2014).

The *Thiomonas* spp, of which strains found in our samples most closely related to *T. delicata* and *T. arsenitoxydans* (Figure 4.5), are chemolithoautotrophs, capable of withstanding

high stress associated with soluble metals, and identified as a moderate acidophile and sulfur oxidizer (Arsène-Ploetze et al. 2010; Battaglia-Brunet et al. 2006; Katayama et al. 2006). *Thiomonas* spp. have been found across multiple mine wastewater sites of various metal mines (Johnson and Hallberg 2003) and their ability to survive in these systems lends well to the use of them as an indicator due to their ubiquitous nature and their genetic and metabolic capabilities towards acid resistance and generation (Arsène-Ploetze et al. 2010).

4.5. Conclusions

Results here identified that circumneutral mining wastewaters collected from tailings ponds exhibit a different microbial community structure than the more well studied waste rock classic AMD context. Wastewater *in situ* microbial communities were more diverse with more unique sequences from Mine 1, resulting in clear NMDS differentiation between the two mines microbial communities. Mine 1 also exhibited a lower Total S concentration and reactive S proportion relative to Mine 2. Suggesting microbial community structure trends in parent wastewater communities were driven by geochemical variation. *Proteobacteria* dominated all wastewater parent and enrichments communities ranging between 58% - 99% of the community abundances. However, a shift in dominance from primarily *Alphaproteobacteria* (28% - 77%) in the circumneutral parent wastewater communities to *Gammaproteobacteria* (>80%) in moderately acidic enrichment communities. A further pH dependent shift from *Halothiobacillus* spp. dominating the pH 7 to 5 enrichments, to *Thiomonas* spp. dominating the pH 5 to 3 enrichments, identifies a successional, pH dependent shift in both the Family and the dominant genus from *Halothiobacillus* to *Thiomonas*. These results provide putative biological indicators that can be explored for better prediction and management of sulfur processing and AMD onset within mining wastewaters.

References

Andrews S (2018) Babraham Bioinformatics - FastQC A Quality Control tool for High Throughput Sequence Data. http://www.bioinformatics.babraham.ac.uk/projects/fastqc/.

Arsène-Ploetze F, Koechler S, Marchal M, Coppée JY, Chandler M, Bonnefoy V, Brochier-Armanet C, Barakat M, Barbe V, Battaglia-Brunet F, Bruneel O (2010) Structure, function, and evolution of the *Thiomonas* spp. genome. PLoS genetics 6(2).

Baker BJ, Banfield JF (2003) Microbial communities in acid mine drainage. FEMS Microbiol Ecol 44:139–152. http://dx.doi.org/10.1016/S0168- 6496(03)00028-X.

Barlow M (2013) *Blue Future: Protecting water for people and the planet forever*. House of Anansi Press Inc.

Bartram AK, Lynch MDJ, Stearns JC, Moreno-Hagelsieb G, Neufeld JD (2011) Generation of multimillion-sequence 16S rRNA gene libraries from complex microbial communities by assembling paired-end Illumina reads. Appl Environ Microbiol 77:3846–3852. doi:10.1128/AEM.02772-10.

Battaglia-Brunet F, Joulian C, Garrido F, Dictor MC, Morin D, Coupland K, Johnson DB, Hallberg KB, Baranger P (2006) Oxidation of arsenite by *Thiomonas* strains and characterization of *Thiomonas arsenivorans* sp. nov. Antonie van Leeuwenhoek 89:99–108.

Bernier L, Warren L (2005) Microbially driven acidity generation in a tailings lake. Geobiology 3:115-133.

Bernier L, Warren LA (2007) Geochemical diversity in S processes mediated by culture-adapted and environmental-enrichments of *Acidithiobacillus* spp. Geochim Cosmochim Acta 71:5684-5697.

Bobadilla Fazzini RA, Cortés MP, Padilla L, Maturana D, Budinich M, Maass A, Parada P (2013) Stoichiometric modeling of oxidation of reduced inorganic sulfur compounds (Riscs) in *Acidithiobacillus thiooxidans*. Biotechnol Bioeng 110:2242-2251.

Buttigieg PL, Ramette A (2014) A guide to statistical analysis in microbial ecology: a community-focused, living review of multivariate data analyses. FEMS Microbiol Ecol 90:543–550. doi:10.1111/1574-6941.12437

Callahan BJ, McMurdie PJ, Rosen MJ, Han AW, Johnson AJA, Holmes SP (2016) DADA2: High-resolution sample inference from Illumina amplicon data. Nat Methods 13:581.

Camacho D, Frazao R, Fouillen A, Nanci A, Lang BF, Apte SC, Baron C, Warren LA (2020) New insights into *Acidithiobacillus thiooxidans* sulfur metabolism through coupled gene

expression, solution chemistry, microscopy and spectroscopy analyses. Front Microbiol 11:411. doi: 10.3389/fmicb.2020.00411

Caporaso JG, Lauber CL, Walters WA, Berg-Lyons D, Huntley J, Fierer N, Owens SM, Betley J, Fraser L, Bauer M, Gormley N (2012) Ultra-high-throughput microbial community analysis on the Illumina HiSeq and MiSeq platforms. ISME J 6:1621–1624. doi:10.1038/ismej.2012.8.

Caporaso JG, Lauber CL, Walters WA, Berg-Lyons D, Lozupone CA, Turnbaugh PJ, Fierer N, Knight R (2011) Global patterns of 16S rRNA diversity at a depth of millions of sequences per sample. Proc Natl Acad Sci 108:4516–4522. doi:10.1073/pnas.1000080107.

Cowie BR, Slater GF, Bernier L, Warren LA (2009) Carbon isotope fractionation in phospholipid fatty acid biomarkers of bacteria and fungi native to an acid mine drainage lake. Org Geochem 40:956-962.

Dockrey JW, Services LE, Lindsay M, Norlund KLI, Warren LA (2014) Acidic Microenvironments in Waste Rock Characterized by Neutral Drainage: Bacteria–Mineral Interactions at Sulfide Surfaces. Minerals 4:170–190. doi:10.3390/min4010170.

Druschel GK, Baker BJ, Gihring TM, Banfield JF (2004) Acid mine drainage biogeochemistry at Iron Mountain, California. Geochem T 5:13-32.

Glassing A, Dowd SE, Galandiuk S, Davis B, Chiodini RJ (2016) Inherent bacterial DNA contamination of extraction and sequencing reagents may affect interpretation of microbiota in low bacterial biomass samples. Gut Pathog 8:24. doi: 10.1186/s13099-016-0103-7.

Hallberg KB, Johnson DB (2003) Novel acidophiles isolated from moderately acidic mine drainage waters. Hydrometallurgy 71:139-148.

Huang LN, Zhou WH, Hallberg KB, Wan CY, Li J, Shu WS (2011) Spatial and temporal analysis of the microbial community in the tailings of a Pb-Zn mine generating acidic drainage. Appl Environ Microbiol 77:5540-5544.

Johnson DB, Hallberg KB (2003) The microbiology of acidic mine waters. *Res. Microbiol*. 154:466-473.

Katayama Y, Uchino Y, Wood AP, Kelly DP (2006) Confirmation of *Thiomonas delicata* (formerly *Thiobacillus delicatus*) as a distinct species of the genus *Thiomonas* Moreira and Amils 1997 with comments on some species currently assigned to the genus. Int J Syst Evol Microbiol 56:2553–2557.

Kelly DP, Wood AP (2000) Reclassification of some species of *Thiobacillus* to the newly designated genera *Acidithiobacillus* gen. nov., *Halothiobacillus* gen. nov. and *Thermithiobacillus* gen. nov. Int J Syst Evol Microbiol 50:511–516.

Kimura S, Bryan CG, Hallberg KB, Johnson DB (2011) Biodiversity and geochemistry of an extremely acidic, low-temperature subterranean environment sustained by chemolithotrophy. Environ Microbiol 13:2092–2104. doi:10.1111/j.1462-2920.2011.02434.x.

Korehi H, Blöthe M, Schippers A (2014) Microbial diversity at the moderate acidic stage in three different sulfidic mine tailings dumps generating acid mine drainage. Res Microbiol 165(9):713-718.

Kuang JL, Huang LN, Chen LX, Hua ZS, Li SJ, Hu M, Li JT, Shu WS (2013) Contemporary environmental variation determines microbial diversity patterns in acid mine drainage. ISME J 7:1038.

Kumar S, Stecher G, Tamura K (2016) MEGA7: molecular evolutionary genetics analysis version 7.0 for bigger datasets. Mol Biol Evol 33:1870–1874. doi:10.1093/molbev/msw054

Langmead B, Salzberg SL (2012) Fast gapped-read alignment with Bowtie 2. Nat Methods 9:357.

Leduc D, Leduc L, Ferroni G (2002) Quantification of bacterial populations indigenous to acidic drainage streams. Water Air Soil Pollut 135:1-21.

Li H, Handsaker B, Wysoker A, Fennell T, Ruan J, Homer N, Marth G, Abecasis G, Durbin R (2009) The Sequence Alignment/Map format and SAMtools. Bioinforma Oxf Engl 25:2078–9.

Lindsay MB, Moncur MC, Bain JG, Jambor JL, Ptacek CJ, Blowes DW (2015) Geochemical and mineralogical aspects of sulfide mine tailings. Appl Geochem 57:157-177.

Liu J, Hua ZS, Chen LX, Kuang JL, Li SJ, Shu WS, Huang LN (2014) Correlating Microbial Diversity Patterns with Geochemistry in an Extreme and Heterogeneous Environment of Mine Tailings. Appl Environ Microbiol 80:3677–3686. doi:10.1128/AEM.00294-14.

Martin M (2011) Cutadapt removes adapter sequences from high-throughput sequencing reads. EMBnet.journal 17:10–2.

Mazuelos A, Iglesias-González N, Montes-Rosúa C, Lorenzo-Tallafigo J, Romero R, Carranza, F (2019) A new thiosalt depuration bioprocess for water-recycling in metallic sulphide mineral processing. Miner Eng 143:106031.

Miranda-Trevino JC, Pappoe M, Hawboldt K, Bottaro C (2013) The Importance of Thiosalts Speciation: Review of Analytical Methods, Kinetics, and Treatment. Crit Rev Env Sci Tec 43:2013-2070. doi: 10.1080/10643389.2012.672047.

Moncur MC, Ptacek CJ, Lindsay MB, Blowes DW, Jambor JL (2015) Long-term mineralogical and geochemical evolution of sulfide mine tailings under a shallow water cover. Appl Geochem 57:178-193.

Niu J, Deng J, Xiao Y, He Z, Zhang X, Van Nostrand JD, Liang Y, Deng Y, Liu X, Yin H (2016) The shift of microbial communities and their roles in sulfur and iron cycling in a copper ore bioleaching system. Sci Rep 6:34744. doi: 10.1038/srep34744.

Oksanen J, Blanchet G, Kindt R, Legendre P, O'Hara B (2010) Vegan: Community Ecology Package.

Quast C, Pruesse E, Yilmaz P, Gerken J, Schweer T, Yarza P, Peplies J, Glöckner FO (2013) The SILVA ribosomal RNA gene database project: improved data processing and web-based tools. Nucleic Acids Res 41:D590–6.

Ramette A (2007) Multivariate analyses in microbial ecology. FEMS Microbiol Ecol 62:142–160. doi:10.1111/j.1574-6941.2007.00375.x

Rethmeier J, Rabenstein A, Langer M, Fischer U (1997) Detection of traces of oxidized and reduced sulfur compounds in small samples by combination of different high-performance liquid chromatography methods. J Chromatogr A 760:295-302.

Salter SJ, Cox MJ, Turek EM, Calus ST, Cookson WO, Moffatt MF, Turner P, Parkhill J, Loman NJ, Walker AW (2014). Reagent and laboratory contamination can critically impact sequence-based microbiome analyses. BMC Biol 12:87. doi: 10.1186/s12915-014-0087-z

Schippers A, Breuker A, Blazejak A, Bosecker K, Kock D, Wright TL (2010) The biogeochemistry and microbiology of sulfidic mine waste and bioleaching dumps and heaps, and novel Fe(II)-oxidizing bacteria. Hydrometallurgy 104:342–350. doi:10.1016/j.hydromet.2010.01.012.

Schippers A, Jozsa P, Sand W (1996) Sulfur chemistry in bacterial leaching of pyrite. Appl Environ Microbiol 62:3424-3431.

Schippers A, Sand W (1999) Bacterial leaching of metal sulfides proceeds by two indirect mechanisms via thiosulfate or via polysulfides and sulfur. Appl Environ Microbiol 65:319-321.

Sheoran AS, Sheoran V (2006) Heavy metal removal mechanism of acid mine drainage in wetlands : A critical review. Miner Eng 19:105–116. doi:10.1016/j.mineng.2005.08.006.

Tyson GW, Chapman J, Hugenholtz P, Allen EE, Ram RJ, Richardson PM, Solovyev VV, Rubin EM, Rokhsar DS, Banfield JF (2004) Community structure and metabolism through reconstruction of microbial genomes from the environment. Nature 428:37-43.

Wang Q, Garrity GM, Tiedje JM, Cole JR (2007) Naïve Bayesian Classifier for Rapid Assignment of rRNA Sequences into the New Bacterial Taxonomy. Appl Environ Microbiol 73:5261–7.

Warren L, Norlund KI, Bernier L (2008) Microbial thiosulphate reaction arrays: The interactive roles of Fe (III), O2 and microbial strain on disproportionation and oxidation pathways. Geobiology 6:461-470.

Whaley-Martin KJ, Jessen G, Nelson TC, Mori J, Apte S, Jarolimek C, Warren LA (2019) The potential role of *Halothiobacillus* spp. in sulphur oxidation and acid generation in circum-neutral mine tailings reservoirs. Front Microbiol 10:297.

Whaley-Martin K, Marshall S, Nelson TE, Twible L, Jarolimek CV, King JJ, Apte SC, Warren LA (2020) A mass-balance tool for monitoring potential dissolved sulfur oxidation risks in mining impacted waters Mine Water Environ 39:291–307. https://doi.org/10.1007/s10230-020-00671-0

Chapter 5

Microbial Sulfur Reaction Pathways from Circumneutral to Acidic pH on Thiosulfate and Tetrathionate in Mine Wastewater Enrichment Communities

David Camacho[1] and Lesley A. Warren[1,2]

[1]School of Geography and Earth Science, Faculty of Science, McMaster University, Hamilton, ON, CA;
[2]Department of Civil and Mineral Engineering, Faculty of Applied Science and Engineering, University of Toronto, Toronto, ON, CA;

Abstract

Here experiments examining the collective influence of (1) sulfur oxidation intermediate (SOI) speciation ($S_2O_3^{2-}$, $S_2O_3^{2-}$ + $S_4O_6^{2-}$, or $S_4O_6^{2-}$); (2) total S concentration ([4mM] or [20mM]); and (3) sulfur oxidizing bacteria (SoxB) enrichments varying in recently identified known mining wastewater *Halothiobacillus* and *Thiomonas* genera, abundances ((A) ~ equal *Halothiobacillus* and *Thiomonas*; (B) *Halothiobacillus* dominant and (C) *Thiomonas* dominant) reveal new potential geochemical signals that signal a shift to initiation of AMD processes in mining wastewaters. Results identify that sulfur reaction pathways, which all ultimately were dominated by oxidation to sulfate reactions at pH < 3, were most strongly driven by SOI speciation for all three SoxB enrichment communities and two total S concentration. They importantly identify that irrespective of whether thiosulfate or tetrathionate, ubiquitous thiosalts species occurring in sulfide ore-based tailings, occur in these mining wastewaters, predictable changes in SOI speciation as a function of pH will occur for each of these two species; and that when both are present, the outcomes reflect additivity. Importantly these results newly identify that the observed relationship between increasing [Elemental S] and decreasing pH as pH decreases from 6 → 3, signals that the system is shifting towards the domination of sulfur oxidation reactions and thus high acidity generation. Further, SO_4^{2-}:H^+ ratios quantifying the relative intensity of acid consuming (i.e., dis/comproportionation) to acid generating (i.e., oxidation) reactions revealed the importance of acid consuming reactions during early stage (i.e., circumneutral pH conditions) microbial S autotrophic metabolism with either or both SOI species as starting substrate (Supplemental Table S3). Collectively, these results identify that under varying occurrence of important mining wastewater SOI species and sulfur concentrations common to base metal mining wastewaters,

important SoxB identified in this thesis (*Halothiobacillus* spp. and/or *Thiomonas* spp.) catalyze a predictive set of SOI reactions that are linked to observable pH changes and sulfate production. These results provide putative indicators that can guide development of new biologically informed, more accurate monitoring tools for mines to manage sulfur compounds within their wastewaters more effectively during circumneutral pH conditions, i.e., before run-away acid generation that is difficult to reverse, initiates.

5.1. Introduction

Microbial sulfur oxidation processes have long been recognized to be involved in the generation of acid mine drainage (AMD) (Pronk *et al.*, 1990; Jonhson and Hallberg, 2003; Bernier and Warren, 2005; Nordstrom *et al*., 2015) associated with oxidation of sulfide minerals in tailings and waste rock impoundments (Schippers and Sand, 1999; Elberling *et al*., 2000; Schippers *et al.*, 2010). Less well studied are the sulfur linked acidification processes occurring in typically circumneutral mine wastewater impoundments containing sulfide ore derived tailings. These wastewaters typically contain a suite of aqueous sulfur oxidation intermediates (SOI; Warren *et al.*, 2008; Miranda-Trevino *et al.*, 2013; Whaley-Martin *et al.*, 2019; Camacho *et al*., 2020a, b). However, the industry monitoring and treatment focus has been on a specific subset of stable (under impoundment pH conditions) sulfur oxy-ion compounds of the form $S_nO_x^{2-}$ (i.e. thiosulfate $S_2O_3^{2-}$, tetrathionate $S_4O_6^{2-}$) termed "thiosalts" by the industry that are commonly generated during extraction of sulfide ores (Druschel *et al.*, 2004; Bernier and Warren, 2005; Bernier and Warren, 2007; Warren *et al.*, 2008; Bobadilla Fazzini *et al.*, 2013; Miranda-Trevino *et al.*, 2013; Whaley-Martin *et al.,* 2020).

The oxygen driven oxidation of these thiosalts in the wastewaters can cause acid generation (Eq 1 and 2) and their relative dominance in the overall microbial catalysis of possible S oxidation reactions relative to dis/comproportionation reactions (that can consume acidity) can be represented by the SO_4^{2-}:H^+ ratio (Suzuki, 1999; Bernier and Warren, 2007; Smuda *et al.*, 2008; Nordstrom, 2015).

$$S_2O_3^{2-} + 2O_2 + H_2O \rightarrow 2SO_4^{2-} + 2H^+ \quad (1)$$

$$S_4O_6^{2-} + 3½O_2 + 3H_2O \rightarrow 4SO_4^{2-} + 6H^+ \quad (2)$$

However, recent results from my thesis (Chapter 3, Camacho *et al.*, 2020a), as well as others (Whaley-Martin *et al*., 2019) have identified that aerobic microbial sulfur oxidation metabolism, highly active in these contexts, catalyzes a greater diversity of SOI cycling reactions. These include dis/comproportionation and/or other acid consuming reactions that maintain a pool of intermediate SOI compounds and disconnect SO_4^{2-}:H^+ ratios from those expected for when oxidation reactions dominate (i.e., Eq 1 and 2). Hypothesized here, microbial processing of thiosulfate is likely to involve more of these S recycling reactions resulting in the maintenance of S in SOI compounds and lower SO_4^{2-}:H^+ ratios not consistent with Eq 1, as the available literature has shown its important role in such reactions (Suzuki, 1999; Bernier and Warren, 2007); while microbial processing of tetrathionate is likely more dominated by oxidation associated with possible energy gain from that reaction for the microbes involved and thus higher SO_4^{2-}:H^+ ratios more consistent with Eq 2 (Druschel, 2002; Camacho *et al.,* 2020a). The characterization of the reactions and associated sulfate and acid outcomes involved in microbial oxidation of these two widespread SOI compounds in mining wastewaters would provide more accurate identifiers of when such reactions are initiating, i.e., pre net acid generating conditions, that would support mines' ability to adaptively manage their wastewaters.

In addition to the importance of SOI specificity, the identities of microbes capable of sulfur oxidation metabolism present within wastewaters affects sulfur cycling (Suzuki, 1999; Li *et al.*, 2017; Wang *et al*., 2019). Very recent results generated by this thesis (Chapter 4, Camacho *et al*., 2020b) as well as Whaley-Martin *et al*. (2019) have identified two important sulfur oxidizing bacteria (SoxB) genera that affect S cycling in a pH dependent manner in these tailings impoundments. Specifically, field and experimental results demonstrated that *Halothiobacillus spp*. appear to dominate associated with initiation of S cycling at circumneutral pH wastewater

values, that ultimately lead to acidic conditions (Whaley-Martin *et al.*, 2019). Here, my experimental results for Objective 2 of this thesis (Chapter 4), determined that *Thiomonas* succeeds *Halothiobacillus* as the pH drops below 5 in SoxB enrichment experiments from seasonally collected wastewaters from two different base metal mines, suggesting an ecological transition that may be important to AMD processes that could serve as microbial signals (Camacho *et al.*, 2020b). However, whether these emerging results reflect specific pH preferences of these two SoxB genera, and/or their respective capacities for processing of different SOI species that typically occur at these different pH values have yet to be determined.

Thus, here, the objectives were to identify the key metabolic pathways, S species and pH outcomes in well controlled microbial SoxB experiments with varying *Halothiobacillus* to *Thiomonas* abundance for the two ubiquitous and important thiosalts species occurring in mining wastewaters, thiosulfate and tetrathionate. The thiosalts were added individually or in combination ($S_2O_3^{2-}$, $S_4O_6^{2-}$, or $S_2O_3^{2-}$ + $S_4O_6^{2-}$), at two total S concentrations (4 mM or 20 mM of S) to prevent exhaustion of a particular SOI species, such as thiosulfate, as commonly occurs as pH decreases below 5. To systematically identify the interactive collective influence of these variables on S speciation and pH outcomes in simulated wastewaters.

5.2. Methods

5.2.1. *Halothiobacillus – Thiomonas* SoxB enrichments

The three SoxB enrichment communities chosen for these experiments were previously reported on in Chapter 4 results, Camacho *et al.* (2020b). These SoxB enrichments were generated from parent wastewaters from two different mines and were selected because they differed in their relative abundances of *Halothiobacillus* and *Thiomonas*, with A) having similar abundances of each, B) having a 3:1 ratio of *Halothiobacillus* and C) being dominated by *Thiomonas* (Table 5.1). A full description on community enrichment methods are provided in Chapter 2 (pages 53-56) as well as in Chapter 4 (pages 122-124).

To regrow the preserved (-80˚C; Chapter 2, page 54) microbial enrichment communities, samples were thawed at room temperature. Once thawed, the tube was shaken/vortexed to ensure cells were suspended in the sample, then poured into fresh acidophilic sulfur oxidizing enrichment media (ASOM) and grown under identical conditions of the initial sample enrichment as described in Chapter 4 (pages 122-123, Camacho *et al.,* 2020b).

Table 5.1: Relative abundances of the three biological SoxB enrichment communities down to genera taxa.

	A (Mine 1 2014)	B (Mine 2 2014)	C (Mine 2 2015)
Halothiobacillus	47	68	<1
Thiomonas	41	24	>99
Other Gammaproteobacteria genera	11	8	<1
Other OTUs	0	<1	<1

5.2.2. Media and synthetic wastewater recipes for experiments

5.2.2.1. Microcosm enrichment media creation

ASOM was made in 1 L batches as follows. In 1 000 ml of distilled water the following salts were added individually until dissolved, 5 g of $Na_2S_2O_3$, 0.2 g $(NH_4)_2SO_4$, 0.5 g $MgSO_4.7\ H_2O$, 0.36 g $CaCl_2.2\ H_2O$, 3 g KH_2PO_4 and 10 mg $FeSO_4$. The solution was then filter sterilized (< 0.2 µm).

5.2.2.2. Synthetic mine wastewater sulfur treatments

Six experimental conditions were created assessing two concentrations of total S, a low [Total S] at 4 mM (in mM of S) and a high [Total S] at 20 mM (in mM of S) comparable to the range of Total S observed in Whaley-Martin *et al.* (2019) and Camacho *et al.* (2020b), and three different combinations of SOI species, $S_2O_3^{2-}$, $S_2O_3^{2-}$ + $S_4O_6^{2-}$ and $S_4O_6^{2-}$ for each of these total S concentrations.

The synthetic mining wastewaters were created in 5 L batches as follows: A base solution was created with 5 000 ml of MQ water and the following salts added individually until dissolved, 1 g $(NH_4)_2SO_4$, 1.25 g $MgSO_4.7\ H_2O$, 1.8 g $CaCl_2.2\ H_2O$, 2.5 g KH_2PO_4 and 90 mg $FeSO_4.7\ H_2O$. The SOI sources (thiosulfate and/or tetrathionate) were then added as per the experimental design: i) $S_2O_3^{2-}$ 4 mM, 2.48 g $Na_2S_2O_3.5H_2O$; ii) $S_2O_3^{2-}$ 20 mM, 12.4 g $Na_2S_2O_3.5H_2O$; iii) $S_2O_3^{2-}$ + $S_4O_6^{2-}$ 4 mM, 1.24 g $Na_2S_2O_3.5H_2O$ + 0.756 g $K_2S_4O_6$; iv) $S_2O_3^{2-}$ + $S_4O_6^{2-}$ 20 mM, 6.2 g $Na_2S_2O_3.5H_2O$ + 3.93 g $K_2S_4O_6$; v) $S_4O_6^{2-}$ 4 mM, 1.512 g $K_2S_4O_6$; and vi) $S_4O_6^{2-}$ 20 mM, 7.56 g $K_2S_4O_6$. The combined $S_2O_3^{2-}$ + $S_4O_6^{2-}$ addition, added equal concentrations of S, i.e., for the 4 mM treatment, 2 mM of S as $S_2O_3^{2-}$ and 2 mM of S as $S_4O_6^{2-}$, and for the 20 mM treatment, 10 mM of S as $S_2O_3^{2-}$ and 10 mM of S as $S_4O_6^{2-}$. The solution was then filter sterilized (< 0.2 µm) and placed in an autoclaved 8 L carboy that served as the experimental systems.

5.2.3. Microbial inoculation, growth and counting for mesocosms

5.2.3.1. Synthetic wastewater "S treatment" enrichment mesocosms design

Four treatments were assessed for these experiments, an abiotic control and three SoxB enrichments varying in the relative proportions of *Halothiobacillus*:*Thiomonas*; Enrichment A, ≈ equal *Halothiobacillus* and *Thiomonas*; Enrichment B, *Halothiobacillus* dominant; and Enrichment C, *Thiomonas* dominant (Table 5.1). Once the enrichment reached the low end of its pH corral (pH = 3), cells were counted via fluorescence microscopy and added to the mesocosm.

5.2.3.2. Cell counting and enrichment inoculation to "S treatment"

Enrichments were centrifuged @10 000 rpm at 4˚C for 20 min, the supernatant discarded, and cells were washed with 0.01 M PBS (pH 7.0). The cells were then centrifuged again, the supernatant discarded, and the resulting cell pellet resuspended in sterile MQ water.

Washed SoxB enrichment cells were enumerated by first drawing a 1 cm circle on microscope slide with marker, then washing the slide with 10% v/v HCl and rinsing with MQ water after a couple hours. A 1% w/v Agarose solution (1 g per 100 ml) was cooked in a glass beaker via microwave until the agarose dissolved, then the solution was poured on the slides and left for a couple hours in a sterile laminar hood until it hardened. 10 µl of an enrichment sample was spread onto the 1 cm^2 area and left to dry in a laminar hood. Once dried, 3 µl of SYTO™ 9 (Invitrogen™) (diluted to a 30 µM solution) and 7 µl MQ water was added and spread onto the 1 cm^2 area then placed in a dark sterile container in the laminar hood to stain for a few minutes. 12-15 field views per slide were then counted via fluorescence microscopy (Leica DM R, Wetzlar, Germany) at 100x magnification under UV light and through the GFP filter. Then cell count

extrapolation based on the area of the field of view for magnification and number of fields for the 1 cm^2 of sample.

The enrichment volume was determined for each biological amendment treatment to ensure $1x10^5$ cells/ml for each mesocosm and that volume was then added to the 5 L synthetic wastewater mesocosm. Mesocosms were buffered to pH = 7 by dilute sterile (< 0.2 μm filtered) NaOH and HCl and were kept static in incubators @ 28˚C with a 12 hour diurnal light cycle.

5.2.4. Sulfur speciation sampling and analyses

5.2.4.1. pH survey and sulfur species sampling regime

For all 24 mesocosm experiments samples were taken every 12 hours from day 0-4, then every 24 hours until day 15, for a total of 20 time points. At each time point pH was aseptically measured immediately (Denver Instrument Model 225, NY, USA) prior to sampling for any sulfur analyses. Samples were then collected for dissolved (< 0.2 μm) total sulfur (total $S_{0.2\mu m}$), unfiltered total sulfur (total S_{UF}) and sulfur species (SO_4^{2-}, S^{2-}, $S_2O_3^{2-}$, SO_3^{2-} and S^0) in triplicate.

5.2.4.2. Sulfur chemistry analyses

For total $S_{0.2\mu m}$, 40 ml of water samples were filtered by Pall Acrodisc® 25 mm 0.2 μm Supor® membrane via polypropylene syringes into 50 ml Falcon™ tubes and for total S_{UF} 40 ml of water samples were transferred directing into the 50 ml tubes. For both total $S_{0.2\mu m}$ and total S_{UF} samples, immediately after 80 μL of HNO_3 (Optima grade, Fisher Chemical) was added to each tube, and stored at 4°C until further processed at CSIRO Land and Water laboratory (New South Wales, Australia). Analyses for total S were carried out using inductively coupled argon plasma emission spectrometry (ICP-AES) (Varian730 ES, Mulgrave, VIC), with sulfur calibration standards

prepared from a certified reference stock solution (AccuStandard New Haven, CT, USA) in 2% *v*/*v* HNO_3. By measuring intensity at the 181.972 nm sulfur emission line concentrations were determined with a limit of detection (LOD) for sulfur of 1 mg L^{-1} (0.03 mM). SO_4^{2-} and S^{2-} samples were immediately fixed and analyzed using the HACH SulfaVer 4 Method and Methylene Blue Method for SO_4^{2-} and S^{2-}, respectively (Hach company, Colorado, USA) by spectrophotometry (Pharmacia Biotech Ultrospec 3000 UV/Visible Spectrophotometer).

Samples for SOI species $S_2O_3^{2-}$, SO_3^{2-} and S^0 were collected simultaneously with those for total S (total $S_{0.2\mu m}$ and total S_{UF}), SO_4^{2-} and $\Sigma H_2S_{(aq)}$. The SOI species were immediately preserved using a monobromobimane derivatization procedure for SOI analyses by HPLC (Rethmeier *et al.*, 1997). The Shimadzu LC-20AD prominence HPLC instrument with Alltima HP C18 (5 µm x 150 mm x 4.6 mm Grace™) reverse phase column was used for all SOI species analyses. Solvents used in protocols were A=Water, B=Methanol, C=Acetonitrile, D=Acetic acid 0.25% *v*/*v* pH 3.5 adjusted with NaOH (1N). $S_2O_3^{2-}$ and SO_3^{2-} were analyzed via fluorescence excitation at 380 nm and emission at 480 nm. Standards and calibrations for $S_2O_3^{2-}$ (0-10 mM) and SO_3^{2-} (0-1.7 mM) were made with $Na_2S_2O_3$ (Sigma Aldrich, 99% purity) and Na_2SO_3 (Sigma Aldrich, ≥ 98% purity), respectively. The thiosulfate and sulfite elution protocol comprised an Isocratic mobile phase B 35%, D 65%, a flow rate of 1ml/min and oven heating to 35˚C for a run time of 15 min. Sample size was 10 µl and elution times were 3 min for SO_3^{2-} and 4 min for $S_2O_3^{2-}$. S^0 was extracted with chloroform from the water samples and analyzed with reverse-phase HPLC and UV-absorption at 263 nm. Standards and calibrations (0-32 mM) were made from S^0 (Fisher, 99.5% purity) dissolved in chloroform. S^0 elution protocol: Isocratic mobile phase A 5%, B 95%, flow rate of 1 ml/min, run time of 12 min. The sample size was 20 µl and the elution time was at 8 min.

A mass balance enabled quantification of any unresolved or "Other SOI" S species not directly analyzed within this study, by the difference between the sum of all measured solution sulfur species concentrations, (i.e., $\sum$[S-SO_4^{2-}, S-S^{2-}, S-$S_2O_3^{2-}$, S-SO_3^{2-} and S-S^0] and the Total S (total $S_{0.2\mu m}$, total S_{UF} and known initial synthetic made "S treatment") concentration. Lastly, by subtracting SO_4^{2-}, the end state of S oxidation, from Total S, the reactive S pool (S_{react}; i.e. all S available for oxidation; Whaley-Martin *et al*., 2020) was also quantified.

5.2.5. Abiotic control experiments: S and acidity results

For all six experiments, abiotic controls (no microbial enrichment addition) evidenced a gradual decrease in pH with the maximum observed pH decrease of 7 to 6.35, equivalent to a maximum [H^+] increase of 0.35 μM, occurring in the $S_2O_3^{2-}$ + $S_4O_6^{2-}$ high total S treatment (Figure 5.1). This pH decrease most likely reflects the equilibrium of initial buffering. The only change in SOI species observed in these abiotic controls: the generation of S^0 which was immediately produced in the $S_2O_3^{2-}$ + $S_4O_6^{2-}$ treatment experiments (Supplemental Table S1), at both high and low Total S concentrations and across all experiments, which would generate acidity (Eq 3 and 4). This was likely due to reactions forming S^0 abiotically (≈ 2.5% M/M), closely related to Wackenroder reactions when $S_2O_3^{2-}$ + $S_4O_6^{2-}$ are present together (Eq 3 and 4) (Thom *et al*., 1978).

$$HO_3SS_n\text{-}SO_3H + HSSO_3H \rightarrow HO_3SS_n\text{-}SSO_3H + H_2SO_3 \quad (3)$$

$$HS_8\text{-}SO_3H \rightarrow S_8 + H_2SO_3 \quad (4)$$

Approximately 0.1 mM of S^0 was produced in the abiotic control $S_2O_3^{2-}$ + $S_4O_6^{2-}$ low [Total S] and ≈ 0.5 mM of S^0 was observed in the $S_2O_3^{2-}$ + $S_4O_6^{2-}$ high [Total S] treatment experiment (Supplementary Figure S1). These initial S^0 concentrations remain stable throughout the time

course in the abiotic experiments, showing no further abiotic sulfur reactions (Supplementary Figure S1).

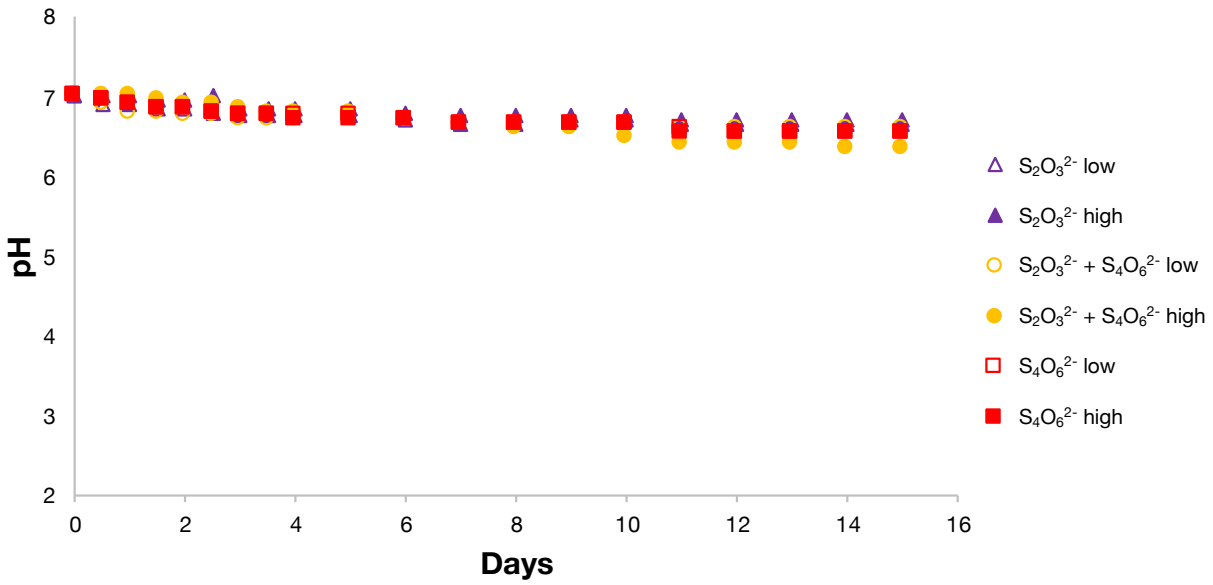

Figure 5.1: pH values for each of the six abiotic S control experiments across the experimental time period.

5.3. Results and Discussion

5.3.1. S and Acidity generation across biological experiments

5.3.1.1. pH

All three microbial SoxB enrichment experiments evidenced acidification with remarkably similar pH trends for each SOI treatment (with one exception: Enrichment A (50:50 *Halothiobacillus* sp. and *Thiomonas* sp.), $S_2O_3^{2-}$, high [Total S] addition), decreasing below pH 4, over the 15 days experimental time (Figure 5.2). pH results indicate that the two $S_2O_3^{2-}$ alone addition experiments, regardless of low or high [Total S], were the slowest to reach acidic pH values (Figure 5.2i), consistent with greater disproportionation and H^+ consuming reactions and/or lower microbial activity relative to the $S_2O_3^{2-}$ + $S_4O_6^{2-}$ or $S_4O_6^{2-}$ treatments (Figure 5.2ii, iii). The $S_4O_6^{2-}$ experiments were the quickest to reach acidic pH values (Figure 5.2iii), while the $S_2O_3^{2-}$ + $S_4O_6^{2-}$ addition experiments reflected an additive blend of the two single S substrate addition treatments (Figure 5.2ii). The slowest pH decreases observed for the Enrichment A, the $S_2O_3^{2-}$ high addition experiment (Figure 5.2i), suggests higher concentrations of thiosulfate will delay acidification onset through acid consuming processes associated with its conversion.

Enrichment A (50:50 *Halothiobacillus* spp. and *Thiomonas* spp.) exhibited the slowest pH decrease, while Enrichment C (*Thiomonas* spp. dominant*)* exhibited the quickest pH decline across all experiments. Since Enrichment A cells were inactive for longer during cryopreservation than Enrichment C, these results may reflect potential effects such as cell lethargy or reduced activity (Hubálek, 2003). Evidenced trends observed no enrichment effect on pH, with factors primarily controlled by the SOI substrate. These results emphasize that though previous results found *Halothiobacillus* and *Thiomonas* to dominate sulfur oxidation reactions at circumneutral and

moderately acidic pH ranges respectively (Chapter 4 of this thesis, Camacho *et al*., 2020b), they are both capable of similar potential acidification and S metabolisms across multiple SOI species from circumneutral to acidic pH (Johnson and Hallberg, 2003; Arsène-Ploetze *et al.*, 2010; Liu *et al.*, 2014; Whaley-Martin *et al.*, 2019).

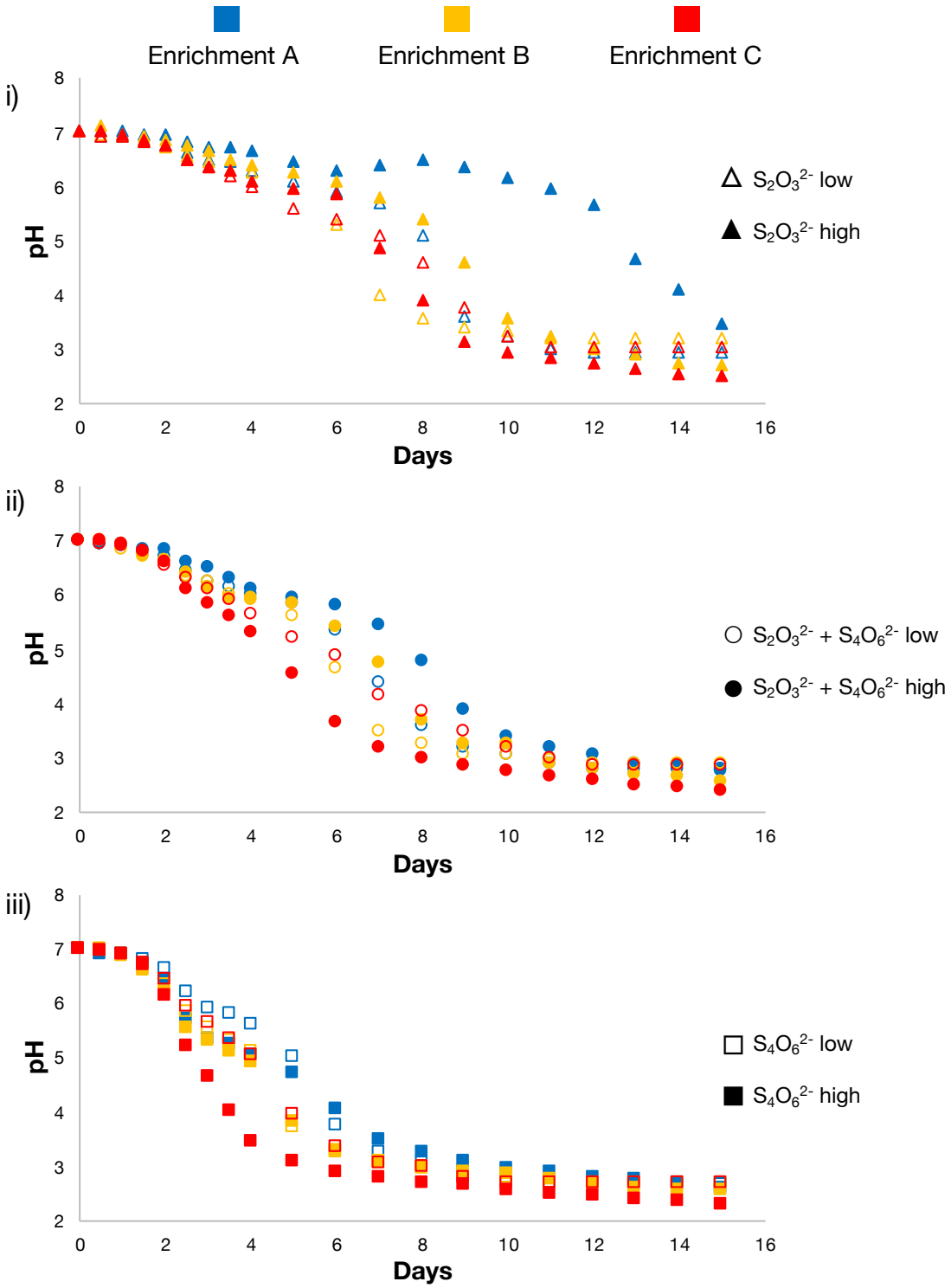

Figure 5.2: pH changes for each of the three biological enrichments (A (~50:50 abundance *Halothiobacillus*:*Thiomonas*) = blue; B (*Halothiobacillus* dominant) = yellow; C (*Thiomonas* dominant) = red) over the experimental time period for the six 'S treatments' (shapes; open = low [Total S], closed = high [Total S]): **i)** triangle = $S_2O_3^{2-}$ treatments; **ii)** circles = $S_2O_3^{2-}$ + $S_4O_6^{2-}$ treatments; **iii)** squares = $S_4O_6^{2-}$ treatments.

5.3.1.2. S_{react} and sulfate generation results

Consistent with the similar decreasing pH trends observed across all microbial SOI and [Total S] treatment experiments (Figure 5.2); a similar trend of increasing sulfate concentrations was also observed across experimental treatments (Supplementary Figure S2). Interestingly across all three enrichments, the highest sulfate concentrations occurred in the two high [Total S] $S_2O_3^{2-}$ (alone or in combination with $S_4O_6^{2-}$) experiments, while sulfate generation in the high [Total S] $S_4O_6^{2-}$ alone experiment was indistinguishable from the three low [Total S] SOI experiments (Supplementary Figure S2).

While trends were similar for all three Enrichments, Enrichment C (highest *Thiomonas* abundance > 99%; Table 5.1) evidenced the greatest decrease in pH (Figure 5.2), and thus the greatest overall oxidative progression of potential sulfur chemical reactions leading to sulfate within the time frame of the experiment. Thus, subsequent examination of which reactions may be occurring were focused on the results for this Enrichment. For Enrichment C results, in all three low [Total S] experiments, > 90% of sulfur was oxidized to sulfate within the experimental timeframe (Figure 5.3A, Supplementary Table S2):

$S_2O_3^{2-}$ experiment (SO_4^{2-}, t=0 2.0 mM $\rightarrow$ t=end, 6.3 mM; S_{react}, 4.6 mM $\rightarrow$ 0.3 mM);

$S_4O_6^{2-}$ experiment (SO_4^{2-}, 2.1 mM $\rightarrow$ 6.0 mM; S_{react}, 4.5 mM $\rightarrow$ 0.6 mM); and

$S_2O_3^{2-}$ + $S_4O_6^{2-}$ experiment (SO_4^{2-}, 2.1 mM $\rightarrow$ 6.4 mM; S_{react}, 4.5 mM $\rightarrow$ 0.2 mM).

In comparison, in the high [Total S] experiments < 70% of sulfur was oxidized to sulfate and variability amongst the rates and concentrations produced was observed across the different S substrate experiments (Figure 5.3; Supplementary Table S2). A greater increase in sulfate concentration occurred in the $S_2O_3^{2-}$ experiment compared to the $S_4O_6^{2-}$ experiment or the $S_2O_3^{2-}$ + $S_4O_6^{2-}$ experiment (Figure 5.3A, Supplementary Table S2):

$S_2O_3^{2-}$ experiment (SO_4^{2-}, 2.0 mM → 15.6 mM; S_{react}, 20.6 mM → 7.0 mM);

$S_4O_6^{2-}$ experiment (SO_4^{2-}, 2.0 mM → 8.8 mM; S_{react}, 20.6 mM → 13.8 mM); and

$S_2O_3^{2-}$ + $S_4O_6^{2-}$ experiment (SO_4^{2-}, 2.1 mM → 12.6 mM; S_{react}, 20.5 mM → 10.0 mM).

The results in the high [Total S] treatments identify that when $S_2O_3^{2-}$ is present, these microbes catalyze reactions that result in more SO_4^{2-} compared to when only $S_4O_6^{2-}$ is present (Figure 5.3A; Supplemental Figure S2), however, with lower net acidity generation. This result identifies that the presence of $S_2O_3^{2-}$ may mask overall progress towards the tipping point when oxidation (and greater acidity generation) dominates. Further, the in-between levels of SO_4^{2-} production observed in both low and high total concentration $S_2O_3^{2-}$ + $S_4O_6^{2-}$ experiments compared to that produced in the individual thiosulfate or tetrathionate addition experiments, suggest both sets of reaction pathways are occurring, i.e., additive SOI influence occurs on sulfate and acid production (Figure 5.2, 5.3).

Clear trends were observed when examining sulfate against pH for the $S_2O_3^{2-}$ experiments indicating that different reactions were likely dominating as a function of pH. From pH 6 → pH 5, an increase in SO_4^{2-} occurred for both low and high [Total S] $S_2O_3^{2-}$ treatments (Figure 5.3B); which was not observed in the $S_4O_6^{2-}$ experiments and was observed at an intermediate level between the two individual SOI treatments in the $S_2O_3^{2-}$ + $S_4O_6^{2-}$ experiments (Figure 5.3B). These results suggest that between pH 6 → pH 5 when $S_2O_3^{2-}$ is present, microbes were catalyzing reactions that resulted in the oxidation end point, SO_4^{2-}, as well as dis/comproportionation reactions that would consume acid (Bernier and Warren, 2007; Camacho *et al.*, 2020a). However, as pH values < 3 across all SOI treatments, oxidation reactions dominated resulting in SO_4^{2-} (and greater acid generation) as previously observed by Warren *et al.*, (2008).

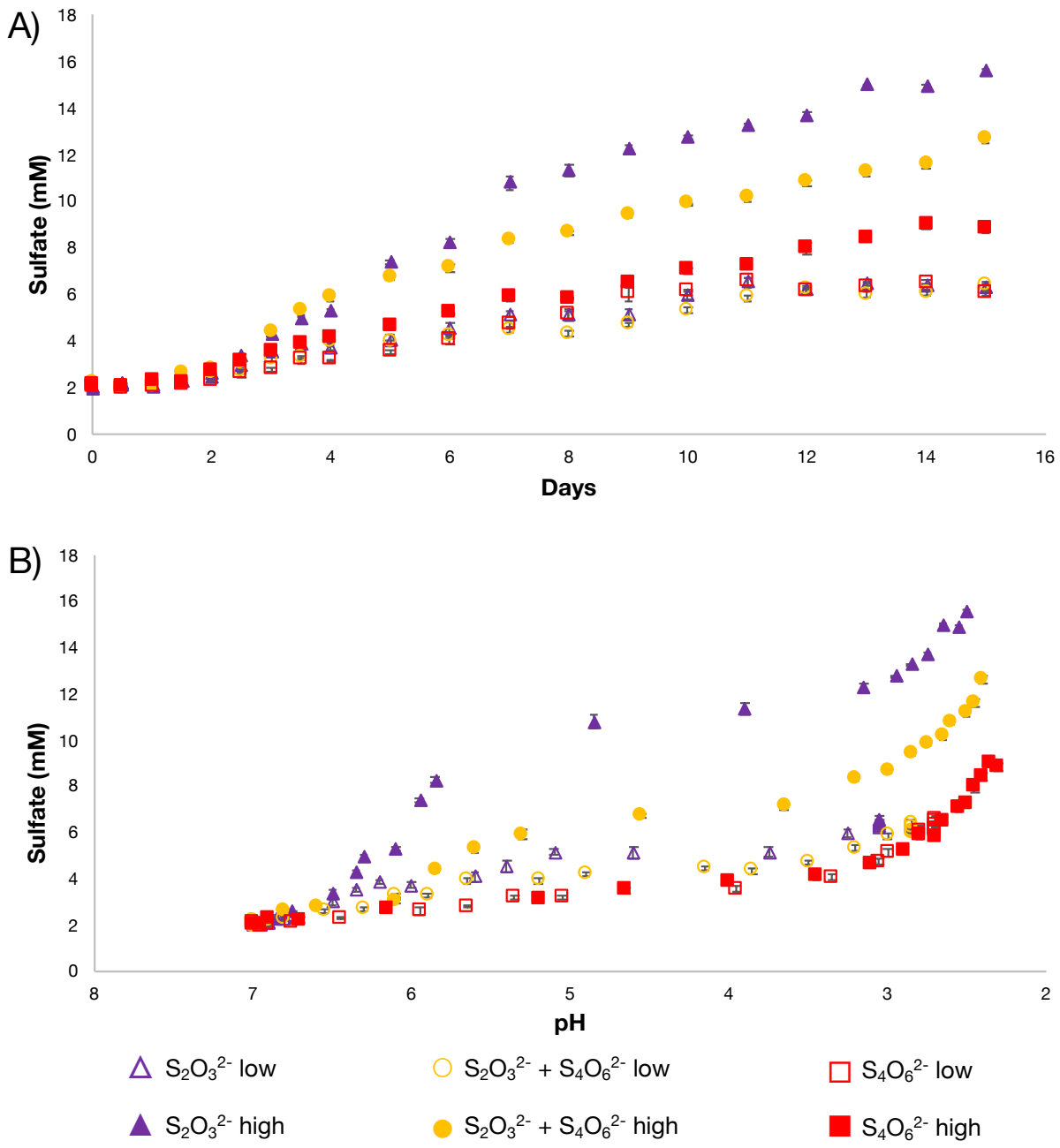

Figure 5.3: Sulfate concentrations observed over the time course of all 'S treatment' experiments for Enrichment C (> 99% *Thiomonas* (Table 1). **A)** Sulfate plotted against time. **B)** Relationship of sulfate to pH.

5.3.1.3. SO_4^{2-}:H^+ ratios

The expected (based on oxygen driven oxidation to sulfate, i.e., Eq 1 and 2) and observed ratios of SO_4^{2-}:H^+ generated by Enrichment C for all SOI and [Total S] experiments were evaluated as a function of pH (Figure 5.4). These ratios were calculated in three ways: A) the ratio depicted from the time of sampling to the initial value **Initial** Δ (T_n-T_1), (T = sampled time point); B) the ratio depicted from the time of sampling to the immediate sample time preceding that point **Continual** Δ (T_n - T_{n-1}); and C) and the ratio depicted from the final end point value to the initial time point **Total** Δ (T_{end} - $T_{initial}$) in SO_4^{2-}:H^+. These ratios were all higher than expected for all treatments indicating higher sulfate to acid generation than Eq (1) or (2) would predict; until a pH of ~ 3 was reached (Figure 5.4).

Results comparing **Initial** Δ**,** which integrates across pH the time of sampling to the initial**,** identified that observed ratios for $S_2O_3^{2-}$ were higher (i.e., greater acid consumption) than expected SO_4^{2-}:H^+ ratios in comparison to $S_2O_3^{2-}$ + $S_4O_6^{2-}$ and $S_4O_6^{2-}$ results indicating greater acid consumption always occurred for thiosulfate (Figure 5.4A).

Continual Δ, which takes the pH values occurring at the time these ratios were calculated, revealed the observed SO_4^{2-}:H^+ gets closer to expected as pH decreases for all S treatments confirming that either dis/comproportionation and/or acid consuming reactions were occurring alongside SO_4^{2-} production, even for the $S_4O_6^{2-}$ metabolic pathways, until pH $\approx$ 3. As pH decreased below 3, observed **Continual** Δ, was approximately equal to the expected value (Figure 5.4B), consistent with a shift of dominant reactions being catalyzed to strict oxidation to sulfate. In some instances at pH values < 3, the observed **Continual** Δ was lower than expected which could be explained by the oxidation of higher chain polythionates to sulfate, which would have been previously generated from the initial S substrates at pH > 3 (Schippers *et al.*, 1996; Warren *et al.*,

2008). These results corroborate findings previously observed in this thesis (Chapter 3, Camacho *et al*., 2020a) of SoxB cycling sulfur even at these low pH values and required generation and subsequent oxidation of higher chain polythionates.

The **Total** Δ SO_4^{2-}:H^+ observed values were greater than expected for all treatments (Figure 5.4C); i.e., less acid generated than expected. Although observed **Total** Δ values (i.e., integrated across the entire experimental time course) differed slightly for high [Total S] versus low [Total S] treatments (Figure 5.4C), the progressive change elucidated by examining the relative change as a function of pH reached from the sampled time point to the initial (**Initial** Δ**)** and between adjacent time points (**Continual** Δ**)** as a function of pH, show that these experiments were not concentration driven (Figure 5.4A and B). Results identified that SOI substrate was the strongest determining factor in determining which S reactions occurred and thus acidity generation. In the high [Total S] experiments, the ratio of **Total** Δ observed SO_4^{2-}:H^+ to expected SO_4^{2-}:H^+ was different across SOI substrates: $S_2O_3^{2-}$ treatments $\approx$ 4:1 was the highest (i.e., lowest acid generation per sulfate produced); $S_4O_6^{2-}$ treatments $\approx$ 2:1 (i.e., highest acid generation per sulfate produced); and $S_2O_3^{2-}$ + $S_4O_6^{2-}$ treatments $\approx$ 3:1 (i.e., intermediate between the two individual SOI treatments). These results explain why the common use of expected (i.e., based on abiotic oxidation reactions) SO_4^{2-}:H^+ ratios as a tool to predict acidity generation risks often fail, as the values associated with microbial S cycling at circumneutral pH are far lower than those expected.

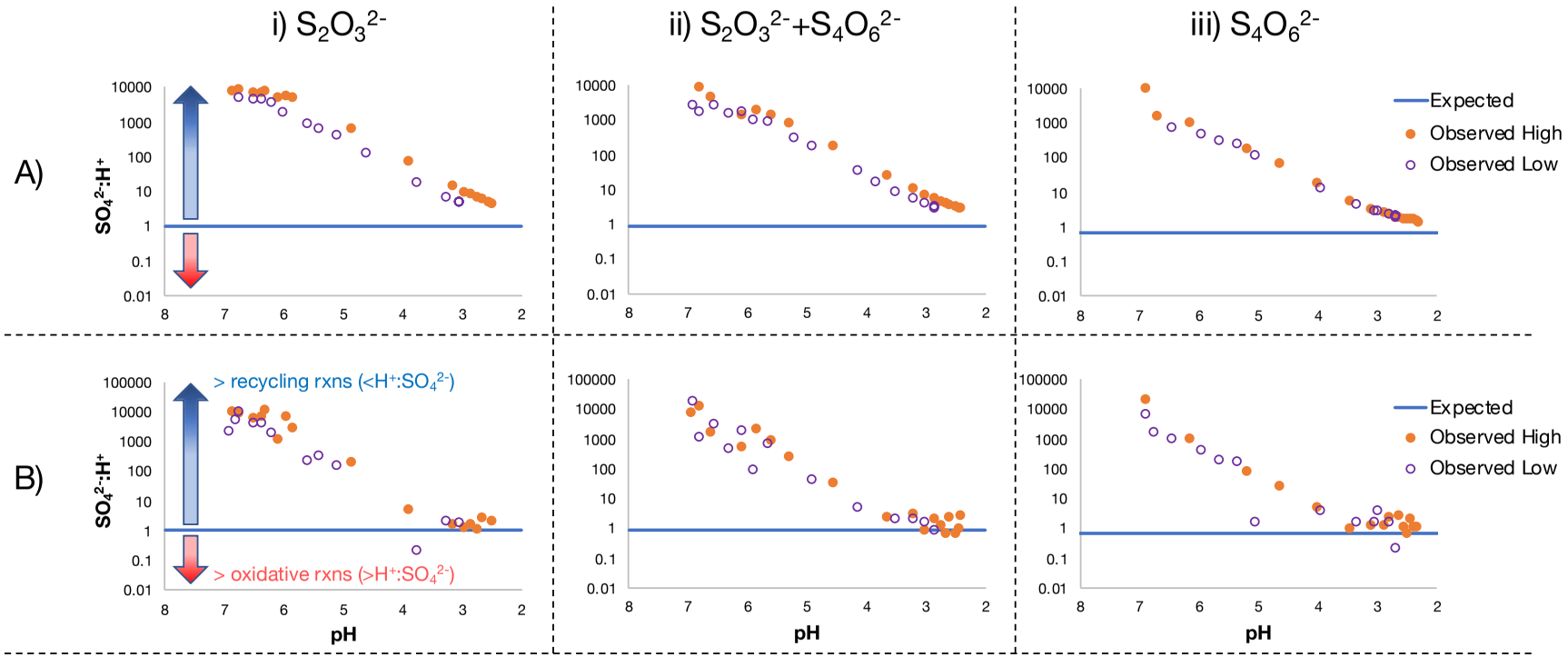

C)

	Observed SO_4^{2-}:H^+	Expected SO_4^{2-}:H^+
High	4.3	1.0
Low	4.8	1.0

	Observed SO_4^{2-}:H^+	Expected SO_4^{2-}:H^+
High	2.6	0.83
Low	3.0	0.83

	Observed SO_4^{2-}:H^+	Expected SO_4^{2-}:H^+
High	1.4	0.67
Low	2.0	0.67

Figure 5.4: Examining the expected and observed ratio of SO_4^{2-}:H^+ as a function of pH for Enrichment C treatments (i) $S_2O_3^{2-}$; ii) $S_2O_3^{2-}$ + $S_4O_6^{2-}$; iii) $S_4O_6^{2-}$) considering the expected ratio as strict oxidation of the initial S substrate. Blue line = Expected, filled orange circles = Observed for high [Total S], open purple circles = Observed for low [Total S]. **A)** the ratio depicted by Initial Δ (T_n-T_1) (T = sampled time point). **B)** the ratio depicted by Continual Δ (T_n - T_{n-1}). **C)** Total Δ (T_{end} - $T_{initial}$).

5.3.1.4. SOI chemistry speciation as a function of pH

The results for SO_4^{2-}:H^+ ratios across the three SOI treatments identify different reactions are occurring dependent on the starting SOI provided, in addition to pH for thiosulfate treatments (Figure 5.4). Thus, evaluating changes in SOI species changes was the first step to identifying the possible reactions occurring. Concentrations of sulfide and sulfite were very low to below detection limits across all experiments, with no discernable trends (Figure 5.5). Thiosulfate, Elemental-S and Other SOI occurred at detectable levels as a function of pH.

Thiosulfate concentrations showed three noticeable trends. First, in the $S_4O_6^{2-}$ substrate experiments. $S_2O_3^{2-}$ concentrations increased specifically between pH 7 → pH 6, consistent with disproportionation occurring (Figure 5.5A-ii, iii). Second, $S_2O_3^{2-}$ concentrations decreased between pH 6 → pH 5 in all experiments (Figure 5.5A). Third, most $S_2O_3^{2-}$ was metabolised as indicated by low to non-detectable concentrations by pH 4 in all experiments (Figure 5.5A). These results identify that thiosulfate is a key SOI species important to microbial S oxidation metabolism irrespective of starting substrate, it was produced initially in the $S_4O_6^{2-}$ treatment, such that across all SOI treatments in pH range of 6 → 5, thiosulfate metabolism occurs. Results show $S_2O_3^{2-}$ was fully metabolised by Enrichment C under more circumneutral pH conditions where it is abiotically stable, as evidenced by its decrease to near or non-detectable levels by pH 4. Thus, thiosulfate loss observed in these experiments is not likely due to possible abiotic instability of this species that has been identified to occur at pH < 3 (Johnston and McAmish, 1973; Druschel, 2002; Vongporm, 2008).

Two major trends emerged for Elemental-S across the three SOI and [Total S] experiments for Enrichment C (Figure 5.5B). First, reflecting the observed generation of Elemental-S in the two $S_2O_3^{2-}$ + $S_4O_6^{2-}$ control experiments that persisted throughout these experiments

(Supplementary Figure S1). Initial abiotically produced S^0 detected in the two Enrichment C $S_2O_3^{2-}$ + $S_4O_6^{2-}$ experiments (Figure 5.5Bii), was subsequently rapidly metabolised between pH 7 → pH 6 (Figure 5.5B-ii). As both these SOI substrates are common to sulfide hosted ore associated tailings (Miranda-Trevino *et al.*, 2013), the importance of S^0 in subsequent microbial S metabolism in mine tailings impoundments is likely to be widespread. Second, in both $S_2O_3^{2-}$ and $S_2O_3^{2-}$ + $S_4O_6^{2-}$ SOI treatments (high and low [Total S]), observed S^0 concentrations increased between pH 6 → pH 3, after which it was then rapidly metabolized to near nondetectable levels in both treatments (Figure 5.5B; Supplementary Figure S3) indicating its generation and subsequent consumption in $S_2O_3^{2-}$ containing experiments. As S^0 is lower on the S electron chain than either of the starting S substrate species, these results confirm disproportionation reactions were occurring (Zopfi *et al.*, 2004; Camacho *et al*., 2020a). Additionally, the increase of S^0 was observed to occur across all Enrichments and SOI and [Total S] treatments under circumneutral pH values that decreased towards acidic values (i.e., ~ 3) along with this observed Elemental-S increase (Supplementary Figure S3). These results demonstrate a convergence to a clearly identifiable pattern in the sulfur reaction chemistry across Enrichment communities, that comprised varying abundances of two important mine wastewater sulfur oxidizing genera (i.e., Camacho et al. 2020b), as well as varying concentrations of SOI substrate containing two important species commonly observed in mining wastewaters. These results suggest the potential of Elemental-S as a chemical marker to signal the initiation of reactions leading to acid generation in mine wastewater systems containing thiosalts.

Results for the calculated Other SOI pool (i.e., non-identified SOI species; calculated as Total S – Σ(all measured SOI species)) identified a pH dependent (7 → 6) decrease in [Other SOI] in experiments containing $S_4O_6^{2-}$ as a substrate, synchronized with the observed increase in $S_2O_3^{2-}$

concentrations (Figure 5.5C-ii, iii). Results further identified an increase in [Other S] across all treatments from pH 6 → pH 4, with a higher proportional concentration increase observed in $S_2O_3^{2-}$ experiments (Figure 5.5C). In all treatments, a slight decrease then occurred between pH 4 → pH 3, followed by a rapid decline at pH < 3 (Figure 5.5C). These results further confirm the prevailing sulfur oxidation mechanisms previously described, that suggested dis/comproportionation alongside oxidation reactions occur contiguously at pH > 3, while rapid oxidation of reduced S towards end-point sulfate dominates at pH < 3 (Bernier and Warren, 2007; Warren *et al.*, 2008; Camacho *et al.*, 2020a).

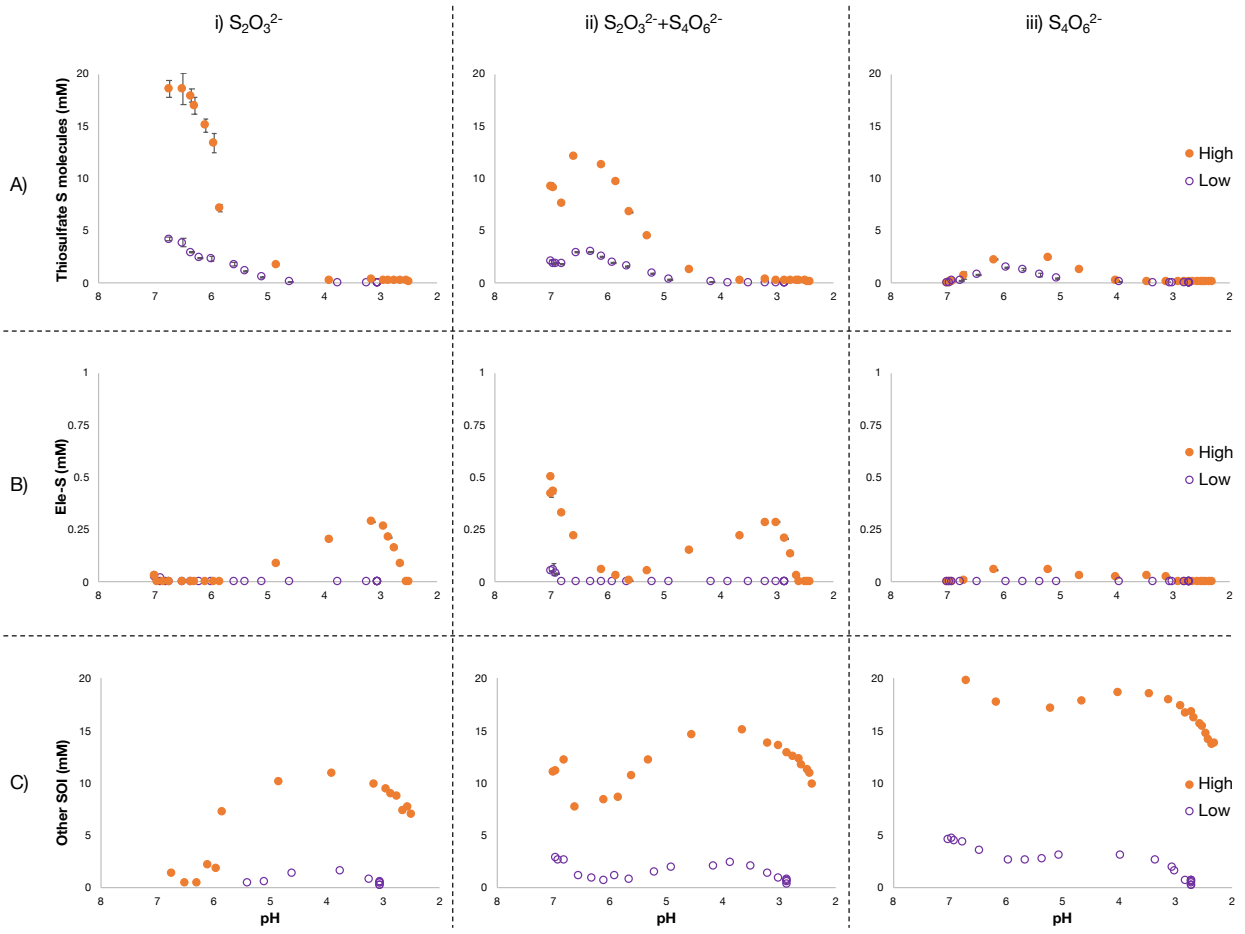

Figure 5.5: Relationship of SOI species as a function of pH for Enrichment C treatments i) $S_2O_3^{2-}$; ii) $S_2O_3^{2-}$ + $S_4O_6^{2-}$; iii) $S_4O_6^{2-}$), filled orange circles = high [Total S], open purple circles = low [Total S]. **A)** Thiosulfate vs pH. **B)** Elemental S vs pH. **C)** Other SOI vs pH. All S concentrations are presented by mol of S, i.e. 1 mol of $S_2O_3^{2-}$ = 2 mol of S.

5.3.2. Sulfur reaction pathways

The observed changes in S speciation results identify that sulfur oxidation reactions were similar for all three Enrichments for each SOI treatment (Supplementary Figure S2), identifying that sulfur speciation is the dominant driver of microbial S catalysis than variations in *Halothiobacillus* spp. and *Thiomonas* spp. abundances (Supplementary Data; Supplementary Figure S2, S4). Here, my results identify a three-phase pathway for both $S_2O_3^{2-}$ and $S_4O_6^{2-}$ metabolism by sulfur oxidizing microbes, than the previously identified two phase array for the $S_2O_3^{2-}$ proposed by Warren *et al*., (2008). Specifically, key sulfur reaction mechanisms for these sulfur species were identified for each of three pH ranges: Phase 1, pH > 5; Phase 2, pH 5 – 3; and Phase 3, pH < 3.

5.3.2.1. $S_2O_3^{2-}$ metabolism

For early phase, i.e., pH > 5, Phase 1 conditions, $S_2O_3^{2-}$ metabolism includes some SO_4^{2-} production, but the observed SO_4^{2-}:H^+ ratio indicated far less acidity than would be expected from dominating oxidation processes (Figure 5.4 A-i, B-i, C-i; Supplementary Table S3). Further, the observed co-incident increase in Other SOI (Figure 5.5C-i), also observed for Phase 1 pH, implies acid-consuming reactions occur in tandem with oxidation to SO_4^{2-}, consistent with microbial oxidation of $S_2O_3^{2-}$ specifically to $S_4O_6^{2-}$ (Eq 5) (Figure 5.6A) (Suzuki, 1999; Wang *et al*., 2019; Camacho *et al.*, 2020a).

$$2S_2O_3^{2-} + ½O_2 + 2H^+ \rightarrow S_4O_6^{2-} + H_2O \quad (5)$$

As pH transitioned from Phase 1 to Phase 2, i.e., as pH decreased below 5, the observed production of S^0 and shifts in Other SOI production (Figure 5.5B, C) imply disproportionation reactions involving either the initial starting substrate $S_2O_3^{2-}$ (Eq 6; consistent with observed decreases in

[$S_2O_3^{2-}$] at this pH interval (Figure 5.5Ai, ii)) or the postulated, now abundant $S_4O_6^{2-}$ (Eq 7 and 8) (Figure 5.6A) (Suzuki, 1999; Ghosh and Dam, 2009; Camacho *et al*., 2020a) are now occurring.

$$S_2O_3^{2-} + ½O_2 \rightarrow S^0 + SO_4^{2-} \quad (6)$$

$$S_4O_6^{2-} + H_2O \rightarrow S_2O_3^{2-} + S^0 + SO_4^{2-} + 2H^+ \quad (7)$$

$$S_4O_6^{2-} + H_2O \rightarrow 2S^0 + H_2SO_3 + SO_4^{2-} \quad (8)$$

Many sulfur oxidizers within the *Halothiobacillus*, *Thiomonas* and other Gammaproteobacteria genera are known to carry out these reactions, associated with the Sox complex and S_4I pathway (Kelly *et al.*, 1997; Friedrich *et al.*, 2001; Rowerder and Sand, 2003; Hensen *et al*., 2006; Sauvé *et al.*, 2007; Arsène-Ploetze *et al*., 2010; Wang *et al.*, 2019; Whaley-Martin *et al.*, 2019; Camacho *et al*., 2020b). Finally, in Phase 3, when pH values decrease below 3, the SO_4^{2-}:H^+ approaches values associated with dominant oxidation and production of sulfate (and associated acidity generation; Figure 5.3B, Figure 5.4B-i; Supplementary Table S3), and consumption of all reduced S following Eq (1), (2) and (9) (Figure 5.6A) (Suzuki, 1999).

$$S^0 + 1½O_2 + H_2O \rightarrow SO_4^{2-} + 2H^+ \quad (9)$$

5.3.2.2. $S_4O_6^{2-}$ metabolism

For the $S_4O_6^{2-}$ treatment experiments, the observed SO_4^{2-}:H^+ ratio was higher (i.e., less acid generated than predicted) than expected assuming only oxidation to sulfate (Eq 2). However, these ratios were closer to expected (i.e., greater oxidation relative to acid consuming reactions) than those observed in the $S_2O_3^{2-}$ containing experiments (Figure 5.4 A-iii, B-iii, C-iii, Supplementary Table S3). During the initial Phase 1 pH range, the observed increase in [$S_2O_3^{2-}$] (Figure 5.5A-iii) implies that the discrepancy in observed SO_4^{2-}:H^+ can be attributed to disproportionation reactions, such as Eq (7) (Figure 5.6B). As pH decreases below 5, (Phase 2), a relatively greater oxidation to

SO_4^{2-} (Figure 5.3B) occurs as evidenced by acid producing reactions (Figure 5.4B-iii) and observed decreases in [$S_2O_3^{2-}$] (Figure 5.5A-iii) and production of S^0 (Eq 2, 4-8; Figure 5.5B-iii; Supplementary Figure S3, Figure 5.6B). The lower concentration of generated S^0 compared to generated $S_2O_3^{2-}$ in $S_4O_6^{2-}$ experiments observed as pH decreased below 5, suggests catalyzed sulfur reactions involve oxidation up the sulfur polythionate chain from the end of Phase 1 into Phase 2, likely decreasing the concentration of $S_4O_6^{2-}$ present, (i.e., Eq 10 - 13) (Figure 5.6B) (Steudel *et al.*, 1987; Schippers *et al.*, 1996).

$$S_4O_6^{2-} + H_2O \rightarrow HSSSO_3^- + SO_4^{2-} + H^+ \quad (10)$$

$$S_3O_3^{2-} + S_2O_3^{2-} + 0.5O_2 + 2H^+ \rightarrow 3S_5O_6^{2-} + H_2O \quad (11)$$

$$S_3O_3^{2-} + S_4O_6^{2-} \rightarrow S_2O_3^{2-} + S_5O_6^{2-} \quad (12)$$

$$S_3O_3^{2-} + 1.5O_2 \rightarrow S_3O_6^{2-} \quad (13)$$

Similar to the observed $S_2O_3^{2-}$ reaction array, as pH decreased below 3 (Phase 3), strict oxidation to SO_4^{2-} dominates in the $S_4O_6^{2-}$ experiments (Figure 5.3B; Figure 5.4C-iii; Supplemental Table S3) via Eq (2) and (9) (Figure 5.6B). The $S_4O_6^{2-}$ pathways also are known to be metabolically available to these sulfur oxidizer enrichment communities (Wang *et al.*, 2019; Whaley-Martin *et al.*, 2019; Camacho *et al*., 2020b).

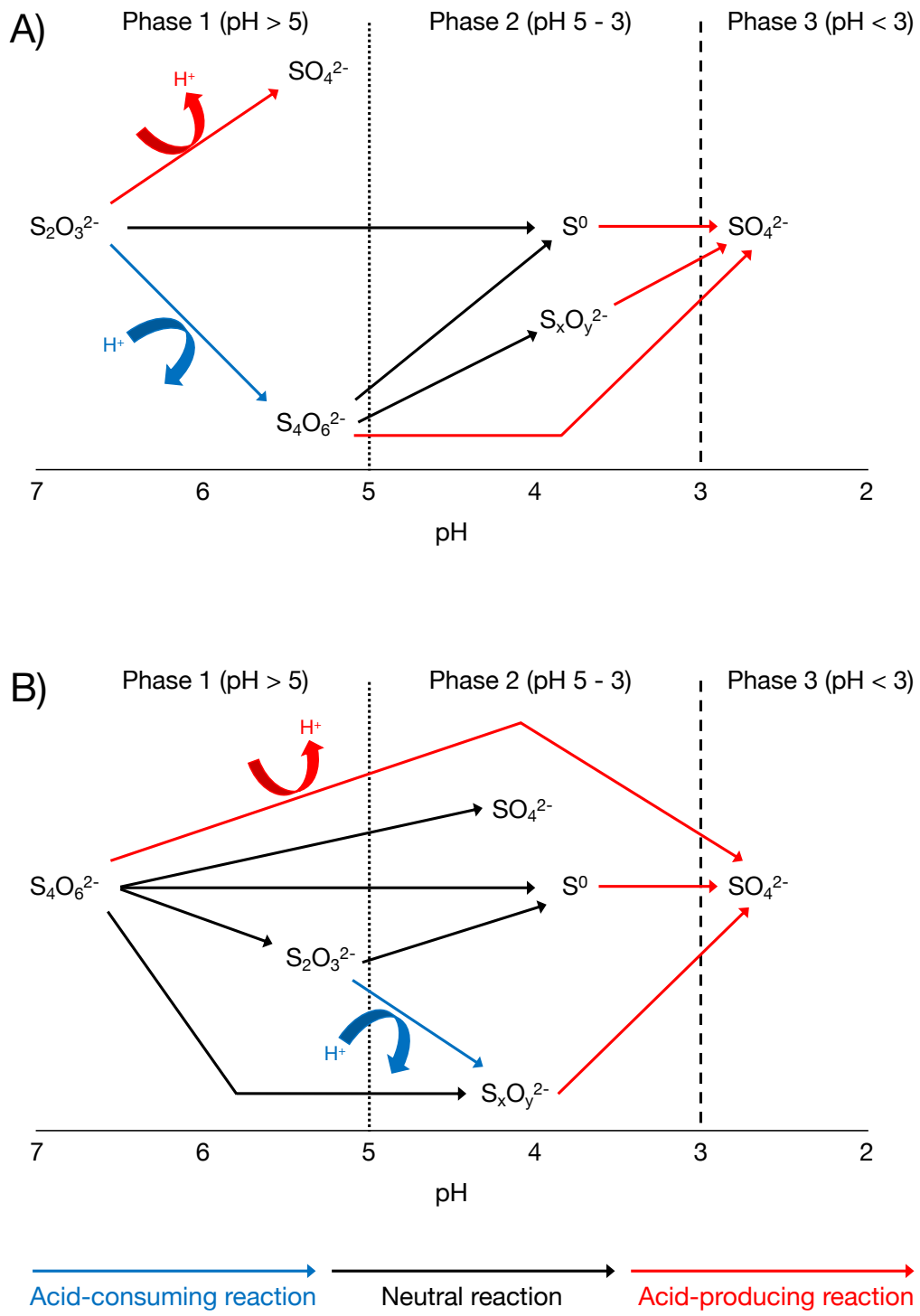

Figure 5.6: Conceptual diagram of sulfur reaction pathways for thiosalts divided into three phases: Phase 1, pH > 5; Phase 2, pH 5 – 3; and Phase 3, pH < 3. Showing the greater amount of dis/comproportionation reactions and acid-consuming reactions for phases 1 and 2, with more oxidation and acid-producing reactions in phase 3. **A)** Reaction pathways for $S_2O_3^{2-}$ as the initial S substrate. **B)** Reaction pathways for $S_4O_6^{2-}$ as the initial S substrate.

5.4. Conclusions

These novel results demonstrate the importance of SOI substrate species in determining the outcomes of microbial S oxidation pathways irrespective of whether *Halothiobacillus* spp. or *Thiomonas* spp., two important autotrophic S metabolising genera identified to occur in mine tailings ponds, dominate (Table 5.1, Figure 5.2). These results suggest predictive model development that incorporates microbially informed understanding of potential thiosalts cycling (and outcomes) based on knowledge of SOI speciation (and pH) in mining wastewaters is possible. They reinforce, why current modeling, based on assumed oxidation to sulfate (Eq 1 and 2) is not an acceptable practice under circumneutral pH conditions, i.e., those during which mines still have the opportunity to adaptively manage their systems to prevent or mitigate possible acid generation, i.e., ARD. Specifically, here, use of the proxy SO_4^{2-}:H^+ ratio, which quantifies acid consuming (i.e., dis/comproportionation) to acid generating (i.e., oxidation) reactions, reveals the importance of acid consuming reactions during early stage (i.e., circumneutral pH conditions) microbial S autotrophic metabolism (Supplemental Table S3), and explains the poor calibration between observed SO_4^{2-}:H^+ ratios and those expected based on current (abiotic) modeling. They importantly identify that irrespective of whether thiosulfate or tetrathionate, ubiquitous thiosalts species occurring in sulfide ore-based tailings, occur in these mining wastewaters, predictable changes in SOI speciation as a function of pH will occur for each of these two species; and that when both are present, the outcomes reflect additivity (Figure 5.3, 5.4). Importantly these results newly identify that the observed relationship between increasing [Elemental S] and decreasing pH as pH decreases from 6 → 3, signals that the system is shifting towards the domination of sulfur oxidation reactions and thus high acidity generation. Thus, examining SOI speciation is likely a crucial step

towards predictive measures in assessing the potential pathways and oxidative or acidification potential of circumneutral mine wastewater systems. Overall, these results set the stage for the development of more microbially informed, and therefore more sensitive monitoring approaches through more comprehensive understanding of the reactions catalyzed by important autotrophic S metabolising mining wastewater genera as well as the associated reaction controls and water chemistry outcomes.

References

Arsène-Ploetze F., Koechler S., Marchal M., Coppée J.Y., Chandler M., Bonnefoy V., *et al.* (2010) Structure, function, and evolution of the *Thiomonas* spp. genome. *PLoS genetics*. 6: 1000859.

Bernier L., Warren L. (2005) Microbially driven acidity generation in a tailings lake. *Geobiology*. 3: 115-133.

Bernier L., Warren L.A. (2007) Geochemical diversity in S processes mediated by culture-adapted and environmental-enrichments of *Acidithiobacillus* spp. *Geochim. Cosmochim. Acta.* 71: 5684-5697.

Bobadilla Fazzini R.A., Cortés M.P., Padilla L., Maturana D., Budinich M., Maass A., *et al*. (2013) Stoichiometric modeling of oxidation of reduced inorganic sulfur compounds (Riscs) in *Acidithiobacillus thiooxidans*. *Biotechnol. Bioeng.* 110: 2242-2251.

Camacho D., Frazao R., Fouillen A., Nanci A., Lang B.F., Apte S.C., *et al.* (2020) New insights into *Acidithiobacillus thiooxidans* sulfur metabolism through coupled gene expression, solution chemistry, microscopy and spectroscopy analyses. *Front. Microbiol.* 11:411. doi: 10.3389/fmicb.2020.00411

Camacho D., Jessen G.L., Mori J.F., Apte S.C., Jarolimek C.V., Warren L.A. (2020) Microbial succession signals the initiation of acidification in mining wastewaters. *Mine Water Environ.* doi.org/10.1007/s10230-020-00711-9.

Druschel G.K. (2002) Sulfur Biochemistry: Kinetics of Intermediate Sulfur Species Reactions in the Environment. PhD Dissertation University of Wisconsin - Madison.

Druschel G.K., Baker B.J., Gihring T.M., Banfield J.F. (2004) Acid mine drainage biogeochemistry at Iron Mountain, California. *Geochem. T.* 5: 13-32.

Elberling B., Schippers A., Sand W. (2000) Bacterial and chemical oxidation of pyritic mine tailings at low temperatures. *J. Contam. Hydrol*. 41:225-238.

Friedrich C.G., Rother D., Bardischewsky F., Quentmeier A., Fischer J. (2001) Oxidation of reduced inorganic sulfur compounds by bacteria: emergence of a common mechanism? *Appl Environ Microbiol* 67: 2873-2882, doi: 10.1128/AEM.67.7.2873-2882.2001.

Ghosh W., Dam B. (2009) Biochemistry and molecular biology of lithotrophic sulfur oxidation by taxonomically and ecologically diverse bacteria and archaea. *FEMS Microbiol Rev* 33: 999-1043.

Hensen D., Sperling D., Trüper H.G., Brune D.C., Dahl C. (2006) Thiosulphate oxidation in the phototrophic sulphur bacterium *Allochromatium vinosum*. *Mol Microbiol* 62: 794-810.

Hubálek Z. (2003) Protectants used in the cryopreservation of microorganisms. *Cryobiology* 46: 205-229. doi:10.1016/S0011-2240(03)00046-4

Johnson D.B., Hallberg K.B. (2003) The microbiology of acidic mine waters. *Res. Microbiol*. 154:466-473.

Johnston F., McAmish L. (1973) A study of the rates of sulfur production in acid thiosulfate solutions using S-35. *J. Colloid. Interf. Sci.* 42: 112-119.

Kelly D.P., Shergill J.K., Lu W., Wood A.P. (1997) Oxidative metabolism of inorganic sulfur compounds by bacteria. *Antonie Van Leeuwenhoek*. 71: 95-107.

Li L.F., Fu L.J., Lin J.Q., Pang X., Liu X.M., Wang R., *et al.* (2017) The sigma(54)-dependent two-component system regulating sulfur oxidization (Sox) system in *Acidithiobacillus caldus* and some chemolithotrophic bacteria. *Appl. Microbiol. Biotechnol.* 101: 2079–2092. doi: 10.1007/s00253-016- 8026-2

Liu J., Hua Z.S., Chen L.X., Kuang J.L., Li S.J., Shu W.S., *et al.* (2014) Correlating Microbial Diversity Patterns with Geochemistry in an Extreme and Heterogeneous Environment of Mine Tailings. *Appl Environ Microbiol* 80:3677–3686. doi:10.1128/AEM.00294-14.

Miranda-Trevino J.C., Pappoe M., Hawboldt K., Bottaro C. (2013) The Importance of Thiosalts Speciation: Review of Analytical Methods, Kinetics, and Treatment. *Crit. Rev. Env. Sci. Tec.* 43: 2013-2070. doi: 10.1080/10643389.2012.672047.

Nordstrom D.K. (2015) Baseline and premining geochemical characterization of mined sites. *Appl Geochem.* 57:17-34.

Nordstrom D.K., Blowes D.W., Ptacek C.J. (2015) Hydrogeochemistry and microbiology of mine drainage: an update. *Appl. Geochem.* 57:3-16.

Pronk J., Meulenberg R., Hazeu W., Bos P., Kuenen J. (1990) Oxidation of reduced inorganic sulphur compounds by acidophilic thiobacilli. *FEMS Microbiol. Lett*. 75:293-306.

Rethmeier J., Rabenstein A., Langer M., Fischer U. (1997) Detection of traces of oxidized and reduced sulfur compounds in small samples by combination of different high-performance liquid chromatography methods. *J. Chromatogr. A*. 760: 295-302.

Rohwerder T., Sand W. (2003) The sulfane sulfur of persulfides is the actual substrate of the sulfur-oxidizing enzymes from *Acidithiobacillus* and *Acidiphilium* spp. *Microbiology*. 149: 1699-1710.

Sauvé V., Bruno S., Berks B.C., Hemmings A.M. (2007) The SoxYZ complex carries sulfur cycle intermediates on a peptide swinging arm. *J Biol Chem* 282: 23194-23204.

Schippers A., Breuker A., Blazejak A., Bosecker K., Kock D., Wright T.L. (2010) The biogeochemistry and microbiology of sulfidic mine waste and bioleaching dumps and heaps, and novel Fe(II)-oxidizing bacteria. *Hydrometallurgy* 104:342–350. doi:10.1016/j.hydromet.2010.01.012.

Schippers A., Jozsa P., Sand W. (1996) Sulfur chemistry in bacterial leaching of pyrite. *Appl. Environ. Microbiol.* 62:3424-3431.

Schippers A., Sand W. (1999) Bacterial leaching of metal sulfides proceeds by two indirect mechanisms via thiosulfate or via polysulfides and sulfur. *Appl. Environ. Microbiol.* 65:319-321.

Smuda J., Dold B., Spangenberg J.E., Pfeifer H. (2008) Geochemistry and stable isotope composition of fresh alkaline porphyry copper tailings: Implications on sources and mobility of elements during transport and early stages of deposition. *Chem. Geol.* 256:62-76.

Steudel R., Holdt G., Göbel T., Hazeu W. (1987) Chromatographic Separation of Higher Polythionates SnO 62θ(n= 3… 22) and Their Detection in Cultures of *Thiobacillus ferroxidans*; Molecular Composition of Bacterial Sulfur Secretions. *Angew. Chem. Int. Edit*. 26:151-153.

Suzuki I. (1999) Oxidation of inorganic sulfur compounds: chemical and enzymatic reactions. *Can J Microbiol* 45: 97-105.

Thom G.C., Waters P.F., Hadermann A.F. (1978) Formation and decomposition of thiosulfate in the ferrous sulfide-sulfur dioxide reaction. *Inorg Chem*. 17: 1693-1696.

Vongporm, Y. (2008) Thiosalt behaviour in aqueous media. MEng Thesis: Memorial University of Newfoundland.

Wang R., Lin J.Q., Liu X.M., Pang X., Zhang C.J., Gao X.Y., *et al.* (2019) Sulfur oxidation in the acidophilic autotrophic *Acidithiobacillus* spp. *Front. Microbiol.* 9: 3290.

Warren L., Norlund K.I., Bernier L. (2008) Microbial thiosulphate reaction arrays: The interactive roles of Fe (III), O2 and microbial strain on disproportionation and oxidation pathways. *Geobiology* 6: 461-470.

Whaley-Martin K.J., Jessen G., Nelson T.C., Mori J., Apte S., Jarolimek C., *et al*. (2019) The potential role of *Halothiobacillus* spp. in sulphur oxidation and acid generation in circum-neutral mine tailings reservoirs. *Front. Microbiol*. 10: 297.

Whaley-Martin K.J., Marshall S.D., Nelson T.C., Twible L., Jarolimek C., King J.J., *et al.* (2020) A mass-balance tool for monitoring potential dissolved sulfur oxidation risks in mining impacted waters *Mine Water Environ.* 1-17.

Zopfi J., Ferdelman T.G., Fossing H. (2004) Distribution and fate of sulfur intermediates−−sulfite, tetrathionate, thiosulfate, and elemental sulfur −−in marine sediments. *Geol. Soc. Am. Spec. Papers.* 379: 97-116 doi: 10.1130/0-8137-2379-5.97.

Chapter 6

6.1 Conclusion

This thesis details advances a comprehensive understanding of the sulfur biogeochemistry of circumneutral mine wastewaters and potential indicators of acid generation for mine waste management through microcosm and mesocosm experiments integrating gene expression, microbial ecology and sulfur oxidation intermediate (SOI) geochemistry.

6.1.1. Gene expression (Chapter 3)

Several metabolic models were developed for the strict sulfur oxidizing bacteria (SoxB) *A. thiooxidans* sulfur metabolism by integrating gene expression levels with bulk solution S speciation of starting substrates S^0 and $S_2O_3^{2-}$. These models provide new insights into the likely pathways involved in *A. thiooxidans* sulfur metabolism closing some of the gaps in current literature. Specifically, results assessing relative changes in gene expression identified that *sox* complex, *sqr*, *hdr*, *tetH* and *rhd* genes are important in both S^0 and $S_2O_3^{2-}$ metabolism by *A. thiooxidans*. However, the results novelly identified a key role of *hdr* in *A. thiooxidans* ATCC 19377 S^0 metabolism expanding the understanding of important genes and their roles in *A. thiooxidans* sulfur metabolism. Relatively high *hdr* expression levels were observed under all conditions in comparison to the low levels of *sdo*. The inclusion of solution chemistry and electron microscopy enabled identification that Hdr is likely the primary S^0 oxidizing enzyme rather than Sdo, which was previously identified as important for internal generation of SO_3^{2-} and $S_2O_3^{2-}$ during growth on S^0 (Rohwerder and Sand, 2003; Bobadilla Fazzini *et al*., 2013; Yin *et al*., 2014). The study identified new insights into the central role of intracellular S^0 generation and transformation in both $S_2O_3^{2-}$ and S^0 metabolism, identifying SO_3^{2-} comproportionation to $S_2O_3^{2-}$

is a critical step in S^0 metabolism. Results confirmed the importance specifically of $S_2O_3^{2-}$ and SO_3^{2-} in *A. thiooxidans* sulfur metabolism, which have been widely proposed in the literature to be important, though not definitively shown to date prior to this thesis (Suzuki *et al.*, 1992; Suzuki, 1999; Bobadilla Fazzini *et al*., 2013). Collectively these results highlight how the integration of molecular biology and analytical chemistry approaches can better inform our understanding of sulfur biogeochemical cycling.

6.1.2. Microbial ecology (Chapter 4)

This dissertation provides new experimental findings demonstrating that circumneutral mining wastewaters have differing SoxB than those identified from more well studied tailings and waste rock AMD associated microbial communities (Schippers *et al*., 2010; Kuang *et al*., 2013; Liu *et al.*, 2014). These results underscore that pH is a key factor influencing which SoxB occur irrespective of total S concentration of SOI substrate. Results identify a greater diversity of SoxB in pre-AMD wastewater contexts than more well-known waste rock and tailings associated AMD systems. In pre-AMD circumneutral wastewaters *Proteobacteria* were found to be most prevalent (58% - 99%), primarily *Alphaproteobacteria* (28% - 77%) families *Sphingomonadaceae*, *Rhodobacteraceae* and *Caulobacteraceae* and *Gammaproteobacteria* (16% - 35%) families *Burkholderiaceae* and *Hydrogenophilaceae*. Experimental results identified that as sulfur oxidation proceeds and pH values become acidic, *Alphaproteobacteria* dominance decreased and *Gammaproteobacteria* become most prevalent. The microcosm SoxB enrichment experiments identified that *Halothiobacillus* spp. and *Thiomonas* spp. dominated the microbial communities between pH ranges 7-5 and 5-3 respectively. This result further corroborated previous findings by Whaley-Martin *et al*. (2019) that identified *Halothiobacillus* spp. prevalence between pH range 7-

5. However, the results of this thesis expand on that study, identifying a pH dependent succession to a dominance of *Thiomonas* spp. from pH range 5-3. These results reveal new opportunities for biological indicators linked to pH changes in mining wastewaters associated with initiation of AMD processes.

6.1.3. Sulfur oxidation intermediate (SOI) geochemistry (Chapter 5)

Results of this chapter novelly identified the influences of SOI chemistry and SoxB consortia containing varying abundances of *Halothiobacillus* and *Thiomonas* on SOI cycling. SOI speciation, $S_2O_3^{2-}$, $S_4O_6^{2-}$, or $S_2O_3^{2-}$ + $S_4O_6^{2-}$, was identified to be a more important determinant of microbial S oxidation and acidification outcomes than the relative abundances of *Halothiobacillus* and *Thiomonas*. The pathways mediated by both SoxB genera were characterized by three pH dependent phases of microbial sulfur processing: Phase 1, pH > 5, dis/comproportionation reactions and acid consuming reactions were prevalent alongside oxidation, with $S_2O_3^{2-}$ identified as an important indicator; Phase 2, pH 5 – 3, further dis/comproportionation occurred, with S^0 emerging as an important indicator signalling the progression of the system towards net acid generation with $S_4O_6^{2-}$ or $S_2O_3^{2-}$ as the major S species present and; Phase 3, pH < 3, i.e. full AMD conditions, with dominant oxidation reactions resulting in SO_4^{2-} and acid generation. Results demonstrate outcomes for the joint SOI substrate $S_2O_3^{2-}$ + $S_4O_6^{2-}$ treatment were additive of results observed for each of the single $S_2O_3^{2-}$ or $S_4O_6^{2-}$ treatment experiments, when SOI substrates were added in excess. Results of this chapter further identified rates of acidification and SO_4^{2-}:H^+ were dependent on the SOI species, indicating different reactions were being mediated. Results revealed $S_2O_3^{2-}$ as the S substrate produced more acid consumption and dis/comproportionation reactions and thus lower acid generation rates compared

to $S_4O_6^{2-}$. Collectively, results of this chapter identified specific SOI species important at different stages in AMD initiation and development for a suite of varying microbial SoxB enrichments that provide new understanding of how microbial identity and sulfur speciation affect sulfur outcomes in mining wastewaters.

6.1.4. Mine wastewater management acid generation indicators

The interdisciplinary approach of this thesis, combining gene expression, microbial ecology and sulfur geochemistry enabled new insights. These novel insights into key processes, important sulfur compounds and SoxB microbial identities and roles will better inform the development of biologically informed, and therefore more effective monitoring tools for circumneutral mine wastewaters before a system reaches AMD. Currently, mines typically rely on geochemical (i.e., sulfate concentrations) and/or physico-chemical (i.e., pH values) to identify if wastewaters may be moving from PNAG to NAG stages; these geochemical proxies are not sensitive to early PNAG conditions associated especially with microbial SoxB activity. Thus, many mines often fail to capture the shift from PNAG to NAG conditions, that can result in an inability to prevent or mitigate NAG conditions in a timely fashion. Results here specifically lay the groundwork for new, microbially informed monitoring capabilities that target early PNAG stages that would enable mines to proactively detect when shifts are beginning to occur and thus adaptively manage to prevent undesired outcomes.

First the improved understanding of sulfur biogeochemistry generated by this thesis identified critical SOI species S^0, $S_2O_3^{2-}$, $S_4O_6^{2-}$ and SO_3^{2-} that are indicators of different stages of the AMD initiation and generation cascade. These results identify that incorporation of these SOI species in a monitoring program would enable mines to proactively identify when AMD may be

initiating and manage the process before it establishes fully. Something that mines still struggle to do around the world by primarily measuring for pH and/or sulfate, which are not sensitive or provide sufficient warning time for mines to intervene.

Second, results of this thesis identify that shifts in abundance of key SoxB groups from *Alphaproteobacteria* to *Gammaproteobacteria* signals pH decline from circumneutral to moderately acidic in the mine wastewater microbial communities. Specifically, *Halothiobacillus* spp. dominated under more circumneutral pH conditions of 7-5, while *Thiomonas* spp. abundance increased as pH decreased below 5. Thus, monitoring assays that identify the relative abundances of these genera may be a promising monitoring tool for mines to employ to catch the initiation of AMD conditions from PNAG stages to the transitionary stage before NAG.

Next steps should build on the new understanding revealed in this thesis and work towards the development of possible monitoring assays that use these potential indicators of S speciation and SoxB abundance in tandem to detect AMD initiation in mining wastewaters. Such tools would enable a proactive monitoring approach that could increase mines' ability to mitigate and prevent AMD conditions, decreasing environmental risks and increasing mining water stewardship.

References

Bobadilla Fazzini R.A., Cortés M.P., Padilla L., Maturana D., Budinich M., Maass A., *et al*. (2013) Stoichiometric modeling of oxidation of reduced inorganic sulfur compounds (Riscs) in *Acidithiobacillus thiooxidans*. *Biotechnol bioeng* 110: 2242-2251.

Kuang J.L., Huang L.N., Chen L.X., Hua Z.S., Li S.J., Hu M. *et al*. (2013) Contemporary environmental variation determines microbial diversity patterns in acid mine drainage. *ISME J*. 7: 1038.

Liu J., Hua Z., Chen L., Kuang J., Li S., Shu W., *et al*. (2014) Correlating Microbial Diversity Patterns with Geochemistry in an Extreme and Heterogeneous Environment of Mine Tailings. *Appl. Environ. Microbiol.* 80: 3677–3686. doi:10.1128/AEM.00294-14.

Rohwerder T., Sand W. (2003) The sulfane sulfur of persulfides is the actual substrate of the sulfur-oxidizing enzymes from *Acidithiobacillus* and *Acidiphilium* spp. *Microbiology*. 149: 1699-1710.

Schippers A., Breuker A., Blazejak A., Bosecker K., Kock D., Wright T.L. (2010) The biogeochemistry and microbiology of sulfidic mine waste and bioleaching dumps and heaps, and novel Fe(II)-oxidizing bacteria. *Hydrometallurgy* 104: 342–350. doi:10.1016/j.hydromet.2010.01.012.

Suzuki I. (1999) Oxidation of inorganic sulfur compounds: chemical and enzymatic reactions. *Can J Microbiol* 45: 97-105.

Suzuki I., Chan C.W., Takeuchi T.L. (1992) Oxidation of elemental sulfur to sulfite by *Thiobacillus thiooxidans* cells. *Appl Environ Microbiol* 58: 3767-3769.

Whaley-Martin K.J., Jessen G., Nelson T.C., Mori J., Apte S., Jarolimek C., *et al*. (2019) The potential role of *Halothiobacillus* spp. in sulphur oxidation and acid generation in circum-neutral mine tailings reservoirs. *Front. Microbiol*. 10: 297.

Yin H., Zhang X., Li X., He Z., Liang Y., Guo X., *et al*. (2014) Whole-genome sequencing reveals novel insights into sulfur oxidation in the extremophile *Acidithiobacillus thiooxidans*. *BMC microbiol* 14: 179.

Appendix

Supplemental Material for Chapter 3

Methods

Metabolism Model Creation

Stoichiometric mass balance based on net changes in solution sulfur and acid concentrations across time, within each treatment, were first used to identify the most likely sulfur reactions occurring (Supplementary Figure S2). These geochemical changes could be balanced via several possible sulfur reactions creating uncertainty in identification of the specific pathways being catalyzed (Supplemental Data). Then, we used the gene expression levels (Figure 3.3a) to refine the reaction pathways identified as most likely from our geochemical results assessing sulfur species and proton changes over time (Supplementary Figure S2). The resulting metabolic maps highlight the genes and pathways being potentially catalyzed (Figure 3.7). The best model predicting sulfur reactions was then determined by narrowing down the range of geochemically possible reactions through observed changes in gene expression levels, which provides clues as to which reactions are most likely occurring (Supplemental Data, Figure 3.7). Further sulfur metabolism models were developed for both S^0 and $S_2O_3^{2-}$ as initial sulfur sources, via stoichiometric balancing and the identified pathways from the entire suite of those proposed, observed, hypothesized and/or putatively suggested in the literature to be catalyzed by specific genes (Table 3.3; Figure 3.1), generating *A. thiooxidans* S^0 and $S_2O_3^{2-}$ dependent metabolism models (Supplemental Data and Figure 3.6).

Results

Stepwise reactions for Figure 3.6 follows.

Step-Wise reactions

$6S^0 \rightarrow 2SO_4^{2-} + 4S^{Other\ SOI} + 5H^+$ (Table 3.3, Eq 1)

$37S_2O_3^{2-} + 0.5SO_3^{2-} \rightarrow 7S^0 + 31.5SO_4^{2-} + 36S^{Other\ SOI} + 20H^+$ (Table 3.3, Eq 7)

$3S_2O_3^{2-} \rightarrow 2S^0 + 2SO_4^{2-} + 2S^{Other\ SOI} + H^+$ (Table 3.3, Eq 8)

Figure 3.6a was theorized via mass balance of total experiment for ASOM-S^0 i.e Eq (1) Table 3.3 to get the closest in describing S-species consumption/production and H^+ production.

Step-wise reactions

$4S^0 + 4O_2 + 4H_2O \rightarrow 4SO_3^{2-} + 8H^+$ (1)

$2SO_3^{2-} + O_2 \rightarrow 2SO_4^{2-}$ (2)

$2S^0 + 2SO_3^{2-} \rightarrow 2S_2O_3^{2-}$ (3)

$2S_2O_3^{2-} + 0.5O_2 + 2H^+ \rightarrow S_4O_6^{2-} + H_2O$ (4)

Figure 3.6b was created using similar steps, based on the observed total S changes from day 0-2 for the ASOM-$S_2O_3^{2-}$ test, Eq (7) Table 3.3.

Step-wise reactions

$7S_2O_3^{2-} \rightarrow 7S^0 + 7SO_3^{2-}$ (5)

$7SO_3^{2-} + 7H_2O \rightarrow 7SO_4^{2-} + 14H^+$ (6)

$$0.5SO_3^{2-} + O_2 \rightarrow 0.5SO_4^{2-} \quad (7)$$

$$30S_2O_3^{2-} + 7.5O_2 + 30H^+ \rightarrow 15S_4O_6^{2-} + 15H_2O \quad (8)$$

$$6S_4O_6^{2-} + 21O_2 + 18H_2O \rightarrow 24SO_4^{2-} + 36H^+ \quad (9)$$

Figure 3.6c was also theorized the same as the others but based on ASOM- $S_2O_3^{2-}$ total experiment (day 0-4) as in Eq (8) Table 3.3.

Step-wise reactions

$$3S_2O_3^{2-} + 0.75O_2 + 3H^+ \rightarrow 1.5S_4O_6^{2-} + 1.5H_2O \quad (10)$$

$$S_4O_6^{2-} + H_2O \rightarrow S_3O_3^{2-} + SO_4^{2-} + 2H^+ \quad (11)$$

$$S_3O_3^{2-} \rightarrow 2S^0 + SO_3^{2-} \quad (12)$$

$$S^0 + SO_3^{2-} \rightarrow S_2O_3^{2-} \quad (13)$$

$$S_2O_3^{2-} \rightarrow S^0 + SO_3^{2-} \quad (14)$$

$$SO_3^{2-} + H_2O \rightarrow SO_4^{2-} + 2H^+ \quad (15)$$

(Eq 13 + 14 can also be replaced directly to Eq 15)

Discussion

RNA-seq on other metabolic characteristics

Whereas we primarily focused on the genes involved in sulfur metabolism, RNA-seq analysis provides genome-wide quantitative information on gene expression patterns. This analysis revealed higher expression of a substantial number of genes of the flagellar assembly pathway at day 3 during growth on S^0 as compared to day 5. The bacteria are probably more metabolically active in the exponential growth phase at day 3 and this could be linked to higher mobility. We also obtained evidence for differential expression of genes encoding ATP synthase components as well as genes encoding components of cytochrome C biogenesis, protein folding and membrane stability, providing additional insights into the distinct metabolic adaptations under the different growth conditions tested here.

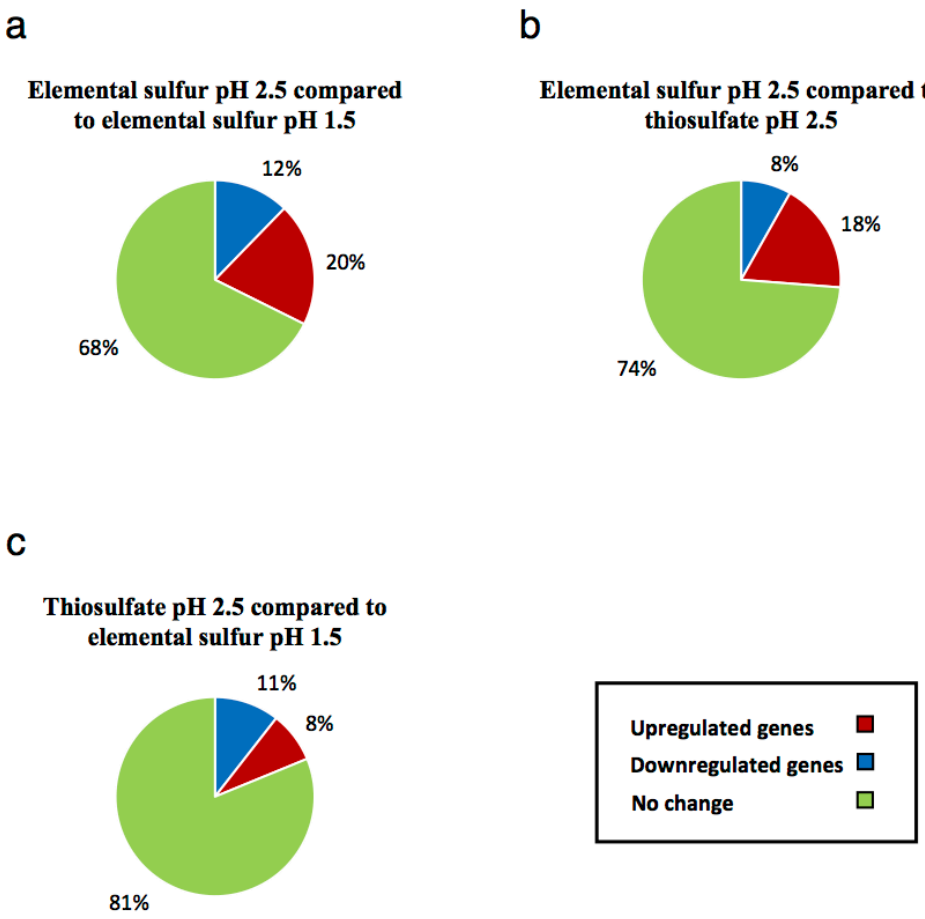

Supplementary Figure S1: Analysis of gene expression regulation on all genes after growth with S^0 or $S_2O_3^{2-}$ as energy source. Comparative gene expression for FPKM values based on Log2 ratio. (**a**) Growth on same substrate (S^0) at different points on pH and growth curve (pH 2.5 = day 3 / pH 1.5 = day 5), (**b**) growth to same pH (2.5) on different substrates and points on growth curve (S^0 = day 3 / $S_2O_3^{2-}$ = day 5), (**c**) growth until day 5 on different substrates and to different pH values ($S_2O_3^{2-}$ = pH 2.5 / S^0 = pH 1.5).

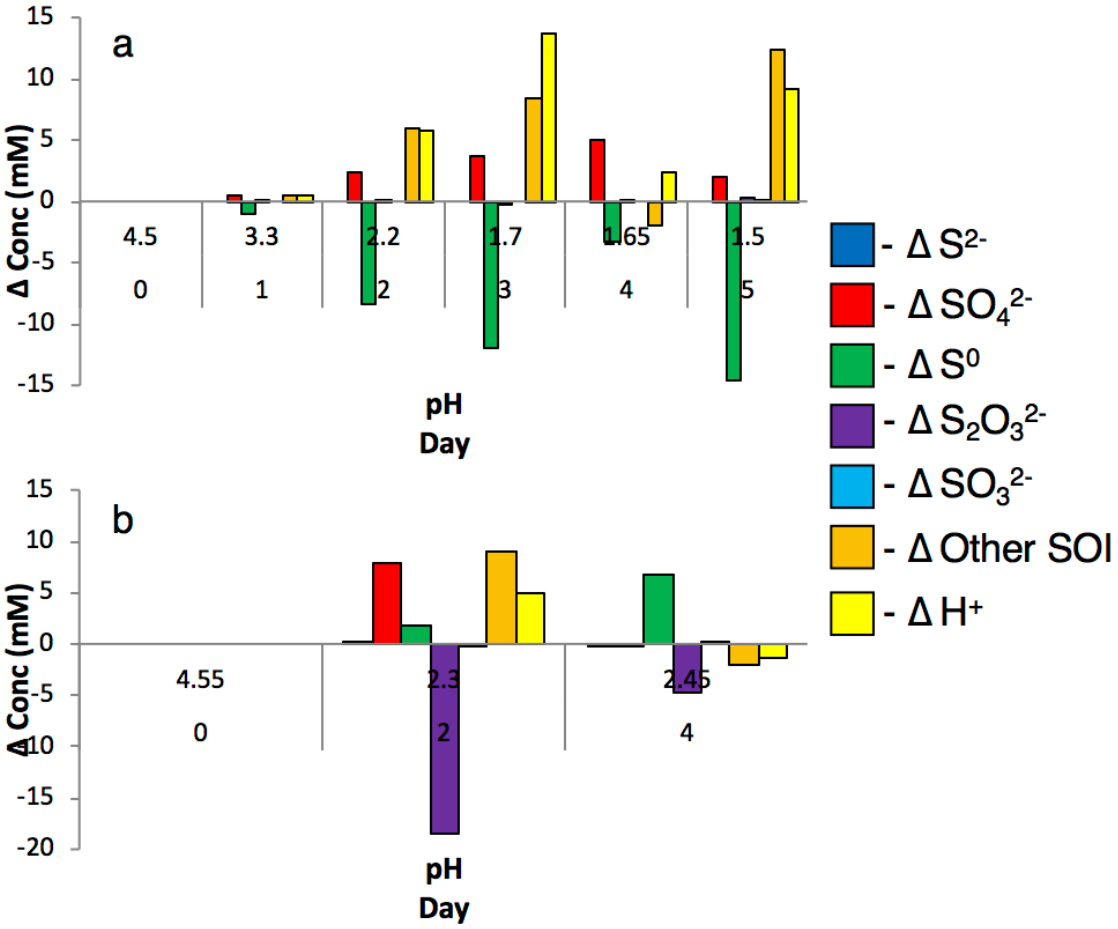

Supplementary Figure S2: Change in sulfur species and H^+ concentration per sampling point. (**a**) For S^0 media. (**b**) For $S_2O_3^{2-}$ media. Concentrations of all S species are mM in mol of S.

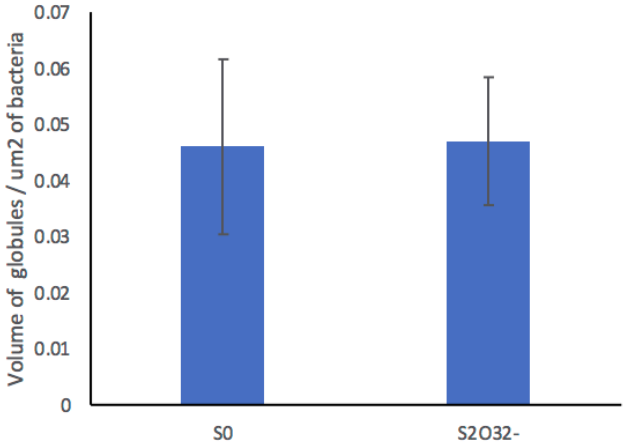

Supplementary Figure S3: Size in volume of the S^0 globules formed in *A. thiooxidans* cells when grown in either S^0 or $S_2O_3^{2-}$, analysis done via Image J.

Supplementary Table S1: More statistical detailed table of Figure 3a, showing analysis of gene expression after growth with S^0 or $S_2O_3^{2-}$ as energy source, with gene expression based on FPKM values and standard deviation on the biological triplicate experiments.

Gene	Gene number	S^0 pH=2.5	S^0 pH=1.5	$S_2O_3^{2-}$ pH=2.5
sdo-1	PROKKA-ALT_00302	82 ± 9	65 ± 17	57 ± 13
sdo-2	PROKKA-ALT_03084	336 ± 34	265 ± 71	297 ± 1
sdo-3	PROKKA-ALT_00833	122 ± 42	40 ± 11	34 ± 1
soxA-1	PROKKA-ALT_01532	8991 ± 650	740 ± 91	27741 ± 776
soxB-1	PROKKA-ALT_01530	6620 ± 519	506 ± 96	18732 ± 1793
soxX-1	PROKKA-ALT_01535	13321 ± 1082	1431 ± 57	48108 ± 233
soxY-1	PROKKA-ALT_01534	18029 ± 1609	1887 ± 81	58197 ± 1804
soxZ-1	PROKKA-ALT_01533	20503 ± 1519	2138 ± 139	63386 ± 2778
soxA-2	PROKKA-ALT_02661	137 ± 8	970 ± 98	1445 ± 125
soxB-2	PROKKA-ALT_02657	453 ± 5	1358 ± 16	3489 ± 181
soxX-2	PROKKA-ALT_02660	126 ± 4	776 ± 106	1307 ± 102
soxY-2	PROKKA-ALT_02655	597 ± 28	1552 ± 67	4122 ± 113
soxZ-2	PROKKA-ALT_02656	723 ± 21	1764 ± 19	5215 ± 222
sqr	PROKKA-ALT_02961	4623 ± 1085	3353 ± 609	3124 ± 57
doxD	PROKKA-ALT_02168	42 ± 0	39 ± 14	54 ± 13
tetH	PROKKA-ALT_02172	251 ± 80	214 ± 98	5968 ± 1143
sor	PROKKA-ALT_00671	21 ± 2	17 ± 0	26 ± 1
rhd-1	PROKKA-ALT_01651	756 ± 189	839 ± 337	916 ± 42
rhd-2	PROKKA-ALT_01545	1345 ± 182	661 ± 134	702 ± 77
hdrA-1	PROKKA-ALT_01550	8668 ± 607	11964 ± 2479	8236 ± 666
hdrA-2	PROKKA-ALT_00063	50 ± 6	27 ± 11	20 ± 3
hdrA-3	PROKKA-ALT_01357	4628 ± 670	19041 ± 3595	15625 ± 2227
hdrB	PROKKA-ALT_01507	1176 ± 329	1354 ± 124	831 ± 68
hdrC	PROKKA-ALT_01552	4903 ± 488	6565 ± 1594	4219 ± 190
paps	PROKKA-ALT_03389	20 ± 1	80 ± 5	148 ± 29
aps	PROKKA-ALT_02667	178 ± 11	68 ± 25	82 ± 14

Supplementary Table S2: More statistical detailed table of Figure 3b-i, showing analysis of gene expression after growth with S^0 or $S_2O_3^{2-}$ as energy source, with comparative gene expression for FPKM values based on Log2 ratio and p-value based on independent t-test between the respective triplicate samples of growth on same substrate (S^0) at different points on pH and growth curve (pH 2.5 = day 3 / pH 1.5 = day 5).

Gene	Gene number	Log2	Err. standard log2	p-value
sdo-1	PROKKA-ALT_00302	0.33	0.12	2.09E-01
sdo-2	PROKKA-ALT_03084	0.34	0.13	3.34E-01
sdo-3	PROKKA-ALT_00833	1.62	1.01	2.96E-02
soxA-1	PROKKA-ALT_01532	3.60	0.71	3.15E-03
soxB-1	PROKKA-ALT_01530	3.71	0.99	3.70E-03
soxX-1	PROKKA-ALT_01535	3.22	0.39	4.12E-03
soxY-1	PROKKA-ALT_01534	3.26	0.43	4.94E-03
soxZ-1	PROKKA-ALT_01533	3.26	0.45	3.43E-03
soxA-2	PROKKA-ALT_02661	-2.83	-0.86	1.43E-04
soxB-2	PROKKA-ALT_02657	-1.58	-0.04	1.70E-04
soxX-2	PROKKA-ALT_02660	-2.62	-0.71	4.75E-04
soxY-2	PROKKA-ALT_02655	-1.38	-0.12	2.87E-03
soxZ-2	PROKKA-ALT_02656	-1.29	-0.05	3.75E-04
sqr	PROKKA-ALT_02961	0.46	0.19	1.52E-01
doxD	PROKKA-ALT_02168	0.10	0.03	7.54E-01
tetH	PROKKA-ALT_02172	0.23	0.18	6.35E-01
sor	PROKKA-ALT_00671	0.34	0.04	6.26E-03
rhd-1	PROKKA-ALT_01651	-0.15	-0.10	7.30E-01
rhd-2	PROKKA-ALT_01545	1.03	0.35	6.29E-03
hdrA-1	PROKKA-ALT_01550	-0.46	-0.13	8.89E-02
hdrA-2	PROKKA-ALT_00063	0.91	0.49	3.22E-02
hdrA-3	PROKKA-ALT_01357	-2.04	-0.68	2.41E-03
hdrB	PROKKA-ALT_01507	-0.20	-0.08	4.29E-01
hdrC	PROKKA-ALT_01552	-0.42	-0.13	1.59E-01
paps	PROKKA-ALT_03389	-1.97	-0.18	3.29E-03
aps	PROKKA-ALT_02667	1.39	0.61	2.31E-03

Supplementary Table S3: More statistical detailed table of Figure 3b-ii, showing analysis of gene expression after growth with S^0 or $S_2O_3^{2-}$ as energy source, with comparative gene expression for FPKM values based on Log2 ratio and p-value based on independent t-test between the respective triplicate samples of growth to same pH (2.5) on different substrates and points on growth curve (S^0 = day 3 / $S_2O_3^{2-}$ = day 5).

Gene	Gene number	Log2	Err. standard log2	p-value
sdo-1	PROKKA-ALT_00302	0.54	0.18	4.58E-02
sdo-2	PROKKA-ALT_03084	0.18	0.02	2.49E-01
sdo-3	PROKKA-ALT_00833	1.83	0.69	2.15E-02
soxA-1	PROKKA-ALT_01532	-1.63	-0.16	1.45E-03
soxB-1	PROKKA-ALT_01530	-1.50	-0.26	1.04E-02
soxX-1	PROKKA-ALT_01535	-1.85	-0.16	5.05E-04
soxY-1	PROKKA-ALT_01534	-1.69	-0.20	1.81E-03
soxZ-1	PROKKA-ALT_01533	-1.63	-0.19	2.72E-03
soxA-2	PROKKA-ALT_02661	-3.40	-0.99	6.10E-05
soxB-2	PROKKA-ALT_02657	-2.95	-0.19	2.16E-04
soxX-2	PROKKA-ALT_02660	-3.37	-0.72	3.90E-05
soxY-2	PROKKA-ALT_02655	-2.79	-0.21	5.47E-04
soxZ-2	PROKKA-ALT_02656	-2.85	-0.21	1.23E-03
sqr	PROKKA-ALT_02961	0.57	0.14	7.51E-02
doxD	PROKKA-ALT_02168	-0.36	-0.09	1.84E-01
tetH	PROKKA-ALT_02172	-4.57	-2.34	9.87E-04
sor	PROKKA-ALT_00671	-0.28	-0.04	1.28E-01
rhd-1	PROKKA-ALT_01651	-0.28	-0.08	2.27E-01
rhd-2	PROKKA-ALT_01545	0.94	0.23	4.83E-03
hdrA-1	PROKKA-ALT_01550	0.07	0.01	4.53E-01
hdrA-2	PROKKA-ALT_00063	1.32	0.38	1.70E-03
hdrA-3	PROKKA-ALT_01357	-1.76	-0.50	1.21E-03
hdrB	PROKKA-ALT_01507	0.50	0.18	1.51E-01
hdrC	PROKKA-ALT_01552	0.22	0.03	8.65E-02
paps	PROKKA-ALT_03389	-2.86	-0.66	2.54E-02
aps	PROKKA-ALT_02667	1.12	0.26	7.80E-04

Supplementary Table S4: More statistical detailed table of Figure 3b-iii, showing analysis of gene expression after growth with S^0 or $S_2O_3^{2-}$ as energy source, with comparative gene expression for FPKM values based on Log2 ratio and p-value based on independent t-test between the respective triplicate samples of growth until day 5 on different substrates and to different pH values (S^0 = pH 1.5 / $S_2O_3^{2-}$ = pH 2.5).

Gene	Gene number	Log2	Err. standard log2	p-value
sdo-1	PROKKA-ALT_00302	0.20	0.10	5.29E-01
sdo-2	PROKKA-ALT_03084	-0.16	-0.04	5.95E-01
sdo-3	PROKKA-ALT_00833	0.22	0.07	4.47E-01
soxA-1	PROKKA-ALT_01532	-5.23	-0.79	4.19E-04
soxB-1	PROKKA-ALT_01530	-5.21	-1.48	4.82E-03
soxX-1	PROKKA-ALT_01535	-5.07	-0.23	1.30E-05
soxY-1	PROKKA-ALT_01534	-4.95	-0.37	5.14E-04
soxZ-1	PROKKA-ALT_01533	-4.89	-0.53	1.03E-03
soxA-2	PROKKA-ALT_02661	-0.58	-0.11	6.58E-03
soxB-2	PROKKA-ALT_02657	-1.36	-0.09	3.63E-03
soxX-2	PROKKA-ALT_02660	-0.75	-0.16	3.37E-03
soxY-2	PROKKA-ALT_02655	-1.41	-0.10	1.31E-03
soxZ-2	PROKKA-ALT_02656	-1.56	-0.08	2.08E-03
sqr	PROKKA-ALT_02961	0.10	0.02	5.51E-01
doxD	PROKKA-ALT_02168	-0.45	-0.27	2.55E-01
tetH	PROKKA-ALT_02172	-4.80	-3.12	9.67E-04
sor	PROKKA-ALT_00671	-0.62	-0.02	7.13E-04
rhd-1	PROKKA-ALT_01651	-0.13	-0.06	7.15E-01
rhd-2	PROKKA-ALT_01545	-0.09	-0.03	6.68E-01
hdrA-1	PROKKA-ALT_01550	0.54	0.16	6.56E-02
hdrA-2	PROKKA-ALT_00063	0.41	0.24	3.78E-01
hdrA-3	PROKKA-ALT_01357	0.29	0.09	2.34E-01
hdrB	PROKKA-ALT_01507	0.70	0.12	3.03E-03
hdrC	PROKKA-ALT_01552	0.64	0.18	6.47E-02
paps	PROKKA-ALT_03389	-0.89	-0.23	8.39E-02
aps	PROKKA-ALT_02667	-0.27	-0.15	4.47E-01

Supplementary Table S5: Top 50 upregulated genes after growth on elemental sulfur at pH 2.5 as compared to pH 1.5.

p-value	FPKM	LOG2	Genes
2.71E-01	42.98	8.78	16S ribosomal RNA
1.11E-01	4926.88	6.15	putative globin-like protein aq_211
2.15E-01	48.31	5.71	16S ribosomal RNA
7.19E-02	735.70	5.00	Xylene monooxygenase electron transfer component
7.70E-05	743.07	4.68	hypothetical protein
1.13E-02	690.12	4.45	Chemotaxis protein CheY
2.44E-02	339.73	4.38	STAS domain protein
4.08E-02	101.34	4.12	hypothetical protein
8.49E-03	792.53	4.01	Methyl-accepting chemotaxis protein 3
4.47E-02	4950.47	3.99	hypothetical protein
4.05E-01	599.51	3.90	tRNA-Lys(ttt)
2.26E-02	374.81	3.88	Chemotaxis protein CheA
4.07E-01	6.51	3.81	hypothetical protein
2.09E-02	199.92	3.72	Chemotaxis response regulator protein-glutamate methylesterase 2
3.79E-03	1123.46	3.72	Flagellar hook protein FlgE
2.48E-02	409.85	3.56	Biofilm dispersion protein BdlA
4.14E-01	6540.13	3.54	tRNA-Trp(cca)
4.48E-03	1169.28	3.54	Basal-body rod modification protein FlgD
4.51E-02	452.51	3.52	DNA-3-methyladenine glycosylase
2.61E-02	576.58	3.52	Methyl-accepting chemotaxis serine transducer
5.39E-03	1059.93	3.46	hypothetical protein
1.40E-05	189.60	3.43	Flagellar biosynthetic protein FliR
1.42E-02	1023.61	3.42	hypothetical protein
1.82E-03	724.00	3.41	Flagellar biosynthetic protein FliP
6.17E-03	561.07	3.38	Chemotaxis protein CheA
2.46E-02	549.99	3.36	putative chemoreceptor glutamine deamidase CheD
1.56E-02	1065.97	3.35	Flagellar basal-body rod protein FlgC
1.17E-02	439.38	3.33	hypothetical protein
4.23E-02	874.01	3.28	Cytochrome bd-I ubiquinol oxidase subunit 2
1.00E-05	160.77	3.27	Flagellar biosynthetic protein FlhB
8.33E-03	554.28	3.26	hypothetical protein
4.69E-01	287.73	3.21	tRNA-Pro(ggg)
8.23E-03	833.92	3.21	Metallo-beta-lactamase superfamily protein
6.19E-03	1142.73	3.19	Chemotaxis protein CheY
1.66E-02	1435.00	3.18	Flagellar basal body rod protein FlgB
1.03E-02	772.58	3.18	FlgN protein
1.56E-02	839.46	3.17	Flagellar basal-body rod protein FlgF
7.00E-02	1220.94	3.16	Cytochrome bd-II ubiquinol oxidase subunit 1
1.25E-02	238.24	3.13	putative signaling protein
4.74E-01	455.44	3.07	tRNA-Gln(ttg)
9.79E-04	286.66	3.07	Flagellar brake protein YcgR
2.16E-02	1347.68	3.06	hypothetical protein
1.01E-02	1017.38	3.05	hypothetical protein
1.69E-03	1391.39	3.05	flagellar protein FliS
4.67E-02	312.68	3.04	Chemotaxis protein methyltransferase 3
7.09E-02	695.87	3.02	Cytochrome c biogenesis protein CcsB
4.37E-03	2725.95	2.99	hypothetical protein
6.46E-03	440.43	2.99	Flagellar hook-length control protein
1.90E-02	413.96	2.98	Chemotaxis protein CheV
1.26E-01	12.18	2.98	Glycosyl transferase family 2

Supplementary Table S6: Top 50 downregulated genes after growth on elemental sulfur at pH 2.5 as compared to pH 1.5.

p-value	FPKM	LOG2	Genes
3.61E-01	26.96	-6.55	hypothetical protein
3.66E-01	129.99	-6.26	hypothetical protein
3.68E-01	90.04	-6.07	hypothetical protein
3.67E-01	70.83	-6.05	hypothetical protein
3.67E-01	75.00	-6.04	hypothetical protein
3.67E-01	42.30	-5.98	hypothetical protein
3.68E-01	72.61	-5.96	hypothetical protein
3.67E-01	63.09	-5.95	hypothetical protein
3.68E-01	46.96	-5.94	hypothetical protein
3.65E-01	42.37	-5.92	hypothetical protein
3.68E-01	67.87	-5.90	hypothetical protein
3.65E-01	55.69	-5.89	hypothetical protein
3.68E-01	112.53	-5.86	hypothetical protein
3.66E-01	49.85	-5.86	hypothetical protein
3.64E-01	41.91	-5.86	hypothetical protein
3.66E-01	60.91	-5.82	hypothetical protein
3.67E-01	98.17	-5.82	hypothetical protein
3.65E-01	204.11	-5.82	hypothetical protein
3.69E-01	60.88	-5.81	hypothetical protein
3.70E-01	254.82	-5.80	hypothetical protein
3.67E-01	86.34	-5.80	hypothetical protein
3.68E-01	37.68	-5.79	hypothetical protein
3.67E-01	52.53	-5.78	Nucleoid occlusion protein
3.66E-01	71.47	-5.77	hypothetical protein
3.68E-01	26.08	-5.76	hypothetical protein
3.69E-01	38.62	-5.74	hypothetical protein
3.67E-01	57.77	-5.74	hypothetical protein
3.69E-01	85.93	-5.71	Single-stranded DNA-binding protein
3.68E-01	96.85	-5.70	hypothetical protein
3.67E-01	40.19	-5.67	hypothetical protein
3.66E-01	47.84	-5.65	hypothetical protein
3.66E-01	55.51	-5.65	hypothetical protein
3.68E-01	37.68	-5.62	hypothetical protein
3.67E-01	40.47	-5.61	hypothetical protein
3.66E-01	79.07	-5.59	hypothetical protein
3.66E-01	56.27	-5.59	hypothetical protein
3.68E-01	127.91	-5.58	hypothetical protein
3.63E-01	11.50	-5.55	hypothetical protein
3.69E-01	76.44	-5.52	hypothetical protein
3.64E-01	59.73	-5.48	ThiF family protein
3.69E-01	65.72	-5.43	Calcineurin-like phosphoesterase superfamily domain protein
3.69E-01	66.37	-5.41	hypothetical protein
3.68E-01	40.16	-5.40	hypothetical protein
3.62E-01	17.67	-5.37	hypothetical protein
3.67E-01	85.81	-5.36	hypothetical protein
3.65E-01	247.11	-5.35	hypothetical protein
3.71E-01	32.22	-5.21	hypothetical protein
3.68E-01	110.20	-5.20	hypothetical protein
3.69E-01	58.58	-5.15	DNA polymerase III subunit beta
3.64E-01	42.33	-5.14	hypothetical protein

Supplementary Table S7: Top 50 upregulated genes after growth on elemental sulfur at pH 2.5 as compared to thiosulfate pH 2.5.

p-value	FPKM	LOG2	Genes
1.61E-02	365.21	4.04	hypothetical protein
1.91E-03	1656.05	4.02	hypothetical protein
6.80E-03	1593.95	3.94	NADH-quinone oxidoreductase subunit L
3.61E-01	151.44	3.71	putative multidrug resistance protein EmrY
1.18E-03	304.67	3.59	hypothetical protein
3.72E-03	223.33	3.42	Nodulation protein NolG
1.19E-04	799.66	3.41	hypothetical protein
6.22E-03	1336.96	3.36	CobQ/CobB/MinD/ParA nucleotide binding domain protein
4.20E-01	2452.55	3.35	tRNA-Thr(ggt)
1.08E-02	3169.29	3.32	hypothetical protein
5.43E-03	296.13	3.27	hypothetical protein
8.36E-02	1019.12	3.19	hypothetical protein
1.88E-02	929.70	3.16	hypothetical protein
8.45E-03	459.09	3.10	hypothetical protein
4.87E-03	232.78	3.08	hypothetical protein
2.90E-05	212.04	3.05	hypothetical protein
6.80E-02	1058.54	3.02	hypothetical protein
1.67E-02	690.12	3.01	Chemotaxis protein CheY
2.88E-02	374.81	3.00	Chemotaxis protein CheA
3.45E-02	339.73	2.98	STAS domain protein
3.16E-01	0.31	2.94	Rhodopirellula transposase
2.33E-01	236.32	2.94	Cytochrome bd-II ubiquinol oxidase subunit 2
1.47E-02	2695.43	2.94	50S ribosomal protein L7/L12
1.41E-02	276.06	2.89	hypothetical protein
5.46E-04	743.07	2.74	hypothetical protein
3.44E-02	576.58	2.74	Methyl-accepting chemotaxis serine transducer
3.45E-01	72.11	2.72	Fusaric acid resistance protein FusA
4.57E-03	377.74	2.71	hypothetical protein
4.65E-03	127.69	2.67	hypothetical protein
2.20E-01	270.40	2.64	Blue copper oxidase CueO
3.40E-03	796.31	2.63	ATP synthase gamma chain
5.35E-03	754.11	2.56	ATP synthase epsilon chain
7.27E-03	3106.66	2.55	50S ribosomal protein L10
1.60E-02	792.53	2.52	Methyl-accepting chemotaxis protein 3
2.19E-01	132.59	2.51	2-isopropylmalate synthase
4.62E-01	303.63	2.51	tRNA-Val(cac)
2.22E-01	216.52	2.50	Cytochrome bd ubiquinol oxidase subunit 1
5.96E-03	2248.89	2.50	TraT complement resistance protein
2.57E-03	1193.21	2.48	ATP synthase subunit alpha
1.39E-04	184.35	2.48	Capsule polysaccharide export outer membrane protein CtrA
3.65E-03	1318.97	2.44	ATP synthase subunit beta
7.61E-02	12.18	2.37	Glycosyl transferase family 2
7.36E-02	36.98	2.34	RNA polymerase sigma factor RpoS
2.39E-03	801.26	2.33	ATP synthase subunit delta
5.19E-02	124.94	2.33	ATP-binding protein BexA
6.48E-03	660.05	2.23	DNA-directed RNA polymerase subunit beta
1.37E-01	439.74	2.22	Cytochrome bd ubiquinol oxidase subunit 1
3.33E-02	96.75	2.21	Capsule polysaccharide export inner-membrane protein CtrC
1.27E-02	693.33	2.20	DNA-directed RNA polymerase subunit beta'
3.47E-03	1481.47	2.18	ATP synthase subunit b

Supplementary Table S8: Top 50 downregulated genes after growth on elemental sulfur at pH 2.5 as compared to thiosulfate pH 2.5.

p-value	FPKM	LOG2	Genes
1.31E-01	0.11	-9.40	hypothetical protein
1.28E-01	0.17	-8.84	hypothetical protein
8.30E-05	13.89	-5.74	putative protein
1.57E-04	23.79	-5.00	Cation efflux system protein CusC
1.06E-02	24.27	-4.92	hypothetical protein
1.05E-04	30.52	-4.72	putative transporter
1.40E-01	3.91	-3.88	23S ribosomal RNA
4.37E-02	217.63	-3.76	hypothetical protein
1.46E-02	13.92	-3.76	Osmolarity sensor protein EnvZ
1.65E-03	150.95	-3.70	hypothetical protein
5.40E-05	4.67	-3.62	hypothetical protein
2.14E-04	407.47	-3.58	hypothetical protein
3.75E-03	33.17	-3.48	hypothetical protein
6.00E-02	117.39	-3.46	Transcriptional regulatory protein OmpR
3.35E-04	5.98	-3.36	hypothetical protein
6.80E-05	0.19	-3.28	Protein TolB
3.70E-05	203.27	-3.22	Transcriptional regulatory protein OmpR
7.37E-03	179.64	-3.18	hypothetical protein
2.37E-04	169.94	-3.17	Cytochrome c biogenesis protein CcsA
3.51E-04	203.15	-3.17	hypothetical protein
1.59E-02	51.46	-3.15	hypothetical protein
2.35E-03	75.13	-3.12	Cytochrome c biogenesis protein CcsB
4.40E-05	7.24	-3.10	ISXO2-like transposase domain protein
2.45E-03	14.92	-2.91	hypothetical protein
1.78E-03	16.08	-2.74	hypothetical protein
9.76E-04	7.01	-2.65	Outer membrane lipoprotein Slp family protein
1.72E-02	70.10	-2.64	hypothetical protein
1.36E-03	0.06	-2.60	Penicillin-binding protein 1A
2.70E-03	486.91	-2.56	hypothetical protein
3.95E-02	665.72	-2.51	hypothetical protein
2.17E-02	21.72	-2.50	Multidrug resistance protein MdtA
9.33E-03	2669.52	-2.46	hypothetical protein
1.12E-04	7.91	-2.46	hypothetical protein
2.47E-03	1446.84	-2.45	Cytochrome c biogenesis protein CcsA
4.79E-02	26.96	-2.44	hypothetical protein
4.59E-03	30.35	-2.43	hypothetical protein
7.70E-04	10.36	-2.43	putative parvulin-type peptidyl-prolyl cis-trans isomerase
3.11E-04	2.42	-2.42	Outer membrane protein assembly factor BamD
4.62E-03	894.49	-2.42	hypothetical protein
3.37E-02	1.48	-2.40	Multidrug resistance protein MdtA
1.31E-02	49.10	-2.40	Thymidylate kinase
6.36E-04	9.44	-2.38	hypothetical protein
2.91E-03	4035.40	-2.38	DsrE/DsrF-like family protein
3.67E-03	1222.25	-2.38	Thiol:disulfide interchange protein DsbG
5.23E-02	0.15	-2.36	Multidrug resistance protein MdtB
5.38E-03	9.80	-2.32	hypothetical protein
5.11E-03	11.93	-2.32	Protein CyaE
1.56E-03	2.56	-2.32	hypothetical protein
3.90E-02	0.76	-2.31	hypothetical protein
2.11E-03	90.42	-2.31	hypothetical protein

Supplementary Table S9: Top 50 upregulated genes after growth on thiosulfate at pH 2.5 as compared to elemental sulfur pH 1.5.

p-value	FPKM	LOG2	Genes
2.93E-01	62.68	9.32	16S ribosomal RNA
1.32E-01	76.35	7.25	hypothetical protein
1.73E-01	6597.13	6.57	putative globin-like protein aq_211
8.00E-05	740.67	6.35	putative protein
2.97E-01	65.53	6.15	16S ribosomal RNA
1.36E-03	17859.50	5.84	hypothetical protein
1.35E-01	1136.18	5.62	Xylene monooxygenase electron transfer component
1.02E-02	734.44	5.48	hypothetical protein
1.50E-04	758.90	5.45	Cation efflux system protein CusC
1.00E-04	802.89	5.19	putative transporter
3.85E-03	14719.90	4.65	hypothetical protein
9.26E-04	20973.40	4.52	DsrE/DsrF-like family protein
1.37E-02	188.27	4.17	Osmolarity sensor protein EnvZ
4.14E-02	2952.08	4.15	hypothetical protein
1.45E-01	680.51	4.11	DNA-3-methyladenine glycosylase
4.52E-03	1178.45	3.91	ABC transporter, phosphonate, periplasmic substrate-binding protein
3.44E-03	369.92	3.90	hypothetical protein
5.69E-02	1291.91	3.78	Transcriptional regulatory protein OmpR
1.49E-03	6352.36	3.64	Thiol:disulfide interchange protein DsbG
8.47E-04	7884.33	3.53	Cytochrome c biogenesis protein CcsA
8.97E-04	2678.03	3.27	hypothetical protein
4.50E-05	1895.24	3.26	Transcriptional regulatory protein OmpR
1.29E-03	819.75	3.26	Cytochrome c biogenesis protein CcsB
2.13E-04	338.77	3.19	Osmolarity sensor protein EnvZ
1.47E-03	115.31	3.13	Lipoprotein-releasing system ATP-binding protein LolD
4.10E-04	4880.44	3.10	hypothetical protein
4.90E-05	960.76	3.08	Cytochrome c biogenesis protein CcsA
1.79E-01	478.14	3.01	putative protein YeaO
8.70E-04	4131.53	2.96	hypothetical protein
2.75E-03	766.06	2.92	Thiol:disulfide interchange protein DsbD
4.12E-03	49.04	2.86	hypothetical protein
3.31E-01	3.34	2.85	hypothetical protein
4.86E-01	280.35	2.80	tRNA-Lys(ttt)
4.99E-03	171.98	2.71	Transcriptional regulatory protein ZraR
2.83E-04	225.84	2.69	hypothetical protein
1.23E-01	8.92	2.67	hypothetical protein
1.05E-03	9721.32	2.67	hypothetical protein
4.76E-04	2491.13	2.63	Glutamate racemase
2.12E-02	122.59	2.63	Multidrug resistance protein MdtA
1.94E-02	441.22	2.55	Sec-independent protein translocase protein TatC
4.41E-04	7.45	2.49	hypothetical protein
9.62E-03	147.88	2.43	Ammonia channel
3.70E-03	279.88	2.43	hypothetical protein
7.90E-05	287.10	2.40	Flagella basal body P-ring formation protein FlgA
7.94E-03	273.44	2.40	Transposase
5.31E-03	59.46	2.39	Protein CyaE
9.51E-03	1627.58	2.34	hypothetical protein
2.69E-04	809.73	2.32	hypothetical protein
6.98E-03	141.62	2.32	HlyD family secretion protein
8.44E-02	7.47	2.31	Hydrolase in pqqF 5'region

Supplementary Table S10: Top 50 downregulated genes after growth on thiosulfate at pH 2.5 as compared to elemental sulfur pH 1.5.

p-value	FPKM	LOG2	Genes
3.62E-01	7.22	-5.42	hypothetical protein
2.77E-02	30.77	-5.24	hypothetical protein
3.47E-01	0.25	-5.24	hypothetical protein
3.35E-01	0.18	-5.14	hypothetical protein
3.76E-01	444.80	-5.00	hypothetical protein
1.06E-02	104.24	-5.00	hypothetical protein
4.63E-02	53.59	-4.83	hypothetical protein
2.45E-02	22.15	-4.73	hypothetical protein
2.24E-02	37.28	-4.66	hypothetical protein
3.36E-01	0.15	-4.61	hypothetical protein
3.77E-01	143.15	-4.59	hypothetical protein
3.78E-01	8.20	-4.55	hypothetical protein
3.20E-02	57.62	-4.49	hypothetical protein
3.95E-01	40.05	-4.40	tRNA-Asn(gtt)
3.82E-01	214.90	-4.39	hypothetical protein
3.82E-01	492.89	-4.34	hypothetical protein
2.58E-02	20.93	-4.32	Nodulation protein NolG
3.77E-01	27.82	-4.28	hypothetical protein
2.54E-02	111.48	-4.28	hypothetical protein
2.14E-02	316.48	-4.25	hypothetical protein
3.84E-01	237.89	-4.24	Single-stranded DNA-binding protein
4.75E-02	25.69	-4.23	hypothetical protein
2.06E-02	130.27	-4.18	hypothetical protein
3.81E-01	8.74	-4.16	DNA ligase
3.86E-01	115.20	-4.16	hypothetical protein
3.71E-01	16.67	-4.16	Helicase associated domain protein
3.80E-01	23.98	-4.15	hypothetical protein
3.84E-01	222.36	-4.13	hypothetical protein
3.84E-01	165.00	-4.13	hypothetical protein
3.80E-01	582.56	-4.11	hypothetical protein
3.87E-01	348.92	-4.11	hypothetical protein
3.85E-01	163.94	-4.11	hypothetical protein
3.87E-01	198.71	-4.10	hypothetical protein
3.82E-01	146.45	-4.10	hypothetical protein
3.86E-01	122.17	-4.10	hypothetical protein
3.86E-01	157.14	-4.09	hypothetical protein
3.83E-01	163.38	-4.09	hypothetical protein
3.84E-01	151.43	-4.08	hypothetical protein
3.87E-01	170.41	-4.08	hypothetical protein
3.87E-01	293.93	-4.07	hypothetical protein
3.84E-01	144.87	-4.05	hypothetical protein
3.87E-01	283.24	-4.05	hypothetical protein
3.80E-01	10.97	-4.05	hypothetical protein
3.87E-01	85.79	-4.04	hypothetical protein
3.86E-01	211.21	-4.03	hypothetical protein
3.85E-01	712.51	-4.01	hypothetical protein
3.86E-01	128.00	-4.00	hypothetical protein
3.88E-01	411.17	-3.99	hypothetical protein
3.73E-01	17.79	-3.98	hypothetical protein
3.81E-01	111.16	-3.95	hypothetical protein

Supplementary Table S11: Mean values for all sulfur species where concentrations for all S are in mM in mol of S.

S^0 Treatment

Day	pH	S^{2-}	SO_4^{2-}	S^0	$S_2O_3^{2-}$	SO_3^{2-}	Other SOI	Total SOI	Total Aqueous S	Total S
0	4.5	0.00	3.55	311.79	0.02	0.00	0.08	311.89	3.65	315.44
1	3.3	0.00	4.06	310.74	0.06	0.00	0.58	311.38	4.70	315.44
2	2.2	0.00	6.42	302.36	0.16	0.00	6.50	309.02	13.08	315.44
3	1.7	0.00	10.16	290.37	0.02	0.00	14.89	305.28	25.07	315.44
4	1.65	0.00	15.22	287.06	0.19	0.00	12.97	300.22	28.38	315.44
5	1.5	0.00	17.18	272.40	0.50	0.0004	25.35	298.26	43.04	315.44

$S_2O_3^{2-}$ Treatment

Day	pH	S^{2-}	SO_4^{2-}	S^0	$S_2O_3^{2-}$	SO_3^{2-}	Other SOI	Total SOI	Total Aqueous S	Total S
0	4.55	0.03	4.27	0.19	28.84	0.12	7.05	36.20	40.30	40.50
2	2.3	0.07	12.14	1.89	10.28	0.004	16.12	28.29	38.61	40.50
4	2.45	0.03	12.07	8.71	5.50	0.22	13.97	28.40	31.78	40.50

Supplementary Table S12: Values for S^0 in mM, for all methods used. **N.B.** the low values of HPLC S_T in the S^0 treatment from day 0-3, are most likely due to the nature of S^0 in the media where initially it is clumped and mostly out of solution. Variation in values for HPLC vs ($\sum S_{in\ media}$ - $\sum S_{aq}$) may also be attributed to external vs internal S^0.

S^0 Treatment

Day	pH	S^0 = HPLC S_{aq}	S^0 = HPLC S_T	S^0 = $\sum S_{in\ media}$ - $\sum S_{aq}$
0	4.5	0.00	10.37	311.79
1	3.3	0.00	63.33	310.74
2	2.2	0.00	128.28	302.36
3	1.7	0.00	219.28	290.37
4	1.65	0.00	261.29	287.06
5	1.5	0.00	172.11	272.40

$S_2O_3^{2-}$ Treatment

Day	pH	S^0 = HPLC S_{aq}	S^0 = HPLC S_T	S^0 = $\sum S_{in\ media}$ - $\sum S_{aq}$
0	4.55	0.00	0.19	0.19
2	2.3	0.00	1.45	1.89
4	2.45	0.00	2.36	8.71

Supplemental Material for Chapter 4

Results

Enrichment generational microbial progression

Analyses to determine the progression of the microbial community in these pH corrals over generations further supported our observations. Where 3 progressions were examined on Mine 1 Summer 2014, Mine 2 Summer 2014 and Summer 2015, with only one for Mine 1 due to its relatively consistent endemic geochemistry and two on Mine 2 due to the great variation in the endemic geochemistry over these time points (Supplementary Figure S3). For Mine 1 Summer 2014 ASOM 7-5, the community after the first gen was primarily comprised of *Halothiobacillus* spp. (48%) and *Thiovirga* spp (41%), where by gen 3 *Halothiobacillus* (79%) outcompeted *Thiovirga* (<1%) and eventually by gen 5 was dominated by *Halothiobacillus* (84%) and *Thiomonas* increased very slowly over the gens (from <1% to 2%) Supplementary Figure S3). However, Mine 1 Summer 2014 ASOM 5-3, we observed the decrease of *Halothiobacillus* over the gens from 66% to 32%, while *Thiomonas* increased from 20% to 64% (Supplementary Figure S3). In spatial comparison for Mine 2 Summer 2014 ASOM 7-5, as neat a progressional trend was not observed with the fluctuation of *Halothiobacillus* over the gens between 47% and 81% and the increase of *Thiomonas* over time from 2% to 22%, though *Thiovirga* was similarly outcompeted again going from 10% to 0% (Supplementary Figure S3). Similarly, the sample's ASOM 5-3, *Halothiobacillus* fluctuates over the gens between 50% and 85% and *Thiomonas* fluctuates between 10% and 43%, with those 2 genera dominating the enrichment community (Supplementary Figure S3). For the temporal comparison, Mine 2 Summer 2015 ASOM 7-5,

showed a clear progression of both *Halothiobacillus* increasing from 13% to 75% and *Thiovirga* outcompeted from 30% to <1%, while *Thiomonas* fluctuates between 6% and 19% (Supplementary Figure S3). Lastly the ASOM 5-3, showed the similar trends of the initial abundance of *Thiovirga* after gen 1 of 65% declined to <1%, while *Halothiobacillus* and particularly in this pH corral *Thiomonas* increase to dominate the enrichment community (2% to 14% and 8% to 85% respectively) (Supplementary Figure S3).

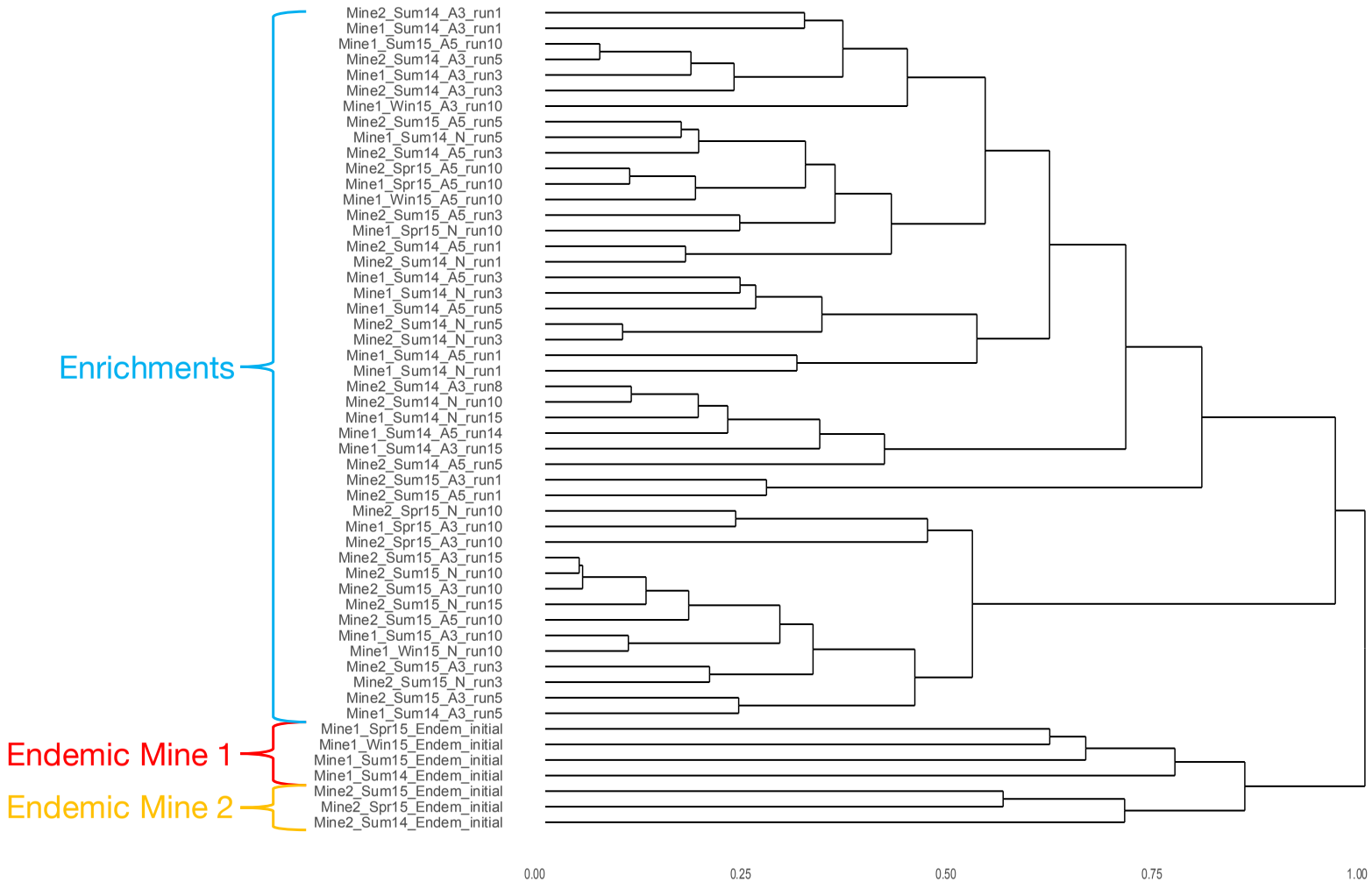

Supplementary Figure S1: Dendrogram showing hierarchal clustering of all samples. (Based on Bray-Curtis dissimilarity from Illumina sequencing of 16S rRNA gene amplicons). Illustrating the clustering of enrichments and the separate clustering of endemic parent microbial communities. Highlighting the clustering of the endemic communities by mine site and level of dissimilarity

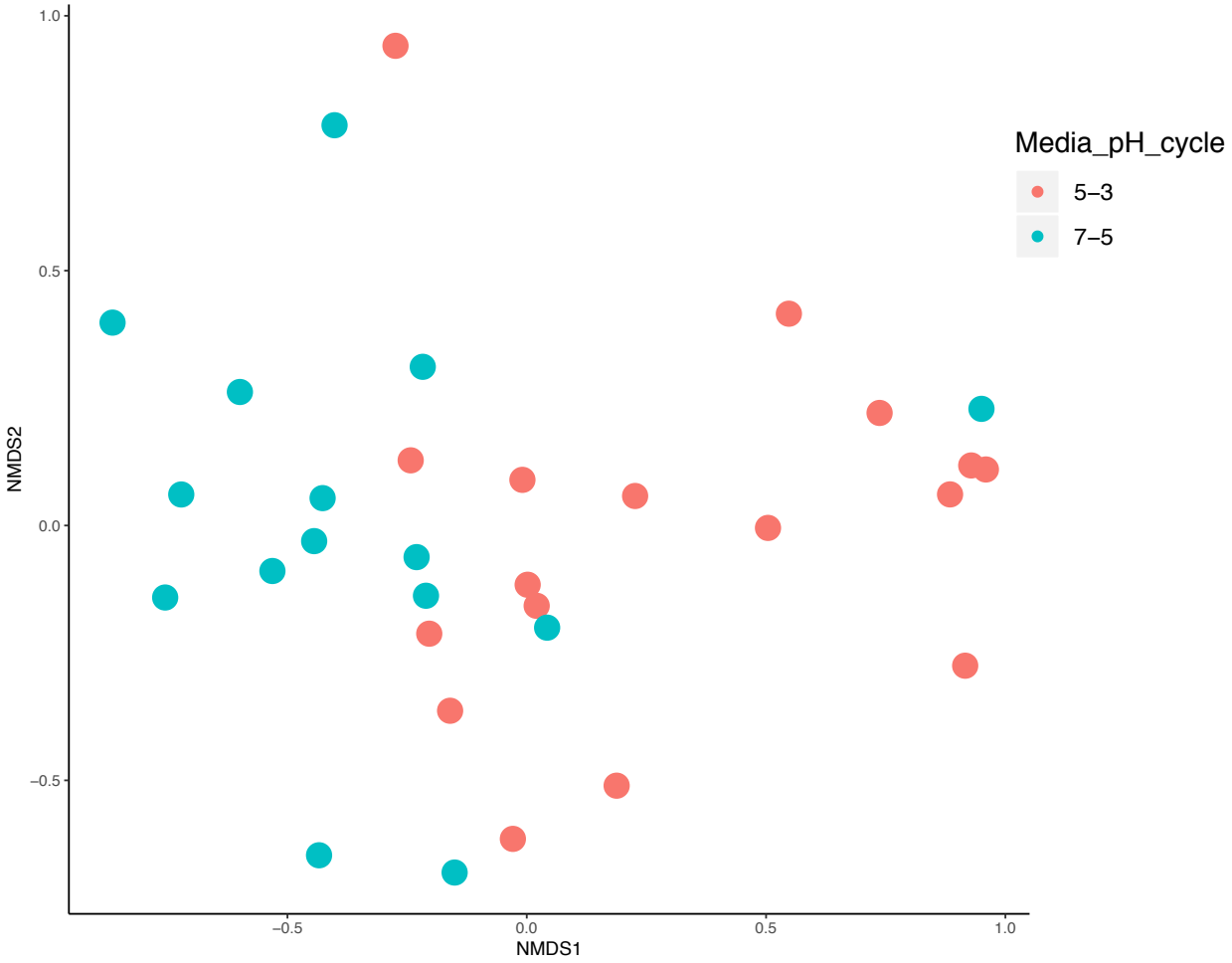

Supplementary Figure S2: Microbial community structure depicting differences between ASOM 7-5 and ASOM 5-3 communities. Non-metric multidimensional scaling (NMDS) plot of ASOM enrichment samples at sequence variants level (based on Bray-Curtis dissimilarity from Illumina sequencing of 16S rRNA gene amplicons) (ANOSIM R^2=0.24, P<0.001, Stress=0.11).

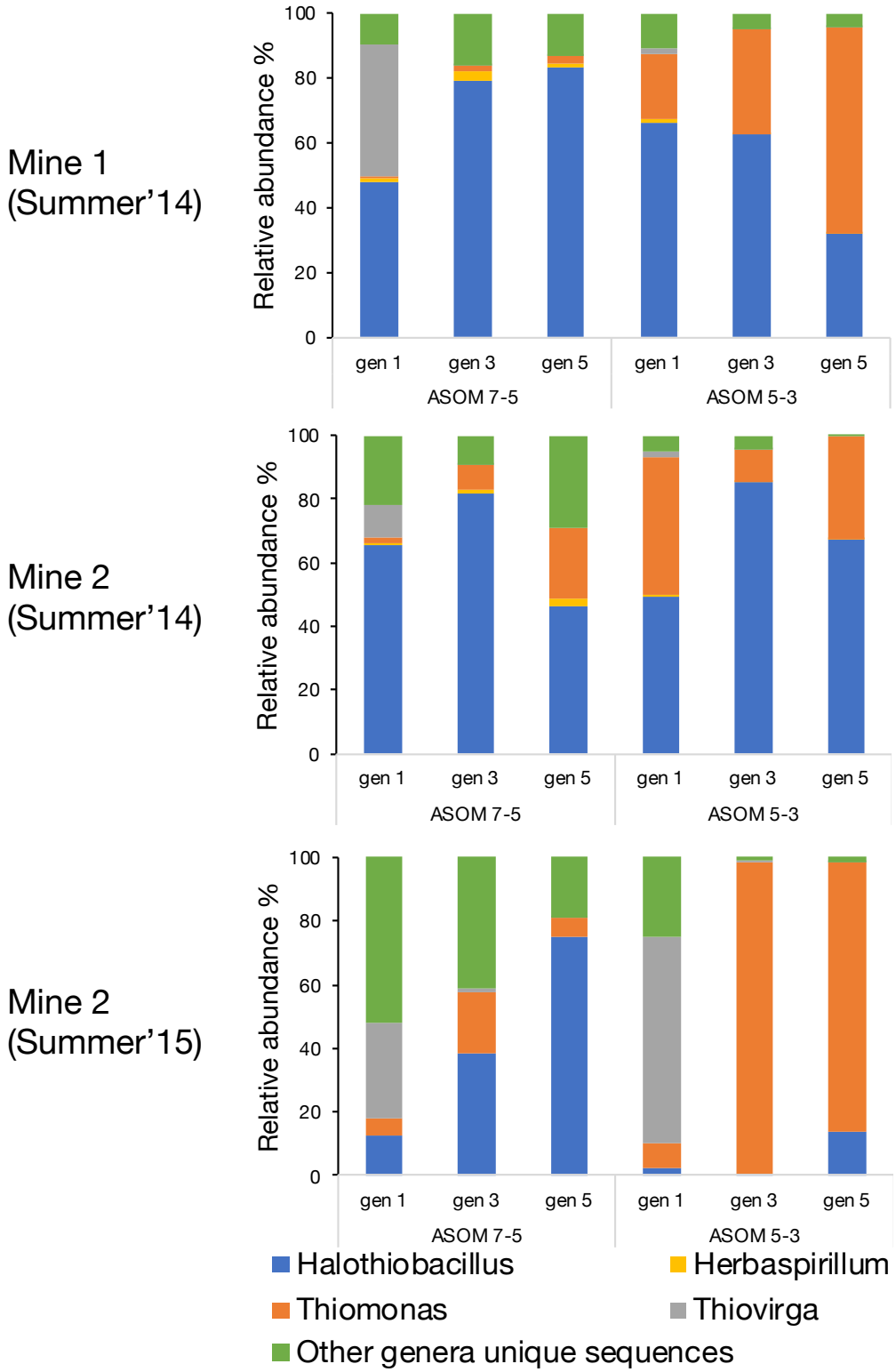

Supplementary Figure S3: Relative sequence abundance of enrichment community classified by genera. Showing succession of generations 1, 3 and 5 within enrichment pH corrals ASOM 7-5 and ASOM 5-3 for three samples: Mine 1 Summer'2014, Mine 2 Summer'2014 and Mine 2 Summer'2015. "Other genera unique sequences" is the remainder of organisms.

Table S1: Number of reads, unique sequences, Shannon diversity and evenness of all genomic samples across both mines and enrichments (based on 16S rRNA gene amplicons).

Sample Name	Mine #	Type (endemic or enrichment)	Media type	Number of reads	Unique sequences	Shannon Diversity	Pielou Eveness
Mine1_Sum14_N_run1	1	Enrichment	NSOM 7-5	111013	38	0.87	0.24
Mine1_Sum14_N_run3	1	Enrichment	NSOM 7-5	125709	18	0.76	0.26
Mine1_Sum14_N_run5	1	Enrichment	NSOM 7-5	113922	13	0.73	0.29
Mine1_Sum14_N_run15	1	Enrichment	NSOM 7-5	7416	19	0.97	0.33
Mine1_Sum14_A5_run1	1	Enrichment	ASOM 7-5	175939	33	1.18	0.34
Mine1_Sum14_A5_run3	1	Enrichment	ASOM 7-5	134157	22	0.86	0.28
Mine1_Sum14_A5_run5	1	Enrichment	ASOM 7-5	137040	24	0.78	0.25
Mine1_Sum14_A5_run14	1	Enrichment	ASOM 7-5	10211	29	1.24	0.37
Mine1_Sum14_A3_run1	1	Enrichment	ASOM 5-3	86667	27	1.09	0.33
Mine1_Sum14_A3_run3	1	Enrichment	ASOM 5-3	74946	11	0.86	0.36
Mine1_Sum14_A3_run5	1	Enrichment	ASOM 5-3	72953	11	0.84	0.35
Mine1_Sum14_A3_run15	1	Enrichment	ASOM 5-3	6509	15	1.20	0.44
Mine1_Sum14_Endem_initial	1	Endemic	-	7546	99	3.46	0.75
Mine2_Sum14_N_run1	2	Enrichment	NSOM 7-5	32486	19	1.41	0.48
Mine2_Sum14_N_run3	2	Enrichment	NSOM 7-5	152507	14	0.58	0.22
Mine2_Sum14_N_run5	2	Enrichment	NSOM 7-5	114981	11	0.75	0.31
Mine2_Sum14_N_run10	2	Enrichment	NSOM 7-5	18451	22	1.07	0.35
Mine2_Sum14_A5_run1	2	Enrichment	ASOM 7-5	110821	23	1.30	0.41
Mine2_Sum14_A5_run3	2	Enrichment	ASOM 7-5	124582	14	0.78	0.30
Mine2_Sum14_A5_run5	2	Enrichment	ASOM 7-5	10435	38	1.98	0.54
Mine2_Sum14_A3_run1	2	Enrichment	ASOM 5-3	78326	16	1.04	0.37
Mine2_Sum14_A3_run3	2	Enrichment	ASOM 5-3	132153	9	0.52	0.24
Mine2_Sum14_A3_run5	2	Enrichment	ASOM 5-3	81898	7	0.68	0.35
Mine2_Sum14_A3_run8	2	Enrichment	ASOM 5-3	9889	14	0.96	0.36
Mine2_Sum14_Endem_initial	2	Endemic	-	7194	49	2.35	0.60
Mine1_Win15_N_run10	1	Enrichment	NSOM 7-5	94666	7	0.35	0.18
Mine1_Win15_A5_run10	1	Enrichment	ASOM 7-5	124669	12	1.00	0.40
Mine1_Win15_A3_run10	1	Enrichment	ASOM 5-3	96122	13	1.41	0.55
Mine1_Win15_Endem_initial	1	Endemic	-	55708	55	2.41	0.60
Mine1_Spr15_N_run10	1	Enrichment	NSOM 7-5	91403	9	1.53	0.70
Mine1_Spr15_A5_run10	1	Enrichment	ASOM 7-5	126704	11	1.12	0.47
Mine1_Spr15_A3_run10	1	Enrichment	ASOM 5-3	83072	13	0.98	0.38
Mine1_Spr15_Endem_initial	1	Endemic	-	78391	154	3.31	0.66
Mine2_Spr15_N_run10	2	Enrichment	NSOM 7-5	83928	11	1.19	0.50
Mine2_Spr15_A5_run10	2	Enrichment	ASOM 7-5	103595	9	0.98	0.44
Mine2_Spr15_A3_run10	2	Enrichment	ASOM 5-3	70272	7	0.72	0.37
Mine2_Spr15_Endem_initial	2	Endemic	-	23707	38	1.94	0.53
Mine1_Sum15_A5_run10	1	Enrichment	ASOM 7-5	104621	6	0.61	0.34
Mine1_Sum15_A3_run10	1	Enrichment	ASOM 5-3	74094	12	0.16	0.06
Mine1_Sum15_Endem_initial	1	Endemic	-	88087	108	3.02	0.65
Mine2_Sum15_N_run3	2	Enrichment	NSOM 7-5	70963	12	0.49	0.20
Mine2_Sum15_N_run10	2	Enrichment	NSOM 7-5	60069	8	0.02	0.01
Mine2_Sum15_N_run15	2	Enrichment	NSOM 7-5	14099	10	0.07	0.03
Mine2_Sum15_A5_run1	2	Enrichment	ASOM 7-5	70796	12	1.90	0.76
Mine2_Sum15_A5_run3	2	Enrichment	ASOM 7-5	77548	11	1.55	0.65
Mine2_Sum15_A5_run5	2	Enrichment	ASOM 7-5	114418	14	0.99	0.37
Mine2_Sum15_A5_run10	2	Enrichment	ASOM 7-5	40846	21	0.12	0.04
Mine2_Sum15_A3_run1	2	Enrichment	ASOM 5-3	132673	13	1.09	0.42
Mine2_Sum15_A3_run3	2	Enrichment	ASOM 5-3	89484	12	0.15	0.06
Mine2_Sum15_A3_run5	2	Enrichment	ASOM 5-3	63344	9	0.48	0.22
Mine2_Sum15_A3_run10	2	Enrichment	ASOM 5-3	65453	7	0.01	0.01
Mine2_Sum15_A3_run15	2	Enrichment	ASOM 5-3	65396	9	0.02	0.01
Mine2_Sum15_Endem_initial	2	Endemic	-	117668	53	2.07	0.52

Table S2: Microbial diversity, evenness, number of unique sequences and relative abundance community structure for all endemic samples. Highlighting the most prevalent or particular recognized as important taxa in the endemic mine samples.

		Mine 1				Mine 2		
		Summer'14	Winter'15	Spring'15	Summer'15	Summer'14	Spring'15	Summer'15
Shannon Diversity		3.46	2.41	3.31	3.02	2.35	1.94	2.07
Pielou Evenness		0.75	0.60	0.66	0.65	0.60	0.53	0.52
Unique sequences		99	55	154	108	49	38	53
Community structure (relative abundance %)								
Bacteria (phylum taxa)	%Bacteroidetes	27	23	19	18	1	1	1
	%Proteobacteria	65	76	58	77	93	95	99
Proteobacteria (class taxa)	%Alphaproteobacteria	28	57	36	60	58	77	73
	%Gammaproteobacteria	32	19	20	16	35	18	26
Alphaproteobacteria (family taxa)	%Caulobacteraceae	<1	9	2	8	44	23	19
	%Rhodobacteraceae	<1	15	16	3	8	<1	6
	%Sphingomonadaceae	25	31	9	24	2	49	40
	%Xanthobacteraceae	<1	<1	1	18	0	0	1
Gammaproteobacteria (family taxa)	%Burkholderiaceae	9	13	15	1	14	2	<1
	%Halothiobacillaceae	7	<1	<1	1	1	3	3
	%Hydrogenophilaceae	6	1	1	7	17	<1	20
	%Legionellaceae	1	3	1	4	1	<1	1
	%Methylophilaceae	5	2	1	3	1	12	1
Gammaproteobacteria (genus taxa)	%Halothiobacillus	1	<1	<1	<1	<1	<1	<1
	%Thiomonas	<1	<1	<1	<1	<1	<1	<1

Supplemental Material for Chapter 5

Methods

Microcosm enrichment media creation

An additional media besides ASOM was used to create enrichments for the endemic mine microbes, a neutrophilic sulfur oxidizing media (NSOM).

NSOM was created in 1 L batches as follows. Part 1: 90 mL of 1.1% (w/v) K_2HPO_4 was added to 400 mL of tap water. Part 2: 5 g of $Na_2S_2O_3$, 90 mL of 0.44% (w/v) NH_4Cl, 90 mL of 0.11% (w/v) $MgSO_4$, 2.2 mL of Solution T and 320 mL of tap water. Part 1 and 2 were sterilized separately by either filtration (<0.2μm) or autoclaving and then combined. Solution T was made by: 50 g of EDTA disodium salt dissolved into 400 mL of water, followed by 9 g of NaOH added to EDTA solution, then the following salts were added individually to 30 mL of water before being added to the EDTA solution: 5 g of $ZnSO_4.7H_2O$, 5 g of $CaCl_2$ (or 7.34 g of $CaCl_2.2H_2O$), 2.5 g of $MnCl_2.6H_2O$, 0.5 g of $CoCl_2.6H_2O$, 0.5 g of $(NH_4)_6Mo_7O_{24}.4H_2O$, 5 g of $FeSO_4.7H_2O$ and 0.2 g of $CuSO_4.5H_2O$.

Microcosm enrichments growth

Water samples collected from both mines during Summer'14 from the mines wastewaters underwent the three enrichment strategies: 1) NSOM within a pH corral between 7-5 (NSOM 7-5); 2) ASOM within a pH corral between 7-5 (ASOM 7-5); and 3) ASOM within a pH corral between 5-3 (ASOM 5-3). These pH corrals were chosen to identify key sulfur oxidizing microbes of mine wastewaters as potential bioindicators as acid generation occurs, as well as to identify

possible microbial SoxB consortia progression from neutral to mildly acidic pH (7-5) and subsequently to moderately acidic pH (5-3) conditions.

The pH was tested at intervals as described in Whaley-Martin *et al.* (2019) until each enrichment achieved the final pH of its specific pH corral, i.e. pH = 5 for the 7-5 enrichments, or pH = 3 for the 5-3 enrichments. Once the final pH was achieved, a new run/cycle/generation(gen) was then created using a 1:2 ratio of the current enrichment to fresh media, i.e. 50 ml of current enrichment cycle and 100 ml of fresh media. It was then buffered to the starting pH of the enrichment types corral, i.e. NSOM 7-5 and ASOM 7-5, starting pH = 7, and for ASOM 5-3 starting pH = 5.

Mine wastewater mesocosms experimental design

Five biological treatment types were assessed for the mesocosms utilizing endemic mine wastewaters. An abiotic and three enrichments; one of each of the three enrichment types (NSOM 7-5, ASOM 7-5 and ASOM 5-3) for either Mine 1 or Mine 2 Summer 2014 latest generation microcosms.

Autoclaved 8 L carboy containers were filled with 5 L of either the filter sterilized (<0.2 μm) mine wastewaters only (abiotic) or filter sterilized (<0.2 μm) mine wastewater and a SoxB enrichment. The enrichments were re-grown from the preserved microcosm enrichments of the latest generations for the samples. Once the enrichments reached the low end of their respective pH corrals, the 150 ml enrichments were filtered through 0.2 μm membranes. Then the membranes were aseptically removed and placed into the 5 L sterile mine wastewaters. This was used to add the SoxB enrichment microbial community while preventing any change to the mine wastewater geochemistry due to addition of S sources or acid contamination from the enrichment media.

Experiments were ran for the 3 enrichments types from both mines, placed individually into their own filtered mine wastewaters and a cross-examination of the enrichments in the other mine's filtered wastewaters. I.e. Mine 1 enrichments were separately placed in Mine 1 wastewaters and in Mine 2 wastewaters, the same was done for Mine 2 enrichments. Samples for pH and sulfur speciation were taken periodically based on any decrease in pH.

Results

Enrichments in mine wastewaters

In Mine 1 (low S) wastewaters neither of the microbial enrichments were able to drive the system to acidic conditions (Supplementary Figure S4a). However, in Mine 2 wastewaters, which was of high S concentration, both enrichments from either parent wastewater drove the system to pH < 4 (Supplementary Figure S4b). Thus indicating that the deciding factor towards acid generation was geochemistry dependent, not microbial. This is further supported by the characterization of the enrichment communities present sharing similar microbial taxa from both mine parent wastewaters (Camacho *et al*., 2020b).

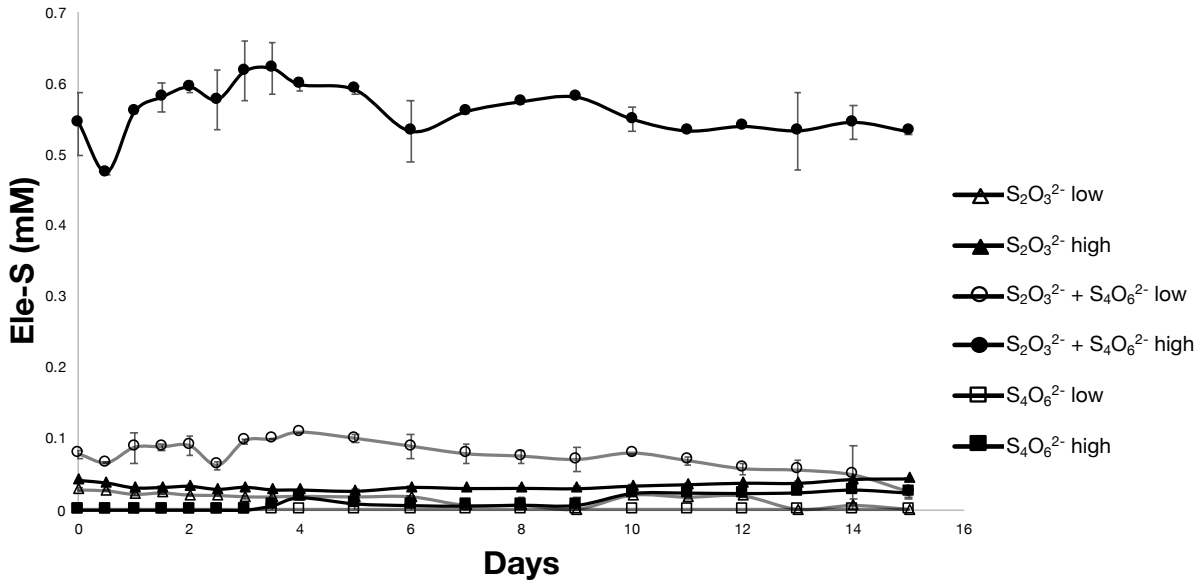

Supplementary Figure S1: Relationship of elemental sulfur over the experimental time period for the Abiotic sulfur treatments. Showing the immediately abiotically formed S^0 as a result similar to Wakenroder reactions.

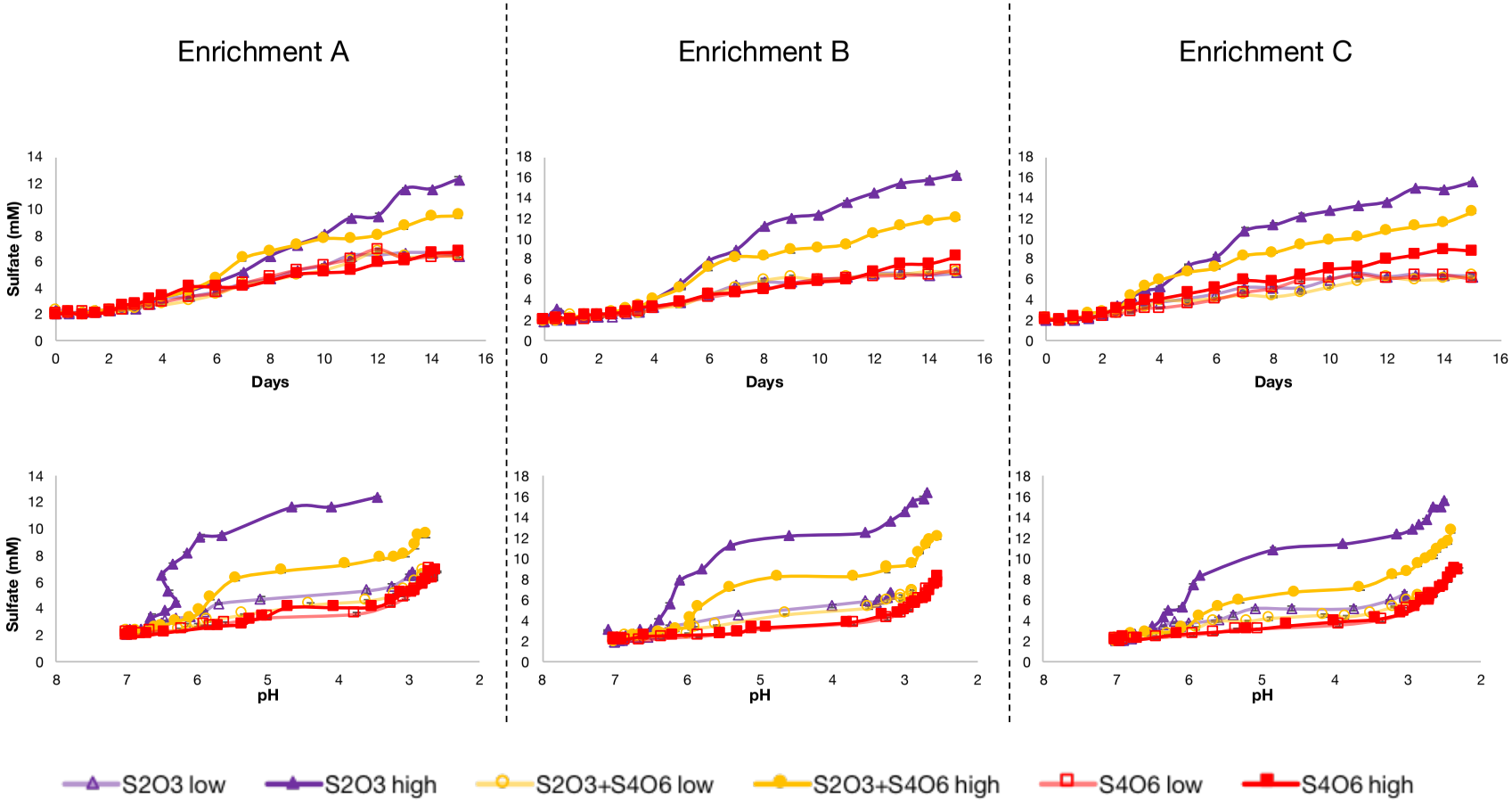

Supplementary Figure S2: Sulfate concentrations for all three biological enrichments, showing against time (top) and against pH.

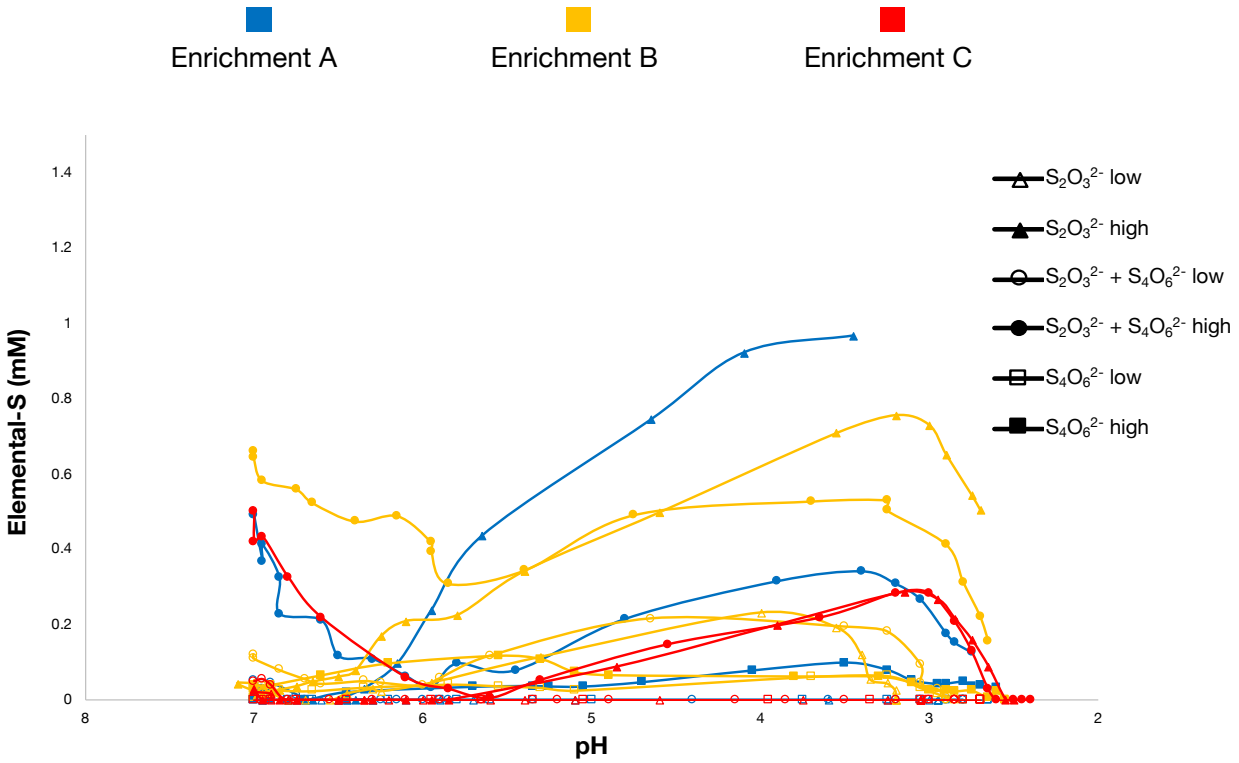

Supplementary Figure S3: Relationship of elemental sulfur as a function of pH, across all three biological experiments.

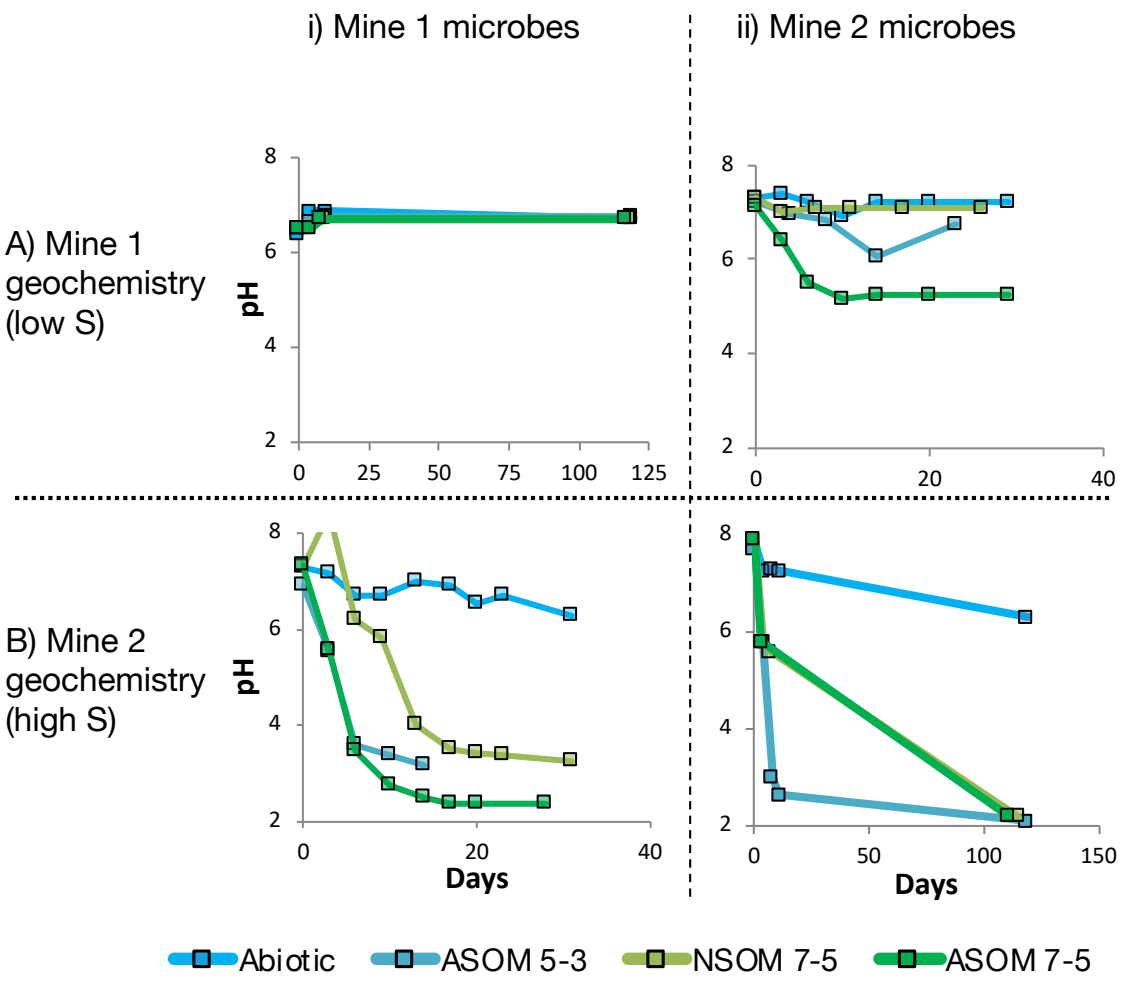

Supplementary Figure S4: pH over the varying time course of three microbial enrichments and a sterile abiotic control from each Mine 1 and Mine 2, in each of the parent mine wastewaters, showing geochemical dependence towards acid generation.

Supplementary Table S1: Initial and final sulfate concentrations for all abiotic sulfur treatments.

Abiotic 'S treatment'	Initial [SO_4^{2-}] (mM)	Final [SO_4^{2-}] (mM)
$S_2O_3^{2-}$ Low	1.71 ± 0.06	1.91 ± 0.06
$S_2O_3^{2-}$ High	2.29 ± 0.05	2.14 ± 0.05
$S_2O_3^{2-}$ + $S_4O_6^{2-}$ Low	2.07 ± 0.06	1.89 ± 0.14
$S_2O_3^{2-}$ + $S_4O_6^{2-}$ High	2.21 ± 0.16	2.56 ± 0.10
$S_4O_6^{2-}$ Low	1.95 ± 0.10	1.93 ± 0.06
$S_4O_6^{2-}$ High	1.94 ± 0.14	2.13 ± 0.04

Supplementary Table S2: Initial and final sulfate and S_{react} concentrations and percentage of [Total S] for enrichment C sulfur treatments.

Enrichment C 'S treatment'	Initial $[SO_4^{2-}]$ (mM)	Final $[SO_4^{2-}]$ (mM)	Initial $[SO_4^{2-}]$ (% of [Total S])	Final $[SO_4^{2-}]$ (% of [Total S])	Initial S_{react} (mM)	Final S_{react} (mM)	Intial S_{react} (% of [Total S])	Final S_{react} (% of [Total S])
$S_2O_3^{2-}$ Low	2.04 ± 0.07	6.28 ± 0.08	31	95	4.56	0.31	69	5
$S_2O_3^{2-}$ High	1.96 ± 0.09	15.56 ± 0.19	9	69	20.63	7.03	91	31
$S_2O_3^{2-} + S_4O_6^{2-}$ Low	2.14 ± 0.05	6.36 ± 0.15	32	97	4.45	0.23	68	3
$S_2O_3^{2-} + S_4O_6^{2-}$ High	2.14 ± 0.11	12.63 ± 0.15	9	56	20.45	9.97	91	44
$S_4O_6^{2-}$ Low	2.11 ± 0.08	6.02 ± 0.07	32	91	4.49	0.57	68	9
$S_4O_6^{2-}$ High	2.02 ± 0.07	8.81 ± 0.18	9	39	20.57	13.78	91	61

Supplementary Table S3: Observed ratio of SO_4^{2-}:H^+ as a function of three pH phases (1: pH > 5, 2: pH 5-3, 3: pH < 3) for Enrichment C treatments. Total phase Δ ($T_{end\ of\ phase}$ - $T_{end\ of\ previous\ phase}$) where T = sampled time point.

Total Phase Δ ($T_{end\ of\ phase}$ - $T_{end\ of\ previous\ phase}$) SO_4^{2-}:H^+			
S treatment	**pH > 5**	**pH 5-3**	**pH < 3**
$S_2O_3^{2-}$ low	395.76	1.29	na
$S_2O_3^{2-}$ high	4781.21	5.67	1.35
$S_2O_3^{2-}$ + $S_4O_6^{2-}$ low	285.80	1.93	1.29
$S_2O_3^{2-}$ + $S_4O_6^{2-}$ high	765.20	2.75	1.34
$S_4O_6^{2-}$ low	120.22	1.99	0.89
$S_4O_6^{2-}$ high	172.78	1.94	0.99